À Biblioteca
da Esc. de Engenharia
POA 08/10/84

CRANFIELD INSTITUTE OF TECHNOLOGY

SCHOOL OF INDUSTRIAL SCIENCE

PhD. THESIS

IVAN GUERRA MACHADO

WELDABILITY ASPECTS OF HIGH YIELD STRENGTH Q & T STEELS

SUPERVISOR: DR. J.H. ROGERSON

APRIL 1984

To LINA. Without you it could never have been done.

In memory of my father. It is really a pity that you could not wait.

To my mother and sister, for the good past.

MACHADO, Ivan G. Weldability aspects of high yeld strength Q & T steels. Cranfield, Cranfield Institute of Technology, 1984. 277p.

RESUMO

Inicialmente, foram estudadas as origens e tendências das trincas de solidificação no passe de raiz, das soldas produzidas num espécimen altamente constrangido, projetado especificamente para esses testes.

Trinta e seis soldas por arco submerso foram feitas sobre dois aços de Alta Resistência Mecânica temperados e revenidos (HY100 e Q2N), com dos arames contendo elementos de liga (LINDE 95 e OERLIKON 53 NiMo 1), dois fluxos básicos (OP41TT e OP121TT) e seis combinações de parametros de soldagem, com os três seguintes níveis de energia de soldagem: 1,9; 2,8 e 4,1 KJ/mm.

O fenômeno de trincas de solidificação mostrou-se extremamente complexo e basicamente dependente da composição química, macroestrutura de solificação, microsegregação, tipo de fluxo, tamanho e orientação das dendritas e estado de tensão do metal base.

Nesse estudo, foram introduzidos dois novos conceitos, o do "tamanho corrigido das dendritas" e "tempo de retenção " da peça de solidificação.

A microestrutura secundária dos metais das soldas foram investigadas e uma boa correlação foi encontrada entre as temperaturas de transformação e o tempo de resfriamento.

Um dispositivo de oscilação do arame foi projetado e usado com sucesso para fabricar soldas exploratorias, no sentido de diminuir a incidencia das trincas de solidificação, atraves da agitação da peça de fusão.

As propriedades mecânicas do metal de solda (tração , escoamento, impacto) foram estudadas, utilizando-se energias de soldagem de 1,9 e 4,1 KJ/mm, com os dois arames e fluxos acima citados. Os resultados mostraram que, mesmo com a mais alta energia de soldagem, é possivel obter metal de solda com relativamente alto limite de escoamento e tenacidade, para qualquer combinação de fluxo/arame, alcançando-se valores maiores do que 600 N/mm^2 e energia absorvida média (Charpy-V) de 80J a -40°C, com temperatura de transição para o modo de fratura por quase-clivagem abaixo de -40°C e igual ou acima de -80°C.

As técnicas básicas utilizadas para o estudo incluiram análise metalografica, pelo microscopio optico (de luz), microscopio eletrônico de transmissão, Microscopio Eletrônico de Varredura e Microsonda; análise térmica "in situ" do metal de solda, ensaios mecânicos.

ABSTRACT

A specially designed, highly restrained specimen test (60^{o} groove angle) was successfully used to study root run weld metal solidification cracking origins and tendencies.

Thirty six submerged arc welds were made on two High Yield Strength Quenched and Tempered base steels (HY100 and Q2N), with two low alloy wires (LINDE 95 and OERLIKON S3 NiMo 1), two basic fluxes (OP41TT and OP121TT), and six welding parameters combination at three energy inputs, viz: 1.9, 2.8 and 4.1 KJ/mm.

The weld metal solidification cracking phenomenon showed up to be extremely complex and basically dependent on chemical composition, solidification (primary) structures, microsegregation, flux type, dendrites size and orientation, and base metals stress state.

The most resistant welds to this defect were those made using Q2N base steel, OP121TT flux and OERLIKON S3 NiMo 1 wire. A combination of the following properties are thought to have induced this result: high carbide-to-ferrite elements forming in the base metal; flux promoting weld centreline equiaxed structure and less microsegregation; wire chemical composition, with high Mn/Si ratio, inducing also less microsegregation at the weld centreline; lower carbon and nickel combined contents in presence of also lower phosphorus and sulphur contents. The Q2N greater ability to relieve the strain around the weld pool at high temperature is another possibility, albeit not practically demonstrated.

The welding parameters' main influence on solidification cracking tendency was found to be through change in centreline solidification macrostructure and dendrite size, but the stress fields within and around the weld pool are also thought to play a significant role.

The dendrite size holds a strong relationship with weld bead geometric factors, such as weld bead height-to-width ratio and, principally, external area-to-perimeter ratio. The dendrite size measured on the weld bead longitudinal section must be corrected, for it depends on the angle between the dendrite growth direction and the weld bead symmetry line in a transverse section. Thus, the actual dendrite size rate of change with welding parameters is not that observed through metallographic analysis.

Four types of centreline solidification macrostructures were identified and associated with solidification cracking tendency, viz: stray, competitive columnar, centreline and equiaxed. The former three macrostructures were found to be dependent on welding parameters, whilst the latter was promoted by the OP121TT flux. Experiments have shown that this flux releases more than twice the amount of gas(es) released by the OP41TT flux.

The time available for reactions between the weld pool liquid metal and the surrounding atmosphere was evaluated through an (approximate) weld pool retention time, given as the weld ripple lag-to-welding speed ratio. Good correlation was found between this ratio and both the amount of fused slag and deoxidants recovery.

The root run welds have shown a secondary microstructure principally composed of ferrite with aligned M-A-C, acicular ferrite and martensite. No differences were detected between weld metals deposited by both wires or fluxes, being noticed the change in microstructure size only. A good correlation was found between transformation temperature and cooling time.

Evidence was found of 'cold' or high temperature (not solidification) cracking propagation from existing solidification cracking, and carbides segregation along the solidification cracking path.

Change in the groove angle to 0^{o} and 120^{o} modified the general weld bead geometry and reduced the solidification cracking tendency.

Cold wire addition reduced the centreline solidification cracking tendency, with no action on transverse cracks.

A device was designed to make exploratory welds with wire oscillation keeping the welding head still. Low oscillation frequencies (below 10 Hz) in the welding direction have shown to be very effective to overcome both, transverse and centreline solidification cracks. Stress relieving the base metals considerably reduced the solidification cracking tendency.

The all-weld metal mechanical properties were assessed through the use of a specimen design which allowed the obtention of practically nil diluted welds, made with 1.9 and 4.1 KJ/mm energy inputs and the two wires and fluxes combinations. The results have shown that even at the highest energy input it is possible to obtain weld metals with relatively high yield strength and toughness, using any one of the available flux/wire combinations. The results yielded not less than 600 N/mm^2 Yield Strength and average Charpy V-notch energy absorbed of 80 J at $-40^{o}C$, with transition temperature to quasicleavage fracture mode occurring below $-40^{o}C$ and at or above $-80^{o}C$.

The basic techniques utilised included metallographic analysis using light microscope, Transmission Electron Microscope and Scanning Electron Microscope; weld metals 'in situ' thermal analysis; all-weld metal mechanical tests; hardness.

ACKNOWLEDGEMENTS

This work certainly would be much more imperfect without the generous help, guidance and friendly relationship of my supervisor, Dr. J. H. Rogerson, and sincere gratitude is here expressed.

The sponsorship of the Brazilian Comissao Nacional de Energia Nuclear (CNEN) is acknowledged.

The author also thanks Dr. F. J. Kiss and Dr. A. Muller from the Universidade Federal do Rio Grande do Sul (UFRGS) for their encouragement.

A special thanks to Professor R. L. Apps for his support in some difficult matters.

Dr. J. C. Borland made many interesting suggestions and these are acknowledged.

The author is indebted to Mr. K. A. Nelson for his constant friendship and advice on all types of subjects. The wire oscillation system would never have been constructed without his help.

A lot of help was received from Messrs. P. Cook and P. Haines, and this is specially acknowledged.

Thanks are also due to Messrs. S. Skevington, D. Smith, C. Matthews, S. D.Moynihan, A. Nelson, D. Timpson and J. Savill for their assistance.

Finally, the author would like to express warm thanks to his colleagues Jorge, Augusto and Nelson for their friendship and fruitful discussions on some subjects.

CONTENTS

CONTENTS (Continued)

CONTENTS (Continued)

LIST OF TABLES

LIST OF TABLES (Continued)

LIST OF FIGURES

LIST OF FIGURES (Continued)

LIST OF FIGURES (Continued)

LIST OF FIGURES (Continued)

LIST OF FIGURES (Continued)

LIST OF FIGURES (Continued)

LIST OF FIGURES (Continued)

LIST OF FIGURES (Continued)

1. INTRODUCTION

The historical launching at Richborough (UK) of the 'Ac 1320', the first all-welded barge, on 11th June, 1918, established the beginning of a new era / 1 /. She had only 240 tons dead-weight but was, for her time, an engineering achievement and, we have to recognise, an act of courage.

Sixty-three years after the floating of the 'Ac 1320' and much experience in this field, the construction of the 'Trident' nuclear submarine in the USA, perhaps one of the most advanced pieces of welding engineering on earth, was delayed several months and 2.6 million dollars were spent on weld repairs only / 2 /.

There is, as a consequence, widespread concern as regards the weldability of steels which have a range of critical applications, such as the High Yield Strength Quenched and Tempered HY100 and Q2N.

An earlier exploratory study / 3 / on hydrogen induced cracking had shown that the two base steels (HY100 and Q2N) have a relatively good resistance to this defect both in the HAZ and weld metal. Weld solidification cracking, however, showed up as a worse problem.

The main objective of this work was, therefore, to study the solidification cracking of High Yield Strength Q & T steels, paying attention to non-compositional factors such as the weld bead geometry, base metals stress state, solidification macrostructure, dendrite size, flux type (some of them neglected in previous studies), as well as compositional factors, and ways to overcome this defect.

The experimental work was carried out on submerged arc welds of Q2N and HY100 steels, and also there were examined the welds secondary microstructure, weld thermal cycles 'in situ' measurements, and all-weld metal mechanical properties.

2. HIGH YIELD STRENGTH QUENCHED AND TEMPERED STEELS

2.1 Outline of their development

The development of High Yield (HY) strength Quenched and Tempered (Q & T) steels is well documented / 4-6 / for example.

Before, however, we must bear in mind the primary objectives of their development. Primarily the materials in question were only intended for submarines operating in a 'marine environment', bringing all its chemical complexity and resultant corrosive consequences; the wide range of temperatures, from the poles to the equator, and the hydrostatic external pressure associated with the depths at which this pressure vessel is operating. By operational demands, the materials employed in these structures must have inherently high Yield Strength (YS), good notch toughness and relatively stable physical properties in a wide range of temperatures (often -34°C to +50°C). Also desirable is a high modulus of elasticity (due to the typical cylindrical configuration of the structure) to prevent premature instability failure, low density and resistance to low-cycle fatigue / 5 /. Moreover, the material should be easily fabricated, readily available and possess good weldability.

Later, the concept was extended and the modern HY Q & T steels are now candidates for nuclear reactor vessels / 7 / and offshore structures / 8 /. Thus, new challenges for these responses to different environments were raised, mainly neutron irradiation embrittlement and stress corrosion cracking (SCC) in the presence of H_2S.

In the UK the early 1950s saw the birth of the grain refined (A1), Mn-Mo normalised and tempered steel UXW (Underwater, eXplosive, Weldable). The high carbon content of this steel and thus weldability problems, soon made it replaced by the lower carbon, Q & T version QT28, guaranteeing a YS of 430N/mm^2. However, the need for a higher strength material to use in the hulls of nuclear submarines, pressed the MoD to design a new steel. A detailed study of the available steels was initiated, and finally in 1957 the QT35 steel was developed. It resulted from nickel additions to a Q & T Mn, Cr, Mo, V steel with minimum YS of 555N/mm^2. This steel was first produced by the basic open hearth process, and silicon killed. In 1966 the practice was changed to an electric furnace technique and primary deoxidation was by aluminium. After an extensive use of this steel in the UK, lamellar tearing in tee-butt joints was detected by ultrasonic examination. Then, at the end of 1965 it was replaced by HY80, an American steel whose first specification was drawn up in the USA in 1951 (see below).

The MoD then decided to have a similar (and perhaps better) steel to the HY80 and the specification for Navy Q1 (Q1N) was drawn up in January 1968 / 9 /. The Q1N is produced by basic electric furnace melting practice, the primary deoxidation is made by aluminium, followed by vacuum treatment. The required mechanical properties are obtained by Q & T.

Between the HY80 and the Q1N steels there are, however, at least three noticeable differences: the Q1N has to be tougher than the HY80; the maximum allowable sulphur and phosphorous content must be lower, and the specification calls for inclusion counts. The steel being designed to have its YS in the range 550-655N/mm^2.

In the USA, a first specification for the HY80 steel was drawn up in 1951, as we have already said above. It too came from a complicated and not less empirical way. After failing to reach the proposed mechanical properties, using modified versions of available High Tensile Steels (HTS), the US Navy researchers turned back more than a half century and found a basic idea in another kind of steel, produced by a different 'school' of metallurgy. The KRUPP 3.5%Ni, 1.5%Cr Q & T steel (developed in 1894), with good toughness and intended for armour purposes was chosen as a starting point. Modifications in the carbon and nickel content and addition of molybdenum led to the low-carbon Special Treatment Steel (STS), which was 'the forerunner of that which is now known as HY80 steel' / 5 /. This steel can be made by either open hearth or electric furnace process, fully killed and grain refined using aluminium. The mechanical properties (minimum 550N/mm^2 or 80,000 psi YS) are obtained by Q & T, with specification calling for not less than 80% of martensite at mid thickness of a plate.

As it could be expected, during 1962, a specification for a minimum 690N/mm^2 (100,000 psi) YS steel was released in the USA, based on the HY80 composition, but with higher nickel and carbon. The British, in counterpart, developed their steel in 1968, similar to the Americans, but again having a specification that calls for an inclusion count, showing greater care for the steel cleanness. Both steels are known as HY100 and Q2N respectively and are the subject of the present study. HY100 is usually melted in electric arc furnaces, fully killed, and vacuum degassing is frequently employed to improve cleanliness. Q2N is understood to be melted by basic electric furnace practice, deoxidation made by aluminium and always vacuum degassed, with inclusion (sulphides and oxides) shape control.

The development of new steels, of course, did not stop at this point, continuing in the USA with the HY series (HY130, HY150, HY180, etc).

Chemical analyses and mechanical properties of Q1N and HY80 steels are found on Tables 2.1 (a,b), while for Q2N and HY100 the author thought it to be more meaningful to place them in Section 6, together with the actual materials on which this work was based (Table 6.1). So, at this point, it is possible to have some idea about the history of the development of the HY Q & T steels. It is clear that it was based on empirical knowledge rather than on systematic scientific research. However, from the HY100/Q2N steels on, the scientific methodology began to be applied / 10/. It was essentially helped by the development of the modern steelmaking practice / 11, 12 /, and a better understanding of its principles / 13 /.

2.2 Metallurgy

It is not the aim of this work to go into detailed discussion of steel manufacture. The objective is only to point out its implications on the properties of the final product, and for that we need to understand the various steps in the production of the steels we are presently handling.

Their properties began to be defined well before the melting of the raw material. The use of scrap, mainly in electric furnace steelmaking, with the recycling and residuals make the point. Recently, a review of the situation in the USA was published by STEPHENSON / 14 /.

The residual elements were defined as those: (a) not efficiently removed from the liquid metal in steelmaking and may therefore build up to relatively high levels with continued recycling, and (b) which significantly affect certain critical properties of steel at residual concentrations of a few tenths of a percent. The same author quotes DUCKETT / 15 / as saying that the element tin will approach limiting values after just four or five recycling operations.

Great care must be taken about the influence of residuals on the processing of the wrought steel, as 'surface hot shortness' or 'adherent scale' as well as on the final product, as strength, ductility, formability, impact resistance and weldability.

The selected process for making the steel will decide the alloying and deoxidation practices. In their turn, amounts of oxygen, hydrogen and nitrogen, as well as shape and amount of second phase particles will be affected. For example, basic oxygen steel is lower in residual content than that from conventional open-hearth, giving a product with better properties. The use of secondary steelmaking processes will bring a series of advantages / 12 / such as: to remove hydrogen from the steels; to improve its mechanical properties; to achieve close control over compositional limits; to produce low sulphur steel; to improve the cleanliness of the steel, and so on. Much improvement can be reached through vacuum degassing of steel and treatment of it in the ladle, today's low level for gases being typically / 11 / 0.002% oxygen and .00015% hydrogen. Nitrogen can be managed to stay in an amount compatible with the nitrides desired, as well as other interstitials, like carbon and boron. Figure 2.1 gives us the enthalpies of formation of those precipitates, being a guide to their formation. The several mechanisms by which steels can be strengthened are relatively well known / see for example, 16 /, and the way by which the inter-relationship among the chemical elements can affect the pursued properties are better known / 13 /. Despite this, much more yet is unknown, and a great degree of uncertainty still persists when one has to design such an alloy. For until today there is not (mathematically speaking), an exact 'law' (if it actually exists) that rules this relationship between elements and the resultant properties. Therefore, the following three points, even today, are held / 17 /:

(a) The effect of an alloying element on properties is not necessarily proportional to the amount present.

(b) The effect of an alloying element on properties may be altered by the presence of another alloying element.

(c) The role of an alloying element may be different in a different phase in an alloy.

As an additional complication, there are the second phase particles, which will affect the steel's properties, mainly toughness, through their shape, size and distribution. The plasticity, thus the shape of these inclusions, can be controlled up to a certain point, after the steel deoxidation, by small additions of elements such as the rare earths, titanium, zirconium or calcium. All these methods were excellently reviewed by PICKERING et al / 18 /, with McLEAN and KAY / 19 / giving us a reasonable picture of the principles that control their formation. WILSON / 20 / specifically showed the beneficial effects

of sulphide control to reduce heat-affected zone cracking in welds and to improve base metal toughness. Figure 2.2 shows the effect of second phase particles on total ductility / 13 /, but the influence of their shape is very important and must be remembered, despite the difficulty of assessment / 20 /.

In the steels studied here, carbon is still by far the most important element, so their solidification generally follows the behaviour described by the carbon-iron equilibrium diagram (more correctly, by the Fe_3C-Fe diagram) / 21 / as shown in Figure 2.3 / 22 /. In this figure, two lines were drawn up showing 0.17%C for Q2N and 0.21%C for HY100, which represent the content of carbon for the actual steels studied in this work. Furthermore, Figure 2.4 / 22 / shows the liquidus projection for the Fe-Ni-Cr system, which are the elements in greatest amount in our two steels. Both steels should be placed at the left bottom corner of this diagram, by their chemical composition. These figures help us to form an idea about the structures found after the solidification. Thus, for these kinds of steel, the solidification transformations are:

$$\text{Liquidus (L)} \rightarrow \delta \text{ dendrite (solid)} + L$$

$$\delta + L \rightarrow L + \gamma + L \quad (\text{probably peritectic } \delta + L \rightarrow \gamma \text{ for Q2N steel})$$

$$\delta + \gamma + L \rightarrow \alpha + Fe_3C$$

The difficulty with these steels resides in the fact that a solidified structure can contain a residual eutectic between the dendrites / 21 /, depending on the amount of impurities. At slower cooling rates the amount of austenite will probably be reduced. Furthermore, the sulphur-iron and phosphorus-iron diagrams / 22 / show that the solubility of S and P in delta iron are respectively 0.18% and 2.8% while those in gamma iron are 0.05% and 0.3%. Therefore, the more solidified gamma phase produced in liquid iron, the more the segregation will be at solidified grain boundaries (dendrites).

It is known that the solidification macrostructure of a steel ingot displays, in general, three structural zones / 23 /, namely, chill, columnar and equiaxed. The resulting macrosegregation is shown in Figure 2.5 / 24 /. The 'banding' phenomenon, or abrupt variations in composition, is not completely clear. It may result from the sweeping of solute from behind the dendrites tips, or due to thermal pulses from convection / 25 /. The dendritic structure is usually continuous through the segregated section, appearing on macroetching only because of local changes in composition / 24 / . The similarity with the 'banding' found in weld sections is remarkable, and we shall come back to this point later (Chapter 3). FLEMINGS / 24 / showed that the original solidification macrostructure above can be profoundly altered by means such as rotation during the pouring, so giving much more homogeneous ingots and different macrostructures with better properties.

The studies of KATTAMIS and FLEMINGS / 26 / pointed out that in the columnar structure of low-alloy steel ingots can be found microsegregation across dendrite arm and interdendritic spaces (in the as-cast condition). The electron microprobe was able to detect at least heavy Ni, Cr and Mn variations. The same FLEMINGS / 25 / gives many examples of the strong relationship between the primary dendrite arm spacing and solidification cooling rate (being smaller for higher cooling rates). In general, the elements diffusion coefficients are at least one order of magnitude

smaller in the gamma-iron than the alpha iron. The solubilities of carbon in gamma and alpha iron are wellknown, while nitrogen changes from 2.8% at 650°C to less than 0.001% at 20°C. The carbides and nitrides of Nb, Ti and V are much more stable than is iron carbide (Figure 2.1), thus combining preferentially with carbon. Consequently, cementite will form only when the carbon concentration exceeds that needed for the micro-alloying elements / 27 /. Figure 2.6 / 28 / shows the solubility products of carbides and nitrides in austenite as a function of temperature (as we quoted this relationship is wt% and not in ats%, as it usually is, the solubility product is defined as wt% solute times wt% carbon or nitrogen). This figure helps us to understand how to employ these carbonitrides. In small amounts and well dosed, carbon and nitrogen can form a relatively large amount of carbonnitride which can retard recrystallization and grain growth of austenite. Aluminium nitride, too, is an effective grain refiner. However, very fine precipitates do not seem to be able to prevent the grain boundary movement once the recrystallization takes place. Coarser particles (greater than 500A) are needed to retard grain growth of austentite.

The final procedure for quenching-and-tempering, specifically for the steels studied in this work, is left to the steel manufacturer / 5 / but two limitations are imposed by MIL-S-16216: the final temperature shall not be less than 593°C for the HY100 and the macrostructure at mid thickness of the plate must contain not less than 80% martensite.

The tempering of martensite at this temperature will trigger the formation of alloy carbonitrides, and the time at the temperature will decide their amount, size, distribution and shape.

2.3 Mechanical/metallurgical properties

The precise Continuous Cooling Transformation (CCT) diagram for the steels HY100 or Q2N is not available. Nevertheless, it is useful to have some idea of its shape, and the diagrams of two similar steels (GY80 and HY130) will give us an approximation. Figure 2.7 (a,b), shows the CCT for HY80 / 29 /, while in Figure 2.8 we can find another one for the HY130 steel, as determined by high speed dilatometry / 30 /. The Ms temperature in both cases is around 370°C and it will stay in this neighbourhood for our steels. Another point of interest is that the 'nose' of the curve is well displaced to the right, due to the alloying, leaving relatively sufficient time for the martensite reaction to occur. This fact is very important if we consider the quenching of thick plates. In Figure 2.7(a) the cooling curves are from a weld thermal cycle having peak temperature of 1315°C (2400°F), 149°C (300°F) preheat in 25.4 mm (1 in) steel plate. The respevtive energy inputs were (as on each curve): 5.8 J/mm (150kJ/in), 3.8kJ/mm (100kJ/in) and 1.9kJ/mm (50kJ/in). Perhaps a better comparison can be made with Figure 2.8 if we look at Figure 2.7b, for the plate thickness is the same and probably the same system was utilized for both tests. Despite the higher alloying of HY130 (but smaller carbon content), for similar cooling rates this steel shows less hardness than the HY80 (see Figures).

The effect of tempering temperature on yield strength, ultimate tensile strength and hardness of ASTMA 543 class 2 is shown in Figure 2.9. / 31 /. The YS and UTS begin to fall around 482°C (900°F), while hardness rises, as a probable consequence of secondary hardening effect.

Hot ductility tests at rapid heating and cooling are available for QT35 and HY80 steels, and as we shall come back to it later (Chapter 4), we just show the results in Figure 2.10 / 32 /. There is a clear difference between both steels related to ductility at high temperature (around 1100°C).

Figure 2.11 shows / 33 / how the time-temperature combination on stress-relieving treatment can cause appreciable decreases in toughness in both HY100 and HY 130 steels.

In Figure 2.12 can be seen the relationships between the Fracture-Appearance Transition Temperature (FATT) at 50% crystallinity, UTS, YS and tempering temperatures. This figure is typical for HY steels and the data were collected by YORKE / 34 /.

Fatigure test yields are of the most concern for designers. Figure 2.13 shows the SN curve for three parent HY steels, while in Figure 2.14 the fatigue test was carried out for three butt welds / 35 /. The weldments on HY80 and HY100 steels were made by manual shielded metal-arc, while those on HY130 by gas metal-arc weld.

The effect of test temperature on the place-strain fracture toughness can be assessed through Figure 2.16 / 36 /, with the ASTM A517 steel being a comparison material.

The corrosion susceptibility of the steels can be shown by Figure 2.16 (a, b, c) / 37 /. The average metal loss (in/1000) in marine environments through the years is quite different for the weldmetal (a), HAZ (b) and parent metal (c).

The susceptibility to stress corrosion cracking (SCC) in the presence of H_2S of these steels is still subject to controversy / 38 /.

The studies of irradiation effects on these steels indicate the care to be taken with impurities and relatively small additions of elements. Figure 2.17 / 39 / shows the effect of test temperature, neutron fluences (as indicated along the lines), and copper content on YS on an ASTM A543 class 1 steel, and its submerged arc (S/A) welds. 'Neutron fluence' is the product of the neutron dose rate and the irradiation time in units of neutron/cm^2. Notice the strong effect of a small difference in copper content.

Still on neutron irradiation, Figure 2.18 / 40 / shows the effect of it on impact strength of type HY80 steel. The displacement to the right of the irradiate samples is clear. A broad picture is given by Figure 2.19 / 41 / where a large number of steels have their transition temperatures increased with irradiation. Notice that the trend is followed by all steels. However, the influence of irradiation on many metallurgical factors such as microstructures, is not perfectly clear, and generalisations must be avoided.

Costs are, of course, a matter of concern in all kinds of societies. For specific use in submarines the problem is critical and, for example, WEEKS / 42 / pointed out that: '(submarines) with the high standard needed, the fabrication price is four times the basic cost of the steel'; and again, in Discussion on Section III of the same Conference: 'the

MoD pays around three times more per ton of steel than a normal buyer'. Clearly this is a direct consequence of the high standard needed.

2.4 Summary

In this introductory chapter we reviewed the development, metallurgy and mechanical/metallurgical properties of High Yield Strength Q & T Steels. The first materials were naturally a product of empirical steel making evolution. Their application, initially directed to submarines only, nowadays, places them among the candidates for nuclear pressure vessels and offshore structures. Thus, to the requirements of High Yield strength, very good notch toughness, stable physical properties in a wide range of temperatures, high modulus of elasticity, low density and good resistance to low-cycle fatigure, there were added good resistance to neutron irradiation embrittlement and stress corrosion cracking in the presence of H_2S.

Due to the relatively low alloying level of these steels, their solidification still follows that described by the carbon-iron equilibrium diagram. However, mainly due to the alloying elements nickel, chromium and manganese, and to impurities like sulphur and phosphorus, there is a real danger of high segregation at the dendrite boundaries.

Through complex steelmaking and rolling practices, the necessary low impurities level and inclusions control are obtained. The final properties are achieved by an elaborate heat treatment, aimed to produce low carbon tempered martensite and a suitable amount of distribution of carbonitrides.

There are available many mechanical/metallurgical properties for this class of steels, like Continuous Cooling Transformation (CCT) diagram, hot brittleness tests, toughness, fatigue, irradiation effects, and so on. However, it is surprising that few of them were made actually on the Q2N steel, and some important ones are missing for the HY100 steel, e.g. CCT diagram.

TABLE 2.1(a) - CHemical Composition and Mechanical Properties Specification for HY 80 Steel Plates (from MIL-S-16216G Ships). / 6 /

Chemical composition

Element	Per cent	
	Not less than	Not more than
Carbon	-	0.18
Manganese	0.10	0.40
Phosphorus	-	0.025
Sulphur	-	0.025
Silicon	0.15	0.35
Nickel	2.00	3.25
Chromium	1.00	1.80
Molybdenum	0.20	0.60
Residual elements		
Titanium	-	0.02
Vanadium	-	0.02
Copper	-	0.25

$S + P < 0.045\%$

Tensile properties

Thickness range mm (in.)	0.2 per cent proof stress, N/mm^2 (tons/in^2)		Elongation on 50mm (2in.) gauge length, %	Reduction in area, %
	Minimum	Maximum	Minimum	Minimum
Less than 16 (0.625)	550 (35.5)	690 (44.5)	19	-
16 (0.625) and over	550 (35.5)	650 (42.5)	20	55 longitudinal 50 transverse

Impact properties

i. Minimum energy absorption in Charpy V notch test

Plate 11.5mm (0.5in.) to 50mm (2.0in.) incl. — 68J (50ft lb) at -84°C; No single specimen < 61J (45ft lb)

Plate over 50mm (2.0in.) — 41J (30ft lb) at -84°C; No single specimen < 34J (25ft lb)

TABLE 2.1(b) - Chemical Composition and Mechanical Properties Specification foe Navy Q1 Steel Plates (from DG. Ships 70.Jan, 1968). / 6 /.

Chemical composition

Element	Per cent	
	Not less than	Not more than
Carbon	-	0.18
Manganese	0.10	0.40
Phosphorus	-	0.015
Sulphur	-	0.015
Silicon	0.15	0.35
Nickel	2.25	3.25
Chromium	1.00	1.80
Molybdenum	0.20	0.60
Residual elements		
Titanium	-	0.02
Vanadium	-	0.02
Copper	-	0.20
Arsenic	-	0.03
Antimony	-	0.005
Lead	-	0.002
Nitrogen	-	0.010
Tin	-	0.02

$S + P < 0.025\%$

Tensile properties

Thickness range mm (in.)	0.2 per cent proof stress, N/mm^2 (tons/in^2)		Elongation on 50mm (2in.) gauge length, %	Reduction in area, %
	Minimum	Maximum	Minimum	Minimum
Less than 16 (0.625)	550 (35.5)	690 (44.5)	20	-
16 (0.625) and over	550 (35.5)	650 (42.5)	20	55 longitudinal 50 transverse

$\frac{0.2\% \text{ proof stress}}{\text{tensile strength}} < 0.88$

Impact properties

i Minimum energy absorption in Charpy V notch test

Plate up to 57mm (2.25in.) incl. — 102J (75ft lb) at -84°C; No single specimen < 88J (65ft lb)

Plate over 57mm (2.25in.) — 68J (50ft lb) at -84°C; No single specimen < 54J (40ft lb)

ii Crystallinity < 50%

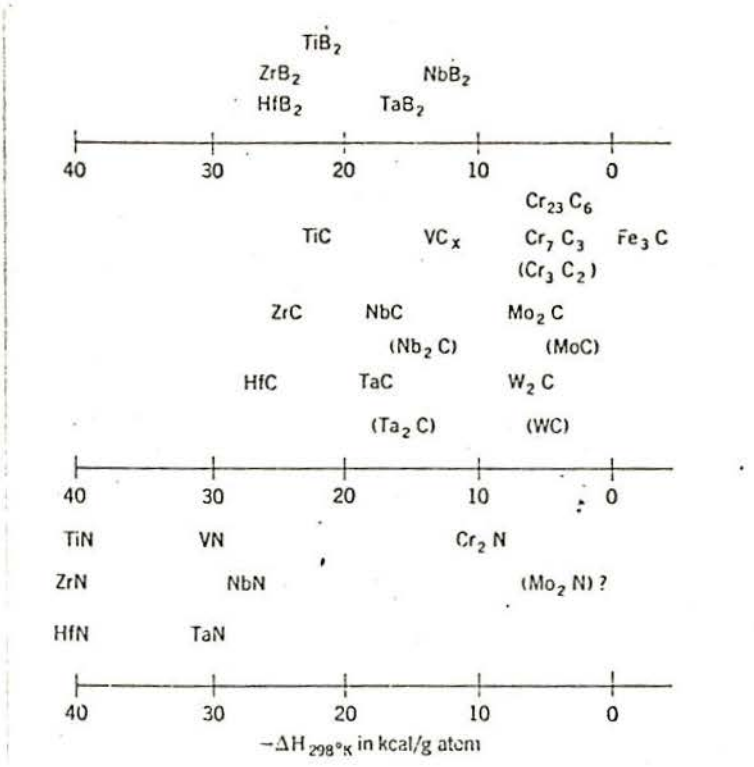

Figure 2.1 - Enthalpies of Formation of Carbides, Nitrides and Borides / 28 /

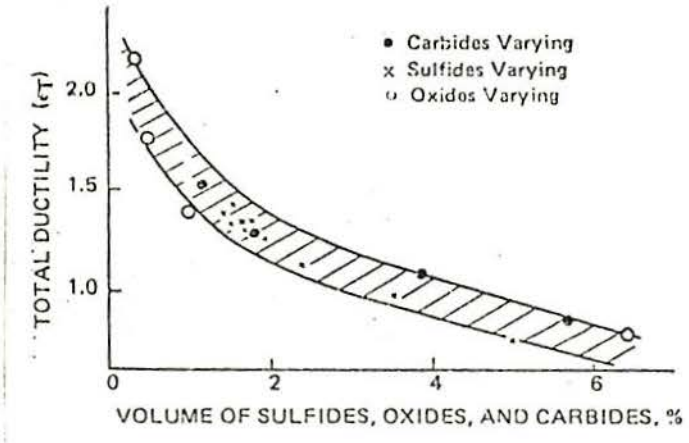

Figure 2.2 - Effect of Second-Phase Particles on Total Ductility / 13 /

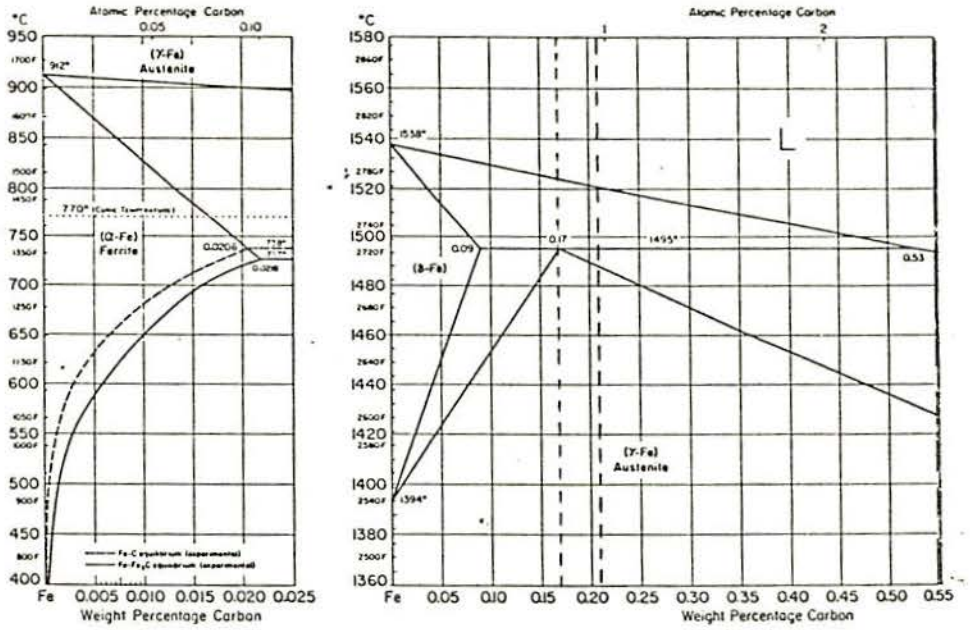

Figure 2.3 - Iron - Carbon Equilibrium Diagram / 22 /

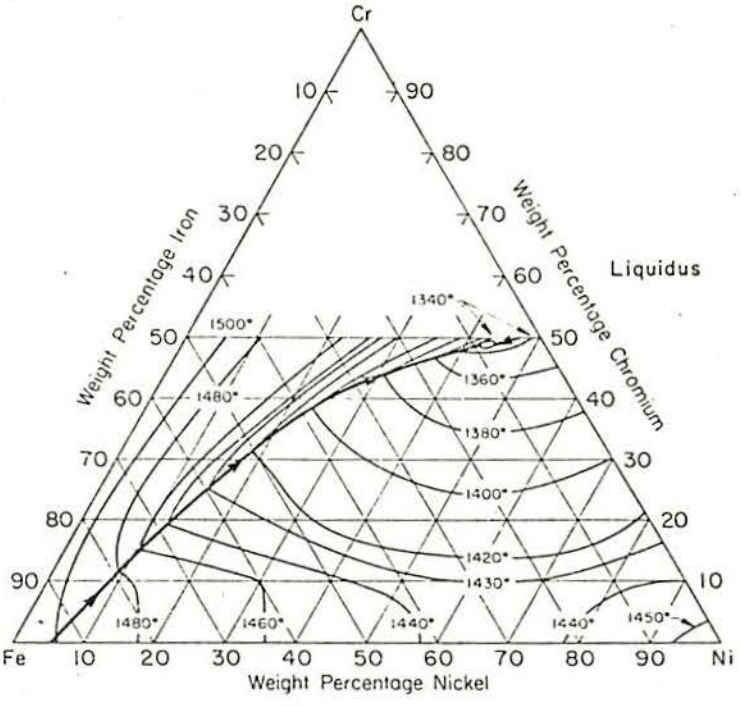

Figure 2.4 - Liquidus Projection for the Cr-Fe-Ni System / 22 /

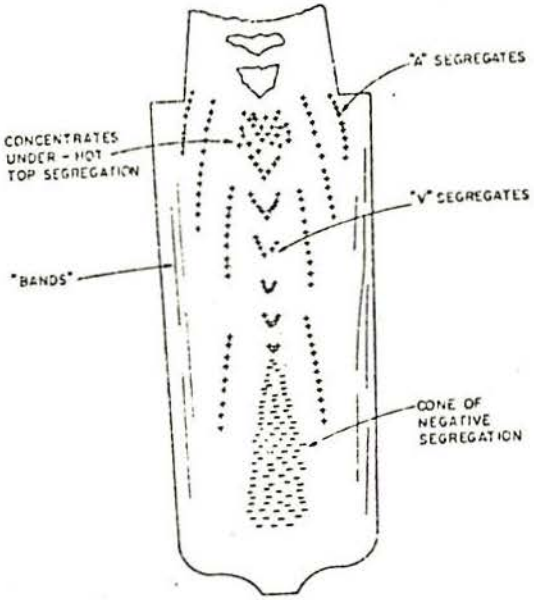

Figure 2.5 - Sketch of Macrosegregation in Large Steel Ingots + Denotes Positive Segregation, - Denotes Negative Segregation. "Bands" Usually involve both Positive and Negative Zones / 24 /

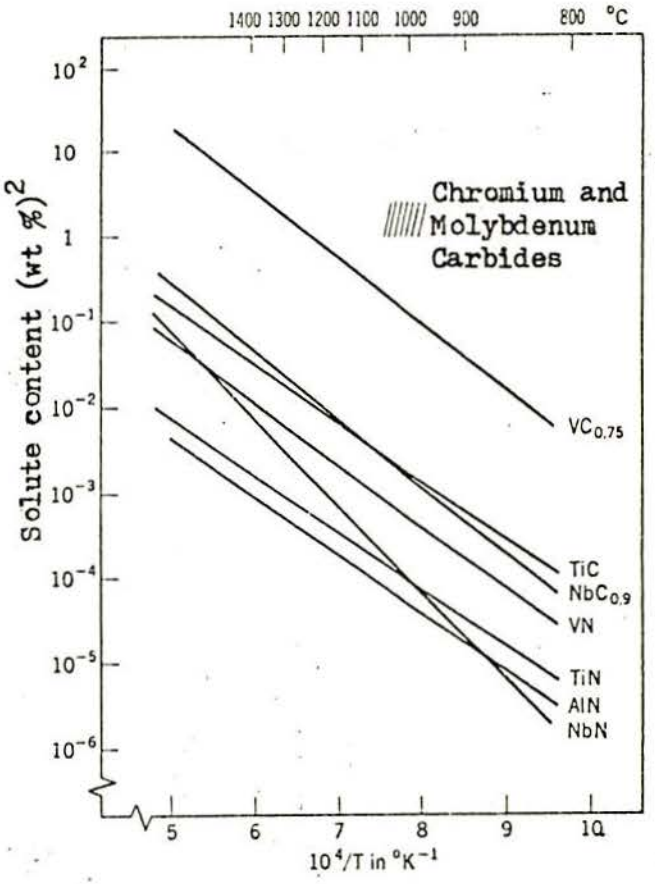

Figure 2.6 -Solubility in $(wt\%)^2$ of Carbides and Nitrides in Austenite as a Function of Temperature / 28 /

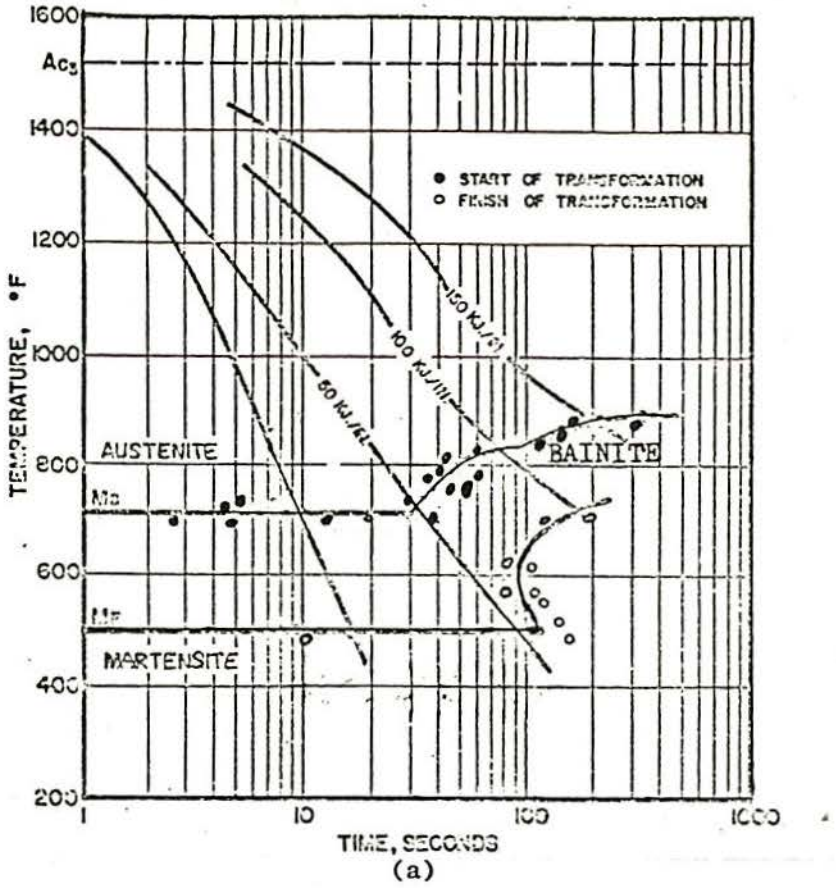

(a)

HY 80-38mm ($1\frac{1}{2}$ in.)

GRAIN SIZE AS RECEIVED (ASTM)														
C	Mn	Si	S	P	Ni	Cr	Mo	V						
0·19	0·28	0·14	0·019	0·008	2·81	1·35	0·44	0·01						

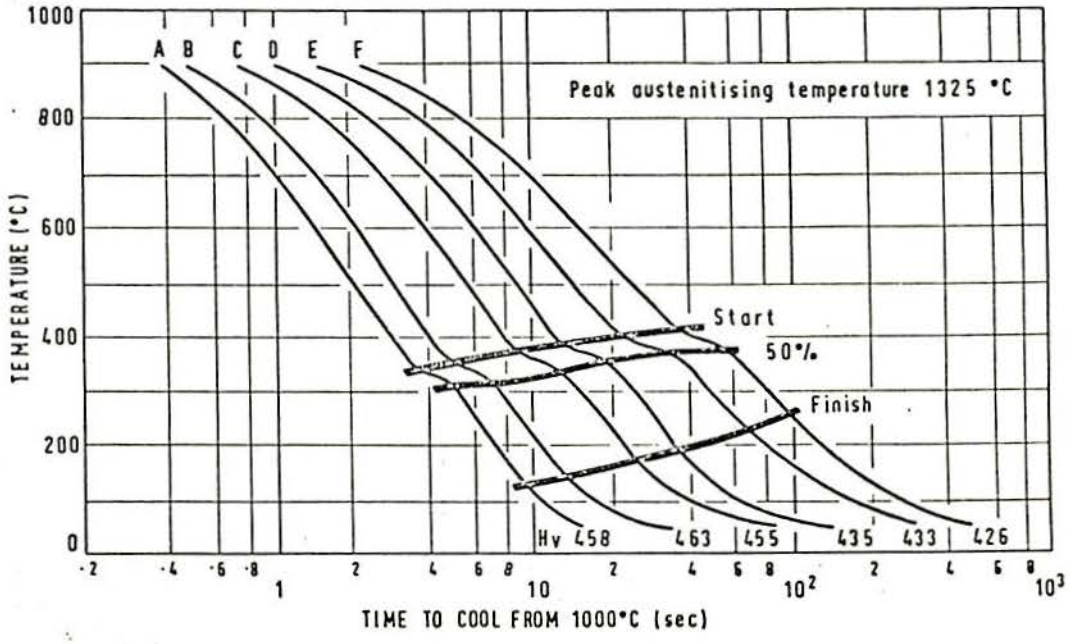

(b)

Figure 2.7 (a,b) - CCT Diagrams for HY80 Steel / 29,6 /

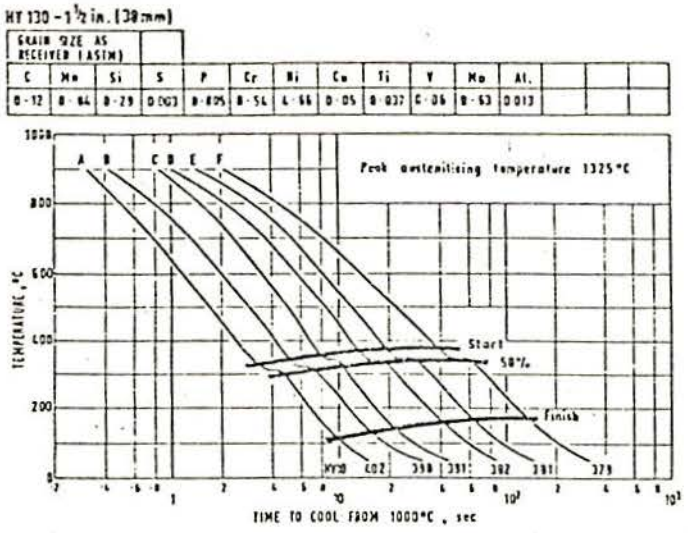

Figure 2.8 - CCT Diagram for HY130 Steel /30/

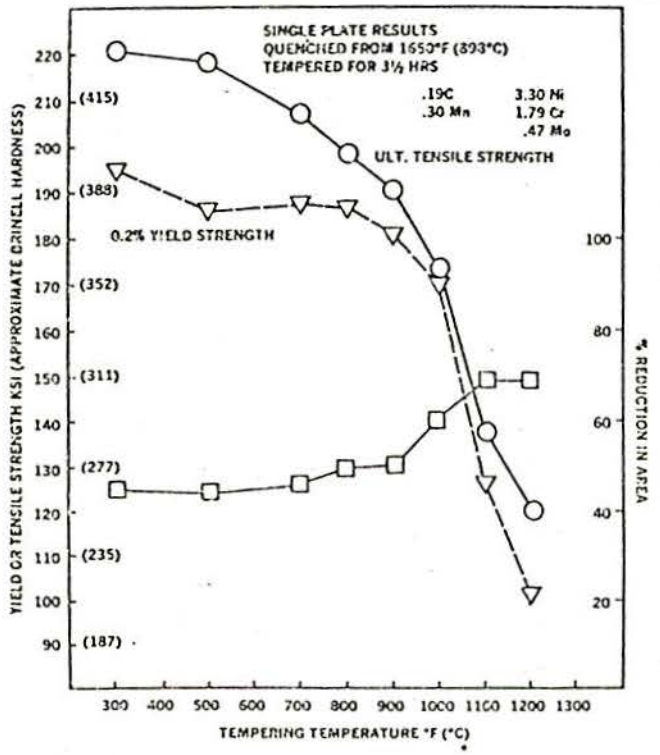

Figure 2.9 - Effect of Tempering Temperature on Properties of 88.9mm thick ASTM A543 Plate / 31 /

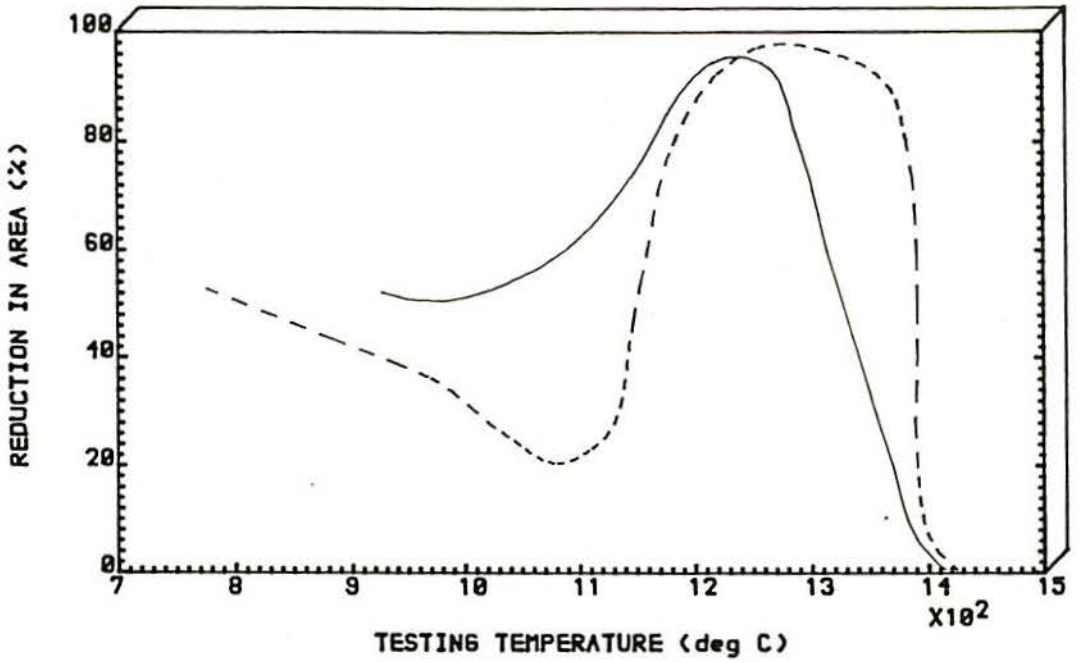

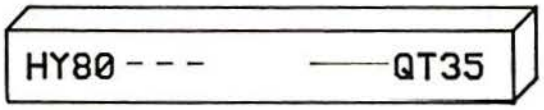

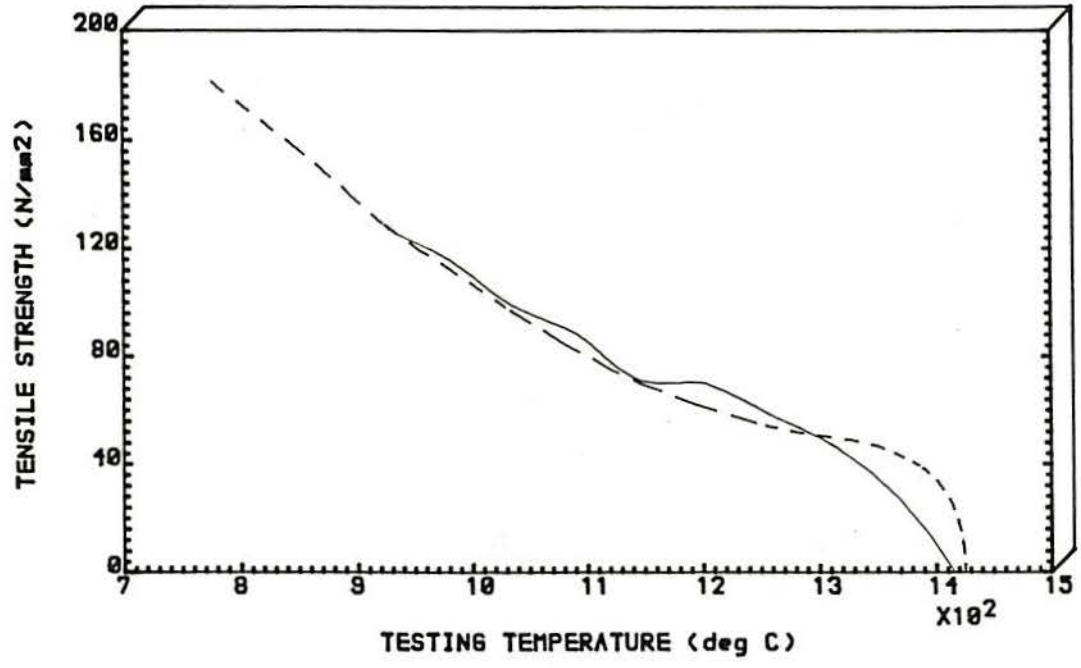

FIGURE 2.10 - REPLOTTING OF 'HOT BRITTLENESS' DATA FROM REF./ 32/. SPECIMENS BROKEN ON COOLING FROM 1414 deg C (STEEL QT35) AND 1422 deg C (STEEL HY80)

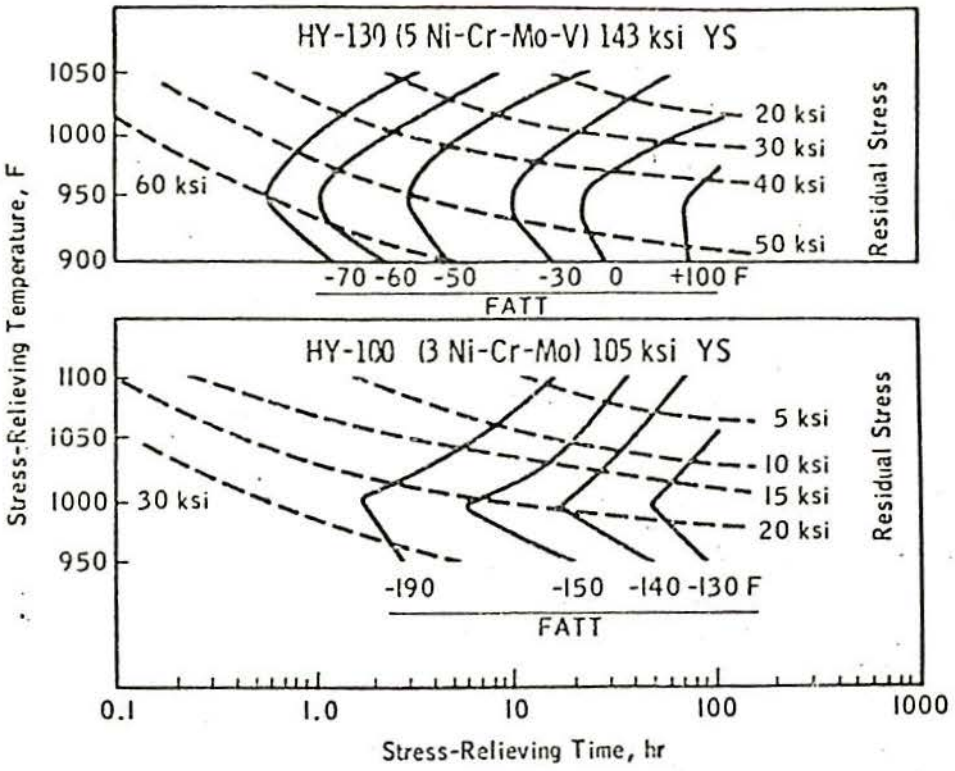

Figure 2.11 - Decreases in the Toughness of HY130 and HY100 Steels Caused by Stress-Relieving Treatment. FATT is the Fracture-Appearance Transition Temperature at 50% Crystallinity / 33 /

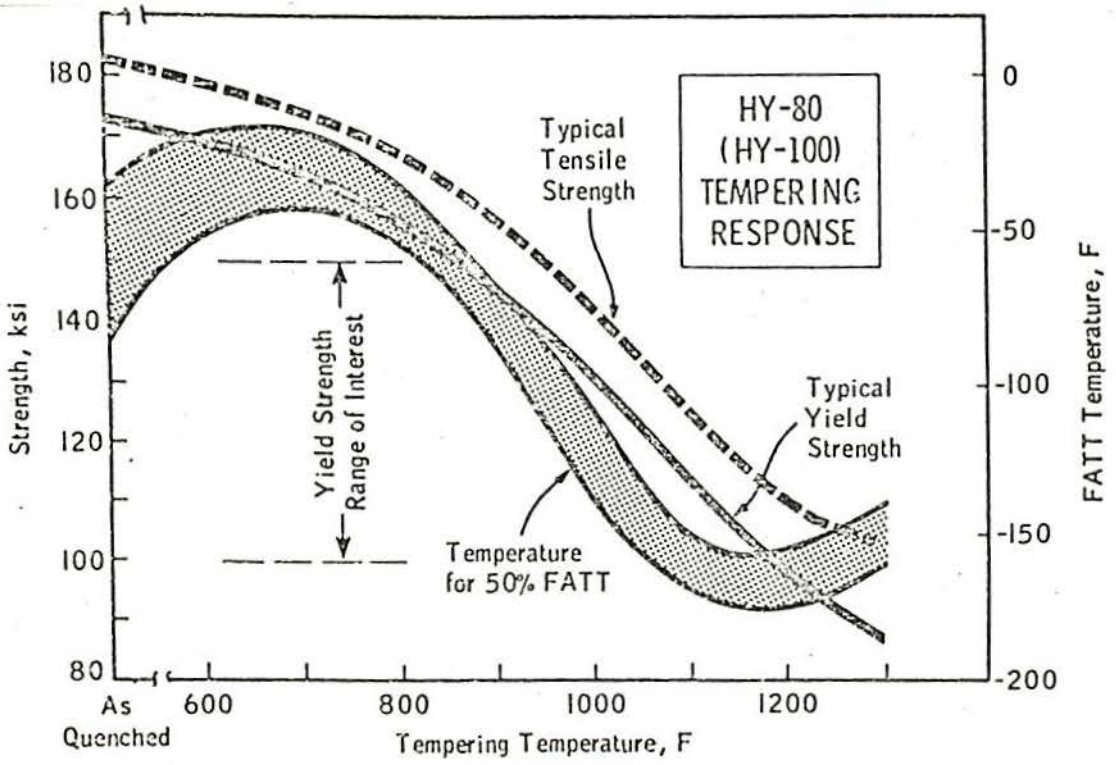

Figure 2.12 - Relationship Among FATT, UTS, YS and Tempering Temperature. This behaviour is typical for HY Steels in general / 34 /

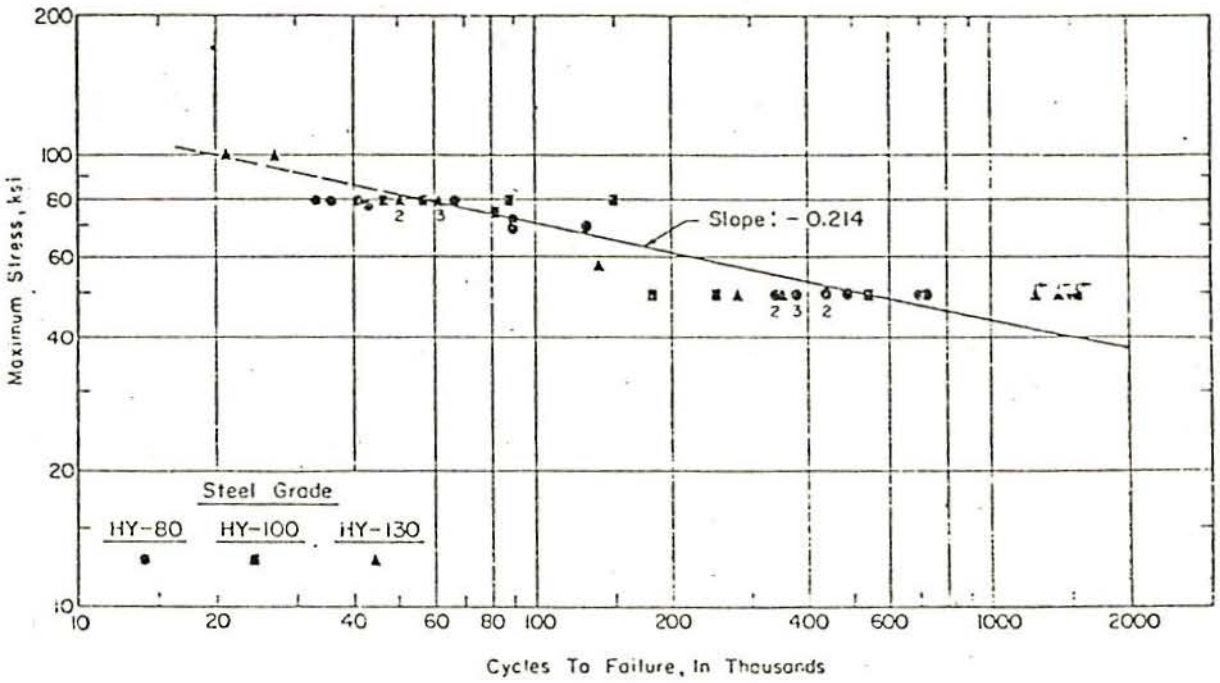

Figure 2.13 - Fatigue test data and S-N Curve for Plain Plate Speciments with mill-scale intact. Numbers adjacent to the data points indicate the failure of two or more specimens of one steel at approximately the same lines / 35 /

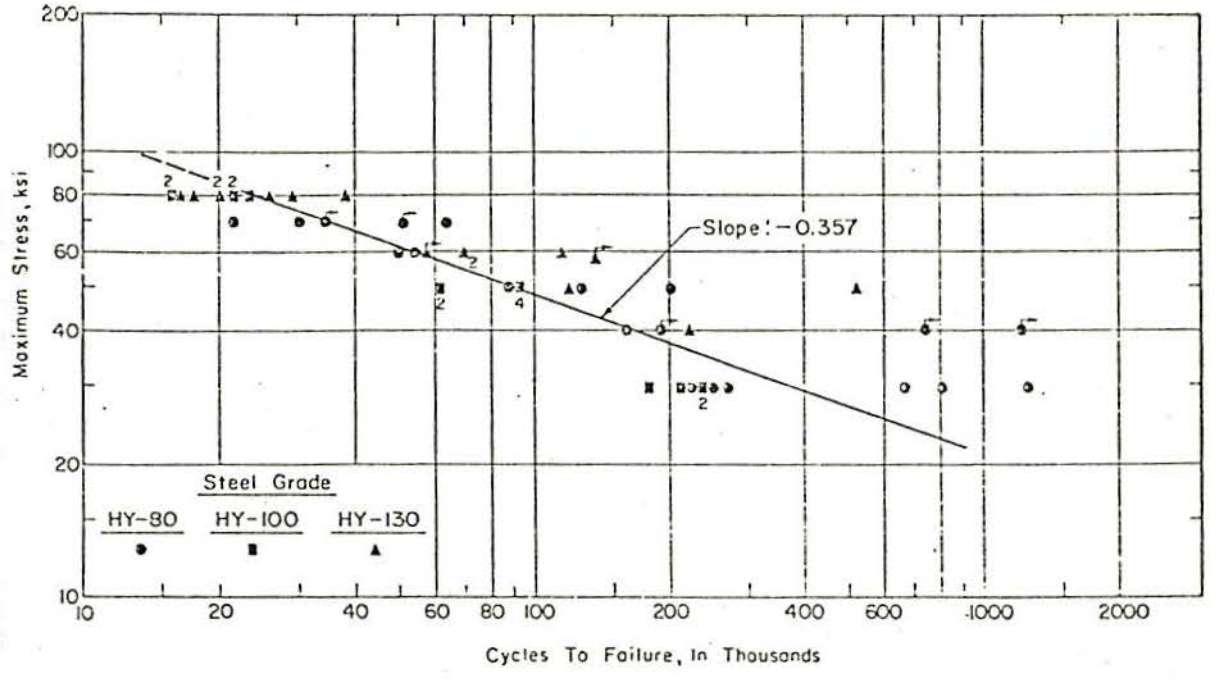

Figure 2.14 - Fatigue test data and S-N Curve for Butt Welds (as-welded) Exhibiting Crack initiation at the toe of the Weld. Arrows indicate specimens in which failure initiate at some other location / 35 /

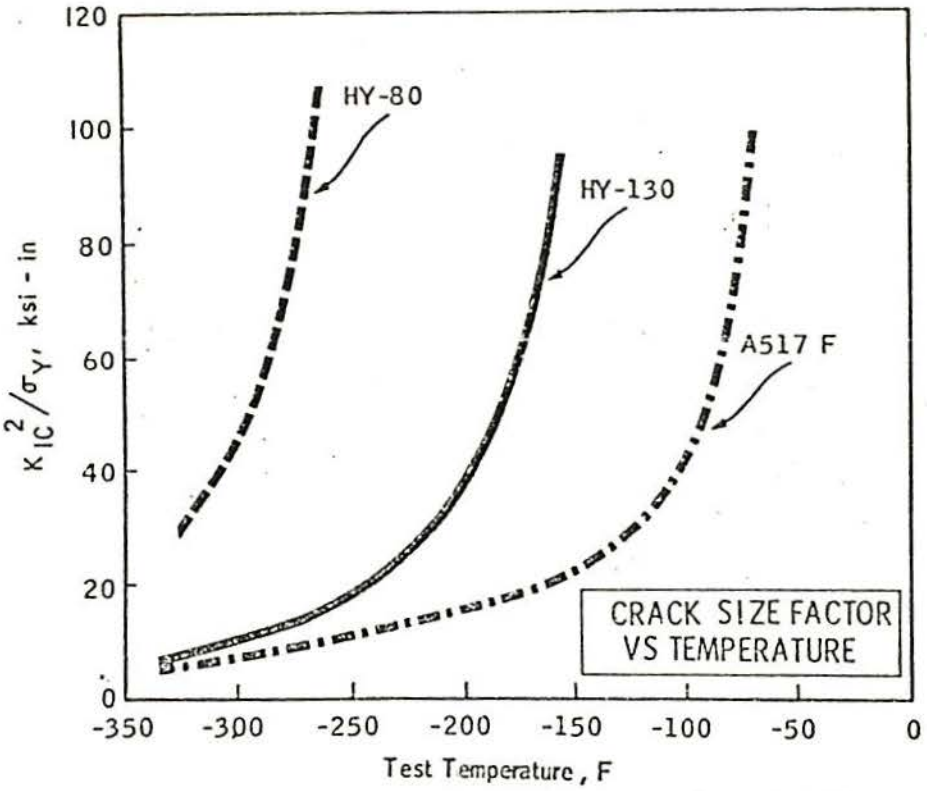

Figure 2.15 - Effect of Test Temperature on the Plane - Strain Fracture Toughness of HY80, HY130 and ASTM A 517F Steels/ 36 /

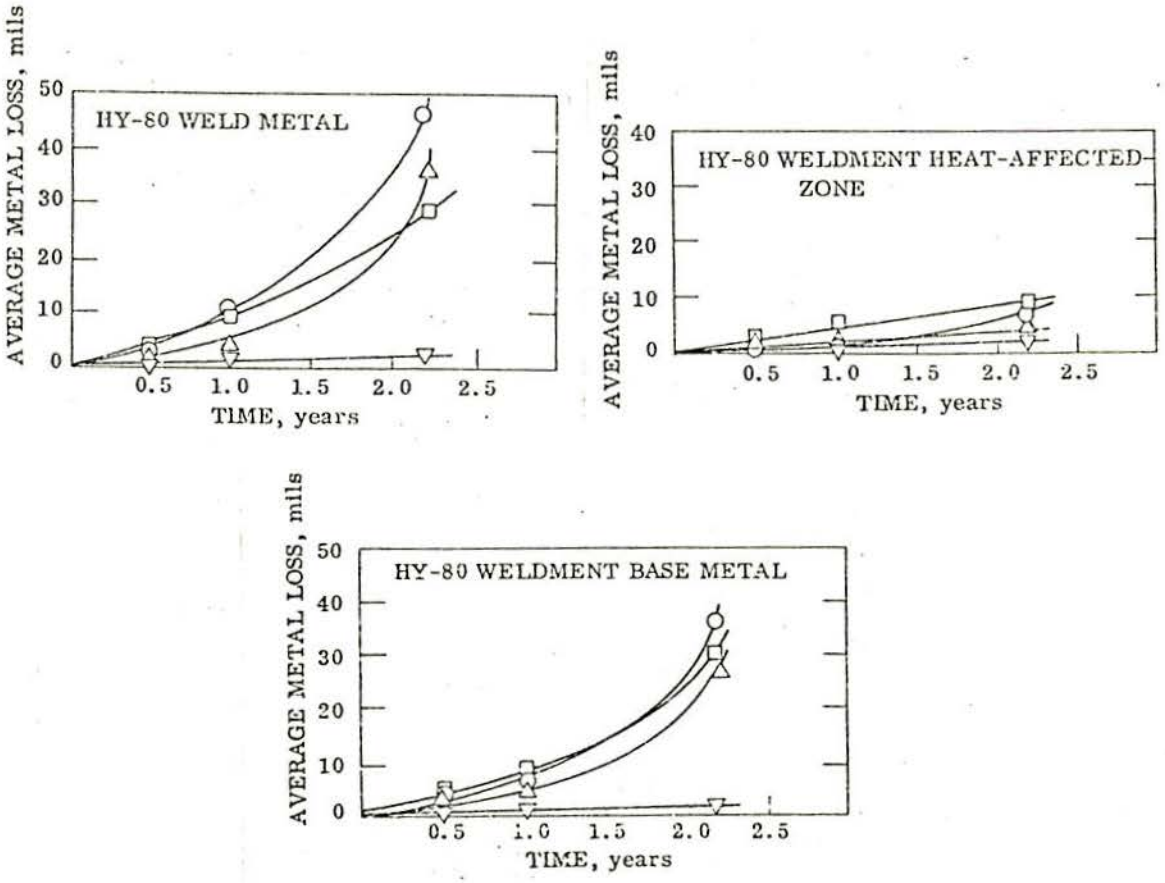

Figure 2.16 - Average Loss of Material in Marine Environment, for Weld Metal (a), HAZ (b), Parent Steel (c) / 37 /

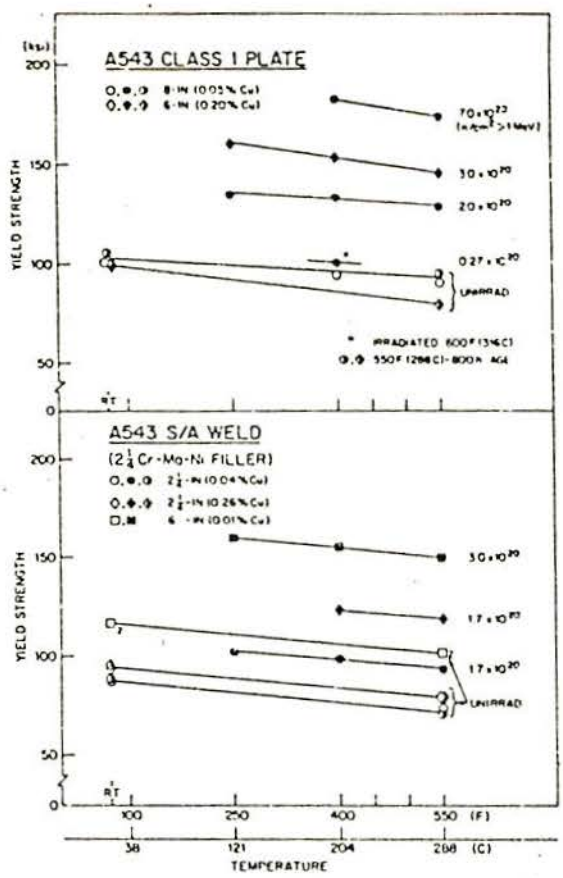

Figure 2.17 - Effect of Neutron Fluence (288°C or 550°F) as indicated along the lines, and different Copper content on YS of an ASTM A543 class 1 Steel and its Submerged Arc Weldment. A 600°F (316°C) Irradiation for one Plate is also shown / 39 /

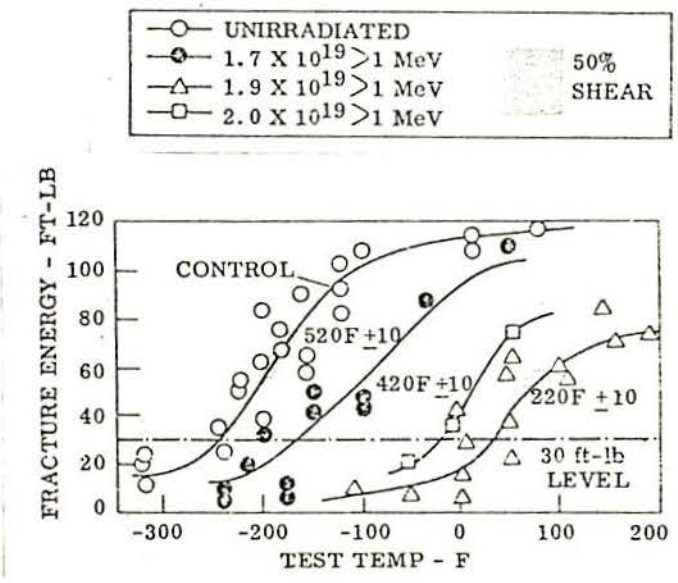

Figure 2.18 - Effect of Irradiation on Impact Strength of HY80 Steel / 40 /

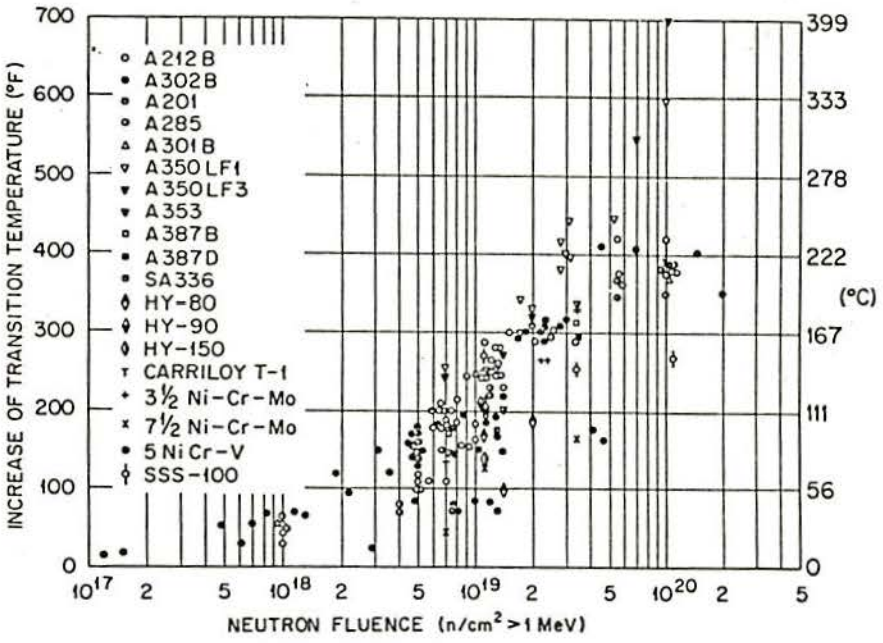

Figure 2.19 - Relationship between the Neutron Fluence at less than 260°C and Charpy - V Notch Transition Temperature / 41 /

3. WELD METAL SOLIDIFICATION PRINCIPLES

3.1 Introduction

The understanding of weld metal solidification mechanisms is of fundamental importance, not only for the scientist interested on welding, but for the practising engineer as well. At this stage of its existence many weld metal properties are decided, some of them irreversibly.

In spite of much effort developed by groups all around the world in the last twenty years or so, up to this date there is neither a completely finished theory about the subject nor are some very basic principles universally accepted. This reflects the problem's complexity and inherent difficulties involves in its 'in situ' observation.

Also, it can be due to the fact that, even nowadays, it is not broadly recognised that it would be much more profitable to the understanding of weld solidification if it is seen as a particular case of the general solidification process. Thus there is a departure from general 'laws' to much more limited ones. Throughout this process perhaps the establishment of boundaries is the largest problem.

Firstly, all general solidification theory principles are applied to the weld metal. Certainly, there will be a number of them which are not suitable for some cases. Together with those principles which proved to be useful, the boundary demarcation is done.

This process of boundary demarcation is still going on, and depends on the number of experiments being made worldwide to test them.

The relevance of the solidification mechanism to weld metal solidification cracking is very great. Any alloy has a solidification temperature range and each solute exhibits different solubilities in the liquid and solid phases. As the cooling through this solidification range proceeds, the solute rejects into the liquid forming an enriched solute layer resulting in microsegregation. Depending on shape, amount and type of the segregated solute and the stress magnitude acting at that layer, the result can be solidification cracking (Chapter 4).

3.2 General solidification theory

3.2.1 Solute segregation: fundamentals

The general solidification theory really advanced during the 1950s due to TILLER and co-workers /43 - 46 / and CHALMERS, summarised in his book / 23 /. Thus, the following lines are based on these works, excluding situations of obvious no relevance for the welding condition.

Consider a crucible with a liquid binary alloy freezing from one end and the solid growing with a plane front of solidification, as shown in Figure 3.1 (a), and its schematic phase diagram in Figure 3.1 (b).

It is convenient to relate the liquidus and solidus concentration at a given temperature by an average distribution coefficient K for an alloy of solute composition C_o. Thus

$$K = C_S/C_L \qquad \text{(Eq.3.1)}$$

where

C_s = equilibrium concentration of the solid phase

C_L = equilibrium concentration of the liquid phase

At any specific temperature, an equilibrium distribution coefficient is defined as K_o for that temperature.

Figure 3.1 (b) shows a phase diagram with $K<1$, or for alloys in which the solute solubility in the solid is less than in the liquid. If $K>1$ the contrary happens, or the solute solubility in the liquid is less than in the solid. The reasoning, however, is the same for both cases.

In most cases of practical solidification the diffusion is limited in the liquid and there is no convection.. Furthermore, as a purely mathematical simplification, K is taken as constant / 43 /.

The initial material to solidify has a composition KC_o and the solute rejected into the liquid by diffusion forms an enriched boundary layer. In general (and this is also valid for welding), the rate of advance of the planar solid-liquid interface is faster than the rate of diffusion in the liquid, and there is not sufficient time for the solute to distribute throughout the remainder of the liquid. Therefore, this boundary layer gradually increases in solute until a steady state solute distribution is reached, as shown in Figure 3.1 (c). TILLER et al / 43, 44 / have shown that the solute concentration in the liquid (C_L) falls off from C_o/k, and at a distance X from the interface into the liquid it is:

$$C_L = C_o' \{1 + \frac{1-K}{K} \text{EXP} \ (-XR/D) \} \qquad \text{(Eq. 3.2)}$$

where

R = rate of interface movement (assumed to be constant)

D = diffusion coefficient for the solute in the melt

At relative large values of X the liquid concentration equals C_o. Furthermore, the ratio D/RK is considered a 'characteristics distance', for it is the distance at which the quantity $(C_L - C_o)$ falls to 1/e of the maximum $(C_o/K - C_o)$, where 'e' is the exponential value.

The initial transient, as shown in Figure 3.1 (d) is obtained / 44 / by

$$C_S(X) = \frac{C_o'}{2} \{ 1 + \text{ERF} \left((XR/D)^{\frac{1}{2}}/2 \right) + (2K-1)\text{EXP}\left(-K(1-K)(XR/D)\right) \ \text{ERF} \left(\frac{2K-1}{2} (XR/D)^{\frac{1}{2}} \right) \} \qquad \text{(Eq.3.3(a))}$$

This equation can be approximated to:

$$C_S = C_o' \{ 1-(1-K)\text{EXP}(-KXR/D) \} \qquad \text{(Eq.3.3(b))}$$

with a maximum error of about 20% / 44 /.

For small K values a characteristic distance for the length of this transient state is (1-1/e) of its maximum, or 67% of its steady state value / 25 /.

The terminal solidification transient can be seen in Figure 3.1 (d). The solute concentration increases continuously from C_o to the maximum, through

$$C_S = C_o \{1 + 3\left(\frac{1-K}{1+K}\right)EXP(-2XR/D) + \frac{5(1-K)(2-K)}{(1+K)(2+K)} EXP(-6XR/D) + \ldots\ldots$$

$$(2n-1)\frac{(1-K)(2-K)\ldots(n-K)}{(1+K)(2+K)\ldots(n+K)}EXP(-n(n+1)(XR/D)\} + \ldots\ldots \qquad \text{(Eq.3.4)}$$

The general importance of this solute build-up must be well understood. The average value for the elements diffusion coefficient (D) in liquid iron is 5×10^{-3} mm^2/s / 23 /. For a typical value of K=0.1 in iron (see / 46 /), and considering a growth rate r = 10^{-1} mm/s, the initial solidification transient distance will be given by

$$X = D/KR = 0.5 \text{ mm}$$

and the concentration at the interface will be 10 times the initial one.

Another case of interest is that in which a sudden change in the solidification rate (R) occurs. It was demonstrated / 44 / that there will exist a transient rise in the liquid concentration near the interface. Thus, after the solidification has been completed the solid will show this solute-rich band.

3.2.2 Constitutional supercooling

In the previous discussion we have seen that a solute-rich boundary layer forms in front of a planar interface. CHALMERS and associates / 23, 43 / demonstrated how this solute build-up could lead to instability of this plane front.

Equation 3.2 describes the liquid composition of an alloy. Thus, every point in the liquid ahead of the interface has a definite liquidus temperature as given by the equilibrium diagram of Figure 3.1 (b). As TILLER / 46 / says: "this is the temperature at which the liquid would like to freeze". The actual temperature distribution is largely determined, however, by the temperature gradient. Figure 3.2 (a) shows the solute enriched layer in front of the interface and Figure 3.2 (b) the 'actual' and 'equilibrium' liquidus temperature. Thus, the liquid at temperatures below the liquidus is said to be 'constitutionally supercooled'.

The local variation in the liquid temperature ahead of the interface due to this solute segregation is given by:

$$m_L (C_L - C_o) = T_L - T_S = m_L \frac{C_o(1-K)}{K} EXP(-XR/D) \qquad \text{(Eq.3.5)}$$

where

m_L = slope of the liquidus line

T_L = melting temperature of the solvent

If the actual temperature gradient in the liquid is given by G_1 (or dT_L/dX at X=0), then the planar interface will stable if:

$$\frac{G_L}{R} \geq \frac{-m_L C_o (1-K)}{DK} = -\frac{\Delta T}{D} \qquad \text{(Eq.3.6)}$$

where ΔT is the melting range at the composition C_o.

In other words, when G_L is less than dT_1/dX at X=0, then the melt temperature locally falls below the freezing temperatures (for some composition) and nucleation of solid occurs in the liquid ahead of the interface.

As the extent of constitutional supercooling increases and the G_L/R ratio deviates from the critical value of equation 3.6, different solidification structures form, viz: cellular, cellular-dendritic, dendritic and equiaxed, which we shall discuss in the next section, related specifically to welding process.

To maintain coherence, we should now describe mathematically each one of the above solidification structures. However, there are not, up to this date, rigorous theories describing their evolution.

It is of much more interest to understand that, in general, the extent of constitutional supercooling for a given alloy depends upon the temperature gradient in the liquid G, and the growth rate R, as Figure 3.3 shows. This figure permits the analysis of four situations, as regards these two factors. Thus, considering initially G_1 and R_1, there is practically no constitutional supercooling. If the growth rate increased to R_2 (and G_1 is maintained), the extent of this phenomenon is very large, as well as the possibility to have one of the structures above quoted. On the other hand, increasing the temperature gradient to G_2 (now maintaining R_1) leads to a plane interface. Now, let us consider G_2 and R_2, a combination which shows some constitutional supercooling. Decreasing the temperature gradient to G_1 (keeping R_2 constant) only increases it, while maintaining G_2 and decreasing the growth rate to R_1 makes possible to have again, a planar interface.

3.2.3 Microsegregation and chemical reaction effects

Microsegregation in the liquid ahead of the solidification front brings about many effects. We have to bear in mind that all elements with distribution coefficient (K) less than one have their solute solubility in the solid less than in the liquid, and the coefficient value determines the amount segregated. Also, reactions may occur and the actual amount of some segregated elements will not have the expected value.

Some of these effects have been investigated and the following lines illustrated this point.

Comparing the effectiveness of Mn, Ti or Zr to form more stable sulphides than FeS, TILLER / 46 / pointed out the importance of the segregation level for the same initial concentrations. For in spite of the fact that Ti or Zr might form more stable sulphides than Mn, the latter segregates about 10 times more at the grain boundary than the former. Thus, Mn acts much more effectively for a same initial concentration

in the melt and this is related to its much smaller distribution coefficient K. As regards the important relationship between the amounts of Mn and S, in Chapter 4 (Section 4.3.1) we will see a theory which modifies the wellknown Mn/S ratio, based on their different distribution coefficient and other considerations on solidification principles.

A very important point related to the deoxidation reactions effects on microsegregation was first introduced by TURKDOGAN / 47 /. As there is a strong interaction between dissolved oxygen and impurities in liquid steel, reactions of the deoxidation type were considered. Based on normal solidification theories, this author plotted the solute enrichment of C, Mn, Si and O in iron, supposing no reactions between them. As expected, there is an overall build-up of all elements as solidification proceeds. However, as reactions between these elements with oxygen are considered, the final level of this latter element will be much less than that expected. Furthermore, practical evidence suggests that these reactions really happen.

Finally, carbides also will be affected by the solidification conditions. The relative stability of the various carbides given by their free energies of formation are not enough to understand their behaviour, as shown by BHAMBRI et al / 48 / and FERNANDEZ et al / 49 /, for example. These authors, among other facts, have shown that some carbides do not melt or are segregated at slower growth rates than other solutes. The importance of these studies, we think, does not need to be overemphasised, for some aspects were seen in Chapter 2 and others will be seen in the next Chapter.

3.3 Weld solidification

3.3.1 Weld pool: growth and geometry

The process of nucleation and growth, normally experienced in castings, is not usually significant in welds (see below) and therefore, will not be discussed here.

The growth mechanism of the solid weld metal occurs by a perfect or near-perfect wetting, depending upon some chemical/metallurgical aspects of the metals involved. Furthermore, liquid metal solidifies from the solid substrate provided by the base metal, and the grains generated in the weld metal are continuous across the fusion boundary. So,at this stage of solidification, there is no grain boundary between a grain in the weld metal and the corresponding grain in the base metal.

Despite the existence of such a solidifcation process in welds being known for some time, as can be seen in the important work of GLADSHTEIN / 50 / and other authors / 51 - 54 /, it was SAVAGE and associates / 55, 56 / who first explained the existence of an 'epitaxial' growth on the base metal, generating grains in the weld metal having the same crystallographic orientation as the grains in the (partially) unmelted base metal. Each crystalline structure exhibits a characteristic preferred growth direction, being <100> in bcc and fcc metals. These phenomena were fully confirmed through careful X-ray analysis by, among others, MATSUDA et al / 57 / and SENDA et al / 58 /, for the most diverse ferrous and non-ferrous metals.

On average, the solid growth rate R at the trailing boundary of a weld pool tends to grow into the moving pool (speed V) through the following relationship due to TERRY and TYLER / 59 /:

$$R = V \sin \theta$$

where θ = angle between the tangent to the solidus isotherm at this point and the line of welding. So far, only one review on this subject of weld solidification was published in Britain / 60, 61 /. Surprisingly, it ignores the credit that must be given to the work of TERRY and TYLER and quotes more recent papers.

Most researchers, however, prefer to define θ as the angle between the normal to the tangent to the pool at the point considered and the welding direction. This gives the same relationship in another form:

$$R = V \cos \theta \qquad \text{(Eq. 3.7)}$$

Thus, the growth of any grain in the weld pool occurs parallel to the preferred growth direction with the greated resolved component of the temperature gradient in the liquid.

In Figure 3.4 is shown schematially two weld pools, with the arrows perpendicular to the trailing edge representing the direction of the maximum temperature gradient at various points along the advancing solid-liquid interface. The different shape reflects the welding speed effect, for in the elliptical pool (Figure 3.4(b), the maximum growth rate occurs at the centreline ($\theta = 0^{\circ}$) and thus corresponds to the welding speed value. However, the maximum rate of latent heat liberation and the minimum rate of heat transfer occurs simultaneously at this location. Therefore, to hold this heat balance at higher (critical) welding speeds, the shape of the pool must change to a tear drop (Figure 3.4 (a)) because the angle θ assumes a minimum compatible value greater than 0°. In the elliptical shaped pool (Figure 3.1.(b)) the direction of the maximum temperature gradient changes continually along the trailing edge. Therefore, there is a continuous competition among the grains, because at one time one has its preferred growth direction aligned with the maximum temperature gradient, and at another time another grain has it. On the other hand, the tear drop shaped pool (Figure 3.4 (a))does not show as intense a competition, because the orientation of the maximum temperature gradient changes by much less.

The crystallographic effect on the growth rate was quantified (NAKAGAWA et al. Journal of the Jap. Weld. Soc. 39, 94, 1970) as quoted by GARLAND / 60 /, and the formula 3.7 is modified:

$$R = V \cos \theta / \cos (\theta' - \theta) \qquad \text{(Eq.3.8)}$$

where θ' is the angle between the welding direction and the direction of preferential crystallographic growth.

Note that the tear drop shaped weld pool induces the grains to converge along the weld centreline. Thus, the tendency for entrapment of low-melting point solute-enriched liquid between the solidus-liquidus interfaces is highlighted. Also there are special conditions where the epitaxial growth does not take place, as LOPER and GREGORY / 62 / have shown welding aluminium. They quote three factors favouring non-epitaxial

growth of essentially single crystals: fine heat-affected zone grain size; high welding speed (such as 850 mm/s); small weld bead size (around 1 mm diameter). As we can see these are conditions completely alien to the normal welding practice.

The spatial weld pool shape has been theoretically studied mainly by PROKHOROV / 63 - 65 / based on RYKALIN's theory of heat propagation during welding / 66 /. The important fact pointed out by these studies is that they recognise, for the first time as far as we know, the role played by the pool geometry. It alters the general form of the equations for the heat conduction, which have to adjust themselves to different weld pool shapes. In Figure 3.5 a schematic three-dimensional weld pool is seen / 63 /. For butt welding, the length OM of the cooling region in the pool is given by:

$$OM = \frac{1}{m} \quad \frac{Q^2}{\lambda c \gamma V \delta^2 T} \qquad \text{(Eq.3.9)}$$

and the half-width

$$ON = \frac{1}{n} \quad \frac{Q}{Vc \gamma \delta T} \qquad \text{(Eq.3.10)}$$

where

m and n are coefficients of proportionality (dependent of material and Q/V)

Q = power input (voltage x current)

V = welding speed

λ = coefficient of thermal conductivity

γ = material density

c = specific heat

δ = plate thickness

T = melt temperature

In this model the energy source is in O, and the weld pool is being heated ahead and cooled behind NN', respectively.

Another very important research on weld pool solidification and shape has been carried out through many years by ISHIZAKI / 67 - 69 /. This author departs from different premises, considering interfacial tensions acting along the various interfaces in the pool. He demonstrated that despite the Young's equation being correct for a liquid drop on a surface, it is wrong for a welding pool, for the contact line of molten metal is supposed always to coincide with the solid edge line intersecting the solid. This is not, obviously, the welding case. Instead, he was able to correlate a solidification angle Φ and the liquid phase angle θ with the interfacial tensions γ, γ_s, γ_i as can be seen in Figure 3.6 through the following equation:

$$\gamma_s \cos \Phi = \gamma \cos \theta + \gamma_i \qquad \text{(Eq.3.11)}$$

So, ISHIZAKI / 69 / explains that the meaning of this equation is: 'the contact line recedes at great velocity, comparable to the speed of heat vibration of atoms, so as to make the solidification angle zero with the progress of solidification, when the liquid phase angle, θ, comes close to θ_s' where θ_s is the characteristic value of θ when Φ is zero.

3.3.2 Mechanisms and modes of solidification

There are many differences between the casting and welding solidification processes. Firstly, as already mentioned, nucleation is different, for in castings it often occurs through heterogeneous means, while in welds it is epitaxial (see Section 3.3.1). Also in welds the relationship of the temperature gradient G and the growth rate R stands in contrast to normal castings, for maximal growth rates occur in the weld centreline where minimal temperature gradients are encountered and vice versa at the fusion boundary. The temperature gradients in welds are high and in large submerged arc weld pools they can change from 110°C/mm at the fusion zone to 20°C/mm at weld centreline / 70 /. Moreover, in welds there is the stirring due to the electromagnetic Lorentz forces / 71, 72 /.

Primarily due to the intense pool turbulence there is a stagnant layer in the liquid at the advancing solid-liquid interface. Thus, within this stagnant layer it is possible to consider the (three) stages in solidification referred to in Section 3.2.1 (see equations 3.2 to 3.4). There is, therefore, a 'microscopic equilibrium' as SAVAGE / 73 / called it, being possible to estimate the distances that the solid-liquid interface moves during the initial and steady state periods. These are 'characteristics' distances, as mentioned previously in Section 3.2.1 At the initial transient period

$$X_c \tilde{=} C\,(D/KR) \qquad \text{(Eq. 3.12)}$$

and in the steady state

$$X_d \tilde{=} C\,(D/R) \qquad \text{(Eq. 3.13)}$$

where C is a constant. At about C=5 the composition of the solid approaches to within 1% of C_o.

Thus, after this point the terminal stage begins, with an increasing solute build-up in front of the solid-liquid interface.

As we have seen (Eq.3.7);

$$R = V \cos \theta$$

Thus, from equations 3.12 and 3.13 respectively,

$$X_c \tilde{=} 5\,D/KV\cos\theta \qquad \text{(Eq.3.14)}$$

and

$$X_d \tilde{=} 5\,D/V\cos\theta \qquad \text{(Eq. 3.15)}$$

As the welding speed once selected is holding constant X_c or X_d are determined by the value of θ which depends on weld pool shape (see Figure 3.4). Therefore, there are at least three factors continuously changing from the fusion zone inwards the pool: temperature gradient, growth rate and solute segregation. Now, in Section 3.2.2 we have seen how the solute build-up could lead the liquid ahead of the solid-liquid interface to be constitutionally supercooled (Figure 3.2(b)), depending on the temperature gradient in the liquid G, and the growth rate R. Figure 3.3 illustrates that, in welding, increasing speed will increase the growth rate R (Eq.3.7), thus extending the constitutional supercooling. The same effect is observed if energy input is increased, for it tends to decrease the temperature gradient.

These changes in G/R ratio, when combined with the solute concentration determine the solidification mode. TILLER and RUTTER / 45 / have already shown this dependence, which SAVAGE / 55 / adapted for welding. Figure 3.7 shows the five possible modes of solidification, all of them reproduced in welding practice. To confirm this point, we made a TIG bead on plate weld on a HY100 steel (see Chapter 6) strip measuring 150 mm x 50 mm x 33 mm, using welding conditions: 1.2 mm/s; 10 V; 200 A; gas argon at 15 1/min flow rate. The nominal energy input of 1.7 KJ/mm allowed a very fast cooling rate, considering the plate thickness and the low arc efficiency for the TIG process. The crater of this bead was examined (untouched) under the Scanning Electron Microscope and Figures 3.8 to 3.10 show that four of the five solidification modes described in Figure 3.7 could really be seen, as we scan the crater from the fusion boundary to its centre. Figure 3.8 shows the transition from cellular (C) cellular-dendritic (CD) structure and was taken at mid-distance between fusion zone and crater centre. As we approach the centre, a beautifully dendritic structure forms, as Figure 3.9 shows. Note the very well formed dendrite arms. Exactly at the 'hill' formed at the cratercentre the structure changes to equiaxed dendrite, as shown in Figure 3.10, with a relatively well defined transition region.

Thus, the G/R ratio changed from the fusion line to the crater centre and the structure followed it. Throughout the experimental part of this study, cellular-dendritic and dendritic structures will be observed in planes generally transverse to the welding direction.

Together with solidification structures, another phenomenon will be seen many times, and it is well characterised in Figure 8.21 (Chapter 8). We are referring to the banding observed in the weld pool, which is still subject to controversy. D'ANNESSA / 74 /, JESNITZER / 75 /, YOSHIMURA and WINTERTON / 76 / have suggested that it is caused by different growth rates resulting from thermal fluctuations in the weld pool. GARLAND and DAVIES / 77 / have shown that it may be caused by cyclic variations from the welding power source, and KOTECKI et al / 78 / that it results from pool oscillation during freezing in GTA spot welds. Nevertheless, it seems that there is a general agreement on the smaller dendrite size, and on the microsegregation of some chemical elements at this zone in the weld. This fact recalls FLEMINGS / 24 / and similar phenomenon in ingots, as we have seen in Chapter 2. Moreover, it was found / 76 / that there are two kinds of relationship between the dendritic structure and banding: one involves the growth of dendrites through the banding, and the other the nucleation and growth of new dendrites when the 'old' dendrite enters a 'new' band.

It was also SAVAGE et al / 79 / who first proposed a new terminology for the regions in welds. In the weld metal there is the 'composite region' which is mechanically mixed by arc forces, and after it the 'unmixed zone' which has been melted but not mechanically mixed and the 'partially melted zone', just before the 'true heat-affected zone'. The 'weld interface' is placed between the 'partially melted zone' and the 'unmixed zone'. Thus, there is a concentration gradient from the base metal composition to that of the filler metal lying in the unmixed zone. The detection of this unmixed zone is only possible through the use of special etching techniques. SAVAGE et al / 79 / used two-stage etchant (described in Chapter 6), while TAKALO and MOISIO / 80 / found the zone in Manual Metal Arc welds of austenitic stainless steels using the potentiostatic technique. Also these authors observed that in moderate oxidising environments, when the weld metal was nobler than the base metal, the unmixed zone was the fastest corroding region.

Finally, there is the point of resultant solidification structure size. As already seen, welds have a much higher solidification rate than castings, and this must reflect in the interdendritic spacing. BROWN and ADAMS / 81 /, using the mass transport phenomenon concept for the interdendritic spacing, applied it to a simplified one-dimensional analysis. Assuming three-dimensionsl heat flow and simplifying the freezing time expression for a small volume of metal at the melting point, the dendrite spacing L is given by:

$$L = \{(8D\Delta T\, HQ)/(2\pi C_p Km(1-K)C_o V(T_m-T_o)^2)\}^{\frac{1}{2}} \qquad \text{(Eq.3.16(a))}$$

where

ΔT = undercooling

m = slope of the liquidus

K = distribution coefficient

C_o = alloy composition

D = diffusivity of solute in the liquid

H = latent heat of fusion

Q = power input (voltage x current)

C_p = specific heat

V = welding speed

T_m = liquidus alloy temperature

T_o = initial material temperature

Thus, the interdendritic spacing should be proportional to the square root of the energy input:

$$L \propto (Q/V)^{\frac{1}{2}} \qquad \text{(Eq. 3.16(b))}$$

This relationship has been confirmed by some researchers, among them PALEY et al / 82 / and JORDAN and COLEMAN / 83 /. However, it must be recognised that Equation 3.16 (a) comes from large over-simplifications. Furthermore, in Chapter 8 we shall show that the dendritic spacing has close relationship with weld bead shape. Also in Chapter 8 is demonstrated the importance of another concept, the dendrite growth

direction, not so far considered in these measurements.

To assess the exact relationship between solidification structure size or mode and mechanical properties is a difficult task, especially if the alloy suffers solid state transformation(s). Nevertheless, there is evidence that this is quite possible, as shown by PROKHOROV and MASTRYUKOVA / 84 / and by THORNLEY / 85 /, who found a very good relationship between dendrites arm spacing and (0.2%) yield strength.

3.3.3 Modifying the normal solidification process

In the previous sections we have seen that the weld solidification process inherently leads to solute(s) microsegregation. Also it was explained how this solute build-up in front of the solid-liquid interface combines with the temperature gradient G and the growth rate R to determine the constitutional supercooling extent and solidification structure modes.

Depending mainly on the microsegregation and weld pool stress level, and solidification structure type, the weld might suffer from severe solidification cracking (Chapter 4). Also its secondary microstructure might present a distribution, constitution or shape which does not enable the weld to fulfil its mechanical duties.

In this section we do not want to make a large discussion on all available methods to modify the 'normal' weld solidification process. Rather, the intention is to provide a general view about them, for in Chapter 9 we shall show the effectiveness in reducing solidification cracking of an oscillation system designed for our studies, in which only the wire oscillates.

Furthermore, the expression 'control' of weld pool solidification / 61 / is here avoided for, as far as we know, up to this date there is not such a device or process which allows exact results to be forecast.

Some weld properties are determined only in their molten state or during their solidification stage. Usually, deoxidation and alloying techniques are employed to obtain these results in castings, but in welding these methods may be much more difficult to apply, for the nuclei must survive the high pool temperature.

In general, any modification of the normal weld solidification process has as primary objective grain refinement but, as we shall see below, some of the experiments were designed specifically to reduce solidification cracking .

The use of inoculants is concentrated mainly in the submerged arc process, due to its relatively large pool and easy addition. Many attempts have been made to modify the weld solidification mode through the use of this method. They were either aimed to refine the structure / 85 - 87 / or to reduce solidification cracking / 88 /, using powdered filler metal. The results, however, were not conclusive, for the control of the various factors involved in this kind of addition is critical and can show heterogeneous distribution.

Other techniques have been developed, such as stirring and vibration. The aim of these methods is the generation of nuclei (through dendrite fragmentation) at the growing solid-liquid interface. These nuclei can be generated either by forced thermal fluctuations or mechanical action and they can survive due to the stirring or vibration which cause reduction in the pool temperature. Due to the electromagnetic Lorentz forces / 71, 72 / stirring occurs in 'normal' welds. Through periodic alternating magnetic fields it is possible to obtain grain refinement / 87 /. Experiments with electromagnetic arc oscillation also have shown to be effective in reducing the grain size / 89 / or solidification cracking / 90 /, where it was highly successful using low frequencies, producing 'growth transition bands', occurring due to solidification structure change of orientation. These bands appear to behave as crack arrestors. Arc weaving has been shown to improve many weld metal properties, including its resistance to cracking / 91 / with frequency of ~ 8Hz and amplitude of 3.5 mm. In spite of the evidence of GARLAND and DAVIES / 61 / that the submerged arc weld pool is too large to suffer the effect of oscillation, in Chapter 9 we shall show that this is not a necessary situation, for oscillation can substantially reduce solidification cracking tendency.

Also ultrasonic vibration has been used and current pulsation is another promising method. Frequencies of ~10Hz / 92 / have shown to be the most effective in aluminium alloys, while it had no effect of titanium alloys but refined the grains in mild steel / 93 / using low pulsation frequencies.

Finally, there are the effects on segregation distribution due, for example to the use of rutile-coated electrodes containing high amounts of iron / 94 / where the sulphur segregation was reduced as was the solidification cracking tendency. Also, the complicated effect of flux in submerged arc welding is an important factor to be considered. It either introduces beneficial or degrading elements to the weld metal properties, alters heat distribution / 95 / and surface tensions, thus influencing the solidification structure. Related to this point, one of the most spectacular effects of flux types is that first reported by COCHRANE / 96 /. It is suggested that in submerged arc weld deposits made under acid fluxes, the secondary grains are confined to the original primary ferrite structure. However with deposits made with basix fluxes, this secondary structure may be appreciably larger than the dendrite spacing.

3.4 Summary

In this chapter we first tried to make a profile of the general metal solidification process, and then to particularise it to welding conditions.

The equations for the initial, steady and terminal transient states (Eqs. 3.2 to 3.4) were given and the equilibrium distribution coefficient defined. The solute build-up in front of the solid-liquid planar interface described by these equations was studied. Its relationship to the temperature gradient G and growth rate R was demonstrated to have fundamental importance in the constitutional supercooling, whose extent determines the interface stability. We also pointed out the effect that chemical reactions might have on solidification, mainly through deoxidation.

In welds, the solid growth mechanism is epitaxial, depending on the base grains. Thus, each grain in the weld metal follows a characteristic crystallographic direction given by that of the base metal.

The solid growth rate is given by the product of the welding speed and cosine of the angle between the normal to the tangent to the pool at the point considered (Eq.3.7). Depending on the welding speed, the pool shape can be elliptical or tear drop, and this has an effect on the segregation mode, for it alters R and in the tear drop case the grains converge along the weld centreline raising the tendency for entrapment of low-melting point solute-enriched liquid between the dendrites.

Also it was seen that maximum growth rates occur in the weld centreline where minimum temperature gradients are encountered and vice versa at the fusion boundary.

The spacial weld pool shape studies are progressing and they are based mainly on the weld pool geometry (Eqs. 3.9 and 3.10). Also, the mechanical interfacial tensions acting along the various interfaces in the weld pool were considered (Eq. 3.11).

In spite of its high kinetic reactions, the weld pool has shown at least five solidification modes: planar, cellular, cellular-dendritic, dendritic and equiaxed. The temperature gradient is very high, but also it is the growth rate and so the G/R ratio in combination with the alloy composition make possible the existence of all solidification modes, as shown in Figures 3.8 to 3.10.

The banding phenomenon in welds is still subject to controversy, or it might be due to all effects suggested in the literature.

The various weld regions were presented, and also it was pointed out that there is a concentration gradient from the base metal composition to that of the filler metal lying in the unmixed zone.

Dendrite size is another important factor in the weld properties, and it is proportional to the square root of the energy input (Eq.3.16(b)) in a first approximation. However, under some circumstances, we found it to be related to weld shape (Chapter 8) and its measurement to be dependent on the dendrite growth direction. Also the influence of dendrite size and solidification mode on weld metal properties were reviewed.

There are many techniques that can be used to modify the 'normal' weld solidification process. Their aim is to generate nuclei and to provide the environment which enables them to survive. Among the most generally known are arc weaving and vibration, ultrasonic vibration, electromagnetic stirring, deoxidation and alloying. Flux can also have an effect on the solidification structure through its physical properties or as a means to make additions of certain chemical elements.

In Chapter 9 we shall show a device used to oscillate only the electrode, thus reducing the mechanical complexity needed to oscillate all the welding head. It was successfully used to reduce solidification cracking tendency. However, the general results have shown that, up to this date, there is not a complete control of the solidification process, for this depends on a number of factors which knowledge is not always available.

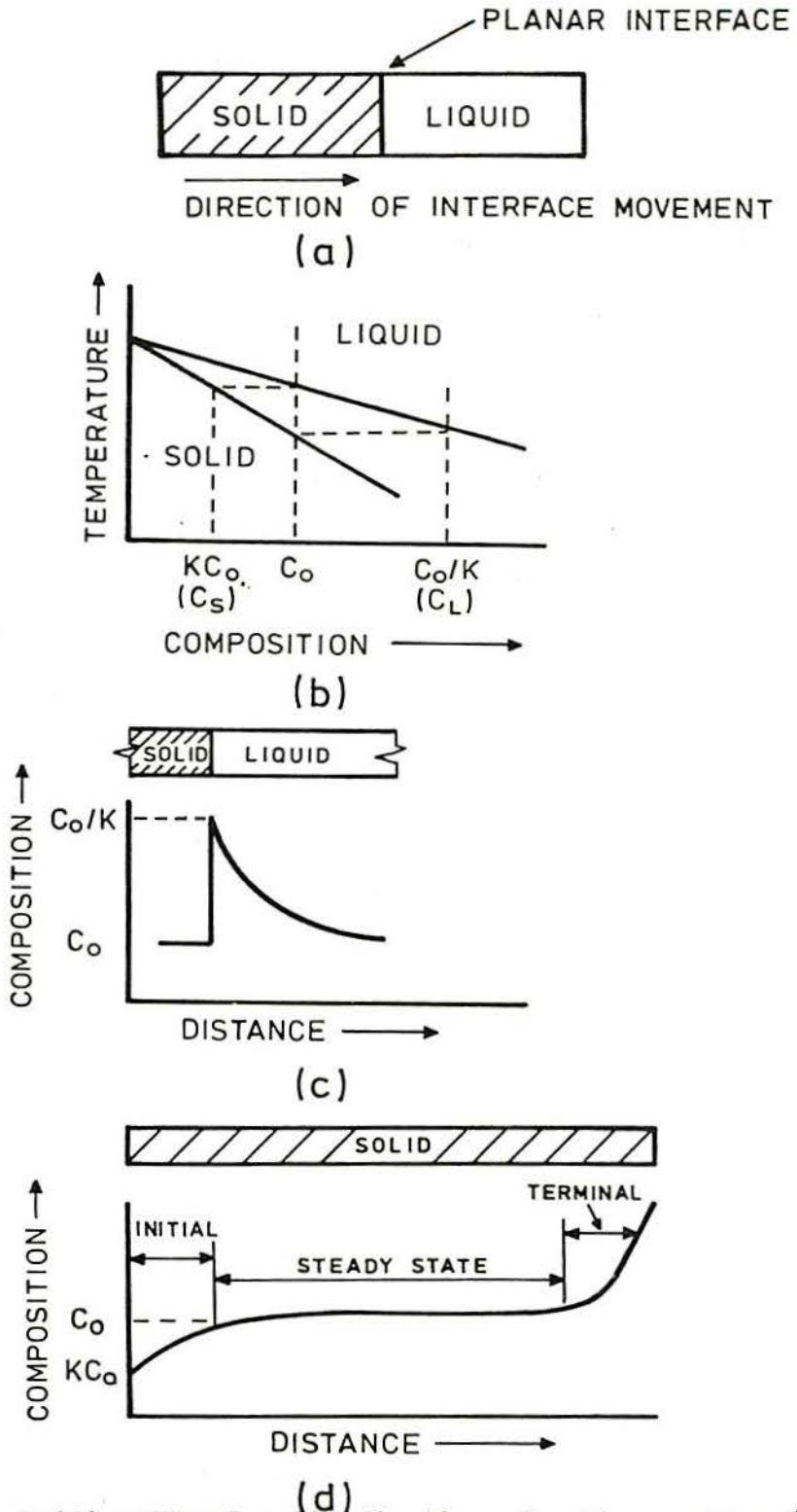

FIG. 3.1 - Unidirectional solidification of a binary alloy (C_o) with limited liquid diffusion and no convection. (a) Liquid metal solidifying with a plane interface. (b) Related phase diagram. (c) Solute concentration profile during steady-state. (d) Solute concentration profile after end of solidification.

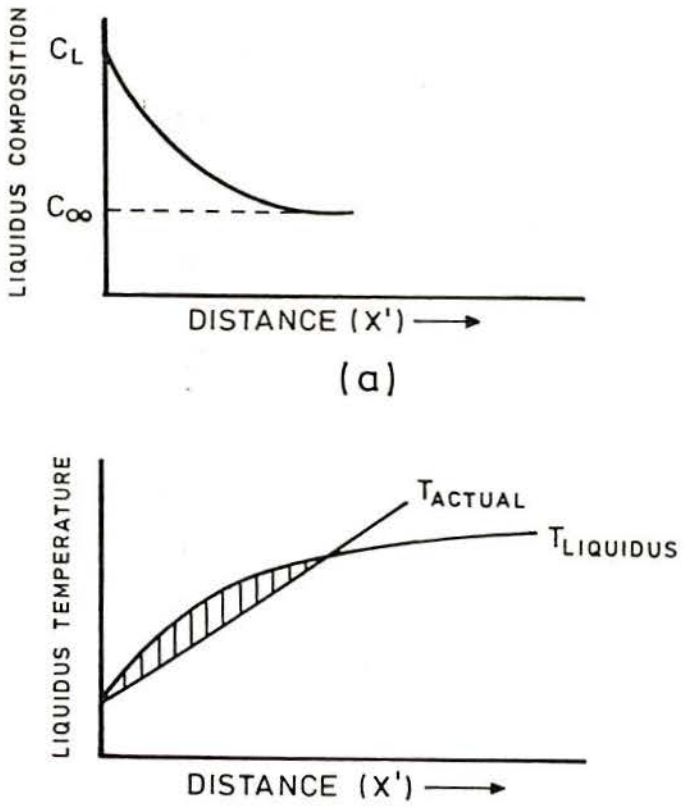

FIG. 3.2 - Constitutional supercooling. (a) Solute enriched layer ahead of the interface. (b) Actual temperature below liquidus temperature due to composition effect.

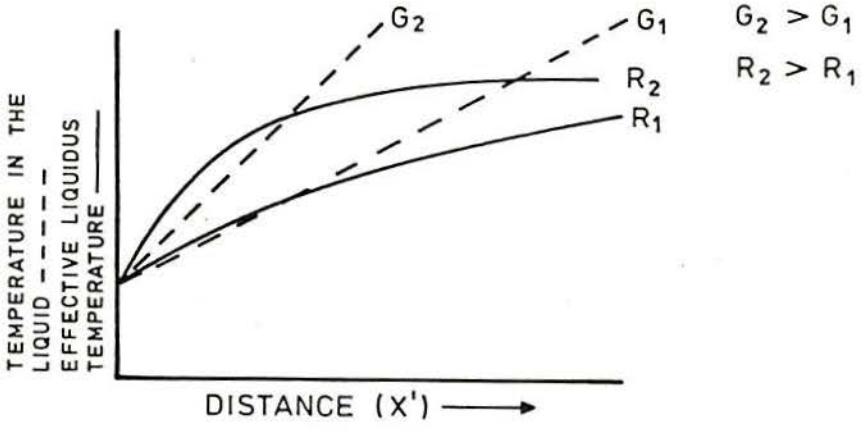

FIG. 3.3 - Effect of temperature gradient (G) and growth rate (R) on constitutional supercooling.

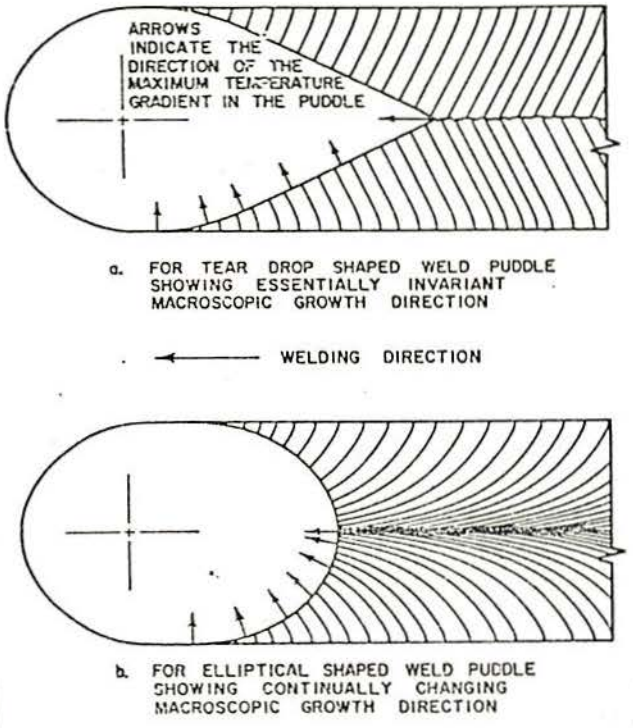

FIG. 3.4 - Schematic Representation of Two Weld Pools, showing their Shapes at (a) High , and (b) Low Welding Speed. / 56 /.

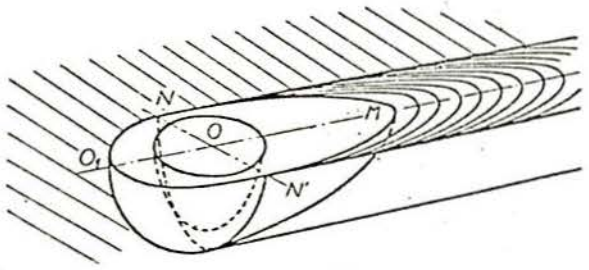

FIG. 3.5 - Schematic Representation of the Spatial Weld Pool Shape (see text). / 63 /.

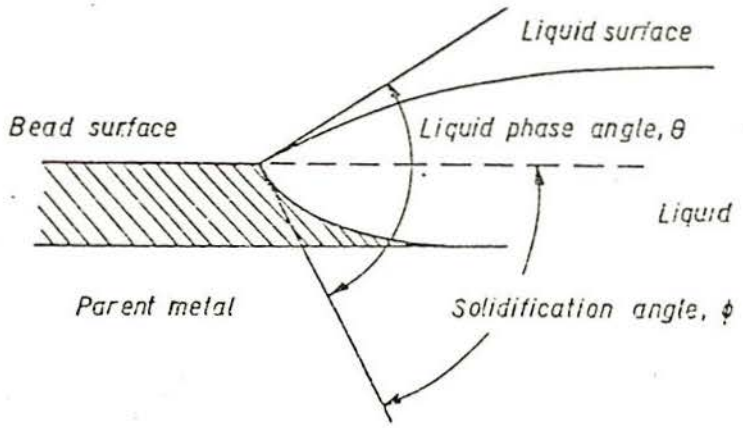

FIG. 3.6 - Relationship between Liquid Phase Angle and Solidification Angle . / 69 /.

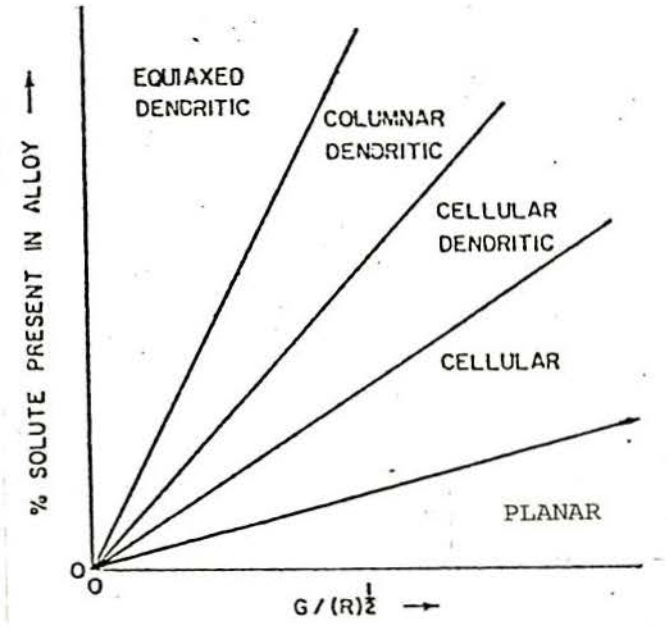

FIG. 3.7 - Schematic Relationship between Temperature Gradient (G), Growth Rate (R), and Solute Concentration on the Solidification Modes. / 55 /.

FIG. 3.8 - Crater of a TIG weld bead. Mid distance between fusion zone and crater centre. Transition from Cellular (C) to Cellular-Dendritic (CD) Solidification Microstructure. SEM, untouched (see text).

FIG. 3.9 - Crater of a TIG weld bead, just before the "hill" at crater centre. Complete Dendrite. SEM, untouched (see text).

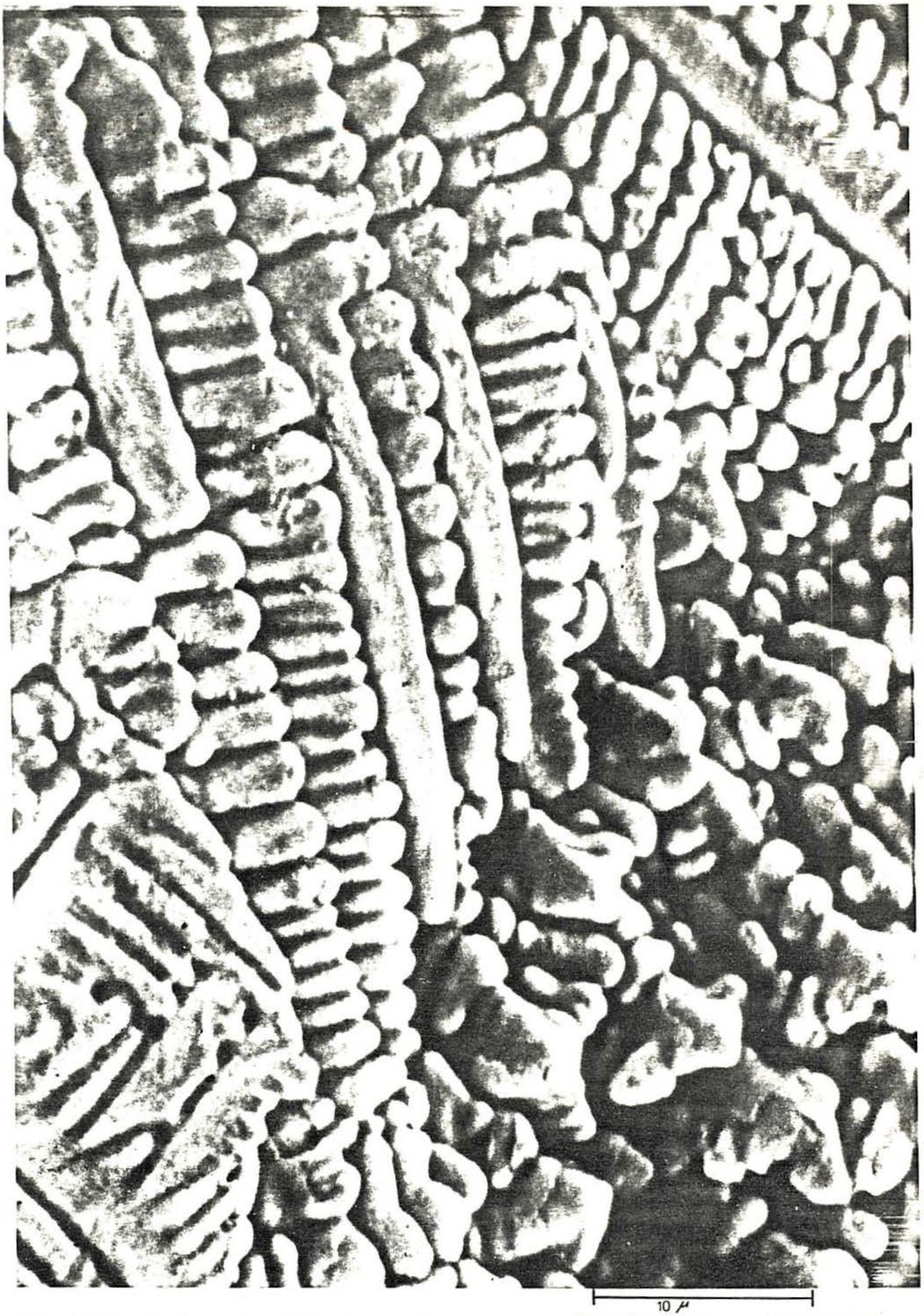

FIG. 3.10 - Crater of a TIG weld bead. Top of the "hill" at the crater centre. Equiaxed Dendrites. SEM, untouched (see text).

4. SOLIDIFICATION CRACKING PHENOMENOLOGY

4.1 Introduction

As we have seen in Chapter 3, the weld solidification process is complex and its last stage is critical, for there is, inherently, solute(s) segregation and its effects are enhanced when the interfaces meet each other.

At this point the association of mechanical/thermal stress, and lack of a suitable (micro) structure to resist it, or sufficient liquid to fill in the gap once it has been open, can cause what is known as 'solidification cracking'.

It is necessary to define what exactly we mean by solidification cracking and how to recognise it.

In a classic work on the subject, HEMSWORTH, BONISZEWSKI and EATON / 97 / proposed a classification for High Temperature welding cracks. There are six categories, classified on the basis of their microstructural characteristics (excluding reheat or stress relief cracking). The area included by the dashed lines in Figure 4.1 shows the types recognised by them. As a result of intergranular (not here exclusively referred to a crystallite) or interdendritic microsegregation leading to the presence of liquid films during welding, Type 1 cracks occur. Type 2 is a solid state phenomenon and may occur together with Type 1, through propagation of liquation cracks (1B or 1C) or by a ductility-dip mechanism (2A or 2C). Type 1A, following the authors, is always a product of microsegregation and strains formed during or shortly after solidification. At first glance, Type 1A could be the only kind of cracking referred to in this study. However, it is one of two possibilities. There is at least one other kind of solidification cracking, not necessarily resulting from microsegregation (for it is possible that this microsegregation might be unable to promote intergranular films in the amount, type or shape necessary to lead to cracking, as we will see in the next section). This cracking can be at the centreline or can be multiple (transverse). Its face always shows dendritic structure (with no films on them) giving us proof of its formation during solidification and, of course, its path is interdendritic. Its formation is a product of the race between solidification mode and strains developing in the weld pool. Thus, cracking occurs when the race is lost by the former factor, and it is accentuated by the lack of more fresh liquid to fill the gap. The amount of liquid phase being primarily dependent on the freezing range of the alloy and solidification mode.

Therefore we propose the addition of this type of cracking (which was named 'Type 0' to be in line with the existing classification) in the quoted work / 97 /. We place it outside the dashed lines in Figure 4.1 at the same level as the Type 1, to highlight the fundamental difference between them. It is clear that the Scanning Electron Microscope and Microprobe analyser are essential tools to identify these two types of cracks correctly.

Without doubt, solidification cracking is one of the best documented topics in welding (and casting) science. This fact is demonstrated

in the next sections by the number of publications on the subject. Moreover, reviews have been regularly issued / 98 - 108 /, thus showing the topicality of the problem and that it is far from being completely clear.

However, we must recognise that we shall never have absolute assurance about which kind of cracks the 'old' papers refer to. There are many reasons for this : the techniques used by some of them to identify the cracks were very subjective; the terminology utilised was confusing and expressions such as 'hot shortness', 'hot tearing', 'hot cracking', and 'hot fissuring' were freely used to identify different phenomena; and instruments with the depth of focus and image definition such as Scanning Electron Microscope were not available at those times and, therefore, three dimensional structures like the dendrites on a solidification cracking face could not be perfectly seen.

Therefore, caution must be taken when we are consulting these papers.

As we shall see in the next sections, great progress has been made in the solidification cracking field in the course of the last years. However, in our opinion, this phenomenon still lacks a more complete study. The majority of the researches done up to now have been designed to elucidate isolated effects only, while we know that this is not the way welding operates.

4.2 The established theories

Perhaps the foundrymen were the first to meet and roughly to identify the solidication cracking problem; BRIGGS and GEZELIUS / 109, 110 /, VERO / 111 /, LUTTS and HICKEY / 112 /, GALPERIN / 113 / and LEES / 114 / were just some researchers who noticed the influence of the alloy constitution on solidification cracking and to give it many different names and definitions.

Specifically in the welding literature, one of the earliest known direct treatments of solidification cracking is found in the review on effect of sulphur on the welding of steel made by SPRARAGEN and CLAUSSEN / 115 / in 1939 and, again, in another review made by them on weld metal cracks / 98 / two years later.

So far, however, there was not a proper theory to explain the solidification cracking phenomenon. It seems that at the end of the 1940s the conditions were propitious and the understanding of the fundamental mechanics of solidification cracking began to be made.

Conventionally, we study these theories in four steps, almost following their chronological order of appearance. In spite of our knowledge that the main factors causing solidification cracking are mechanical and metallurgical, the study of these theories is justified, for we yet do not know how to quantify these effects. As we shall see below, these theories are much more concerned with the characteristics of the weld pool itself and little was investigated on the mechanical/thermal base metal effects. This shall be seen in Section 4.4.1.

4.2.1 The shrinkage-brittleness theory

(i) The British view

This theory was advanced in some pioneer studies / 111, 113 /, but it was really developed in later works / 114, 116 - 118 / on aluminium alloys (castings first, later extended to welding.) The first important point reached was the relationship found between the 'hot shortness' of these alloys with their range of temperature above the solidus. At this stage the alloy possesses a finite strength yet has no appreciable ductility. The theory suggests a 'brittle temperature range' between the temperature at which a coherent dendrite structure is first developed in the alloy during the cooling from the liquid state, and the effective solidus temperature in the relevant conditions. The basic cause of cracking would be that the semirigid network of interlocked dendrites formed during the solidification of an alloy is unable to withstand strain. If sufficient liquid is available, the gaps (cracks) may be filled, or 'healed'.

PUMPHREY and JENNINGS / 118 / stated that crack initiation would be a function of the contraction per unit volume during cooling through this 'brittle range' of temperatures. They also developed a very simple mathematical approach for cracking conditions and highlighted the importance of the rate of increase in width of the gap.

(ii) The Soviet view

As BORLAND recognises / 106 /: "much current understanding of the fundamental mechanics of crack formation stems from Russian sources".

This is a theory developed by MEDOVAR / 119 / and, principally, by PROKHOROV / 120 - 123 /. The crack susceptibility is related to the temperature and strain rate within the solidifying weld metal. The temperature range over which permanent cracks are formed is defined as the 'brittle temperature range' (BTR). The upper temperature limit of the BTR is that in which the dendrites grow together thus preventing the liquid phase from circulating around them. The lower limit is just beneath the solidus, and is the temperature at which the strength of the grain boundaries is sufficient to resist the shear stress arising from contraction. Thus, within the BTR the metal can absorb some strain if is not applied too rapidly. On the contrary, the grain boundary films can rupture and cracks are created.

Comparing the initial assumptions of this theory / 119 - 121 / with the British view above, the main difference is that the latter stated that the lower limit of the BTR is the solidus. As BORLAND / 106 / suggests, the Soviet view is more precise, but in many practical situations both theories are virtually the same.

Developments were made on this theory / 122 - 124 /. The straining of solid-liquid "assemblies" are treated as a process of relative crystallite displacement against counter-currents of the liquid between them. The strain limit (ductility) of the "assembly" can be calculated from the condition of free crystallite displacement up to the stage of mutual jamming.

Thus for a three-dimensional "assembly" assuming that the liquid is distributed uniformly in the thin liquid interlayers and that the crystallite size in the direction at right angles to the applied forces $\delta=\delta_1=\delta_2=\delta_3$:

$$\varepsilon = K_S \{ (1 - (K/(1-K))((T-T_S)/(T_1-T)) + m_\rho)^{-n} - 1 \}$$

where

ε = ductility

K_S = flow coefficient for the solid phase (experimentally determinable)

K = distribution coefficient of the solute at the solid-liquid interface

T_S = solidus temperature

T_1 = liquidus temperature

T = temperature of interest

m_ρ = amount of liquid cut off by crystallite and unable to flow around them (experimentally determinable)

n = 1/3 for three-dimensional "assembly" (1/2 for two-dimensional)

4.2.2 The strain theory

This theory was developed in the USA to explain 'hot tearing' in castings by PELLINI et al / 125 - 127 /. It does not consider the 'brittle range temperature' concept, stating that cracks cannot occur during this semi-solid ('mushy') state. It will occur later, when an essentially continuous thin film separating solid grains cannot accommodate the strain imposed on it. The total strain applied to this film is a time/temperature dependent property.

Using these principles, SAVEIKO / 128 / was able to calculate the force (F) required to separate the liquid film and its thickness (d), when the liquid is exposed to the environment:

$$F = 2A \gamma_{lv}/d$$

where

A = area of liquid film in contact with the solid

γ_{lv} = liquid-vapour interfacial energy

d = film thickness

Thus, as the film thickness increases the force decreases.

A significant analysis on solid-liquid component fracture in welds was made, BORLAND / 106, 107 /, and will be the subject of the following section.

4.2.3 Borland's generalised theory and beyond

BORLAND is one of the most important and constant researchers in this field, and the wellknown 'generalised theory' / 99 / was soon followed by an incursion on the implications of solidification on weld cracking / 100 /. His latest papers refined, expanded and added new ideas to this important phenomenon / 106,107 /.

The generalised theory /99/includes relevant points from the initial developments of the shrinkage-Brittleness and strain theories. It considers four stages during the solidification process:

(a) Primary dendrite formation: the solid phases are dispersed in the liquid, with both phases capable of relative movement.

(b) Dendrite interlocking: both liquid and solid phases are continuous, but only the liquid is capable of relative movement. The liquid can move freely between the dendrites.

(c) Grain boundary development: the solid crystals are in an advanced stage of development and the movement of the liquid is restricted; relative movement of the two phases is impossible.

(d) Solidification: the remaining liquid has solidified.

In Figure 4.2 these stages can be seen in a schematic form. The stage 3 is considered by BORLAND / 99 / as the most significant in cracking, and named the 'critical' solidification range' (CSR). Due to the undercooling found in weld, the liquidus and solidus can be depressed and the solidus may be further depressed by the lack of time for diffusion to occur. Thus, the CSR is increased as is the susceptibility to solidification cracking. At this stage 'healing' cannot occur, and the material will crack unless it can resist the strain at this high temperature.

An important suggestion is made in that the presence of a wide freezing range is not a sufficient condition for cracking to occur. BORLAND's reasoning / 99, 100 /, is that a liquid phase covering almost all the grain faces during freezing will allow the development of strains that it cannot accommodate in the narrow bridges joining adjacent grains, and could give rise to cracking. On the other hand, a liquid confined mainly to grain edges and corners will allow large areas of the grain faces to unite. These areas should be able to resist higher strains without cracking. ROGERSON and BORLAND / 129 / applied dihedral angle measurements to determine the shapes of liquid phases at temperatures above the liquidus in three binary aluminium alloys. Correlation was found between the 'hot' cracking susceptibility and the relative free energies of grain boundaries. This latter factor is a function of the dihedral angle of the second phase, as SMITH / 130 / has shown:

$$\gamma_{SL} / \gamma_{SS} = 1 / 2 \cos \frac{\theta}{2}$$

where γ_{SL} is the interface energy of the liquidus-solidus, γ_{SS} is the grain boundary energy and θ is the dihedral angle. As shown in Figure 4.3, when $\theta = 0^{o}$ the liquid completely covers the grain faces. When the ration $\gamma_{SL} / \gamma_{SS}$ reaches 0.57 (θ=60°) there is only a network of liquid along the edges of the grain. This should be the best condition to resist cracking.

For the sake of justice, we have to record that MASUBUCHI in his relatively recent book / 131 / is mistaken. For he presents BORLAND's generalised theory as being borne in the review (year 1964) prepared by KAMMER, MASUBUCHI and MONROE / 101 /. However, in that Report the authors recognised BORLAND's authorship.

BORLAND / 100 / was able to foresee the harmful effects of many chemical elements using a 'relative potency factor' (RPF), which includes considerations of the equilibrium phase diagram of binary alloys and the extent of the freezing range and constitutional supercooling. This factor is given by:

$$RPF = mC_s (1-K)/K$$

where

m = slope of liquidus

C_s = maximum solid solubility

K = distribution coefficient

Thus, to be judged harmful, an element must attain a certain minimum value of maximum potency (RPF), combined with conditions imposed on freezing range and constitutional supercooling. As the author recognises, this theory igmores the mechanical strain factor imposed by the welding process. Nevertheless, it has been useful for a first analysis of cracking tendency.

As we previously said, in his later papers BORLAND / 106, 107/ highlights the importance of other factors not so widely discussed in his former works. Much attention is given to the problem (unsolved) of tensions around the weld pool, methods to decrease it (as heating - see Chapter 9) and interfacial tensions. One of the subjects covered in details is the fracture of solid-liquid components in welds. He considers that, at least, three aspects are important:

(a) The presence and /or penetration of liquid between grains or along crystallographic planes;

(b) Fracture initiation at the solid-liquid interface or parting within the liquid phase;

(c) Propagation of the crack.

After some considerations on the interfacial energies involved in the process of liquid separation, including the expression developed by SAVEIKO / 128 / (see Section 4.2.2) he (tentatively) concludes that: "while the continuous liquid phase provides an easy extension path for an existing crack, the presence of the liquid does not

necessarily account for the initial formation of the crack ."

This (tentative) conclusion reinforces what we have said in Chapter 3, when studying interfacial tensions acting on welding, in that much more attention should be given to this point.

4.3 The role of chemical elements

A very complex relationship holds between solidification cracking and the chemical composition. This is not only due to the interactions among the elements themselves, but because relatively simple metallurgical phenomena became complex under the reactions kinetics found in welding processes. Moreoever, there is the additional problem of the range of composition studied and effect reported. Therefore, we can just review the general trends of chemical composition on solidification cracking, and present some empirical equations which prove to be useful in avoiding this type of defect in low alloy steels.

4.3.1 The individual action

(a) Sulphur

This element was detected as harmful to solidification cracking from a very early stage / 115 / and there is a widespread agreement on this / 100, 102, 132, 134 /. The sulphur action through grain boundary Fe-S films of low melting point, and its rejection from the austenite phase, is a wellknown one. At ≈988°C the Fe-S equilibrium diagram shows, as pointed out by BORLAND / 100 /, that austenite is in equilibrium with a liquid containing nearly 30% sulphur / 135 /. The non-equilibrium weld pool solidification as a result of the fast cooling rates enhance the tendency for sulphur-rich liquid films to form over the austenitic solidification range. As the contraction strain in the weld pool increases with cooling, this film may be a real danger to solidification cracking.

Consequently, sufficient addition of elements that form strong links with it, like manganese, will assure the formation of sulphides of different nature and melting point (see manganese, sub-section d). Furthermore, lowering the amount of carbon or adding elements which reduce the austenite range (extending the delta ferrite region) will help to avoid solidification cracking.

(b) Phosphorus

The analysis of the Fe-P binary equilibrium phase diagram alone is insufficient to make predictions on the possible segregation of the phosphide segregation of the phosphide eutectic, which melts at 1050°C, and that under departure from equilibrium in welds is able to be a solidification cracking promoter / 136 /. There is no peritectic reaction in the iron-phosphorus binary phase diagram and, in contrast to sulphur, there is a closed γ-loop in which phosphorus is soluble to the extent of 0.2% at 1100°C / 102 /.

The evidence is clear of this harmful effect / 102, 133, 136 / and a very interesting find is due to GARLAND and BAILEY / 132 /, which states that there is a large interaction between phosphorus and manganese

and the inability of the latter to control cracking (combining with sulphur) at high phosphorus levels.

(c) Carbon

It is agreed / 98, 100, 102, 132, 133 / that this element has a negative effect on solidification cracking.

Firstly, because carbon acts as austenite former, enhancing the segregation of sulphur and reducing the rate of phosphorus diffusion in austenite. However, its effect on extending the solidification range is stronger than was earlier believed and it is thought now as the most important factor increasing cracking tendency / 132 /.

The iron-carbon phase diagram might help to understand the carbon effect (Figure 2.3 in Chapter 2) through the formation of gamma phase as its content increases. However, caution ought to be taken when discussing critical levels of carbon above which susceptibility to cracking is increased.

Contrary to this common belief, in a relatively recent paper / 137 / it was found that, among other not quantified factors, an increase in carbon and nickel content is beneficial to solidification cracking, when weld metals with carbon content ranging between about 0.04 and 0.22% are deposited using MMA (cellulosic electrode) and GMA (100% CO_2) processes. It was concluded that the main origins of this type of cracking is the shrinkage in the transformation from delta to gamma phase in low carbon steels (less than 0.09%), which enhances the normal shrinkage of the solidifying weld metal. As carbon and nickel are gamma formers, they were said to cooperate to prevent this defect. A relationship between carbon, welding speed and weld crack-no-crack boundary was also established, being noticed a minimum welding speed for the cracking occurrence. However, this paper left doubts in the author's mind for it ignores a series of important factors. The most striking is that the base steels and electrodes are not differents in carbon and nickel content only, being important chemical elements to solidification cracking tendency, such as Ti, Nb, V, S, P and Mn also different for each weld metal. Therefore, we think that caution is required in the analysis of these results.

(d) Manganese

The beneficial action of this element on solidification cracking has been recognised for a long time / 100, 102, 133, 138 /through its combination with sulphur. The general suggestion (inherited from the foundry industry) is that there is certain Mn/S ratio above which the susceptibility to solidification cracking can be reduced. JONES/ 139 / found that in low alloy steels a ratio above 50 reduces considerably the cracking tendency, but there is a strong relationship with the carbon content. GARLAND and BAILEY / 132 / arrived at the conclusion that there is not a critical Mn/S ratio, because this implies a change in the effectiveness of manganese. Therefore, they recommend an arithmetic expression like X.Mn - Y.S as a best guide.

There are two explanations available for the beneficial action of manganese. The best known / 102 / is that in which FeS (melting

point 988°C) is not allowed to form as a separated phase. Instead with the addition of manganese the phase will be MnS (melting point 1610°C) with FeS dissolved in it. This is because MnS has a lower free energy of formation than FeS. Thus, MnS will dissolve FeS until a solid containing 75% of it solidifies. So, the higher the manganese content of the steel, the higher the manganese-to-iron ratio in the sulphide and the higher its melting point. With sufficient manganese available, the formation of grain boundary films of low melting point is avoided.

Another theory was introduced by NAKAGAWA et al / 134, 140-144 /. The parameter Mn/S is said to have only an inherited meaning, rather than a metallurgical one. Firstly, by reference to a ternary Fe-S-Mn equilibrium phase diagram these authors were able to demonstrate that in an Fe-rich Fe-S-Mn alloy steel the iron manganese (and also a very little amount of sulphur) solidifies as the primary phase. Using the weld metal solidification model (see Chapter 3), they also have shown that, as the solidification proceeds, the sulphur and manganese concentration in the remaining liquid increases, because their solute distributions are less than unity. However, sulphur has a much smaller distribution coefficient than manganese and, therefore, the Mn/S ratio in the liquid ahead of the solid-liquid interface will decrease.

Based on this changing in the liquid composition and applying distribution coefficient of both Mn and S, these authors concluded that a better parameter to describe structure and shape of the sulphides and the solidification cracking susceptibility depends on the Mn^3/S ratio in steels where δ phase solidifies, while it depends on Mn^5/S ratio in steels where γ phase solidifies.

The same authors carry on studying a series of steels like HY100, HY130, etc and found that for them the parameter Mn^5/S shall be employed, and that even 0.005% sulphur has a detrimental effect on their solidification cracking susceptibility.

(e) Nickel

This element, in general, increases the solidification cracking tendency in the levels employed in steels like those in the present experimental study (Chapter 6 on). It widens the 'brittle temperature range' / 145 / and acts in combination with other elements. KAL'NER and RUSSIYAN / 146 / quote the presence of low melting points sulphides of nickel (800°C) and its eutectic NiS+Ni (melting point 690°C) as being responsible for wide bands of low strength around the dendrite boundaries. MASUMOTO and IMAI / 147 / also reported heavy sulphur and nickel segregation at the dendritic boundaries, and values of less than 0.01% S, 2.5% Ni being needed to prevent cracking. They did not observe any remarkable phosphorus segregation, but stated that limiting amounts of 3.0% Ni and 0.02% P must be the rule. NAKAGAWA et al / 144 / in a work previously described (sub-section (d)), concluded that nickel and carbon promote the detrimental effect of sulphur and phosphorus. They correlated cracking susceptibility with a 'carbon equivalent for solidification cracking' - CE (SC), given by:

$$CE(SC) = C + Ni/23 \qquad (wt\%)$$

Using this formula, the maximum permissible limit of phosphorus, in the HY class of steel considered, is about 0.005%, when CE(SC) = 0.2%.

(f) Silicon

Silicon has not shown a very clear effect on solidification cracking and it is used in relatively low amounts in HY class of steels. However, it is expected to exert a slight beneficial influence on solidification cracking as a ferrite former / 102 /, for sulphur and phosphorus will be more soluble in this matrix as silicon increases / 103 /.

WOLSTENHOLM and BONISZEWSKI / 148 / have shown that a low Mn/Si ratio increases the solidification cracking severity through two-dimensional arrays of silicate-type inclusions which tend to form intercrystalline films.

(g) Aluminium

Due to its deoxidising action it is suggested that this element has a complex influence upon solidification cracking tendency. By analogy with steel castings, BORLAND / 100 / suggests that it is harmful, at least in its first addition, combining with oxygen and inducing production of intergranular Type II sulphide films. If further additions are made it can be beneficial, for then there is production of (AlFe)S. In welds it has been found to be beneficial / 105 /.

(h) Oxygen

The oxygen action "should not be harmful" to solidification cracking, as BORLAND / 100 / stated based upon considerations related to his theory on the dihedral angle (see Section 4.2.3). A powerful crack-inhibiting effect of oxygen was also reported by MORGAN-WARREN and JORDAN / 149, 150 /.

However, it is the author's opinion that yet there is not a reasonable explanation for the oxygen behaviour and theories on microsegregation and chemical reactions effects (Section 3.2.3 - Chapter 3) should be much more investigated, although they are not directly related to solidification cracking. From these theories it seems that the effects of this element cannot be generalised.

(i) Titanium

This element is also a deoxidant and promotes ferrite formation / 102 /. It has been reported to inhibit solidifiation cracking in the relatively high range 1.5-2.0% / 145 / in HY80 steel. Also it is reported / 151 / that with the addition of titanium there is a sharp change in composition, shape and distribution of the sulphide inclusions. The form and composition of other non-metallic inclusions are also altered. With the formation of refractory complex Ti sulphide and titanium carbosulphides, along the grain boundaries, there is a beneficial influence on the resistance to solidification cracking.

In effect, it seems that titanium has varying influence, depending on welding composition, for as it was found beneficial / 145, 151-153 / it also was detrimental / 154 /, for it acts as deoxidant.

(j) Other elements

Other elements can have an influence on solidification cracking tendency in at least three ways / 102 /:

(I) By combining with impurities such as sulphur, thus preventing the formation of low melting point phases;

(II) By encouraging the formation of austenite or ferrite;

(III) By altering the ability of liquid phases to wet the matrix grain boundaries.

In CO_2 welding WIDGERY / 155 / did not notice any increase in solidification cracking due to copper addition up to 0.86%.

Molybdenum and tungsten are not found in the sulphide inclusions and the former increases the resistance to solidification cracking up to 13% while the latter seems to play no role on its tendency / 156 /.

Through its affinity for oxygen, carbon and nitrogen, vanadium has influence on shape, nature and distribution of non-metallic inclusions, reducing the solidification cracking tendency / 157 /.

Chromium tends towards reduction of solidification cracking / 133, 158 /, through its action as carbide former.

Niobium is said to act as a vigorous carbide-forming element and increases the resistance to solidification cracking / 159 /. However, this is not the general observed trend. Additions in a weld metal up to 0.13% were found to reduce solidification cracking tendency. Subsequent additions up to 1.0% improved this resistance, but further additions increased the cracking tendency / 160 /. On the other hand, GARLAND and BAILEY / 154 / found that niobium increases weld metal solidification cracking in concentrations up to 0.09%. This effect is due to the formation of FeCNb films on solidification sub-boundaries, or regions created by a slight mismatch between adjacent dendrites in the same grain.

The effect of boron has been reported to be complex / 161 / for it increases solidification cracking tendency up to ≈ 0.4%. Above this amount the susceptibility decreases. Boride phase distribution along the grain boundaries might be the explanation for this behaviour, for at 0.4% a continuous network exists. Increasing boron content interlayers of liquid eutectic form and the interdendritic spacing is increased. So, the liquid can move and fill in ('heal') gaps.

One of the few data concerning arsenic influence on solidification cracking is given by HUXLEY / 162 /. He reported that it slightly promotes cracking, being its effect 1/20th that of sulphur, and that tin also increases solidification cracking, being its effect 1/40th of sulphur.

While zirconium has been used as deoxidant in wires / 163 / little data is available as regards its influence on solidification cracking. The addition of more than 1.0% of zirconium in HY80 steel abruptly in-

creased the solidification cracking tendency / 145 / and was noticed a high segregation of this element and nickel at the interdendritic regions.

Rare-earth metals are in general beneficial to solidification cracking / 164 / and should act as desulphurising agents. Preventing the formation of low melting point sulphides, cerium improves the weld metal and HAZ resistance to solidification and liquation cracking / 139, 20 /.

4.3.2 Prediction of their effects

Throughout the analysis of the chemical elements individual effect on solidification cracking, it was clear that they interact among themselves. This interaction phenomenon is not a well established one. In general, carbide formers have a favourable influence in reducing the susceptibility of steel to solidification cracking, as we have seen in the previous section. In the strict sense of an analysis of the trend pursued by the literature, the following formulae are offered (all elements contents in wt%):

1. The WILKINSON, COTTRELL and HUXLEY formula / 133 /, as a result of TIG welding on high tensile steel sheets, in a modified HOULDCROFT test:

$$HCS = \frac{C(S+P+Si/25+(Ni/100))}{3\,Mn + Cr + Mo + V} \times 10^3$$

The HCS (Hot Crack Sensitivity) value should not be less than 4 for satisfactory welding. The authors reported that the effect of speed must be more accurately investigated.

2. The BOLLENRATH and CORNELIUS formula, as quoted by / 165 /:

$$S + P < \frac{0.007}{C}$$ for satisfactory resistance to 'SC'.

It is reported that it may be modified for higher Mn steels (in that work it was around 0.50%). Notice the year this formula was proposed: 1936.

3. The three OSTROVSKAYA formulae / 166 / reported as 'carbon equivalent', claimed to be applicable to any fusion welding process on high strength C-Mn steels, and aimed to be used as a comparison mean:

(a) $0.09 < C < 0.14$

$$CE = C + 2S + P/3 + (Si-0.4)/10 + (Mn-0.8)/12 + Ni/12 + Cu/15 + (Cr-0.8)/15$$

(b) $0.14 < C < 0.25$

$$CE = C + 2S + P/3 + (Si-0.4)/7 + (Mn-0.8)/8 + Cu/10 + (Cr-0.8)/10 + Ni/8$$

(c) $0.25 < C < 0.35$

$$CE = C + 2.5S + P/2.5 + (Si-0.4)/5 + (Mn-0.8) + Ni/6 + Cu/8 + (Cr-0.8)/10$$

4. The CSF (Crack Susceptibility Factor) of HUXLEY / 167 /, for autogenous TIG welding on high strength steels:

$$CSF = P(C+Ni/30 - Mo/10 - Cr/100 - V/100)$$

5. The CSF of COTTRELL / 168 /, produced from TIG welding on sheets of high strength steels, some of them used for rocket cases:

$$CSF \propto (P\ (C + 0.142Ni + 0.282Mn + 0.2Co - 0.14Mo - 0.224V) + 0.195S + 0.00216Cu) \times 10^4$$

COTTRELL reported that when the CSF value falls below about 20, the percentage of cracking in production is very low (near 0%). This relationship was based on the combined effect of phosphorus on ferrite and austenite stabilisers.

6. The MORGAN-WARREN and JORDAN / 149 / CFS for high strength steels, considers the effect of oxygen:

$$CSF = 42C + 847S + 265P - 10Mo - 3042\ O + 19$$

7. The latest available version of the UCS (Units of Crack Susceptibility) of GARLAND and BAILEY / 154 /. This formula was developed from Transvarestraint tests / 169 /, for high strength C-Mn steels, as reported by BAILEY and JONES / 105 /.

$$UCS = 230C^* + 190S + 75P + 45Nb - 12.3Si - 5.4Mn - 1$$

where C* indicates that C values below 0.08% should be taken as equal to 0.08%. If UCS is less that 19 for fillet or 25 for butt welds, the probability of cracking is low.

Taking the effect of weld pool shape into consideration they proposed an OCS (Overall Crack Susceptibility) factor:

$$OCS = UCS + 0.4\,\frac{WD}{U} + W/D - 15.5$$

where W is the width, D is the depth and U is the unfused ligament of the weld bead. This OCS value being reported as of 'difficult' correlation with actual welding practice.

The above quoted formulae must be looked at with great caution. The statistical significance of the data as well as the use of different steels to simulate change of chemical elements is open to discussion. Thermal history of the base material is seldom reported and, in general, specific tests and welding processes are extrapolated with excessive freedom.

4.4 Base metal behaviour surrounding the weld pool

The stress/strain pattern generated by highly localised heating and cooling which occurs in welding is very complex. This subject has received a great deal of attention by MASUBUCHI / 170, 171 / and Figure 4.4 / 170 / shows the general distribution of temperature and associated stress during welding. Thus, at least three effects are known / 170 / to happen:

(a) Transient thermal strains and stresses during welding;

(b) Transient metal movement or distortion during welding;

(c) Residual stresses and distortion after welding is completed.

As far as weld metal solidification cracking is concerned, the two first phenomena are very important, for they take place during welding.

Figure 4.5 shows another example, where actual transverse strain changes on a HY130 steel weldment are seen / 172 /. The weld was made on a 19 mm thick., 45º included angle, using MIG process and backing plate, and it is shown in some of the last runs. The word 'ARC' in this figure means the closest distance from it to the gauge location. We have to highlight the strains developed very near the weld pool. Notice that depending on the weld pool size, its trailing edge (liquidus-solidus state) may be within this zone. One clear consequence may be solidification cracking in the weld pool.

Thus, it is very important to know the base metal mechanical/metallurgical behaviour at these high temperatures and load rates, if we want to make any prediction of its effect on weld metal solidification cracking.

In this section we will analyse works which demonstrated some (or total) concern with this subject. Firstly, it will be seen those works which simulated the high temperature and strain rates in the base metal surrounding the weld pool. Here we must emphasise an important point: whilst a great number of them were designed to look for possible base metal metallurgical discontinuity effects (like grain boudary liquation, for example) we are more concerned with properties like ductility and strength.

Then it will be seen the (few) works using actual welding processes and concerned with the base metal effect on solidification cracking.

Thermal stresses are directly proportional to the product of the coefficient of thermal expansion and increment of temperature. Furthermore, variations of more than 200% in thermal conductivity can be expected, not just on distinct materials, but in identical steels, which have been submitted to different heat treatment / 173 /. Moreover, the thermal properties like thermal conductivity, specific heat and density are, to a greater or lesser degree, temperature dependent.

There is a way to assess the hot ductility behaviour of a material under rapid heating and cooling cycles similar to those experimented in a HAZ of a weld. The Gleeble machine was introduced in 1949 / 174 /. Since then much valuable information on crack sensitivity of materials

has been gained through the measurement of strength and reduction of area (ductility) of specimens during the cooling cycle.

There are at least five distinct criteria by which the hot ductility curves are interpreted / 175 /: minimum arbitrary ductility; recovery rate of ductility; recovery rate of ultimate strength; zero ductility range; zero ductility in mid-temperature range. To discuss all of them, however, is beyond the scope and interest of this work. What most concerns us is the effect the testing parameters can have on hot ductility response, and the results themselves. In general, alloys become increasingly more crack-sensitive as / 175 /:

(a) The 'peak' temperature is increased;

(b) The cooling rate is increased

(c) The strain rate is increased

Furthermore, the composition and microstructure have significant effects on hot ductility response.

Figure 4.6 shows the three-dimensional representation of the 'zero ductility plateau' / 176 /. It exists next to the weld pool and it gets smaller further away from the fusion zone, until a limiting temperature is reached when it does not exist any more. Using this concept, YENISCAVICH / 175 / was able to propose a cracking criterion which is of interest in our subsequent reasoning. Figure 4.7 shows schematically half of a weld pool moving on a thick (3D) plate of metal (plan view). Knowing the isotherms, we can draw parallel lines to the welding direction tangents to each isotherm. Then, the locus of these tangent points forms a boundary. While one area is being cooled the other is being heated, as indicated. In the former area, the metal is expanding and developing plastic compression stresses. On the other hand, the stresses on the cooling region get smaller further away from this boundary. Beyond the line of zero stress, the material is in tensile stress and eventually reaches its yield strength / 177 /. That point is difficult to define because the yield strength is another temperature dependent material property. Thus, YENISCAVICH's proposition / 175 / is: if the ductility plateau intersects the yield strength line as shown in Figure 4.8, the material cracks.

Thus, during an actual weld the part which will likely crack within the weld pool is its trailing edge, for it is in the solidus-liquidus ('mushy') state (see Section 4.2).

WELLS / 178 / states that the three major factors in the production of 'hot cracks' during welding are: restraint; cooling rate; thermal cycle peak temperature. The plastic strain imposed on the specimen is calculated for each test between the heating and cooling solidus temperatures using a uniaxial thermal strain equation. Thus, he argues that the elastic strain above the solidus temperatures is very small and the total contraction is negligible, and arrives at the following conclusions:

(a) The magnitude of the tensile plastic strain is given by the restraint against thermal contraction.

(b) The magnitude of the strain rate depends on the cooling rate;

(c) The amount of liquid present at the grain boudary during cooling is related to the peak temperature of the thermal cycle.

STEENBERGEN and THORNTON / 179 / extended the work of WELLS / 178 /. After considerations on the elastic and plastic strains involved in the process, they presented a plastic strain theory to outline the interactions during contraction. Thus, the strain at or near the cooling solidus is responsible for the initiation of 'hot cracks'. So strains generated below the cooling solidus influence crack propagation only, and the plastic strain above it governs strain for 'hot cracking'.

Figure 2.11 (adapted from / 32 / shows the high temperature behaviour of two steels, quite similar in mechanical properties (see Chapter 2) at room temperature. Both steels show nearly the same high temperature tensile strength. However, the ductility (or 'hot brittleness' as the authors of that paper prefer to call it) at high temperature shows a remarkable difference, the QT35 being ≈ 40% more ductile than the HY80 at ≈ 1100°C.

The loss of ductility phenomenon has been studied, but seems to be a difficult one. LOW / 180 / suggested it can be caused by quench-ageing, and is a consequence of fast heating and cooling of the material. PROKHOROV et al / 181 / observed the development of macroscopic plastic strain in the base metal adjacent to the weld pool by watching the relief patterns from on a steel coated with scale. They concluded that their point of initiation lies ahead of the fusion front. Microscopic strain distribution was also observed through major grain displacements.

The plastic deformation in regions of the HAZ was also studied by KASATKIN and TSARYUK / 182 /, and they conclude that it has a substantial effect on its fine microstructure. Using interferogram, these authors detected slip shears due to displacements of the grains relative to one another (not to be confused with slip caused by crystallographic shear within the grains). Displacement among grain boundaries of the order of 100-150% were detected. Moreover, there is an accumulation of dislocations at the grain boundaries, with consequently stress concentration at these places. The authors / 182 / conclude that those micro-mechanisms can have a substantial effect on the physical and chemical properties of the HAZ, and do not make any noticeable changes in the structure, when analysed by the usual metallographic methods. This assumption is also supported by OUDEN / 183 /.

WEISS et al / 184 / found that an increase in the dislocation density has no effect on hot ductility, due to a larger number of recrystallization sites.

The hot ductility can also be substantially lowered by the precipitation of nitrides / 185 / or alloy carbides / 186 /, as well as by the precipitation of sulphides.

A definite correlation between the loss of ductility in the HAZ and the total amount of nitrogen and carbon in interstitial solid

solution was found by OUDEN / 183 /. This author explains the fact through the dissolution of a significant amount of nitrides and carbides at the high temperature reached by the HAZ near the weld pool. Because there is a relatively fast cooling rate, some of the dissolved atoms will remain in solid solution. WILBERG et al / 187 / observed a loss of ductility in low carbon steels associated with decreasing Mn/S ratio. Later, is was minimised by an 'appropriate' heat treatment.

Exhaustion of ductility caused by cyclic strains was studied by SOETE et al / 188 / and DE CHAENE et al / 189 /, both groups using a moire fringe technique, but no conclusive explanations were given.

The determination of stresses and strains during welding has been relatively little studied, considering the importance of the phenomenon.

JOHN and RICHARDS / 190 / made a theoretical analysis of the transverse thermal stresses caused by the differential expansion and contractions around the weld pool, as well as MORGAN-WARREN and JORDAN / 191 /, who studied the relationship between cracking, composition and welding speed. However, theoretical studies are not in themselves sufficient and JOHNSON / 192 / using a moire fringe technique characterised the transient strain fields around the weld pool. He concluded that the straining around the arc consists mostly of shear strain, being the normal strains much smaller. He also observed that the planes of maximum shear strains are oriented almost exactly parallel and perpendicular to the weld bead, when sheets of aluminium alloy are TIG welded.

In our opinion, CHIHOSKI / 193, 194 / made the most original and complete observations on the stress and strain on cracks during the TIG welding of an aluminium alloy. Particularly interesting is the fact that the increasing welding speed may increase welding cracking, but it may, too, diminish it after some point. Moreover, he suggests that every alloy may have an optimum welding speed for a given set of conditions. Another very important conclusion that he arrived at was: "the gap change rate is more important than the gap value itself." His observations highlighted the importance of the right choice of welding parameters, and that the stress fields ahead and behind the weld pool can, under come circumstances, be of the compression type. Further, a very complex situation is created around the pool, but any extrapolation of the stress fields around it must be done with great caution. Different materials, heat flow and process can cause radical changes in that pattern. Furthermore, a high energy input, high deposition rate process can profoundly alter the importance and position given by him to the stresses in compression or tension around the pool.

The influence of the base material heat treatment and strength over the susceptibility to solidification cracking is a very unclear point not helped by the small number of works published on the subject. That it plays a fundamental role is not a matter of dispute, mainly among experienced welders who 'feel' the problem in practice, but in general cannot explain it. So far, the most important work on the subject is that made by GARLAND / 195 /, who was able to show that increasing the yield strength of the base steel leads to a sharp rise in the solidification cracking tendency, at constant chemical composition.

As his work was on mild steel (as received and strengthened by heat treatment) and on high strength C-Mn-Si-Nb steel, research on HY Q & T steels is necessary. Incidentally, in one of the experimental parts of this investigation (Chapter 8), we shall see an exploratory test which confirms the importance of the base metal stress state.

Finally, we would like to summarise the works previously seen through an hypothetical example, which will emphasise our point.

Thus, considering the facts seen on thermal properties, high temperature ductility, stress/strain fields around the weld pool, and how they interact among themselves. Now, considering two materials, similar in chemical composition and heat treatment, but possibly with different residual stress levels, and different amounts of nitrides, carbides and second phase particles and minor elements. During welding the evidence suggests that it is possible for the HAZ of these materials to show a different stress/strain response at high temperature and under rapid heating and cooling. Moreover, if at the trailing edge of the weld pool there was a tensile stress (or compression acting on a slightly different plane in each side) of the same magnitude for each, trying to 'tear' the pool, it seems that it is possible for one material to 'relieve' the HAZ more than the other, such that more strain is 'absorbed' and therefore there is less likelihood of cracking in the weld metal.

4.5 Other factors

Welding is such a complex process that it is almost impossible to find one factor causing only one effect. From what we have seen up to now, any change in one welding condition (maintaining constant the others) has immediately, to a greater or lesser degree, at least the following recognised consequences: alters the spatial weld bead shape (Chapter 3); alters the extent of the constitutional supercooling and thus the solidification mode and the microsegregation distribution (Chapter 3); alters the weld metal resistance to solidification cracking (Section 4.2.3); alters the stress/strain within and around the weld pool (previous section and Section 4.2); alters the weld pool solidification time and thus the recovery of chemical elements and amount of fused slag (as we will see in Chapter 8).

It seems to be elusive, therefore, to analyse individually all the conditions involved in the welding process, with the objective of completely establishing their effects. However, general trends can be observed for some of them, and it is this what we propose to do in this section. Factors like dendrite growth pattern and solidifcation mode were already analysed in Chapter 3, and joint angle will be discussed in Section 9.4(i).

The influence of weld bead shape on solidification cracking is relatively well documented / 104, 105/ and the importance of the width to depth ratio is highlighted. However, a definite crack-no-crack boundary is not yet clear and perhaps it does not exist in a general form for all types of materials and welding processes. The reasons for that can be found in all the facts we have seen until now. A value greater than 1.6 for this ratio is, in general, accepted as a starting point to inhibit cracking due to this factor. Also it has been

observed / 104 / that convex-topped welds are less susceptible to solidification cracking than concave-topped welds. The explanation would be that part of the solidification contraction can be accommodated from the overfill. Possible different dendrite orientation and its effect on solidification cracking tendency was not discussed by these authors, but seems to us this can be another cause.

The weld bead shape is mainly dictated by the welding conditions. Despite the great importance of their individual action, only general trends are known. When effects are compared to one another, dispute arises over the influence of welding parameters, as can be seen in the works of APPS, GOURD and NELSON / 196 / and DRAYTON / 197 /. Moreover, the influence of the use of different fluxes can be greater than expected, and commercial brands show spectacular compositional changes through the years or even for different batches, as will be shown in Chapter 6 of this study.

The increase in welding speed is often regarded as deleterious to solidification cracking. However, as we have seen in the previous section, important works such as of CHIHOSKI / 193, 194 / suggest that there is not a straight relationship between speed and cracking. Rather, this is a complex parameter, at least with a double effect, and a fact nowadays supported also by BORLAND / 106, 107 /.

The change in welding speed causes, at least, alterations in those factors mentioned right at the beginning of this section, and in the angle between the growing dendrites and the welding direction, changing the pool shape from tear drop shaped to elliptical, or vice versa (Chapter 3). So, there is some kind of 'balance' among these factors when cracking does not exist. However, the exact determination of which one is the dominant one is not an easy matter.

BORLAND and ROGERSON / 198 / felt this difficulty when examining the 'Patch' test. They found that decreasing welding speed does not necessarily decrease the 'inherent' (as they called it) crack susceptibility. However, their conclusion was that it 'appears' to increase the severity of the test. Now we could explain this increase in the severity of the test through the change in the pool shape leading to different strain fields, within and around the weld pool. Incidentally, the specimen test design is another factor to be considered, for it can induce changes in the welding speed (or other parameters) apparent influence on solidification cracking susceptibility. An interesting example of thermal analysis applied to sort out test specimen design effects on cracking is given by ROGERSON et al / 199 / when studying the 'Houldcroft' test. They concluded that, necessarily, the cracks produced in this test are of the solidification type, but that the cracking susceptibility is not proportional to the total crack length throughout the weld bead extension. BORLAND and ROGERSON / 200 / comparing the 'Patch Circular' and the 'Houldcroft' tests arrived at the conclusion that the latter is more susceptible to cracking than the former. However, the 'Circular Patch' test seems to be closer to welding practice than the 'Houldcroft'.

SAVAGE et al / 201 / in their study of HY80 bead-on-plate welds highlighted the importance of the distribution of solute accompanying solidification. They found that high welding speeds leading to a

tear-drop shaped pool is the worst condition for solidification cracking. As they produced a constant width bead-on-plate weld, they said that it was'unrestrained' or having the same distribution of tensions. Firstly, even in this condition there is a stress field surrounding the weld pool, and it changes for different welding speeds as the bead-on-plate welds made by JOHNSON / 192 / have shown in the previous section. Their conclusion is important, but they did not isolate the phenomenon as they concluded. This is surprising for some years before SAVAGE and LUNDIN / 202 / developed a test (the 'Varestraint'), in which the mechanical and metallurgical factors are almost totally independent. However, it is felt that the Varestraint test is limited to the parent metal and results cannot be extrapolated to actual welding situations.

TERRY and TYLER / 59 / reported an increase of solidification cracking with increasing speed and a subsequent reduction at higher welding speeds, stating carbon as an element which affected the speed at which crack-free welds could be made. They did not report, perhaps because at that time it was not well established, that this carbon/welding speed relationship seems to have strong links with the microsegregation resulting from different solidification modes.

The above result seems to be confirmed in part by the work of MORGAN-WARREN and JORDAN / 191 / when studying TIG welds on sheets of low alloy steels. The highest practicable welding speeds produced low crack susceptibility in all cases they investigated. They also found a complex relationship between welding speed and steel composition acting on solidification cracking. Their conclusion was that there are two opposing effects due to an increase in welding speed, viz: an increasing length of the crack-susceptible zone behind the weld pool, and a reducing level of transverse tensile stress behind the same pool.

Up to this date there is not a complete understanding of the flux effect on solidification cracking. The matter is complex and further complicated by the general lack of precise information on flux chemical compositions and physical behaviour.

Two ways fluxes can affect weld solidification cracking are through weld chemical composition and solidification pattern. Flux type affects compositional changes during welding in a number of ways / 104 / and, for example, the highly basic can reduce sulphur whilst the neutral bauxite can increase it. However, the same highly basic can reduce manganese as well, affecting the Mn/S ratio.

Also, oxygen content descreases as flux basicity increases / 203, 204 /. This can have effects as regards either the deoxidation process and further changes in chemical composition, or through mechanism not yet clear (see Section 4.3.1(h))on solidification cracking. In spite of these factors, BAILEY / 205 / did not find a simple relationship between flux basicity and solidification cracking, emphasising the fact that more than one effect is operating.

Also the amount of gas evolved from the flux during welding can have an influence on the bead roughness / 206 / and welding cooling rate / 207, 208 / and seems that there is a correlation between the ripple surface lag and the weld solidification / 77 /.

Another way flux can act is through its physical properties, for its slag is part of the interfacial system of tensions discussed in Chapter 3. Furthermore, the flux depth above the pool can influence the bead shape. An excessive depth may result in a narrow bead width, which may increase the solidification cracking tendency.

In Section 3.3.3 (Chapter 3) we have seen some principles to modify the normal solidification process, and some works specifically concerned with ways to reduce the solidification cracking tendency / e.g. 86, 90 /. In general, arc vibration, oscillation, etc., are effective methods to alter the weld solidification mode and also to overcome solidification cracking.

4.6 Summary

In this chapter we have seen some of the most relevant aspects concerned with weld metal solidification cracking in low alloy steels.

This type of crack was defined right at the beginning. It can be produced either by the combination of microsegregation leading to the presence of liquid films and stress/strain during welding, or by stress only and lack of liquid metal to fill the gap once it has been open through a susceptible (micro) structure. Its path is always interdendritic, showing dendrites on the crack surface.

The main theories on the subject were reviewed (Section 4.2), viz: the 'shrinkage - brittleness', 'strain' and 'generalised'. The latter seems to best explain the phenomenon when only considerations on factors acting within the pool are accepted. This theory claims that during the weld solidification stage there is a 'critical solidification range' (CSR) in which relative movement of the liquid and solid phases is impossible and 'healing' cannot occur. Thus, the material will crack unless it can resist the strain at this high temperature.

The developments since these theories were proposed were also reviewed. The influence of solidification mode and chemical composition was seen through the 'relative potency factor', which includes considerations on freezing and constitutional supercooling. The importance of interfacial tensions was highlighted.

The chemical composition was examined in some detail, through the individual and combined action of the elements on solidification cracking tendency. Manganese was one element which deserved a relatively lengthy discussion,for new theories do not accept Mn/S ratio as being representative for its effect on sulphur. Instead, it is proposed Mn^3/S or Mn^5/S ratio, depending how the steel solidifies. Empirical formulae were collected from the literature, with the aim to predict or analyse how the elements are generally thought to influence solidification cracking.

A relatively large amount of attention was given to the base metal around the weld pool and its effect on solidification cracking (Section 4.4). It can be concluded that this point is much more important than usually thought and that relatively little work has

been done on it. The facts showed the importance of base metal strength, heat treatment, residual stress level, and amounts of second phase particles (nitrides, carbides etc) on solidification cracking. The evidence suggested that slight difference in these factors between two materials can make them to show different response to cracking susceptibility.

It is clear that the study of welding parameters influence on solidification cracking is a difficult task, for any change in one of them (maintaining constant the others) causes more than one effect.

Weld bead shape influences solidification cracking susceptibility mainly through its width to depth ratio and convex-topped welds are said to be less susceptible to solidification cracking than concave-topped welds. Solidification contraction and different dendrite orientation are possible explanations for this effect.

In spite of welding speed increase to be regarded as deleterious to solidification cracking, it is accepted that many factors are involved (including compositional) and that it can increase crack but, also, to reduce it after some point. This suggests that it has, at least, a double effect.

The flux effect on solidification cracking is not completely clear. The ways it can affect its tendency are known: through chemical composition change and solidification pattern. However, changes in basicity could not be simply related to solidification cracking tendency. This fact illustrates the complexity of the problem.

Methods to overcome solidification cracking were reviewed in Chapter 3, through the use of arc oscillation, vibration etc. and were not again discussed here.

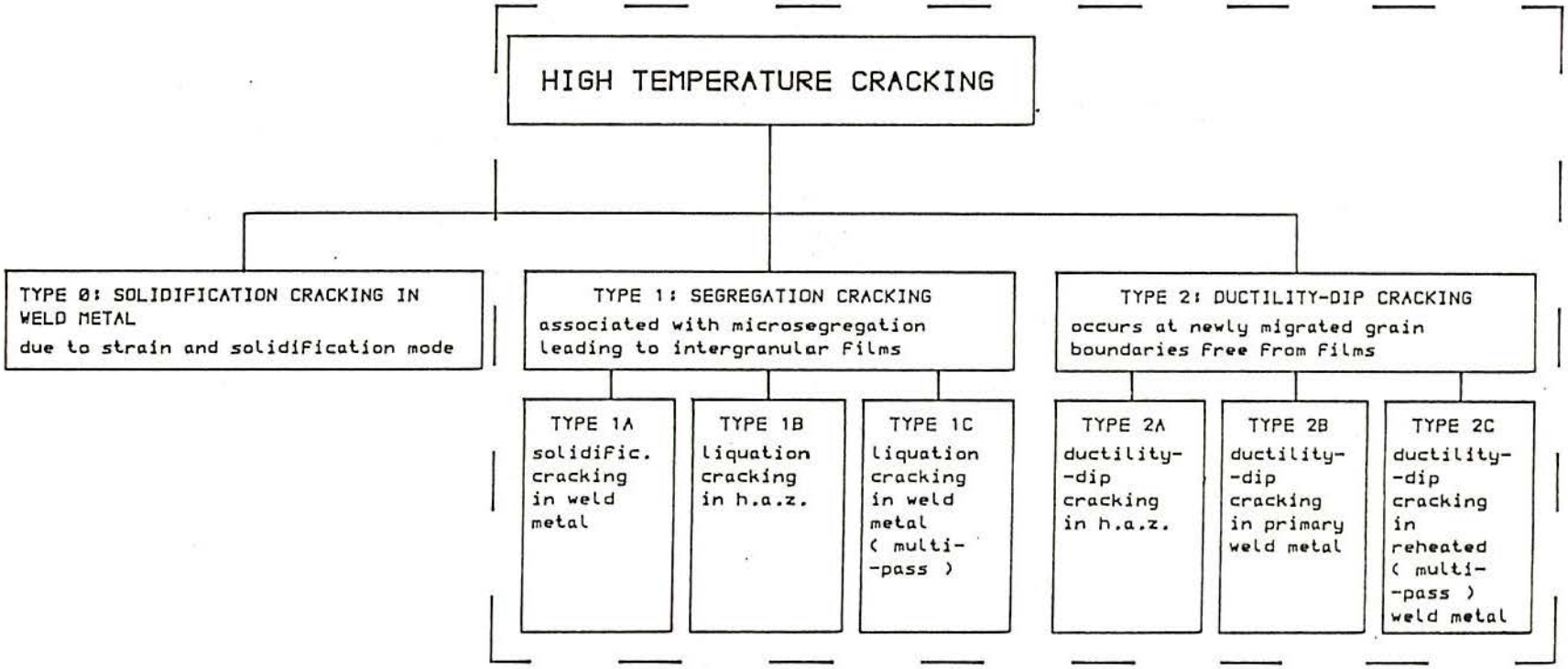

FIGURE 4.1 - CLASSIFICATION OF HIGH TEMPERATURE INTERGRANULAR WELDING CRACKS

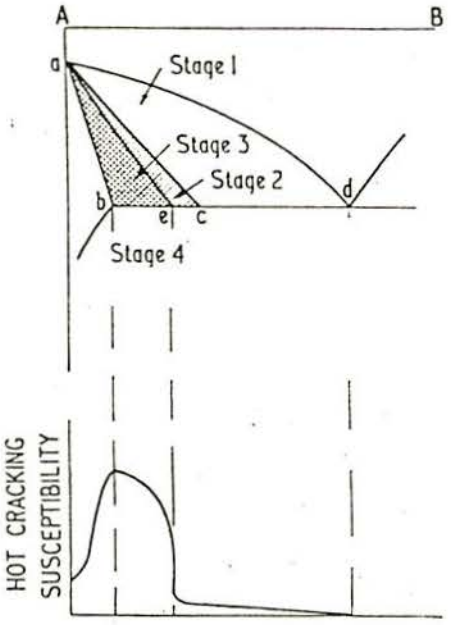

Stage 1-Dendrites freely dispersed in liquid. No cracking.

Stage 2-Interlocking of grains. 'liquid healing' possible if cracks form. 'Accommodation' not important.

Stage 3- Critical solidification range. No 'healing' of cracks possible if 'accommodation' strain exceeded.

Stage 4-Solidification. No cracking.
a-c-e Brittle range.

FIG. 4.2 - Effect of Constitutional Features on Cracking Susceptibility in Binary Systems. / 99 /.

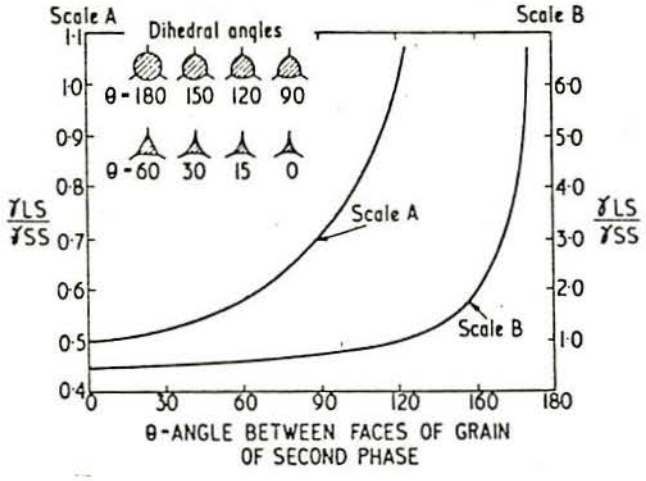

FIG. 4.3 - Relationship between Dihedral Angle and Ratio of Interfacial Energies. / 130 /. After / 100 /.

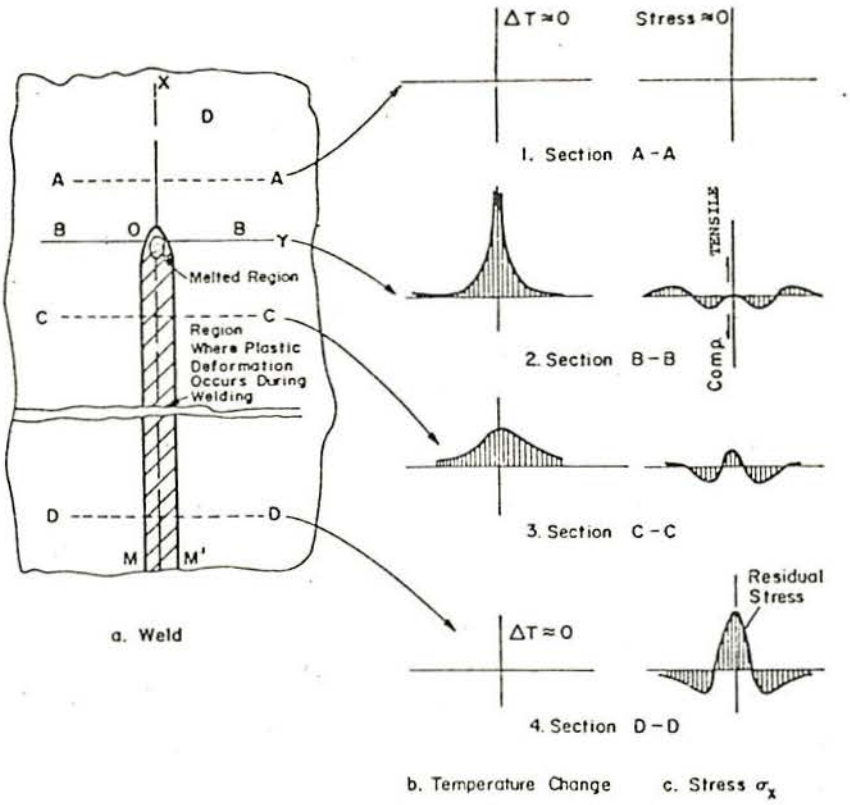

Figure 4.4 - Schematic Representation of Changes of Temperature and Stresses during Welding / 170 /

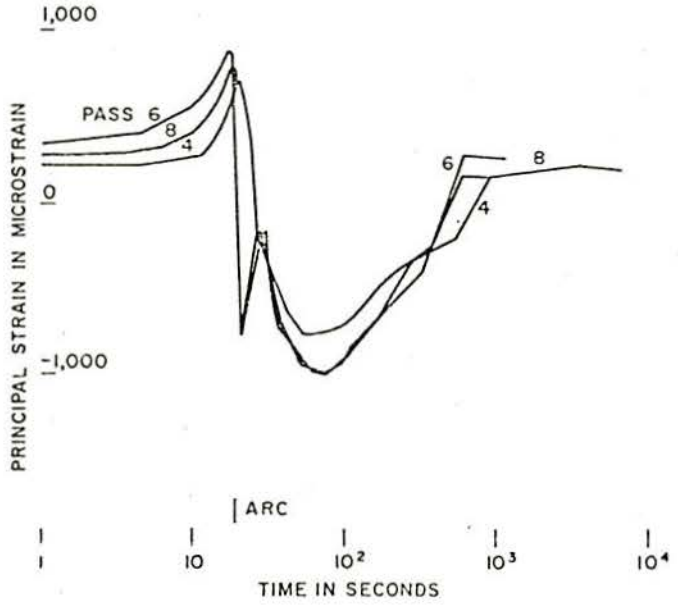

Figure 4.5 - Measured Strain changes for HY130 Weldment / 172 /

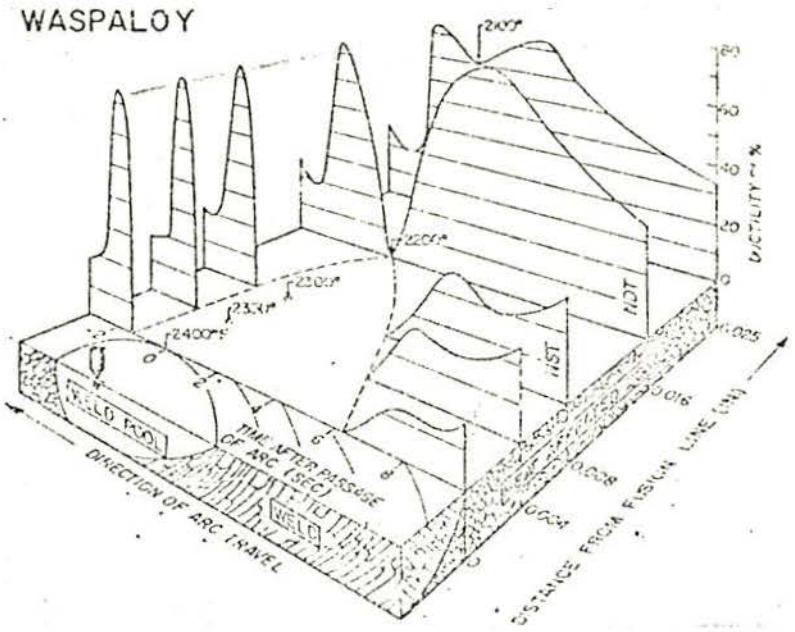

Figure 4.6 - Ductility in the HAZ of a Waspaloy Weld During Passage of Welding Arc, Showing the 'Zero Ductility Plateau' / 176 /

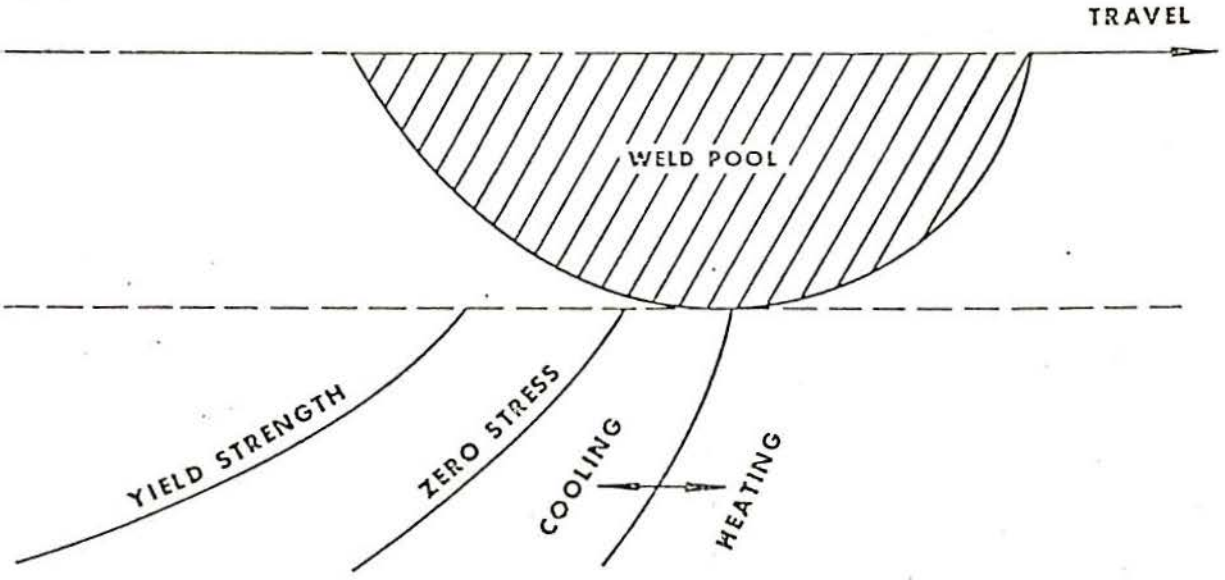

Figure 4.7 - Zero Stress and Yield Strength Lines in a Weld HAZ / 175 /

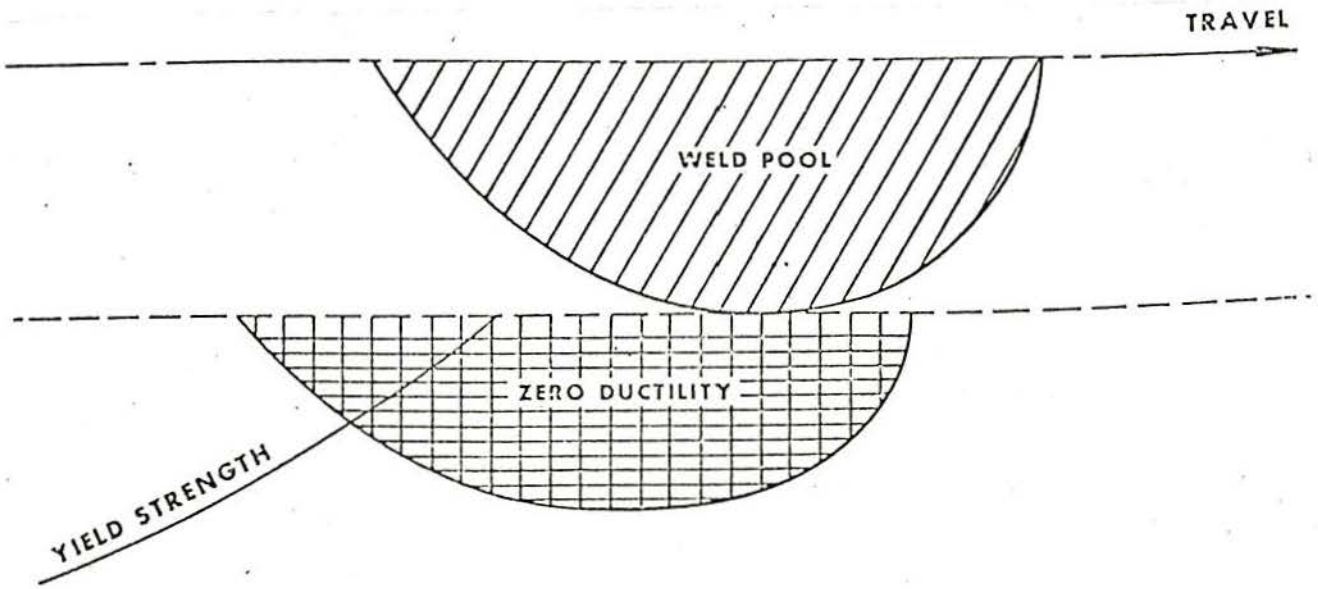

FIG. 4.8 - Yield Strength line and Zero Ductility Plateau of a Crack Sensitive Alloy . / 175 /.

5. WELD METAL TOUGHNESS AND ITS RELEVANCE: AN OVERVIEW

5.1 Introduction

In general, it is of little value to have a weld metal with very high resistance to defects such as solidification cracking, hydrogen induced cracking etc., but very low mechanical properties.

The achievement of the necessary strength in welds on High Yield Strength Quenched and Tempered steels (Chapter 2) proved not to be very difficult / 5 /. Toughness, however, showed up as a persistent problem.

Therefore, before we begin the experimental part of this investigation (next chapter) it is worth pausing to reflect, however briefly on the general circumstances at which weld metal toughness is affected. This will permit us a better understanding on results to be analysed from Chapter 6 on.

In these chapters the welds (multi and single pass) were made using submerged arc. As it is known, this is an automatic or semi-automatic process which allows highly sophisticated metallurgical factors, such as reactions between slag and molten metal, to be manipulated towards practically any desirable weld metal property, in a wide range of deposition rates.

However, this was not always so, and until 1961 the weld metal deposited by this process did not reach the minimum toughness required on HY80 steel / 5 /. The breakthrough came in that year with the electrode-fluxes combinations developed by LEWIS, FAULKNER and RIEPPEL / 209 /, which provided weld metal with toughness even better than that deposited through the MIG process.

Roughly speaking, the toughness of submerged arc weld metal depends primarily on complex interactions between the following factors: (a) wire and base metal chemical composition; (b) cooling rate, and (c) type of flux.

Of course, these factors will affect the toughness through their apparent effects, viz., primary (solidification) and secondary microstructure, residual stress, inclusions, elements in solid solution and precipitated particles.

In a way compatible with an overview, in the following lines we would like to point out some of the major factors involved in the achievement of high toughness in weld metal deposited by the submerged arc process.

5.2 The flux factor and oxygen

Basicity is a way to express the overall metallurgical effect of the flux and has been used for a long time in the steelmaking. One approach is based on the ratio of the sum of basic oxides to the sum of acid oxides. As this dimensionless number becomes higher, the more basic the flux is. As the flux becomes more complex, an immediate problem is the (exact) definition of which are the acid or basic

compounds. However, we will not discuss this point here. Another method defines basicity as being the number of free oxygen anions O^{2-} which are one of the products of the dissociation of the oxygen components of the flux / 210 /. Thus, according to the ionic theory, basicity is expressed as the excess of O^{2-} ions in 100 gr. of slag.

The improvement on weld metal toughness with reduced oxygen levels through high flux basicity was recognised many years ago / 209, 211 /, as well as the Mn/Si ratio importance on weld metal cleanness / 212 /.

However, the understanding of the principles involved in the flux influence was triggered off by the work of TULIANI, BONISZEWSKI and EATON / 203 /, who definitely proved the viability of submerged arc as a process able to deposit weld metal with toughness superior to manual metal arc. These authors proposed a new Basicity Index (BI) for the flux, considering fluorine present as CaF_2 and, also as a basic compound. The formula used is:

$$BI = \frac{CaO + MgO + BaO + SrO + Na_2O + K_2O + Li_2O + CaF_2 + \frac{1}{2}(MnO + FeO)}{SiO_2 + \frac{1}{2}(Al_2O_3 + TiO_2 + ZrO_2)}$$

Nowadays, this BI is widely quoted and used in welding, probably due to its relative simplicity and reasonable balance of the compounds. In the experimental part of this study it was the formula used for flux basicity.

In a very interesting reply to some criticisms on this formula, BONISZEWSKI / 213 / mastered a way to demonstrate the general validity of the assumptions there made, and to explain the relationships among a complex hypothetical function Z = f (deoxidants (wire/flux) energy input, microstructure, with impurities and residuals (wire/flux), and flux basicity and its effects on weld metal toughness. Figure 5.1 shows how these factors can be schematically assembled. Line AA' shows that it is possible to have some toughness with fluxes of BI so different as 1 and 3, depending on the 'Z' value, while for a same 'Z' toughness can have a wide variation as function of BI ('U' shaped curves in this figure).

There is some controversy on the ways weld metals pick up oxygen, but it seems that it is not a simple function of the oxygen potential of the flux. Rather, as studies have suggested / 214, 215 /, it is related to the stability of flux components.

Figure 5.2 illustrates the data collected by EAGAR / 214 / relating to BI and oxygen in the weld metal. He calculated the former factor through the formula given above / 203 /, with and without CaF_2. As can be seen, the shape of the curve is only slightly shifted in value when CaF_2 is not included in the formula, and this may be a reason to use this formula in this way, for assuming CaF_2 as a neutral component is a fact supported by thermodynamic measurements / 214 /. Also in Figure 5.2 is shown that after some basicity value ($\sim$1.6 and $\sim$1.2 in Figures 5.2 (a) and (b) respectively), the oxygen level is constant (250 ppm, or 0.025%)), not following the increasing in BI. To complicate even more this picture, the BI will also affect silicon and

manganese recovery, desulphurisation etc. / 203 /, and carbon content of the filler metal and welding parameters can also affect oxygen / 216 /.

The important work of GARLAND and KIRKWOOD / 217 / pointed out that the energy input may overlap the metallurgical effect of the flux. At 7.6 KJ/mm, for example, a flux with BI = 0.78 had higher Charpy V-notch fracture absorbed energy than a flux with BI = 3.0 for all test temperatures. They explained this behaviour based on the relative ease of microvoid coalescence in the two systems. Examining the welds made under basic flux only, they are much more clean and depend critically on cleavage resistance. At low energy input (1.9 KJ/mm) this cleavage resistance is good, for the microstructure has not upper bainite, little lath martensite and its size is (likely) relatively small. At higher energy input (7.6 KJ/mm), this microstructure has poor cleavage properties for it is coarser and it has been increased upper bainite and lath martensite content. So, in the matrix produced by low energy input the microvoid coalescence mode of fracture can be one of the factors involved in the fracture process, as temperature is increased and it has good resistance to it at low test temperatures due to its high cleavage resistance. However, at high energy input the microvoid coalescence mode will participate at very high temperatures only. At low test temperatures it will depend critically on the cleavage fracture mode, which is very poor, as we have previously seen. In both cases, the welds made under acid flux are dependent on microvoid coalescence mode of fracture and will be more resistant to the impact test. However, in this same work / 217 / it was advanced a way to overcome this problem in the basic flux welding, using wires microalloyed with Mo-B-Ti.

Therefore, the overall picture of flux effect on toughness is far from being complete, for certainly there are many complex interactions still not explained.

5.3 The microstructure and chemical composition

Sulphides and oxides are the principal types of non-metallic inclusions found in welds. They affect the microvoid coalescence (ductile) fracture mode, as have been shown by WIDGERY / 218 /, and there is a general decrease in upper shelf Charpy energy absorbed with an increase in inclusion content / 219 /.

The works of LEVINE and HILL / 220 / and CHOI and HILL / 221 / have shown that the microstructural phases order of appearance as the temperature decreases in welds is: Grain Boundary Ferrite; Ferrite with aligned M-A-C (ferrite containing Martensite-Austenite or Carbide phases); Acicular Ferrite; Pearlite; Bainitic lath structure; and Martensite. In Chapter 8 we will analyse these microconstituents but a detailed description for each of them may be found in the works either of ALCANTARA / 222 / or DOS SANTOS / 223 /.

When the fracture mechanism is by cleavage, the toughness may be increased by increasing the percentage of acicular ferrite at the expense of other microconstituent(s) / 220 /. Thus, the lower shelf toughness depends on chemical composition, microstructure and yield strength, as can be assessed from DOLBY's work / 224 /. The oxygen

level is still very important because as ABSON, DOLBY and HART / 225 / have shown, the intergranularly nucleated Widmantatten ferrite (acicular ferrite) depends upon number, size and appropriated dispersion of oxide inclusions. The same author advanced some of the complex ways oxygen acts on the CCT weld diagram. Also COCHRANE and KIRKWOOD / 226 / have shown that oxygen can increase the ferrite nucleation rate and help lamellar ferrite nucleation at the austenite boundaries. From these works it can be inferred that there is an optimum range for high acicular ferrite content formation around 300 ppm (or 0.03%) of oxygen.

There is still another microstructural effect on weld metal toughness, as first pointed out by GARLAND and KIRKWOOD / 204 / through the deleterious formation of pools of martensite microphase, forming from austenite entrapped between ferrite plates. These authors also have made perhaps the first attempt to correlate, using vector models, metallurgical factors and toughness.

As regard alloying influence on toughness, only general trends are known, for the basic factor microstructure cannot be exactly foreseen due to interactions among the elements and different responses for different cooling rates / 96 /. In deposits not containing microalloying elements, DOLBY / 227 / states that elements such as Mn, Mo, Ni, Si and Cr influence toughness in two main ways: (a) particularly Mn, Mo and Ni promote acicular ferrite and eventually martensite at high alloy content; (b) these elements increase yield strength as a result of the changes in microstructure and through solid solution hardening effects.

However, it is not possible to have continuous improvement in toughness by increasing alloying, for it starts to fall after a critical level is reached / 227 /. This is due to the increase in yield strength by solid solution hardening and the promotion of brittle martensite regions which may segregate.

Furthermore, as DOS SANTOS / 223 / pointed out for manual metal arc, with the increasing in alloy content the microstructure becomes more sensitive to changes in chemical composition.

The effects of microalloying elements on toughness seem to be strongly dependent on both, the addition level and other elements present in the metal.

As will be seen in Chapters 6 and 8, there is only one microalloying element that seems to be significantly different in both base steels there studied, and that is vanadium. From DOLBY's review / 228 /, amounts of up to 0.05% V combined with weld cooling time (800/500°C) less than 50s and deposits with Mn greater than 1.1% or alloyed with Ni, Mo etc. leads to a decrease in Charpy V-notch transition temperature. It is interesting to quote that this is basically the composition of single run welds on Q2N steels, with 5 times more vanadium than in welds on HY100 steel, and the cooling rate of all welds was less than 50s.

In spite of all difficulties involved in its production, it is nowadays quite possible to have welds with relatively high toughness

as we will see in Chapter 7. However, it also will be shown the dramatic fall in toughness as the energy input increases.

Having the capability to decide upon the microstructure, there is still another decision to be taken, as regards fracture toughness. One approach is to produce a structure resistant to initiation of a running brittle crack from any defect likely to be present. The other is to have in this structure areas capable of arresting a crack already propagating out of a localised region of low ductility. As KEELER and GARLAND reported / 229 /, it seems that at present the former philosophy is that adopted in offshore platform for oil production.

5.4 Summary

This overview on weld metal toughness was directed mainly to submerged arc process, but the general principles are also applied to any welding process.

Flux basicity is an important factor and, in general, basic type produces tougher welds. However, there is a complex relationship with energy input, which can overlap the basicity effect. The level of oxygen content is, likely, an effect of the stability of flux components and has an important influence on the formation of the acicular ferrite microconstituents. High percentage of this microstructural phase leads to higher toughness at low temperatures. However, at relatively high temperatures the fracture mode is through microvoid coalescence and inclusions exert the principal role.

Microstructure and chemical composition have not a completely established relationship, for factors such as weld metal cooling rate, oxygen content and interactions between the elements play an important role to decide the microstructural phases, and only general trends can be foreseen.

The present philosophy seems to be to produce a structure resistant to the initiation of a running brittle crack from any defect likely to be present.

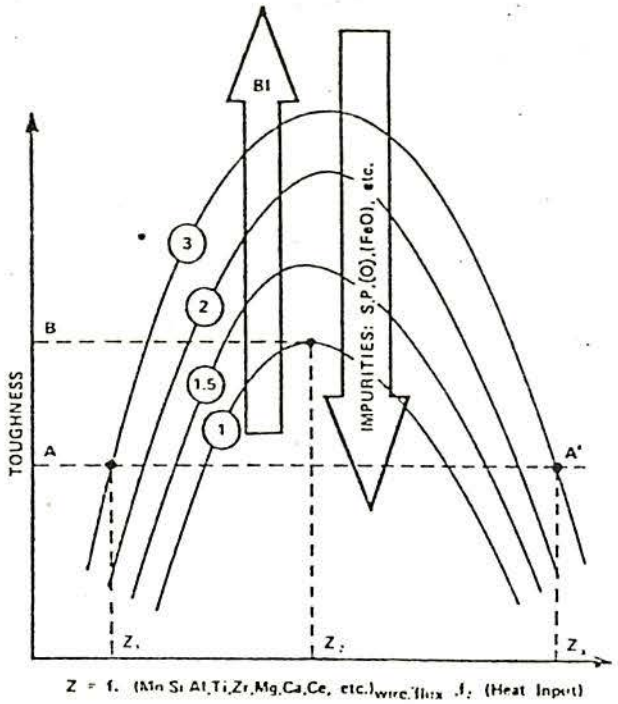

Fig 5.1 Schematic Representation of the Complex Effect of Flux Basicity, Deoxidants in Wire and Flux, and Residuals in Wire and Flux on the Toughness of Weldmetal / 213 /

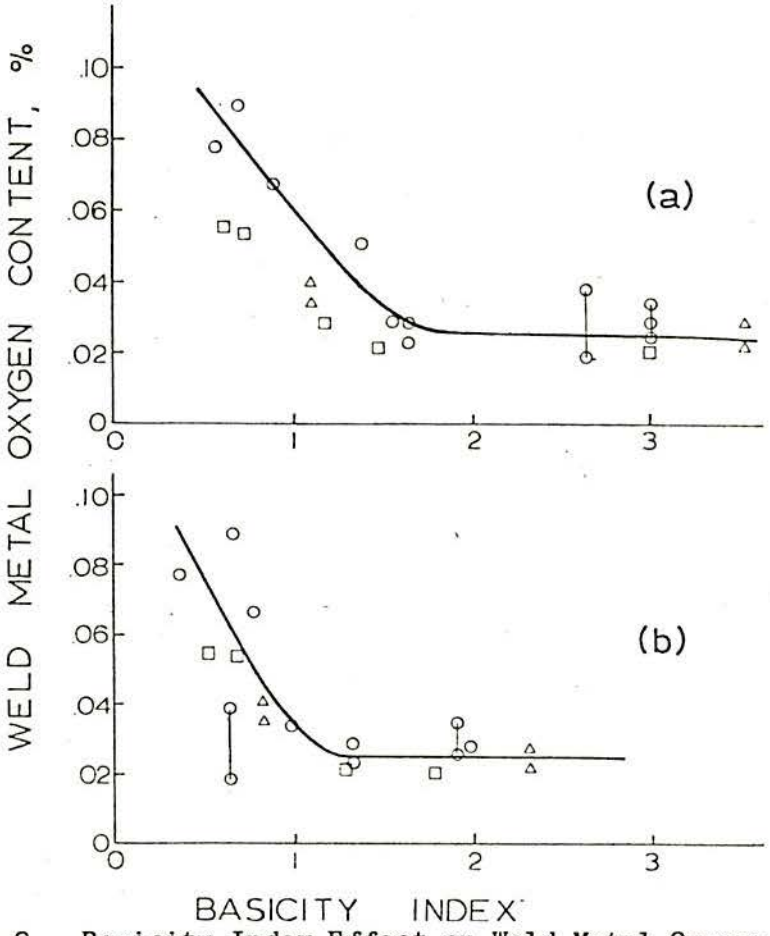

Fig 5.2 Basicity Index Effect on Weld Metal Oxygen Content / 214 / (a) BI Calculated Through / 203 / . (b) BI Calculated Using the Same Formula, Without CaF_2.

6. MATERIALS AND EXPERIMENTAL TECHNIQUES

6.1 Equipment and procedures description

6.1.1 Metallography and microanalysis

When required, the polishing of the specimens was done in the traditional way. The cut sections were flattened and roughly polished on emery paper under running water. Then they were polished in diamond paste from 6 microns to 1 micron (or 1/4 micron in some cases).

The etchants used and the names they were referred to are:

- Nital: A 2% solution of nitric acid in methanol. Used for general metallographic analysis of the secondary microstructure;

- SASPA: a hot (~60°C) saturated aqueous solution of picric acid and drops of 'Teepol' (wetting agent). Used to reveal the primary (solidification) macro/microstructure.

- Ammonium Persulfate: A 5% aqueous solution of ammonium persulfate. Used mainly to disclose weld metal microsegregation and to show primary microstructures.

- Sodium Bisulfite: a two-stage etchant consisting first of very light nital etch, followed by a 3% hot (~37°C) aqueous solution of sodium bisulfate and drops of 'Teepol' (wetting agent). This two-stage etchant reveals weld metal alloy-rich pools and bands, and the unmixed zone at the fusion boundary / 79 /.

The solidification cracking test welds had the average dendrite size measured on a longitudinal centreline section (plane parallel to the welding direction) at half bead height. The SASPA etchant was used at a magnification of x 100. The 'mean lineal intercept method' was utilised for the measurements (1 mm line length) and not less than 200 interceptions were counted in each weld.

A Leitz Panphot microscope was used to perform the optical (light) metallography, with maximum magnification of 1,000 x.

A Cambridge Stereoscan 600 Scanning Electron Microscope (SEM) was utilised for some metallographic studies on polished specimens, as well as in all the fractographic research. It has a resolution of 250 Å and a range of magnification from 20 to 50,000 x. Attached to it there is an Energy Dispersive Analyser, which was used to identify some second phase particles, and in the trials to record some possible matrix segregation.

A Transmission Electron Microscope (TEM) Jeol - JEM 200 B was used for inspection of the secondary microstructure. It has a resolution of 4-5 Å and a magnification range from 1,000 to 180,000 x.

6.1.2 Preheat, interpass temperature and plate preparation

The submerged welds were made using a Hagglunds Type L SIT1200 transformer rectifier rated at 84 KVA giving 1200 A, 44 V DC output, and a drooping static power characteristic. This unit was connected to a Hagglunds HSA 150 voltage controlled wire feed system. The welding head was held stationary whilst the test pieces were traversed beneath it.

All specimens welded throughout this work were preheated at 120°C and those used for all-weld mechanical tests (multipass) the interpass temperature was maintained at 145°C. A 0.5 mm diameter chromel/alumel thermocouple pair was flash welded to the plate down face, 100 mm from the weld centreline, and a COMARK Electronic Thermometer Type 1602-3 was used to control these temperatures.

The preheat was obtained through the use of electrical heaters which covered all specimen surface, and complete thermal insulation. For the solidification cracking specimens the heating rate was 45°C/h, whilst in the bigger plates used for mechanical tests, it was 30°C/h.

The grooves were flame cut and smoothed by grinding. Just before welding they were brushed and degreased.

6.1.3 Thermal analysis

Weld metal thermal analysis was performed using the wellknown technique of "harpooning", or injecting a thermocouple into the weld pool behind the welding electrode, as first shown by GRANJON and GAILLARD / 230 /. Weld metal temperature measurements were made using a 0.5 mm diameter 30% Rhodium/Platinum - 6% Rhodium/Platinum thermocouples, heated in twin-bore alumina insulation. In short, the electromotive force generated at the thermocouple junction by the weld pool heat is amplified/ filtered. The signals are stored in a Transient Recorder DL 901 (DATALAB), whilst an oscilloscope (PHILIPS PM 3230) monitors this operation. The data are then coded through a paper tape punch (DATA DYNAMICS 1133 series). Finally, a suitable computer program is run using the data which were previously fed into the computer from the punched paper tape. The cooling curve and its first derivative are then generated and plotted. The equipment in present use was developed by RODRIGUES / 231 /.

This technique is particularly difficult to apply to submerged-arc welding for two main reasons: the large amount of flux covering the pool, and the fact that the thermocouple, in our laboratory, is hand implanted. Both problems make accurate and repeatable positioning of the thermocouple within the pool very difficult.

6.1.4 Mechanical tests and hardness

Mechanical tests and hardness were carried out on the multipass welds (Chapter 7) made exactly for this purpose, whilst hardness only was done on all single pass weld solidification cracking tests. The exact specimen positions in the weld bead are shown in the related Chapter (7 and 8).

All-weld metal HOUNSFIELD number 17 (32.1 mm gauge length; 9.07 mm diameter) standard tensile test specimen was used. The tests were

carried out at room temperature (~20°C) in a SAML. DENISON & SON LTD machine, with 6.7 ton capacity. Two specimens were tested for each welding condition at a strain rate of 2 mm/min (0.033 mm/s) and followed BS 18 / 232 /. The specimens were taken from the weld centreline, with their centres located at the weld middle height.

Charpy V-notch specimens were tested in accordance with BS 131 / 233 / for all welding conditions of Chapter 7 (multipass welds), at temperatures of 20, 0, -20, -40, and -80°C. The latter four temperatures were obtained through an appropriated mixture of acetone and liquid nitrogen. The specimens were immersed into this mixture, and they were broken only 15 minutes after reaching the thermal equilibrium. The tests were done using a pendulum impact tester manufactured by LOSENHAUSENWERK, with a capacity of 217 ft-lbs (294.4 J). The temperature control was done immersing a chromel/alumel thermocouple in contact with one specimen, using the same device described in Section 6.1.2 for preheat temperature measurement. The Charpy specimens were taken from the weld centreline, 2 mm below the last run, and a detailed explanation is given in Chapter 7.

A Vickers-Armstrong Ltd machine with 5 Kg load and a 136° diamond pyramidal indenter was used for the hardness tests. They were done on transverse bead sections of each welding condition, at the middle bead height and from top to bottom. The total number of indentations was ~25 for the multipass (Chapter 7) and ~15 for the single pass (Chapter 8) welds.

6.1.5 Chemical analysis and dilution

The chemical analyses were supplied by an independent laboratory, utilising spectrography for the main elements. The analysed area on the specimen surface covered 78.5 mm^2 (a 10 mm diameter circle). Nitrogen was analysed through a LECO TN 15 automatic determinator, and a LECO RO 17 automatic rapid determinator was used for oxygen analysis, both instruments being connected to a LECO EF 10 furnace. It is known that the analysis of the latter two gases involves melting the samples in a crucible (usually graphite) and a carrier gas technique.

The above referred to laboratory supplied the following list of 'standard deviation' (SD) for some elements:

- carbon: ± 0.01%
- silicon, manganese, chromium, nickel, molybdenum: ± 0.02%
- sulphur and phosphorous: ± 0.005%
- vanadium and niobium: ± 0.002%

The weld dilution was estimated through two different methods, viz, from macrophotography and from chemical analysis taking the nickel recovery as 100%. The latter process is highly reliable / 234 /, whilst the former showed up a great error (~15%) in the areas measurements of known geometrical figure (rectangle) used to test its reliability. Many sources may be responsible for this deviation. Among them, different print enlargement each time the negative has to be used; not uniform printer paper thickness; errors due to weighing and paper sections not exactly cut.

Using the same known geometrical figures, areas were measured using a fixed arm Planimeter produced by ALLBRIT. The measured areas showed up errors as high as 25%. This kind of instrument has in general a gliding correction for both axes (X and Y), but not this one in consideration, which had only correction for one axis. This is believed to induce the high deviation from the average value.

Therefore, when chemical analysis was available for the weld the dilution was estimated through it and Appendix A shows in detail how the dilution and related (small) error is obtained. Also in that Appendix is found a derivation for the 'expected' amount of any chemical element and its error. In this work the 'expected' amount is the one that would be obtained if reactions of oxidation and reduction had not operated in the welding process. When chemical analysis was not available, the macrography was the technique preferred to estimated dilution.

6.1.6 Cracking and bead geometry measurements

The bead and cracking dimensions were measured twice. First, a vernier was used on the actual specimens, for all welds had a size that allowed such measurements. Then, the measurements were repeated using a Vickers Projection Microscope, manufactured by Cooke Troughton & Simms. The three times magnification provided by this projection microscope, for our deception did not improve the results and they held within the error range of $\pm$ 0.5 mm.

6.2 Base steels characterisation

6.2.1 Chemical composition and mechanical properties

All the experimental work was carried out on two steel plates, each measuring 2,400 mm x 910 mm x 33 mm and denominated Q2N and HY100.

The chemical composition and mechanical properties of both materials, as provided by the supplier, are in Table 6.1 (notice that the elements are given in wt% x 10^{-2}), together with the US specification MIL-S / 235 / and ASTM / 236 /. One of the plates (Q2N) arrived with a relatively heavy distortion in part of its length (around 200 mm from one edge) and this portion was discarded.

The comparison between the supplied and Cranfield analysis shows up a noticeable difference only in the amounts of carbon for both steels (being higher in the Cranfield analysis) and for aluminium (again, higher in the Cranfield analysis). All other differences were considered too small to deserve comments. It is worth to mention that the element carbon was analysed three times (in two independent laboratories) in the Q2N steel and its level confirmed to stay within the range 0.15 - 0.17%.

Thus from now on 'chemical analysis' of parent steels in this work is defined by Table 6.1 (Cranfield analysis) and Q2N or HY100 steel to the plates in our possession on which the welds were made.

As far as chemical analysis differences between both steels are concerned, attention is drawn to the elements carbon, chromium, nickel and vanadium. As seen in Table 6.1 the Q2N steel has seven times more vanadium than the HY100 steel, which shows less nickel, but more carbon and chromium (the difference of this last element being considered not

great at this range). As we have seen when Solidification Cracking (SC) theories were described, perhaps more important than the content of each chemical element alone, it is the 'balance' among them. This 'balance' together with other factors already presented, can have a profound influence on the welds susceptibility to 'SC', and should always be carefully analysed.

It is important to point out that there are some differences in chemical analysis between the quoted Standards and the actual analysis of both steels. The HY100 steel shows up carbon just on the maximum allowable by MIL-S-16216 (allowing the possible 'SD' for minus), as well as nickel, which is slightly above the ASTM A 543-B. On the other hand, the Q2N steel has manganese just on the maximum allowable (considering its 'SD' for minus), and vanadium, which is well above (at this range) of the maximum, both elements by MIL-S-16216. The Q2N steel has other differences, when compared with ASTM A 543-B. The manganese is just above maximum limit, chromium is slightly below the minimum, vanadium is well above the maximum and nickel is 0.24% above the maximum allowable by this standard. There is no reference in the above quoted Standards to the elements oxygen and nitrogen.

On the mechanical properties side, following the results given by the supplier, all of them far exceed the minimum Standards, noticeable being the relatively high toughness values quoted for both steels at -84°C.

The formula for carbon equivalent used is that developed by KIHARA et al / 237 /, and adopted by the NCRE (UK) as shown by WINN / 238 /.

$$CE = C + 1/6\ Mn + 1/24\ Si + 1/40\ Ni + 1/5\ Cr + 1/4\ Mo$$

all elements in wt%.

Thus, considering the Standard Deviation (SD) for each element:

For the HY100 steel: $CE = 0.79\% \pm 0.02\%$
For the Q2N steel: $CE = 0.74\% \pm 0.02\%$

the difference (if it actually exists) is so slight that it does not deserve comment.

6.2.2 Metallography, inclusions identification and hardness

Both steels were carefully analysed through three distinct techniques: light microscope, Scanning Electron Microscope (SEM) and Transmission Electron Microscope (TEM). Furthermore, an Energy Dispersive Analyser was used to identify inclusions and possible matrix segregation.

The Q2N and HY100 microstructures (taken transverse to the rolling direction) are shown in Figure 6.1 and Figure 6.2 respectively. Etching in Nital and 100 x magnification shows up few details, but they give a general view of the second phase particle distribution and grain size. Some black spots on both microphotographies are just the result of a differential etching action, probably due to some chemical or metallurgical inhomogeneity. However, Figure 6.2.(b) shows, at a larger magnification, the central area of Figure 6.2 (a) which seemed to hold some inclusions. In fact, relatively large second phase particles were found in the HY100 steel. The elongated ones measuring around 20 micros in length and the spherical shaped ones more than 6 micros in diameter.

This fact confirmed former findings / 3 / that the HY100 steel has, apparently, a larger number of inclusions than the Q2N. Colonies like this were not found in any of the sections taken from the Q2N steel. To confirm the origins of these inclusions, SEM and Energy Dispersive analyses were performed on both steels. From an area as close as possible to that in Figure 6.2 (b)(which shows HY100 microstructure), a SEM image was recorded (Figure 6.3 (a)). Details of it are shown in Figures 6.3(b and e). Using the Analyser, 'maps' showing elements distribution were made. Figures 6.3 (c and d) show the distribution of manganese and sulphur respectively in the grey area. Furthermore, through the 'point' technique, the presence of titanium and calcium was detected in this same area. The amounts were, however, very small, not enough to be mapped. In the 'black' portion of this complex inclusion there is a relatively large amount of aluminium and traces of magnesium. Figure 6.3 (e) (SEM) shows another detail of Figure 6.3 (a) (right bottom corner) and the aluminium trace can be seen in Figure 6.3 (f). This is practically a pure oxide inclusion and no other elements were detected. Oxides of this type were found in the Q2N steel as well and, therefore, they can be taken as typical for both steels. However, we were unable to find any colony in the Q2N steel, and in general the second phase particles of this steel were smaller.

The microstructure of both steels (Figures 6.1(b) and 6.2(b))is typical of a quenched and relatively high temperature tempered low alloy steel. There is a ferritic matrix containing a dispersion of carbides, (as will be seen in the TEM). The grain size, obtained by comparison with ASTM charts, was estimated to be around number 9.

Figure 6.4(a,b) shows the Q2N and HY100 steels microstructures, respectively. The technique now employed ('pseudo-relief'), allows a better view of the surfaces and highlights the fact that the ferrite lath like structure remained (inherited from martensite). Therefore, the tempering temperature for both steels was around 600°C, for at higher temperatures the ferrite should begin to recrystallize.

Some difference in microstructure between both steels became noticeable at much bigger magnification. At the carbide level, as shown in Figure 6.5 (TEM), their size and distribution are clearly distinct. Figure 6.5 (a, b) gives a general view, and at this magnification (x 4K) the HY100 steel (Figure 6.5 (b)) shows carbides distributed all around the surface, whilst the Q2N shows them (Figure 6.5 (a)) sited mainly at grain boundaries, as confirmed at higher magnifications in Figures 6.5 (c-e). Moreover. the carbides in the Q2N seem to be bigger than in the HY100.

A 'banding' phenomenon in the microstructure was observed, and can be seen in Figures 6.6 (a, b) for both steels. The special etchant used discloses that heterogeneity and possibly the light bands are higher in alloy content than the dark bands / 79 /. However, we were unable to detect any chemical heterogeneity of this kind using our Analyser. Furthermore, caution must be taken when comparisons of these bands between the steels are done. After many etches at different stages in our research, we conclude that they cannot reliably be compared. This is because many factors are involved on the final resultant etching, making it just a qualitative one.

The average hardness of these steels was 277 HV5 for Q2N and 290 HV5 for HY100. However, microhardness survey (300 gm) showed an average of 271 HV for the 'white' band and 256 for the 'dark', in the Q2N steel. For the HY100 steel, these averages were 280 HV for the 'white' band and 290 HV for the 'dark'.

6.2.3 Comments

Both steels have a quite similar chemical composition and mechanical properties. However, a careful observation of the final 'balance' among the elements leads us to a different point of view over the resultant effect of them. The Q2N steel has less carbon, and much more vanadium than the HY100, the levels of nitrogen for both steels being nearly the same. It is shown by COOLEN et al / 239 / that the same yield strength can be obtained in two ways: without vanadium but a low finishing temperature, or with vanadium (0.05%) and a high finishing rolling temperature. The second method is the preferred, because better tensile and impact properties are obtained.

It is possible that the Q2N has more carbon combined with carbon-nitrides than the HY100. It is known / 28 / that a number of alloying elements in steel can form carbonitrides (or borides) which are thermo-dynamically much more stable than cementite. As can be seen in Figure 2.2 / 28 /, the enthalpies of formation place the iron carbide as the least stable compound situated at the extreme right of the diagram. Thus, stronger carbonitride former elements are Cr, Mo, V, W, Al and Ti. Consequently, cementite will normally only form when the carbon concentration exceeds that needed for those elements / 27 /.

Thus, let us follow the idea advanced in Chapter 4. There it was said that carbide formers have a favourable influence in reducing the susceptibility of steels for Solidification Cracking (SC). Or, that ferrite stabilisers suffer the effect of elements like P and are promoters of 'SC'. In that chapter, too, was listed a number of formulae which are said to be a 'guide' in relation to 'SC', being able therefore, to give us a 'hint' on the resultant 'balance' from the combined action of the elements. Thus, what follows is the direct application of three of those formulae, elected because they were developed for use in high strength steels. Caution, however, must be taken when using these formulae. They were obtained under welding conditions, parent steels and consumables different from ours.

(i) The WILKINSON, COTTRELL AND HUXLEY / 133 / formula:

Q2N steels: HCS = 2.9

HY100 steel: HCS = 4.4

The HCS (Hot Crack Sensitivity) of the HY100 is greater than the Q2N. Moreover, the HCS for the HY100 is above 4, the limiting value for satisfactory welding.

(ii) The COTTRELL / 168 / formula:

Q2N steel: CSF = 74.4

HY100 steel: CSF = 102.2

The CSF (Crack Susceptibility Factor) is above 20 for both steels, and this value is said to be the safe one for welding. Nevertheless, the CSF value for HY100 is 27% greater than for the Q2N.

(iii) The MORGAN-WARREN and JORDAN / 139 / formula:

Q2N steel: CSF = 15.6

HY100 steel: CSF = 23.3

Again the HY100 steel seems to be more prone to 'SC' than the Q2N steel (its CSF is 33% greater than that for the Q2N steel). Notice that in this formula oxygen acts as a strong beneficial element.

Therefore, by the analysis of the above results, the Q2N steel should show less susceptibility to 'SC' than the HY100 steel. However, these are empirical 'hints' only and cannot be taken as definite answers.

The carbide size, shape and distribution are clearly different between these steels, as we have seen. It is unwise to attempt the identification of carbides by their shape only, and the identification (chemical and crystallographic) of (probably) complex carbides and nitrides is a very time-consuming research without guaranteed positive results. Furthermore, this is not one of the objectives of our study on weldability.

The Q2N steel shows its carbonitrides, in general, to be bigger than those in HY100 steel, and it does not have the very thin needle-like aligned structures that the latter steel has. Furthermore, the former steel seems to have the carbonitrides mainly along the grain boundaries. DOLBY / 240 / in his study of HY80 and QT35 steels has found that carbides distributed on all the surfaces are indicative of tempered martensite, as they are in the HY100. On the other hand, the same author / 240 / stated that carbides mainly at high angle boundaries can be due to mixed tempered martensite and bainite structures. In fact, there is a slight difference in macrohardness between the steels, the HY100 being the hardest. The microhardness survey confirmed this trend, but they contradict one another in that for the Q2N the 'white' band is the hardest, whilst for the HY100 it is the 'dark' which shows higher microhardness.

6.3 Welding consumables characterisation

6.3.1 Wires

Wires from two different manufacturers were used throughout this work: the OERLIKON S3 Ni Mo 1 (4.0 mm diameter), produced by 'Welding Industries Oerlikon Buehrle Ltd' (Switzerland), from now on referred to simply as 'OERLIKON S3', and the LINDE 95, produced by 'Union Carbide Corporation - Linde Division' (USA) in two different diameters (4.0 mm and 1.2 mm).

The wires' chemical analyses are shown in Table 6.2. The 1.2 mm diameter LINDE 95 was used for welds with 'cold wire' addition and will be discussed in Chapter 9. Both 4.0 mm diameter wires have shown some degree of kinking, higher than that normally expected for wires of this diameter, in the opinion of an experienced technical adviser / 241 /. As this class of wire cannot be copper coated, special precautions against corrosion must be taken once the pack is open.

There are striking differences in the chemical composition of both wires, as can be seen in Table 6.2. There is more carbon, manganese and molybdenum in the OERLIKON S3 than in the LINDE 95, whilst the latter wire has more nickel, silicon and chromium than the former.

6.3.2 Fluxes

Two types of agglomerated fully basic fluxes were used throughout this study. Both of them made by the same producer (OERLIKON). One flux is the wellknown 'OP41TT' and the other the 'OP121TT', which contains more carbonate(s).

Table 6.3 shows their specifications as drawn up by the producer. However, this Table shows up what the Basicity Index (BI) and the chemical composition should be. In fact, a quick look in the available fluxes chemical compositions listed in the literature shows a different figure. Table 6.4 shows the wide variation in chemical composition both fluxes experience, which reflects in their BI (Table 6.4(R) has the quoted References in Table 6.4). So, Figure 6.7 (a) shows the trend pursued by the BI (OP41TT) through the years 1974 to 1980, which in spite of the limited amount of data indicates that there is a definite tendency to higher basicities. For the OP121TT flux little data is available, but it shows differences in the BI in the range 2.6 to 3.8. It is noticeable that References / D, E / were taken from the same journal issue, and even so they show remarkable differences in their analyses. Furthermore, if we consider amounts of compounds, the differences between them can be as large as 42% (CaO, / D, G /) for the OP41TT, or 54% (CaO, / D, H / for the OP121TT. Just to illustrate these differences, Figure 6.7 (b) shows the amount of SiO_2 and CaF_2 analysed through the years 1974 to 1978 by the quoted References. Again, it seems that there is a trend for higher CaF_2 (BI) percentage and lower SiO_2. We still have to quote that /B, E / shows exactly the same analyses, the only difference being that / B / has 1.29% FeO, whilst / E / has 1.29% Fe_2O_3.

Thus, there is a large difference in chemical composition (and BI) for these fluxes, in general not only for analyses made in different years, but probably for different batches. Despite this fact, these different fluxes have the same brand names, but worst yet, this 'fluctuation' in chemical composition is not necessarily particular to the quoted fluxes. This indicates the difficult task when flux dependent welding properties must be compared, and the welds were not made using exactly the same batch of flux.

Therefore, it seems that a complete flux chemical analysis is an important datum, mainly if further comparisons are required.

Only the chemical composition, however, does not completely characterise a flux. The amount of gas evolved from the flux at high temperature can have some influence on the bead roughness / 206 / and welding cooling rate / 207, 208 /. Therefore, a simple experiment was carried out to assess the amount of gas(es) released at 950°C from each flux. Small amounts of each flux (OP41TT and OP121TT) were baked for 25 hs at 450°C. The furnace was then switched off, and the fluxes were left inside to cool down until the temperature dropped to 140°C. In the meantime, ten ceramic boats had been heated inside a furnace for 6 hs at 1,000°C. Five samples were taken from each flux, weighing

around 5 gm each. The boats (now at room temperature), as well as the flux samples, were weighed up to 5 decimals. Each boat was loaded with a sample and all ten were placed into another furnace for $1\frac{1}{2}$ hs after to reach 950°C. After this time had been completed, the furnace was unloaded and the samples and boats were re-weighed.

No difference in weight was detected for the boats (as expected) but the five samples from each flux have shown the following average loss of mass (as a percentage of the original weight):

Flux OP41TT: 0.62% $^{+\ 0.04}_{-\ 0.02}$

Flux OP121TT: 1.35% $\pm$ 0.01

Therefore when each flux is heated to 950°C gas(es) is (are) released from them. We do not know which type of gas is reacting. However, from our fluxes analysis compilation (Table 6.4), it can be seen that at least $MgCO_3$, $CaCO_3$, Li_2CO_3 (OP41TT only), and K_2CO_3 are compounds which can decompose at the conditions of our experiment.

Thus, the important fact, we think, is that OP121TT released more than twice the weight of gas than OP41TT. Whether or not it means that during welding the heat lost through flux decomposition and gas released for each flux is actually proportional to the amounts we found, is a question we are not now prepared to give a categorical answer to without much more research on the subject. Unfortunately, this is not one of the immediate aims of our study.

Table 6.1- Chemical Composition and Mechanical Properties of HY100 and Q2N Parent Steels

MECHANICAL PROPERTIES

	YS (0.2%) (N/mm^2)	UTS (N/mm^2)	EL (%)	Red Area (%)	Cv (^oC) (J)
HY100 (SUPPLIER)*	761	865	20	69	172 (-84)
HY100 (MIL-S-162116)	690/793	-[a]	18	50[b] min	68 (-49)
A543 cls.2 (ASTM)	690 min	793/931	14 min	-	48 (-12)
Q2N (SUPPLIER)*	735	820	22	68	219 (-84)

CHEMICAL COMPOSITION (wt % x 10^{-2})

	C	Mn	Si	Ni	Cr	Mo	V	P[c]	S[c]	B	O	N
HY100 (SUPPLIER)*	18.5	35	21	320	162	42	0.8	1	0.7	-[a]	-	-
HY100 (Cranfield)*	21	38	23	328	155	45	1	1.2	0.7	<0.1	0.3	1.7
HY100 (MIL-S-16216)	20[d]	10/40	15/35	225/350	100/180	20/60	3	2.5[d]	2.5[d]	-	-	-
A543 cls 2 (ASTM)	23[d]	40[d]	20/35	260/325	150/200	45/60	3[d]	2[d]	2[d]	-	-	-
Q2N (SUPPLIER)*	13.5	39	19	346	150	45	7	0.7	0.3	-	-	-
Q2N (Cranfield)*	17	42	17	349	142	50	7	0.9	0.5	<0.1	0.4	1.4

	Al	As	Cu	Sn	Pb	Ti	Sb	Co	W	Nb	Fe
HY100 (SUPPLIER)*	2.3	1.1	7	0.9	0.03	0.3	0.24	1.3	-	-	Bal
HY100 (Cranfield)*	3	-	9	< 1	-	<1	-	2	< 2	< 1	Bal
HY100 (MIL-S-16216)	-	-	25	-	-	2	-	-	-	-	Bal
A543 cls 2 (ASTM)	-	-	-	-	-	-	-	-	-	-	Bal
Q2N (SUPPLIER)*	2.3	1.3	4	0.5	0.04	0.4	0.05	0.5	-	-	Bal
Q2N (Cranfield)*	5	-	7	< 1	-	< 1	-	1.8	< 2	< 1	Bal

(*) Actual Values. Not Standard.
(a) Not Specified (Standard) or not Analysed.
(b) Longitudinal.
(c) For MIL-S-16216 and ASTM, P(%) + S(%) shall be 0.045% MAX
(d) Maximum

Table 6.2 - Wires Chemical Composition (wt % X 10^{-2})

Diam (mm)	Designation	C	Si	Mn	P	S	Cr	Mo	Ni	Al	B	Co	Cu	Nb	Sn	Ti	V	W
4.0	LINDE 95-A	3	47	155	0.8	0.4	11	33	171	< 1	< 0.1	1.	2	< 1	0.2	1.8	< 1	2
4.0	OERLIKON-S3	11	18	170	0.6	0.3	3	57	101	< 1	< 0.1	< 1	4	< 1	< 1	< 1	< 1	< 2
1.2	LINDE 95-B	5	40	168	0.9	0.2	10	33	176	< 1	< 0.1	1	3	< 1	< 1	1.6	< 1	< 2

Table 6.3 - OP41TT and OP121TT Fluxes: Producer Specifications

FLUX	BI	MAX.CUR (A) -TYPE	GRAIN SIZE (TYLER MESH)	SiO_2 $+TiO_2$	CaO +MgO	Al_2O_3 +MnO	CaF_2
OP41TT	3.1	800-DC^+	8 x 48	10%	35%	20%	30%
OP121TT	3.1	1200-DC&AC	8 x 48	15%	35%	20%	25%

Notes: See Text and Table 6.4

BI (Basicity Index) as in /j/. This Reference is together with those for Fluxes Analyses (Table 6.4(R))

TABLE 6.4 - ANALYSES OF FLUXES TAKEN FROM REFERENCES AS QUOTED (Wt% x 10^{-1})

EXPT	REF	BI [ ]	SiO_2 (Si)	Al_2O_3 (Al)	MgO (Mg)	CaO (Ca)	FeO (Fe)	MnO (Mn)	TiO_2 (Ti)	CaF_2 (F)	Na_2O (Na)	LiO_2	K_2O (K)	ZrO_2 (Zr)	BaO	Fe_2O_3
OP 41 TT	A	[3.8]	(56)	(73)	(223)	(221)	(13)	-	(3)	(119)	(5)	-	(6)	(2)	-	-
	B	[2.6]	137	196	290	125.8	12.9	1	5	180	4.2	3.2	7.6	-	-	-
	C	[3.0]	125	197	334	61	-	-	-	276	-	-	-	-	-	-
	D	[3.6]	103	181	355	59	23	1	7	265	7	-	6	-	-	-
	E	[2.6]	137	196	290	125.8	-	1	5	180	4.2	3.2	7.6	-	-	12.9
	F	[3.5]	130	140	350	110	-	2	7	250	-	-	-	-	-	-
	G	[3.7]	108	162	244	140	22	< 1	6	283	27	-	8	-	-	-
OP 121 TT	H	[2.9]	139	168	294	114	13	9	8	212	10	-	18	< 1	-	-
	H		(65)	(89)	(177)	(190)	(10)	(7)	(5)	(103)	(7)	-	(5)	(<1)	-	-
	I	[3.3]	134	142	400	110	17	8.5	5	144	9	-	8	-	1*	-
	C	[2.8]	139	189	322	62	7	8	8	251	8	-	8	-	1	-

* Compound form Barium Carbonate

Note: See Table 6.4(R) for References.

TABLE 6.4(R) - List of References as Quoted in Table 6.4

/ A / DAVIS,M.L.E, PARGETER,R.J. and BAILEY,N. The Effects of Titanium and Boron Additions to Submerged-Arc Fluxes on Weld Metal Chemistry and Microstructure. The Welding Institute Res. Rep. 116/1980 Aug. 1980.

/ B / KIRKWOOD,P.R. and CLARK,A. Mechanical Properties of Submerged - -arc Weld Metals after a Post-Weld Normalizing Treatment. Welding and Metal Fabrication.42(12):427-435. Dec 1974.

/ C / STILL,J.R. The Effect of Titanium, Boron and Molybdenum additions on the Weld Metal Toughness in High Heat Input Welds. M.Sc.Thesis, C.I.T., 1978.

/ D / TULIANI,S.S. A metallographic study of chevron cracks in submerged arc weld metals. Welding Research International.6(6):19-45, 1976.

/ E / KEVILLE,B.R. An investigation to determine the mechanisms involved in the formation and propagation of chevron cracks in submerged arc weldments. Welding Research International.6(6):47-66, 1976.

/ F / KIRKWOOD,P.R. and GARLAND,J.G. The influence of vanadium on sub - merged arc weld metal toughness - 1. Welding and Metal Fabrication. 45(1):17-28.Jan/Feb 1977.

/ G / NOOR,M.A.B., NORTH,T.H. and BELL, H.B. Characteristic properties of flux formulations used in submerged arc welding. Welding and Metal Fabrication.46(3):193-199. Apr 1978.

/ H / TERASHIMA,H. and HART,P.H.M. Effect of Aluminium in C-Mn Steels on Microstructure and Toughness of Submerged-Arc Weld Metal-Part 1. The Welding Institute Rep.,1982.

/ I / KEVILLE,B.R. and COCHRANE,R.C. Strain-induced hot cracking in ferritic weld metals. Trends in steel and consumables for welding. The Welding Int. Conf.1:519-530, 1978.

/ J / TULIANI,S.S., BONISZEWSKI,T. and EATON,N.F. Notch Toughness of Commercial Submerged-Arc Weld Metal. Welding and Metal Fabrication. 37(8):327-339. Aug 1969.

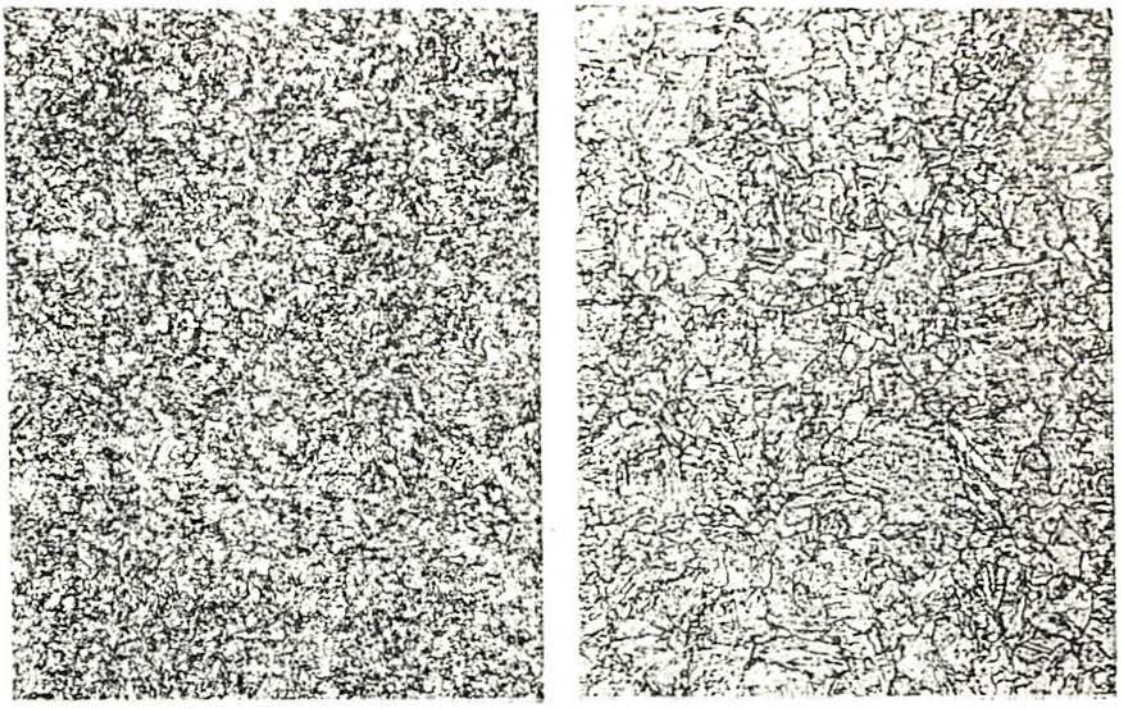

(a) (b)

Figure 6.1 - Q2N Steel Microstructure. Nit. (a) X100, (b) X500.

(a) (b)

Figure 6.2 - HY100 Steel Microstructure,Nit, (a) X100, (b) X500.

FIG. 6.3(a) HY100 SEM Image of Inclusions. General View of Inclusions Shown in Figures 6.3(b) and 6.3(e). Nital, X 1K.

FIG. 6.3(b) HY 100 SEM Image of Inclusions. Nital, X 5K.

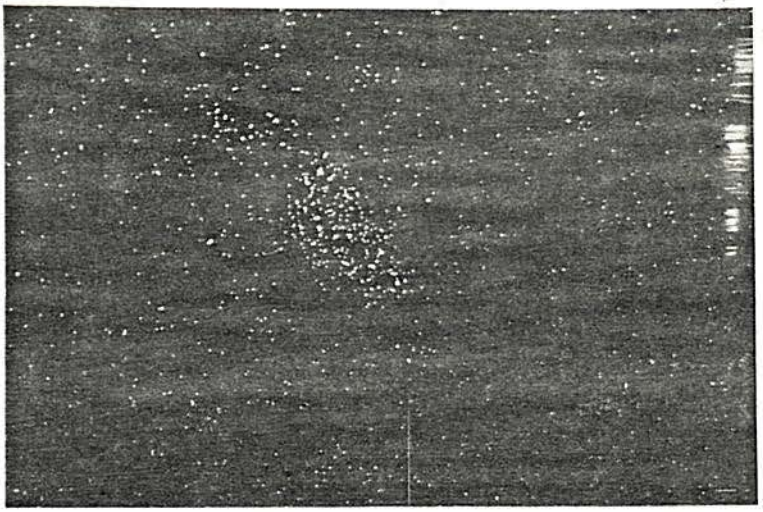

FIG. 6.3(c) Manganese Map for Inclusion Shown in Figure 6.3(b).

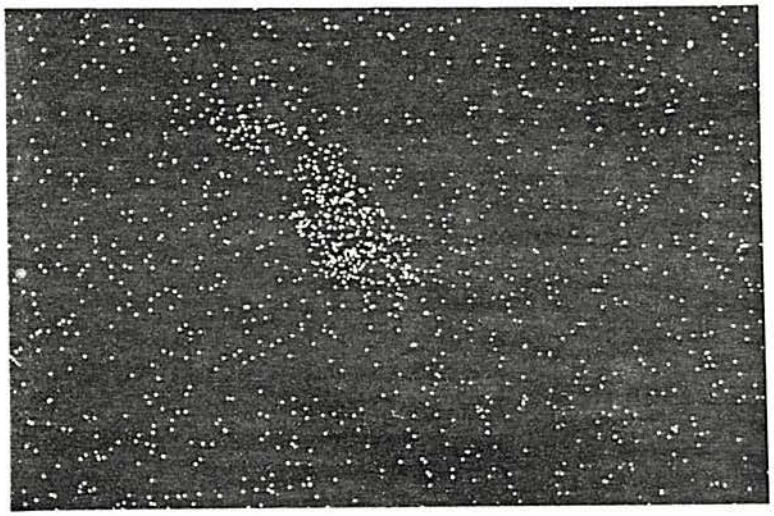

FIG. 6.3(d) Sulphur Map for Inclusion Shown in Figure 6.3(b)

FIG. 6.3(e) HY 100 SEM Image of Inclusions. Nital, X 5K

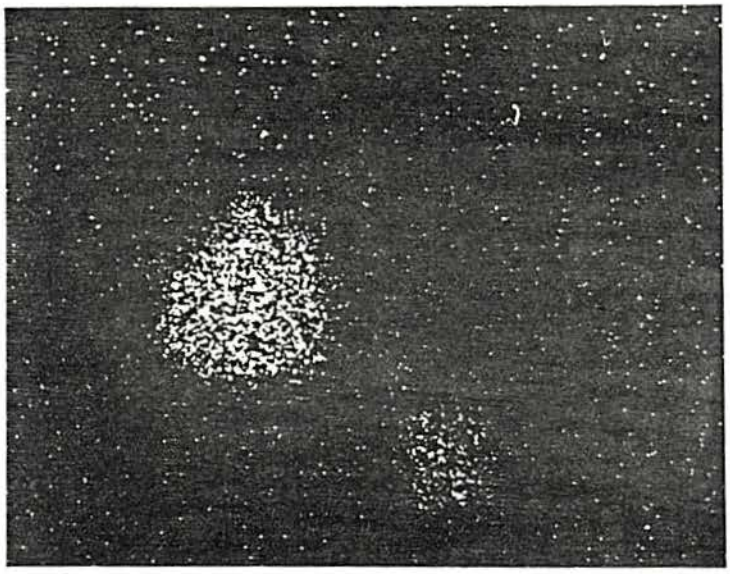

FIG. 6.3(f) Aluminium Map for Inclusions Shown in Figure 6.3(e).

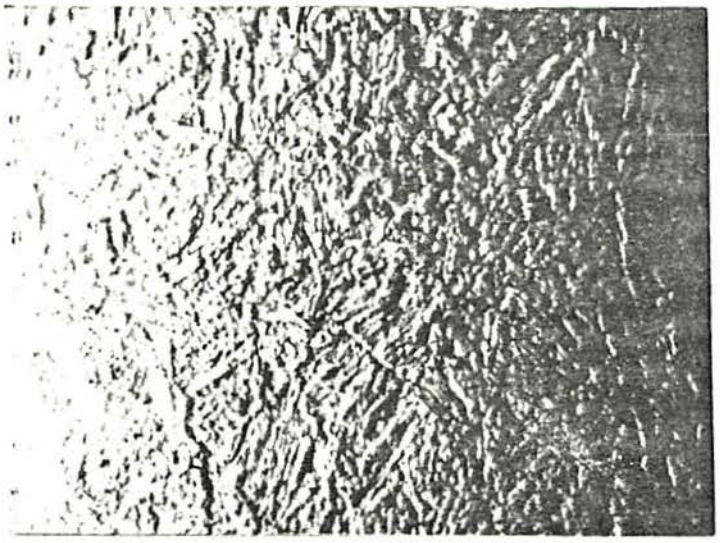

Figure 6.4 (a) - Q2N Steel Microstructure. 'Pseudo-Relief' Technique. SASPA, X1000.

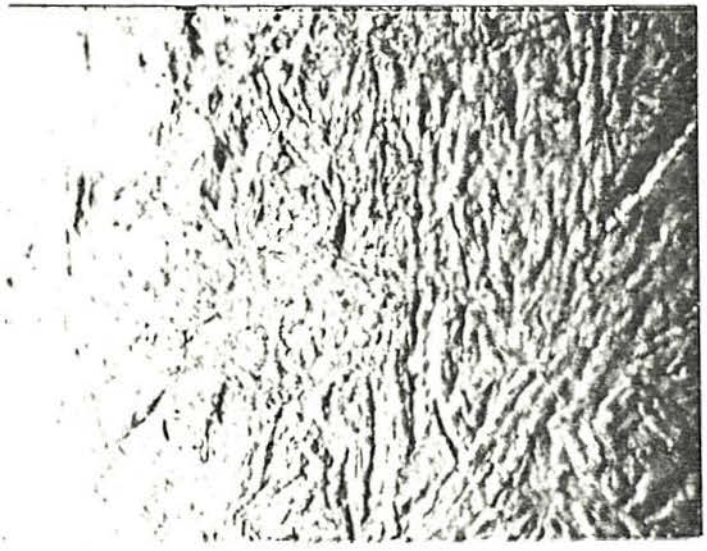

Figure 6.4(b) - HY100 Steel Microstructure. 'Pseudo-Relief' Technique SASPA, X1000.

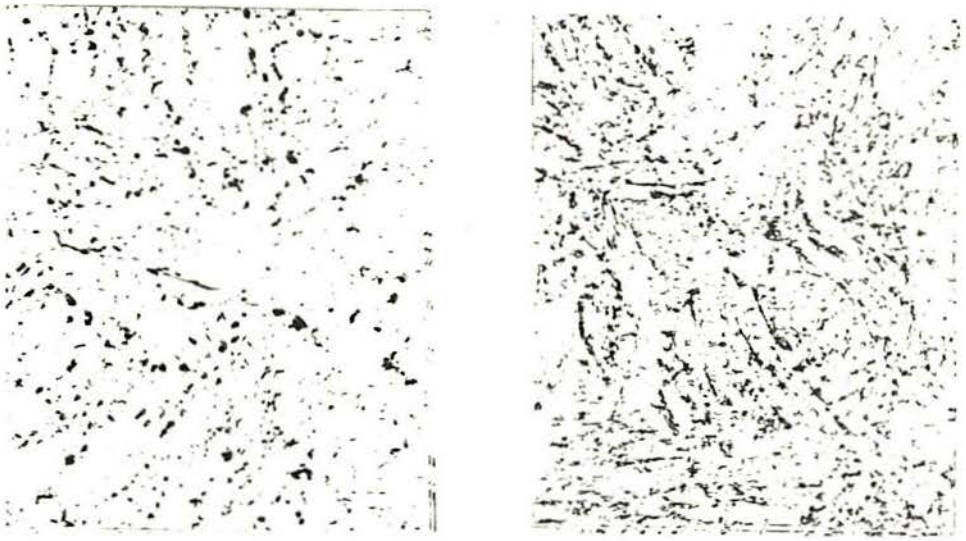

(a) (b)

Figure 6.5 - Tem Image. Carbon Extraction Replica. X4K.
(a) Q2N Steel, (b) HY100 Steel.

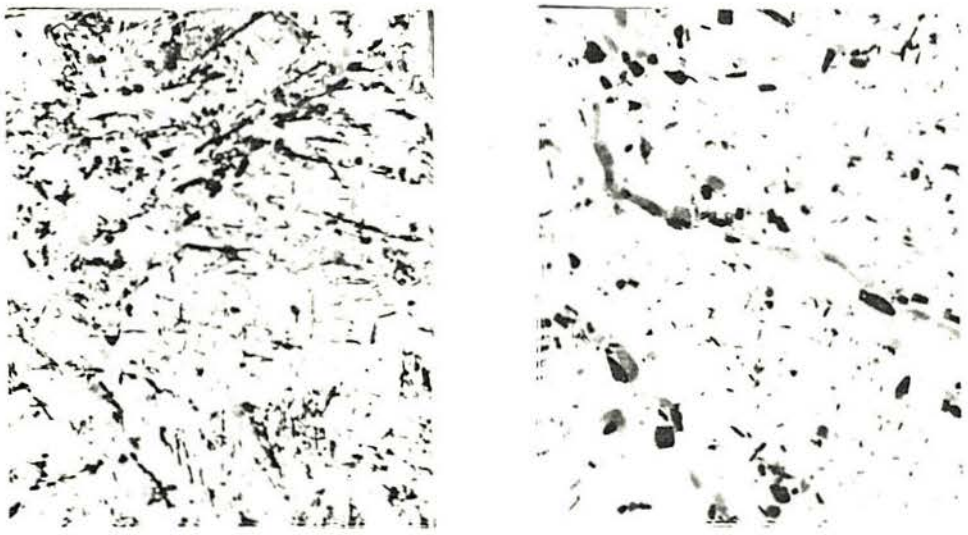

(c) (d)

Figure 6.5 - TEM Image. Carbon Extration Replica. X13K,
(c) HY100 Steel, (d) Q2N Steel.

Figure 6.5 (e) - Q2N Steel TEM Image. Carbon Extraction Replica X14K.

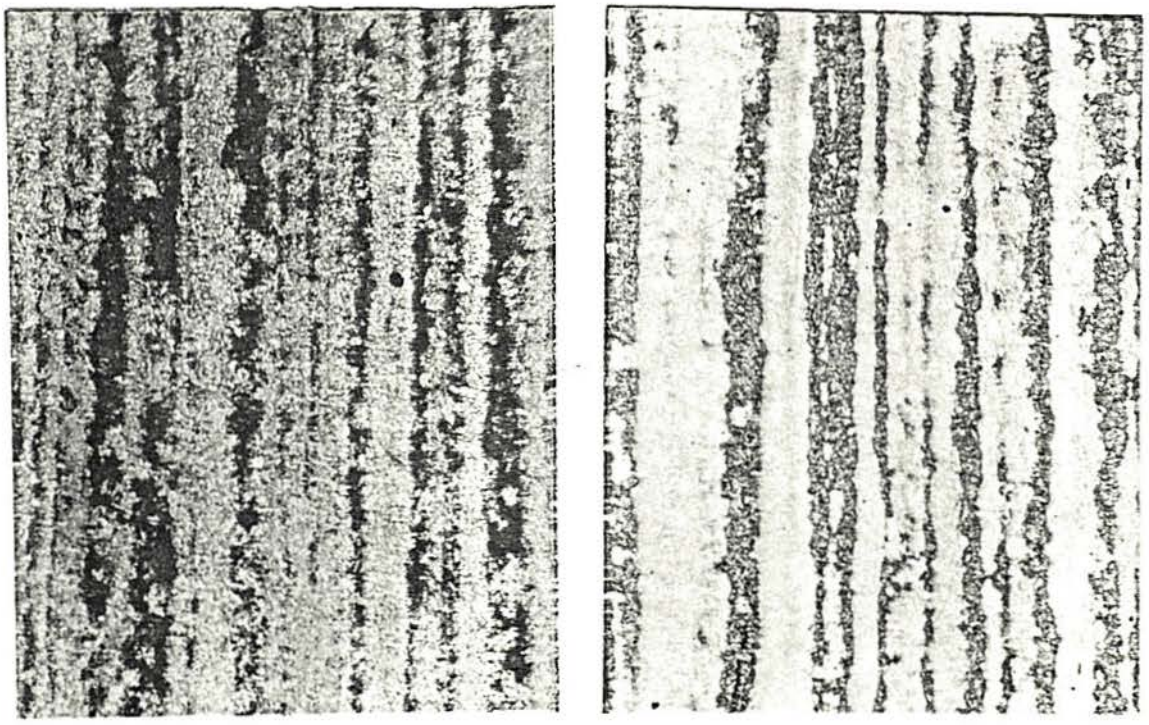

(a) (b)

Figure 6.6 - Steel Microstructure. 'Banding' Phenomenon. Nit + Sodium Bis. X32, (a) Q2N Steel, (b) HY100 Steel.

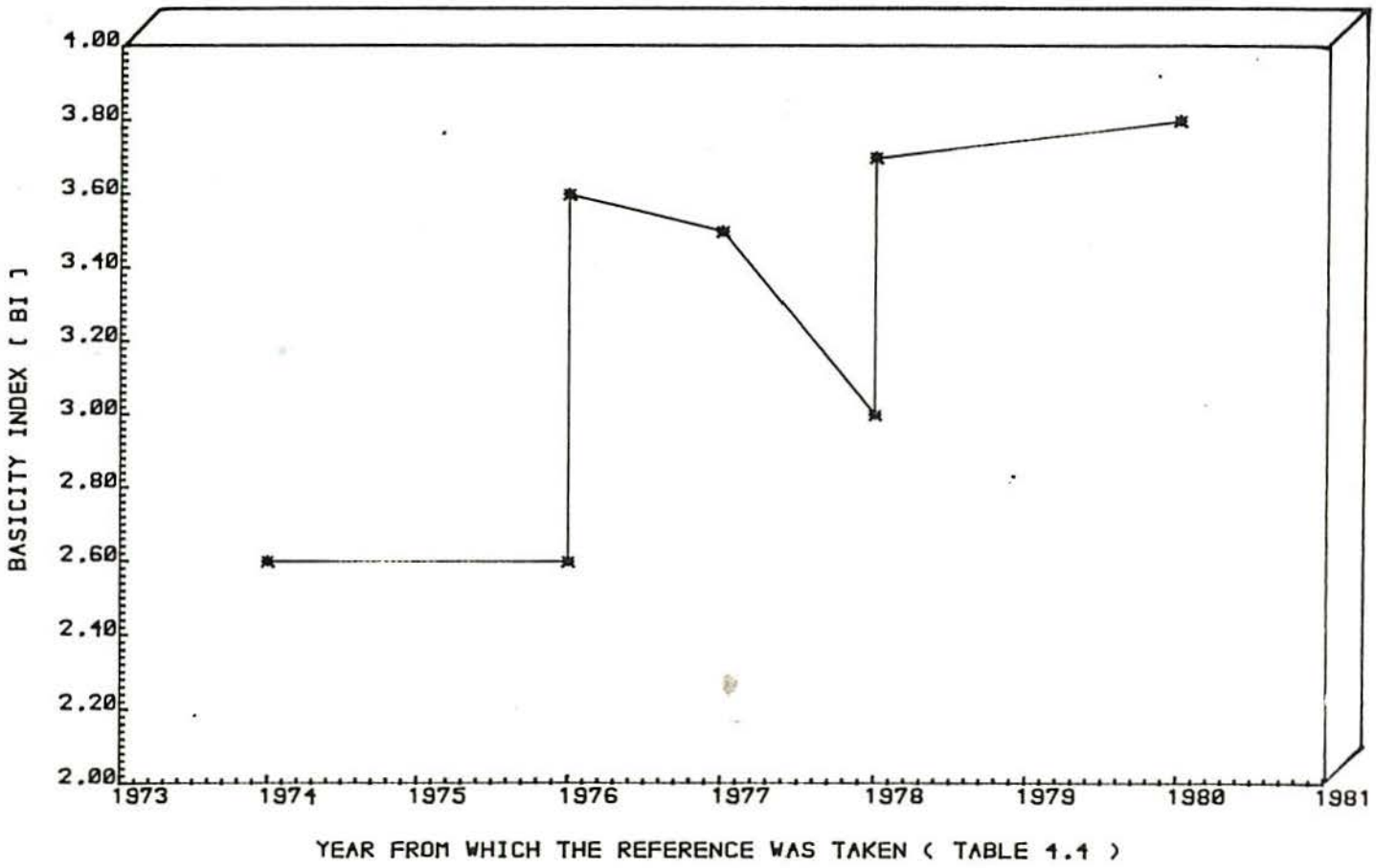

FIGURE 6.7(a)– RELATIONSHIP BETWEEN BASICITY INDEX AND YEAR FOR FLUX OP41TT

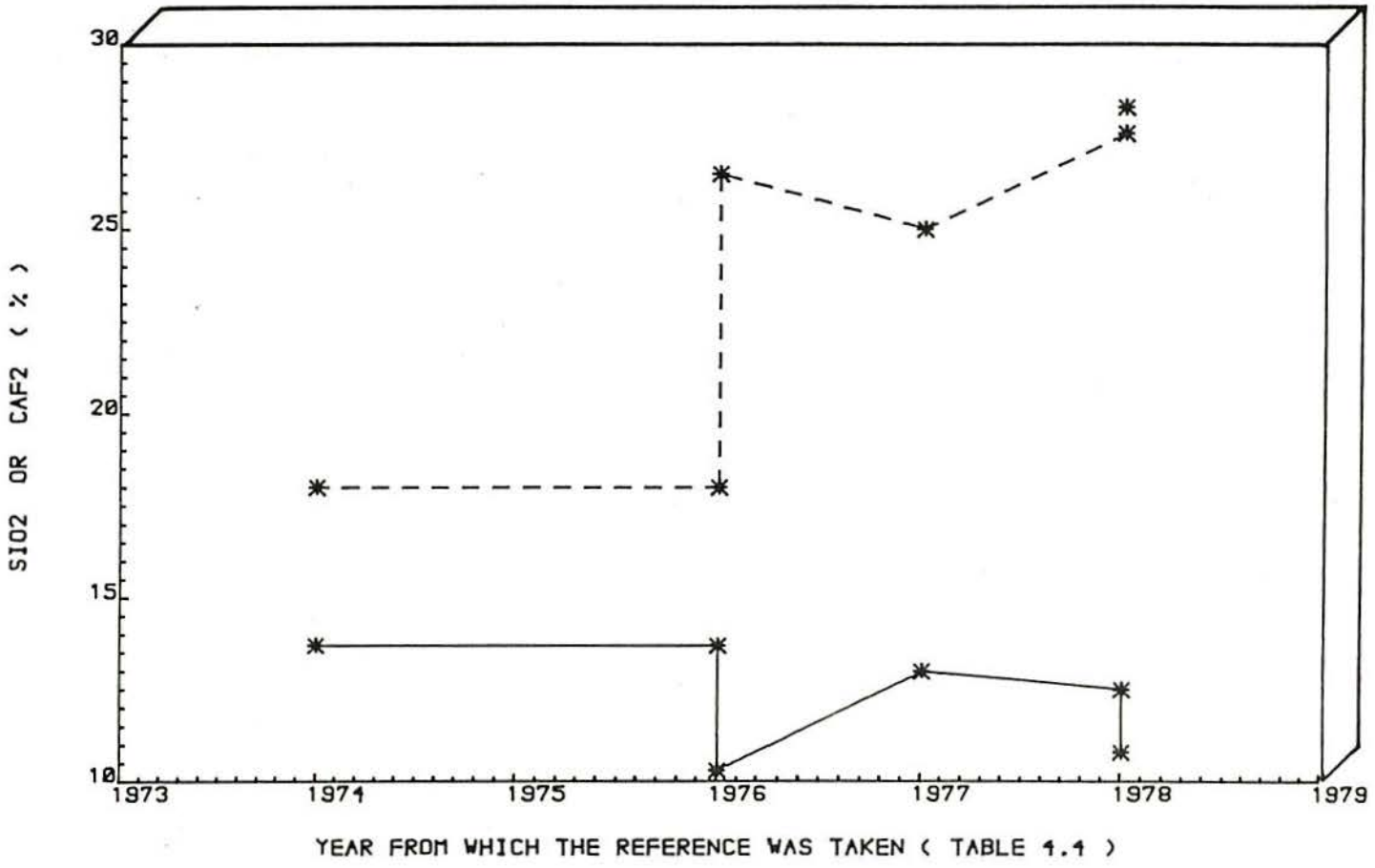

FIGURE 6.7(b) - RELATIONSHIP BETWEEN YEAR AND AMOUNTS OF SIO2 AND CAF2 (DASHED LINE)

7. ALL WELD METAL (MULTIPASS) MECHANICAL TESTS

7.1 Welding conditions and coding

A series of submerged-arc multipass welds were made in order to assess all-weld metal impact and tensile properties of the consumables (Section 6.3) used throughout this study. A specially designed specimen (Figure 7.1), single V nearly vertical groove angle and wide gap surely can reduce dilution to the minimum, allowing the study of the weld metal only.

We were limited to weld five specimens of those dimensions for each parent steel, and little information is available on mechanical properties of weld metal of this type at the relatively high 4.1 KJ/mm energy input. Thus, we decided on the following welding conditions (repeated for each steel).

(a) 1.9 KJ/mm energy input welds:

Welding parameters: 30 V, 400 A, 6.3 mm/s

Flux: OP41TT

Wire: OERLIKON S3

Weld code: WH/WQ 641 S4

(b) 4.1 KJ/mm energy input welds:

Welding parameters: 34 V, 770 A, 6.3 mm/s

b(i) - Flux: OP41TT

Wire: LINDE 95

Weld code: WH/WQ 674 L4

b(ii)- Flux: OP121TT

Wire: LINDE 95

Weld code: WH/WQ 674 L1

b(iii)-Flux: OP41TT

Wire: OERLIKON S3

Weld code: WH/WQ 674 S4

b(iv)- Flux: OP121TT

Wire: OERLIKON S3

Weld code: WH/WQ 674 S1

The 'weld code' above referred to gives the welding condition by itself. Consider an example weld coded WQ or WH VAE XF:

- 'WH' or 'WQ' means weld on HY100 or Q2N steel, respectively
- 'V' means welding speed: 6 = 6.3 mm/s
- 'A' means welding current: 4 = 400 A
  7 = 770 A

- 'E' means energy input: 1 = 1.9 KJ/mm
  4 = 4.1 KJ/mm
- 'X' means wire type: L = LINDE 95
  S = OERLIKON S3
- 'F' means flux type: 1 = OP121TT
  4 = OP41TT

The following general observations are valid for all welds:

- The slag detachability was good and the weld surface appearances were in general, smooth;
- To fill up the joints 27 and 12 runs were necessary, for 1.9 and 4.1 KJ/mm energy input welds, respectively
- For both energy inputs, each weld layer was composed of three runs, using the electrode at 0°.
- The fluxes were baked 2 hs at 450°C before use as a measure recommended by the manufacturer to have very low levels of moisture content, avoiding hydrogen induced cracking due to it;
- The plates were preheated to 120°C and the interpass temperature was maintained at 145 $\pm$ 5°C, also as a measure to avoid hydrogen induced cracking.

7.2 Results and discussion

7.2.1 Thermal analysis and metallography

In spite of the difficulties to get a good 'harpooning' (Section 6.1.3), the measured thermal cycles are reliable, as will be seen in Chapter 8. Therefore, they can give a fair indication of, at least, first and second transformation temperatures, and they can be associated with the microstructures order of appearance.

In Figures 7.2 and 7.3 are seen typical thermal analysis for 1.9 and 4.1 KJ/mm energy input welds, respectively. The plotting of the thermal cycle is composed of two curves, as explained in Chapter 6. The thick line is just the weld thermal history through the time, whilst the line marked with a 'd' on it is its first derivative, which accentuates the transformation temperatures. Besides the graphic there is a table with average cooling rate and time, for temperatures range of interest. As already shown in the CCT diagrams (Chapter 2) for similar materials used in this research and in the metallographic analysis to be presented, the first (solid) phase transformation will happen in the temperature range of 1100 to 500°C. Therefore, special attention was drawn to the ranges 1100/800°C and 800/500°C. Furthermore, the time spent by the weld metal in the range 1400/1000°C has an effect on the grain size mainly and it is given as Retention Time - RT (1000).

Comparing Figures 7.2 and 7.3 it is immediately seen that going from 1.9 to 4.1 KJ/mm energy input more than doubles the time spent in the range 800/500°C, whilst the RT (1000) are nearly the same. This behaviour will be confirmed by all thermal analyses made throughout this work, and simply reflect the characteristic weld heat flow process. Thus, very high temperature cooling rates are only affected by very great changes in energy input.

The estimated phase transformation temperatures (first and second) and average cooling times, in the ranges 1100/800°C and 800/500°C for the 1.9 and 4.1 KJ/mm energy input welds are found in the last two lines on Table 8.10 (Chapter 8), together with specimens of that chapter. The reason to place there these results is of pure coherence, for in that chapter a much broader discussion of the subject will be carried out.

As regards metallographic analysis, we cannot comment on it without considering further aspects, like chemical composition and weld thermal history.

Firstly, we have to bear in mind that these are very low or nil dilution multipass welds. The single-pass welds chemical analyses will show (Chapter 8) that, probably due to the types of flux used, there is a small loss or gain in chemical elements. Therefore, we here assume that the present welds do not have great difference in chemical composition from the wires they were welded. However, some differences do exist, for the different welding parameters induce distinct 'weld pool retention time', e.g. the available time to proceed the metallurgical reactions within the pool/slag system (Chapter 8).

Furthermore, we remind the reader that a detailed metallographic analysis of each zone, from each one of the ten weld beads would be, by itself, a work as long as the present one, and this is not one of the main objectives of the exercise. A more detailed metallographic analysis is found in Chapter 8, for single-pass welds. Nevertheless, this qualitative assessment of microconstituents follows the ABSON and DOLBY / 242 / proposed notation.

We can divide the metallographic analysis into two groups:

(i) General aspects

The typical bead shapes for 1.9 and 4.1 KJ/mm energy input welds are shown in Figures 7.4 (a,b), respectively. From these figures at least three immediate deductions can be made: the 4.1 KJ/mm induces a much coarser microstructure than the 1.9 KJ/mm energy input; the 4.1 KJ/mm has a greater HAZ than the 1.9 KJ/mm energy input weld; both are visually sound welds.

The microstructural zones of 1.9 KJ/mm energy input weld are seen in Figure 7.5 (a). A columnar one (not refined), followed by the first and second refined zones (coarse and fine), originated on the previous weld metal. After this fine microstructure begins the reheated (but not fully transformed) region of the lower run. If followed to its end it would show a similar columnar microstructure, above referred to, because the run is insufficiently deep to affect completely the previous one on which it was laid. In Figure 7.5 (b), taken from a 4.1 KJ/mm energy input weld, it is seen that a much wider and deeper run

than one made by a 1.9 KJ/mm energy input. It is clear that this high energy input run develops a much coarser columnar microstructure, but at the same time it affects (tempering) a much bigger volume of metal under it.

Obviously, independent of wire/flux combination, all other 4.1 KJ/mm welds follow this trend.

(ii) Details

The main microstructural phases of the last run will be shown without, however, a detailed analysis of microphase regions among them, which clearly exist.

Firstly, Figure 7.6 (a) shows the columnar zone of a 1.9 KJ/mm energy input weld (sp.WQ 641 S4). Grain boundary ferrite, acicular ferrite and some ferrite with aligned M-A-C are the main microconstituents seen at this magnification. A detail can be seen in Figure 7.6 (b), which shows grain boundary ferrite, acicular ferrite, some ferrite with aligned M-A-C, martensite (grey phase), and carbides precipitated mainly along grain boundaries. This carbide precipitation was found in the 4.1 KJ/mm energy input welds columnar zone, too.

In Figures 7.7 (a-c) can be seen microstructures at the columnar region of 4.1 KJ/mm energy input welds: Figure 7.7 (a) shows it for OERLIKON S3 wire and OP121TT flux (sp. WQ 674 Sq); Figure 7.7 (b) for OERLIKON S3 wire and OP41TT flux (sp. WQ 674 S1); Figure 7.7 (c) for LINDE 95 wire and OP41TT flux (sp. WQ 674 L4). The use of OP121TT flux seems to induce higher amounts of acicular ferrite, but this possibility must be checked in a future research.

The wire chemical composition effect is much less clear. Table 6.2 (Chapter 6) shows the wire chemical compositions and their differences were discussed in Section 6.3.1. As can be seen (Chapter 5), the balance of acicular ferrite promoters may well be equivalent.

7.2.2 Tensile properties, hardness and fractography

Figure 7.1 illustrates the position in the weldment from where the all-weld metal tensile specimens were taken, and Section 6.1.4 gives details of both specimen and testing.

Table 7.1 shows the average results for weld metal Hardness, Yield Strength (YS-0.2%). Tensile Strength (UTS), Elongation (EL), and Reduction in Area (RA), for all welding conditions, grouped by energy input and cooling time.

It can be seen that all properties are quite homogeneous within each group, mainly hardness, elongation and reduction in area. It was expected to be so, since they should not show great differences in chemical composition.

The 4.1 KJ/mm energy input group were found to be ~30 HV5 harder than the 1.9 KJ/mm welds. So, yield strength and tensile strength are the highest for the same 4.1 KJ/mm energy input, as illustrated comparing welds in the two groups which use the same OERLIKON S3 wire and OP41TT flux, viz: specimens WH/WQ 641 S4 in the 1.9 KJ/mm energy

input group with specimens WH/WQ 674 S4 in the 4.1 KJ/mm energy input group. In consequence, elongation and reduction in area are the best for the lower 1.9 KJ/mm energy input.

The hardness results can be explained through the microstructure size effect, for the 4.1 KJ/mm energy input welds have shown it to be much coarser than the 1.9 KJ/mm ones, as seen in Section 7.2.1. The yield and tensile strength behaviour can be much more complex. Factors like the greater tempered area caused by the subsequent bigger runs of the 4.1 KJ/mm energy input welds can increase these two properties, or complicate interactions between microstructures and the microvoid coalescence mode of fracture can also lead to these higher figures. Nevertheless, the literature shows examples where the weld metal yield strength increased from 2.0 to 4.0 KJ/mm energy input, and then decreased with subsequent increase in energy input / 217 /, or it varied randomly with energy input (1.2 to 4.4 KJ/mm), as put by its authors / 243 /.

Values in Table 7.1 were averages of two specimens by welding condition, and the data did not show any significant difference between similar welds made on HY100 or Q2N steels (as expected from the very low or nil dilution). Therefore, the minimum and maximum values for each property were plotted in Figures 7.8 (a-e). Thus, each bar in these figures shows the lowest and the highest value for the considered property and welding condition (as shown in the coordinate axis).

As regards the very important yield strength property, Figure 7.8 (a) shows that the best range is found combining OERLIKON S3 wire and OP121TT flux at 4.1 KJ/mm energy input (sps. WH/WQ 674 S1). These specimens also have shown good to excellent elongation (Figure 7.8 (c)) and reduction in area (Figure 7.8 (d)) and the best range for tensile strength (UTS), as seen in Figure 7.8 (b).

These results might be due to difference in wires chemical analysis (Table 6.2) and flux behaviour (Section 6.3.2). The OERLIKON S3 wire has higher carbon level than the LINDE 95 and its Mn/Si ratio is 9.4, much greater than the 3.3 value shown by the LINDE 95 wire. Carbon increases yield strength and UTS (Chapter 5). This higher Mn/Si ratio means that it is likely that the OERLIKON S3 wire produces weld deposits much cleaner than the LINDE 95 wire / 212 /. Therefore, being the inclusion volume fraction of such welds with OERLIKON S3 wire very low, the energy required to initiate microvoid coalescence mode of fracture is very high / 217 /. Furthermore, the OP121TT flux might exert a refining action on the microstructure, if its ability to extract more heat from the arc than the OP41TT flux is confirmed. This beneficial action is again shown up by the yield strength range observed for welds made at the same conditions, but flux (compare specimens WH/WQ 674 S4 with specimens WH/WQ 674 S1).

Figure 7.9 (a) illustrates the general great ductility shown up by the welds. In this figure, two broken pieces of a tensile test specimen were assembled, while Figure 7.9 (b) shows the 'cup' and 'cone' fracture. A best view of these fractures is given by the SEM in Figures 7.10 (a,b), whilst Figures 7.10 (c) characterises its microvoid coalescence mode of fracture. Notice that in most of the dimples the small particles that initiate the voids are visible, highlighting the inclusions importance on the fracture process.

7.2.3 Impact and fractography

Figure 7.1 shows the position of the Charpy specimens in the weldment. As they were taken 2.0 mm below the last run their exact position, of course, will change for different energy input welds. Specimen and testing details can be found in Section 6.1.4.

Figures 7.11 (a-e) show impact transition curves for all welding conditions, which are given in the upper left corner of each figure.

From these figures it is clear that there is no practical difference in energy absorbed for specimens taken from welds on HY100 or Q2N steels. This is due to the welds very low or nil dilution. Another striking deduction is that 1.9 KJ/mm energy input welds have shown the highest values for energy absorbed in all test temperatures.

The energy input effect can be best seen comparing Figures 7.11 (a,b) in so far they use the same OP41TT flux and OERLIKON S3 wire, but were welded at 1.9 and 4.1 KJ/mm energy input, respectively.

In the same way we previously used the barchart to analyse tensile properties, we use it now for impact results. Figures 7.12 (a-e) show the lowest and the highest value of energy absorbed for each welding condition, at each test temperature. As can be seen, the spread in energy absorbed values is high, mainly from 0° downwards. Among the 4.1 KJ/mm energy input welds, at -40°C the lowest impact value (54 J) is given by the OERLIKON S3 wire and OP121TT flux combination (sps.WH/WQ 674 S1), as can be seen in Figure 7.12 (d). However, due to the spread in results such values need many more experiments before to be statistic significant.

The fine weld microstructure produced by 1.9 KJ/mm energy input was already seen in Section 7.2.1 and it can be responsible for the high toughness level shown by these welds.

The LINDE 95 wire has higher nickel level that the OERLIKON S3, and this could be a cause of the apparent better toughness shown by the welds which use it. However, no definite wire influence on toughness can be assessed; perhaps due to chemical composition balance (Sections 6.3.1 and 7.2.1), or the microstructure degradation provoked by the high 4.1 KJ/mm energy input (from which comparisons could be made).

Transition in crystallinity is illustrated in Figure 7.13 for 20, -40 and -80°C, respectively. Apparently, this is the behaviour followed by all welds, with large shear lips besides the fracture surface at the highest temperature. The fracture mode is well characterised through SEM. Figure 7.14 (a) shows the microvoid coalescence type of fracture for Charpy specimens broken at 20°C. In many dimples the micro particles that initiate the voids are clearly seen. At -80°C quasicleavage fracture mode actuates, with ill-defined cleavage facets, as shown in Figure 7.14 (b).

Therefore, the weld metals investigated in this study change their fracture mode to quasicleavage only below -40°C, but before or at -80°C.

7.3 Summary

In order to investigate mechanical properties of the consumable used throughout this work, ten welds were successfully made, five on HY100 and five (repeated) on Q2N steel.

The welding energy inputs used were 1.9 KJ/mm (one wire/flux combination only) and 4.1 KJ/mm (four wire/flux combinations), and the groove preparation allowed a very low or nil dilution. Thus, the emphasis was placed on the highest energy input because it has the less known behaviour, using these consumables.

The all-weld metals were tested for tensile properties, impact and hardness. Furthermore, metallography and thermal analysis were carried out.

As expected, the 4.1 KJ/mm energy input welds have shown a much wider and deeper run and coarser microstructure than the 1.9 KJ/mm. However, it is also true that this higher energy input affects (tempering) a much larger weld metal volume under it.

Bother energy inputs last run main microconstituents were grain boundary ferrite, acicular ferrite, ferrite with aligned M-A-C, martensite and carbides around grain boundaries. Therefore, for 1.9 KJ/mm energy input grain boundary ferrite and acicular ferrite appear and develop in the ranges 600-510°C and 510-470°C, respectively, as given by the thermal analysis. For the 4.1 KJ/mm these same microconstituents have a higher phase transformation range temperatures: 690-600°C and 600-540°C, respectively.

There is a slight indication that the OP121TT flux is a stronger promoter of acicular ferrite thatn OP41TT, but this is not a definite conclusion.

The wire effects were not clear. As each one has acicular ferrite elements promoters, a balance of their effects is suggested.

Tensile properties and hardness average results are shown in Table 7.1, whilst Figures 7.8 (a-e) show the minimum values for each property.

Comparing welds using the same wire/flux combination, but different energy input, the 1.9 KJ/mm welds have shown the best elongation and reduction in area. The 4.1 KJ/mm energy input welds have shown the highest hardness, yield and tensile strength.

To explain the 1.9 KJ/mm welds higher elongation and reduction in area (and lowest hardness), their smaller microstructure size is suggested as a cause.

The yield and tensile strength increasing from 1.9 to 4.1 KJ/mm can be resultant of the larger tempering effect of the latter energy input, or from complex interactions between microstructure and fracture mode (microvoid coalescence, as assessed through SEM).

Among welds made using the same energy input (4.1 KJ/mm) OERLIKON S3 wire and OP121TT flux have shown the best range of yield and tensile

strength, and also good to excellent elongation and reduction in area. These results are suggested to be caused by the likely, much cleaner weld metal deposited by the OERLIKON S3 wire, for its Mn/Si ratio is 9.4, much greater than the 3.3 of LINDE 95, and also because the former wire has a higher carbon content.

The OP121TT flux probably exerts a refining action, superior to OP41TT, if its ability to extract more heat from the arc is confirmed and if it actually is a stronger promoter of acicular ferrite than the OP41TT (being the latter condition, probably, consequent from the former).

The impact transition curves for all welding conditions are shown in Figures 7.11 (a-e), whilst Figures 7.12 (a-e) show the ranges of energy for each test temperature.

Comparing welds made at different energy inputs, but the same wire/flux combination, the highest energy absorbed at all test temperatures is shown by 1.9 KJ/mm. The finer microstructure size is again suggested as a cause for this result.

At -40°C and 4.1 KJ/mm energy input, the best range in toughness is achieved by that weld using LINDE 95 wire and OP121TT flux. This wire has higher nickel content than the OERLIKON S3, and this difference might be a cause of its best toughness. However, due to the spread in energy absorbed, more tests must be done before a definitive conclusion can be reached.

The welds fracture mode transition from microvoid coalescence type at 20°C to complete quasicleavage happens at some point below -40°C, but before or at -80°C.

TABLE 7.1 WELD METAL MECHANICAL TESTS (MULTIPASS): TENSILE PROPERTIES, COOLING TIME AND HARDNESS.

ENERGY INPUT: 1.9kJ/mm

AVERAGE COOLING TIME

1100-800°C: 5.9S

800-500°C: 20.5S

Weld Code	YS(0.2%) (N/mm^2)	UTS (N/mm^2)	El (%)	R.A. (%)	HARDNESS (HV5)
WH641S4	594	641	46	75	224 ± 3
WQ641S4	601	653	31	72	229 ± 8

ENERGY INPUT: 4.1kJ/mm

AVERAGE COOLING TIME

1100-800°C: 10.4S

800-500°C: 45.9S

Weld Code	YS(0.2%) (N/mm^2)	UTS (N/mm^2)	El (%)	R.A. (%)	HARDNESS (HV5)
WQ674L4	630	716	27	68	251 ± 8
WH674L4	615	714	28	65	253 ± 7
WQ674L1	616	734	28	67	246 ± 9
WH674L1	624	732	29	67	259 ± 4
WQ674S4	609	709	27	66	251 ± 11
WH674S4	603	720	28	67	263 ± 8
WQ674S1	627	733	28	66	251 ± 9
WH674S1	624	714	28	69	250 ± 8

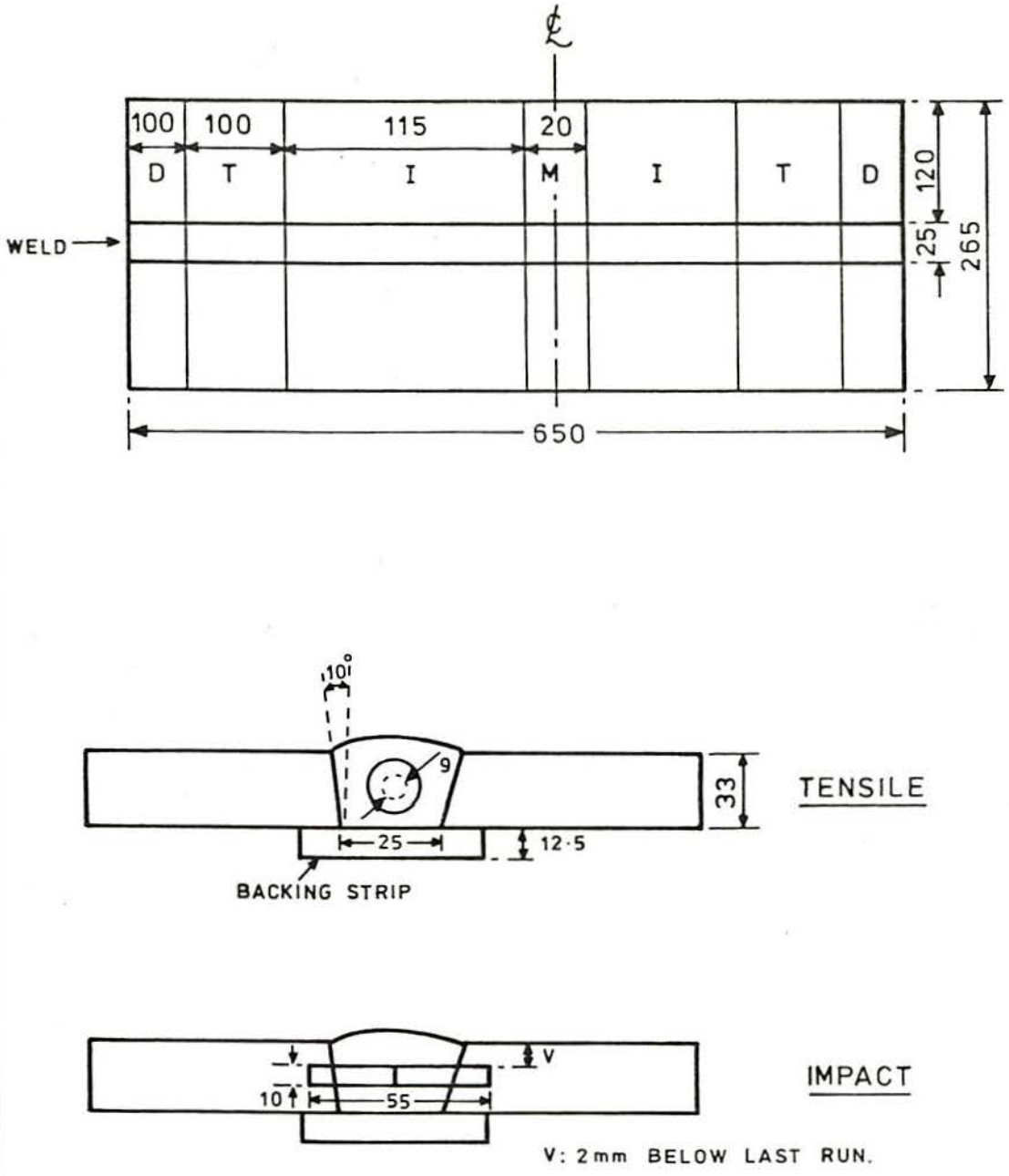

- SPECIMENS TAKEN FROM AREAS:-

I IMPACT.
M METALLOGRAPHY.
T TENSILE.

- AREAS "D" (100mm EACH SIDE) WERE DISCARDED.

FIGURE 7.1 - LOCATION OF ALL-WELD METAL TENSILE AND IMPACT SPECIMENS.

Temperature range (deg C)	Average Cooling Rate (deg C/s)	Average Cooling Time (s)
RT(1000)	--	5.1
1100- 800	-50.00	5.9
800- 500	-14.63	20.5

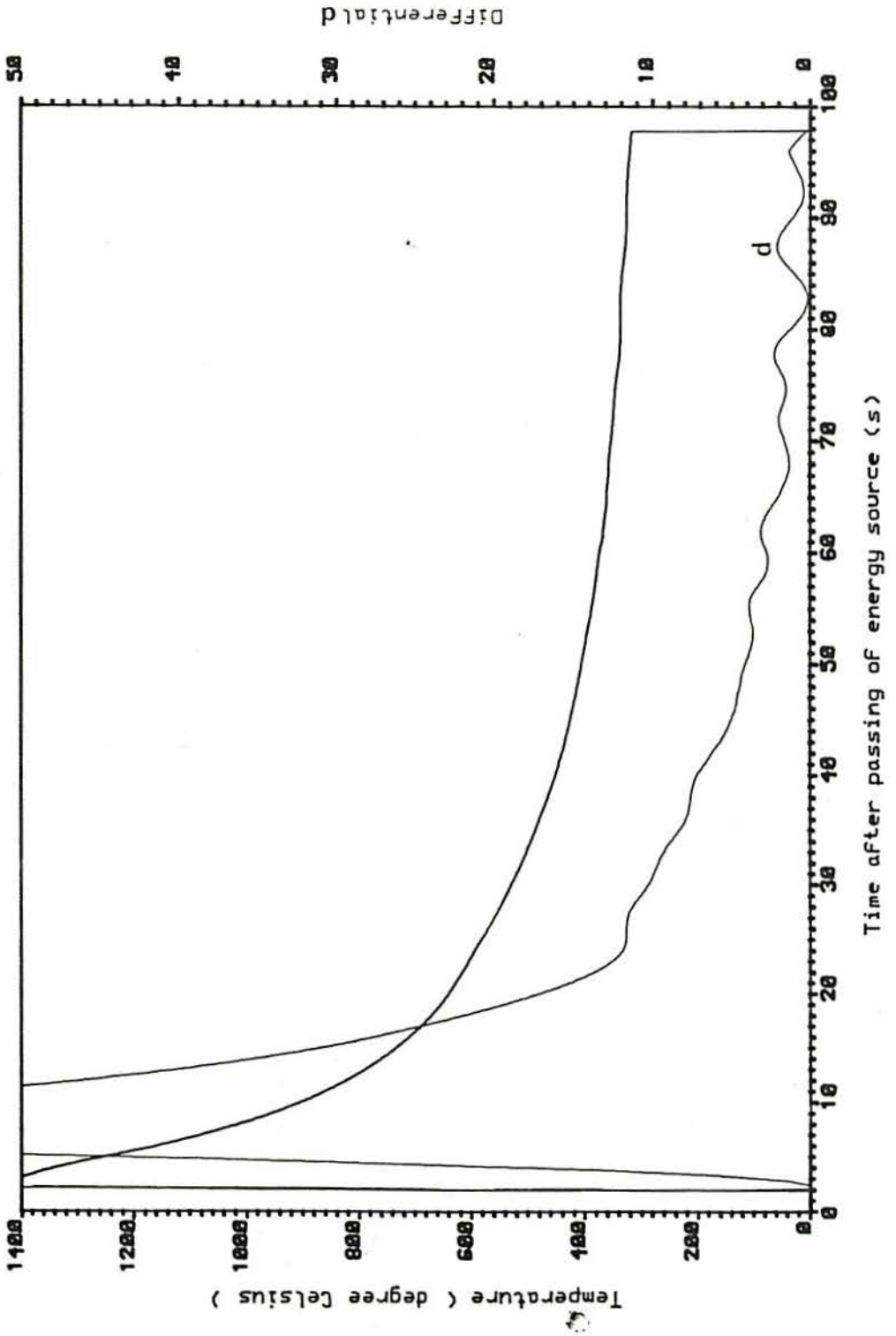

FIGURE 7.2 - WELD METAL THERMAL ANALYSIS - WELDMENT: WH641S4

Temperature range (deg C)	Average Cooling Rate (deg C/s)	Average Cooling Time (s)
RT(1000)	--	5.4
1100- 800	-28.37	10.4
800- 500	-6.51	45.9

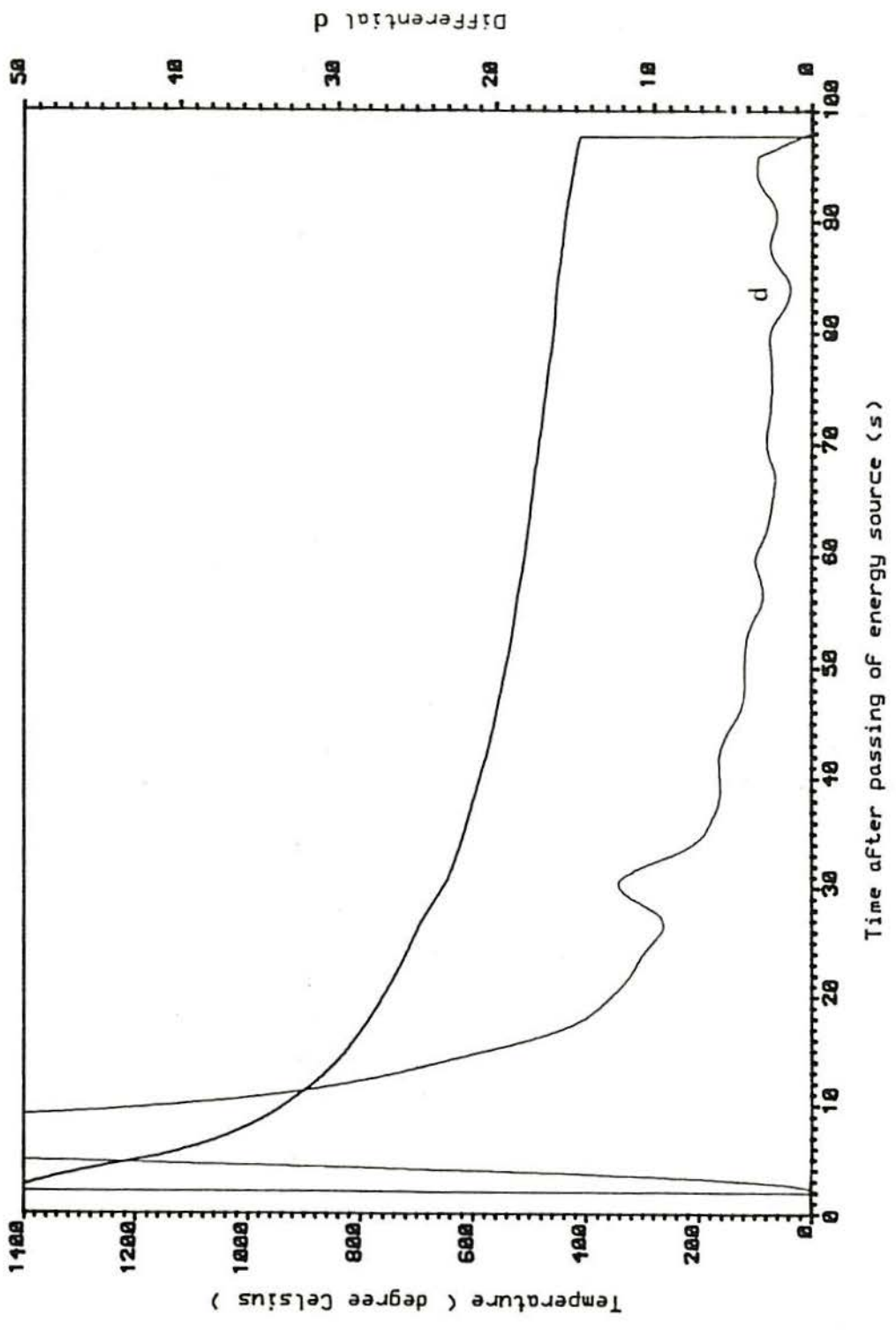

FIGURE 7.3 - WELD METAL THERMAL ANALYSIS - WELDMENT: WQ674L4

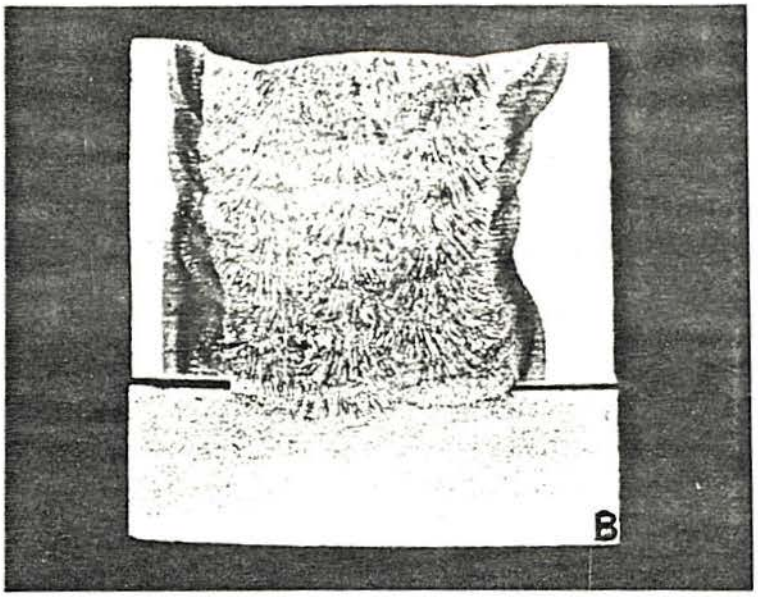

(a) 1.9 KJ/mm energy input welding.

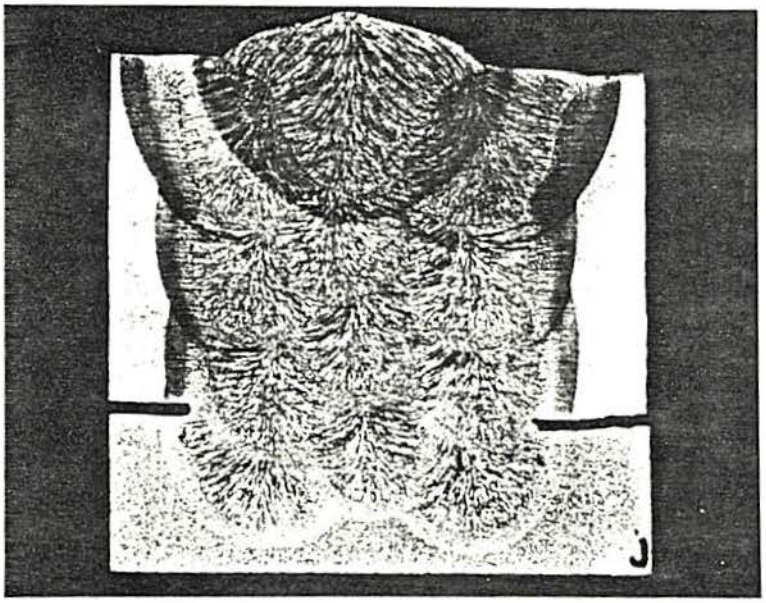

(b) 4.1 KJ/mm energy input welding

FIG. 7.4 Transverse Weld Bead Section Macrostructure. Nital, X 1.

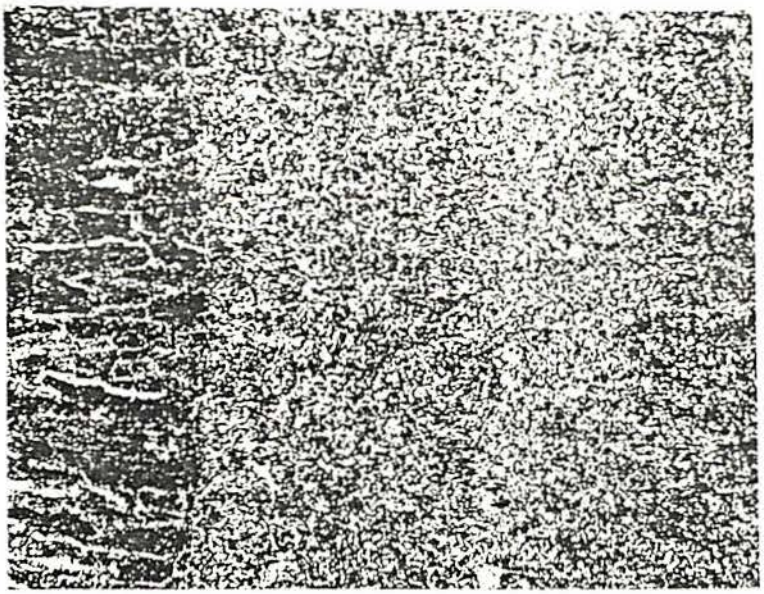

(a) Sp. WQ 641 S4 (1.9 KJ/mm)

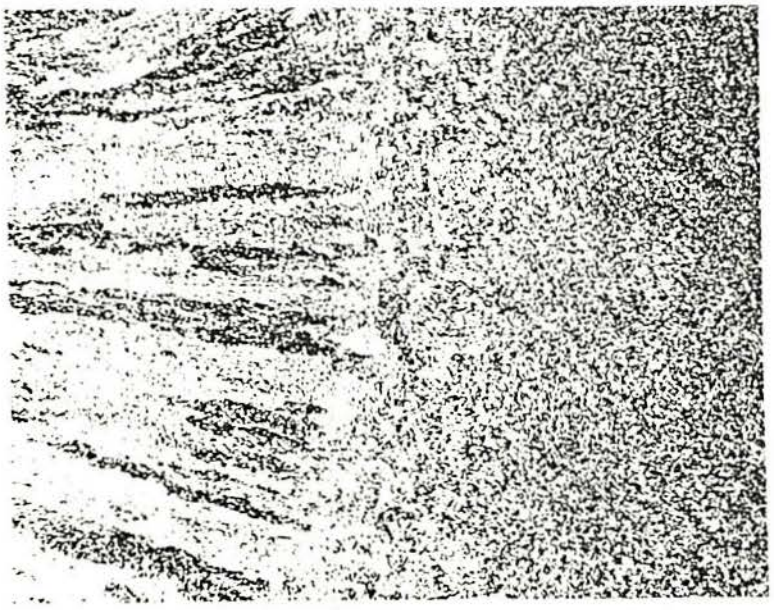

(b) Sp. WQ 674 S4 (4.1 KJ/mm)

FIG. 7.5 Three Microstructural Zones.
Nital, X 50.

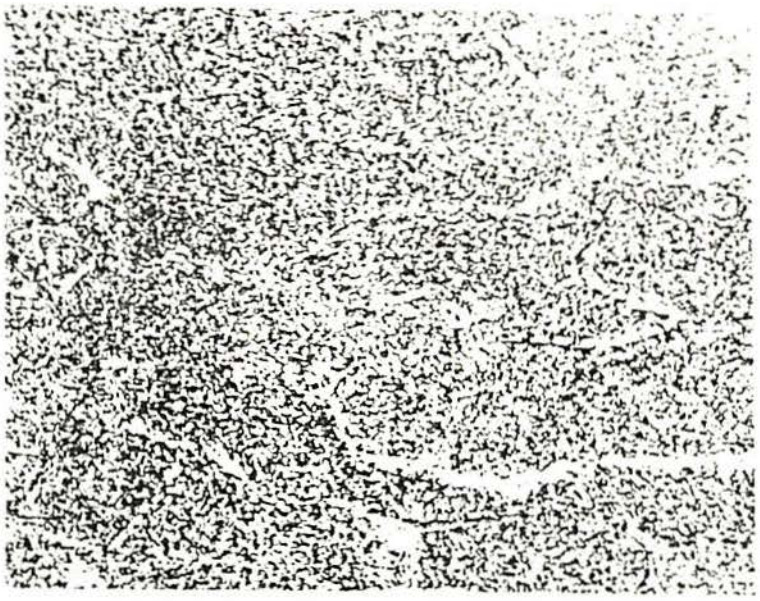

FIG. 7.6(a) Columnar Zone of Sp. WQ 641 S4 (1.9 KJ/mm). Nital, X 200.

FIG. 7.6(b) Detail of (a). Grain Boundary Ferrite (GB), Acicular Ferrite (AF), Martensite (M) , Ferrite with aligned M-A-C (FC), and Carbides (C) Precipitated mainly alon Grain Boundaries. Nital, X 1000.

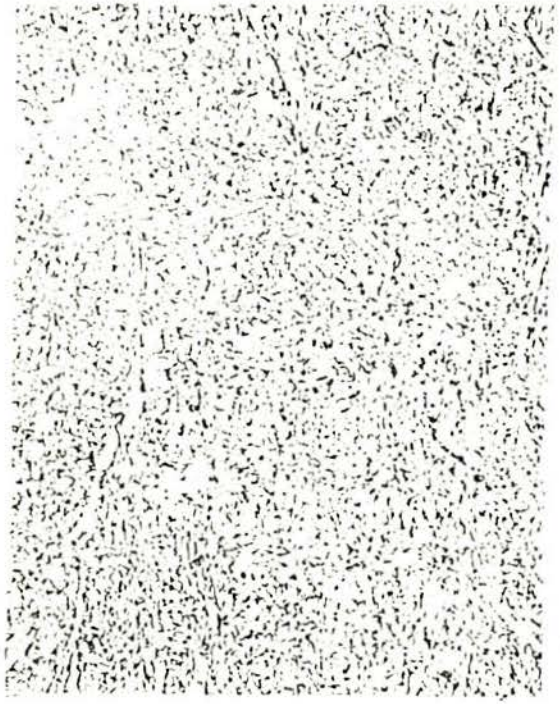

(a) Sp. WQ 674 S1 (OERLIKON S3 wire and OP121TT flux)

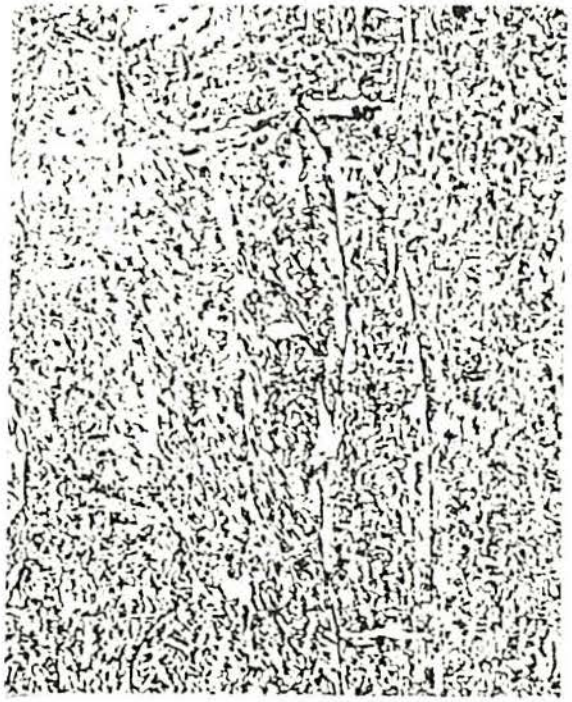

(b) Sp. WQ 674 S4 (OERLIKON S3 wire and OP41TT flux)

(c) Sp. WQ 674 L4 (LINDE 95 wire and OP41TT flux)

FIG. 7.7 Microstructures at the columnar columnar region of 4.1 KJ/mm energy input welds. Nital, X 500.

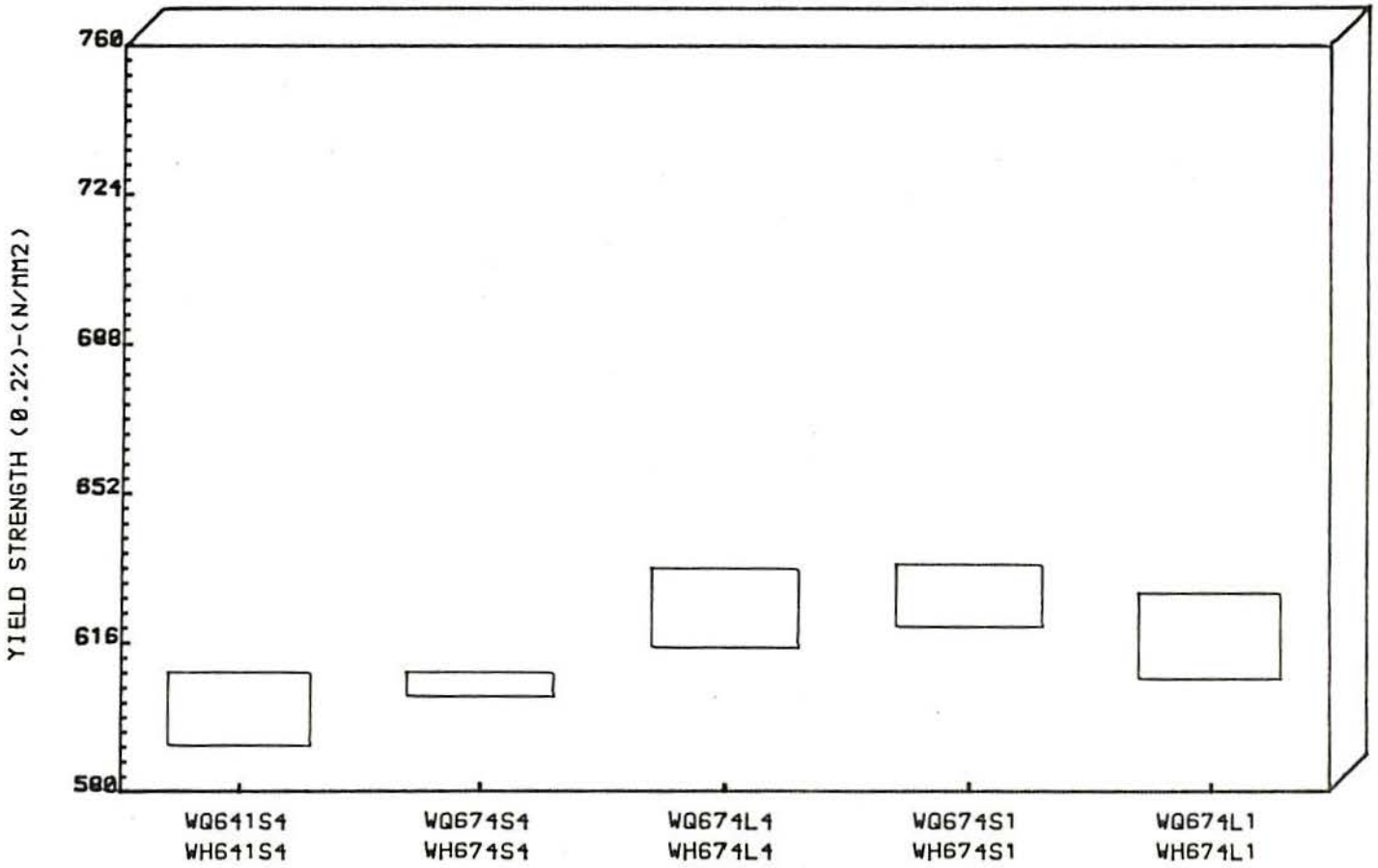

FIGURE 7.8(a)-YIELD STRENGTH RANGE FOR ALL WELD METALS

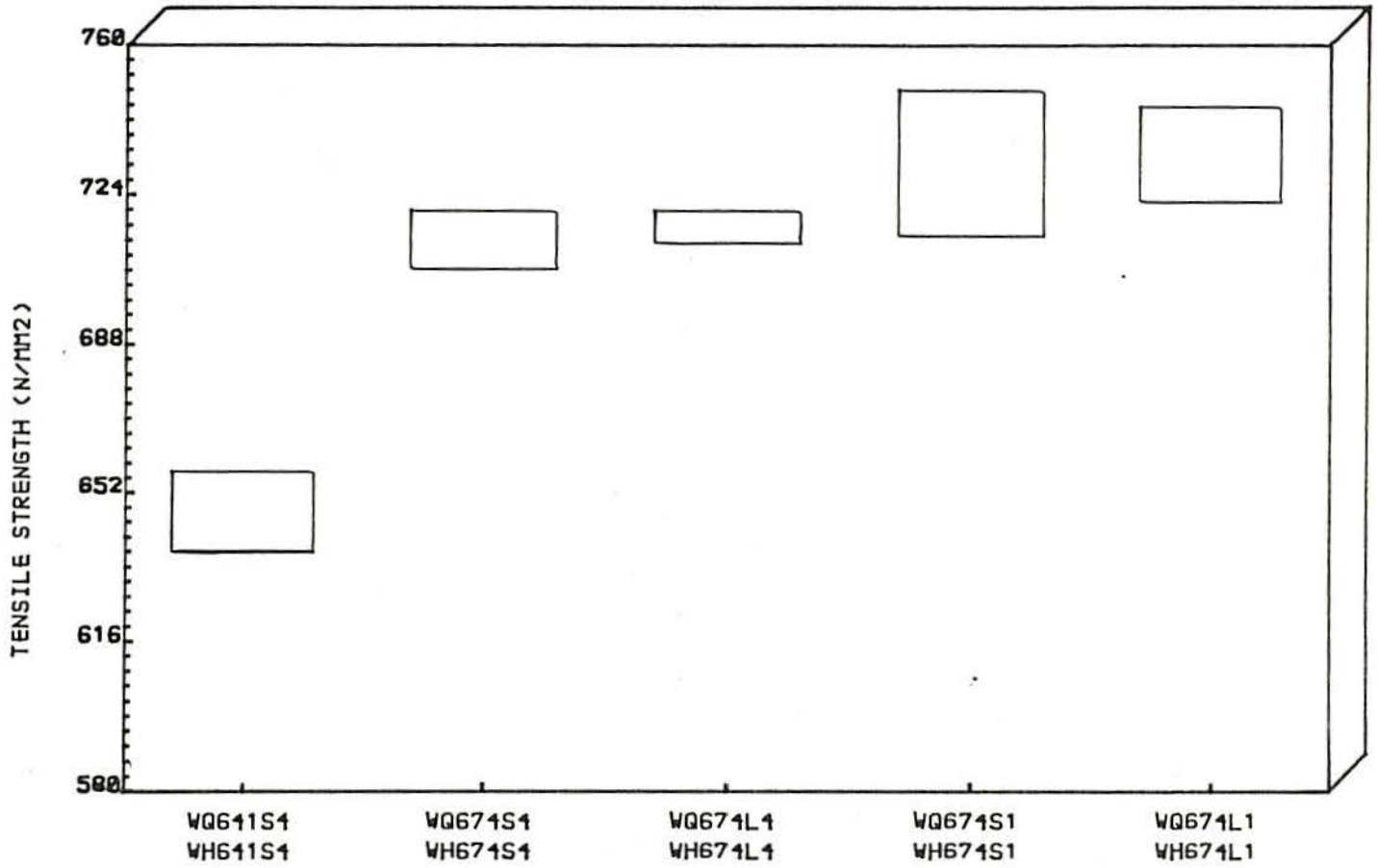

FIGURE 7.8(b)-TENSILE STRENGTH RANGE FOR ALL WELD METALS

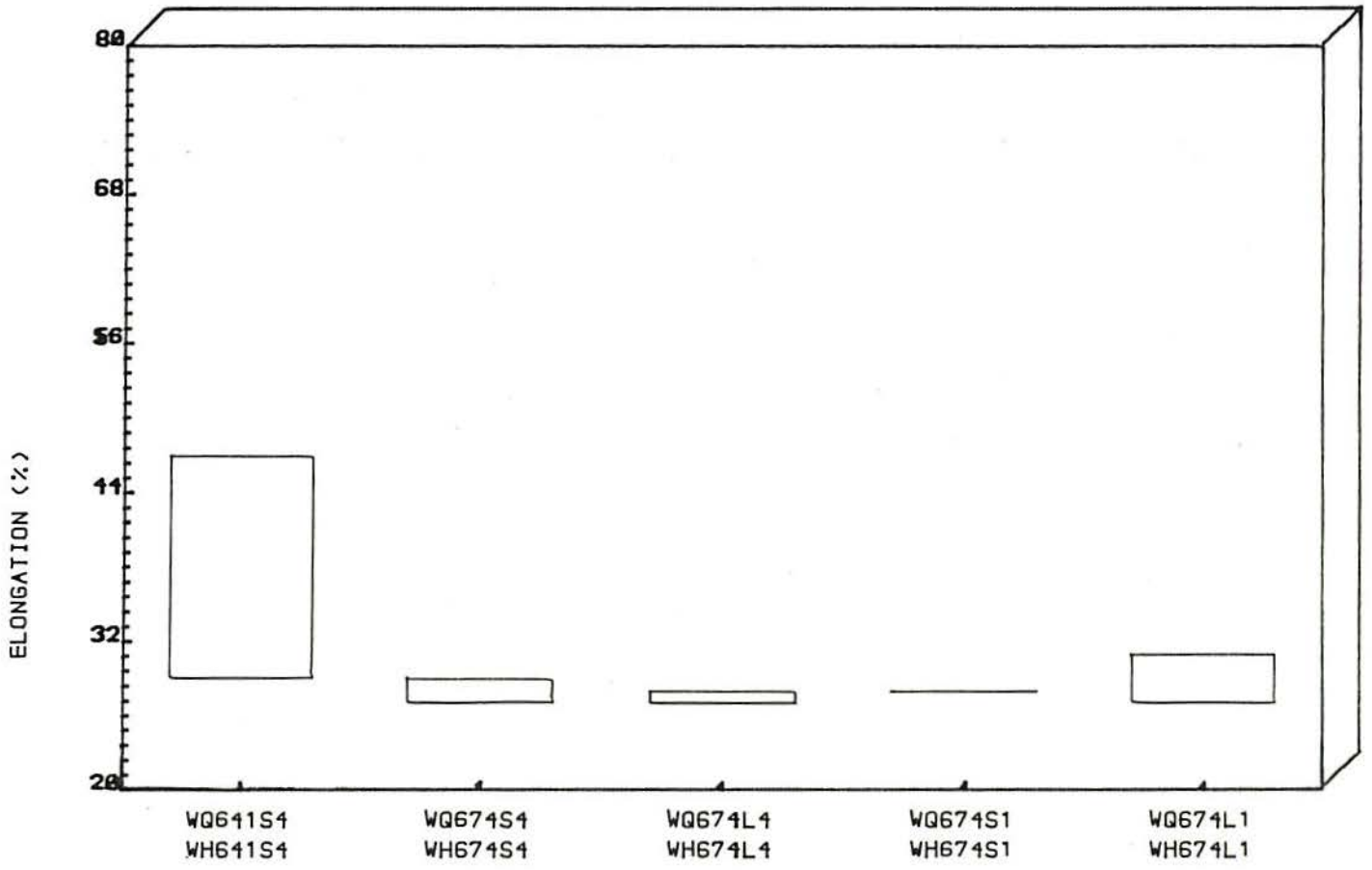

FIGURE 7.8(c)- ELONGATION RANGE FOR ALL WELD METALS

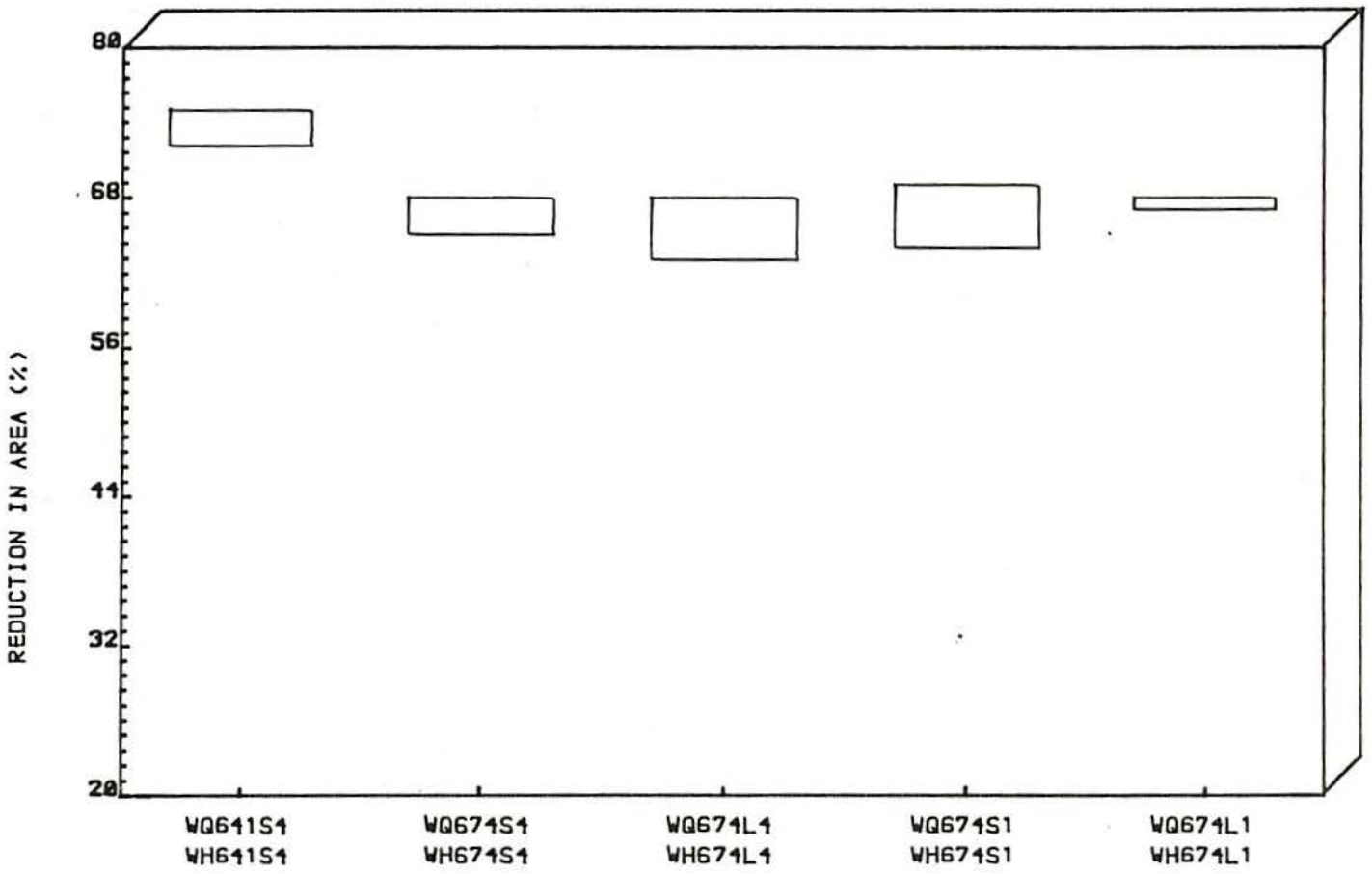

FIGURE 7.8(d)-REDUCTION IN AREA RANGE FOR ALL WELD METALS

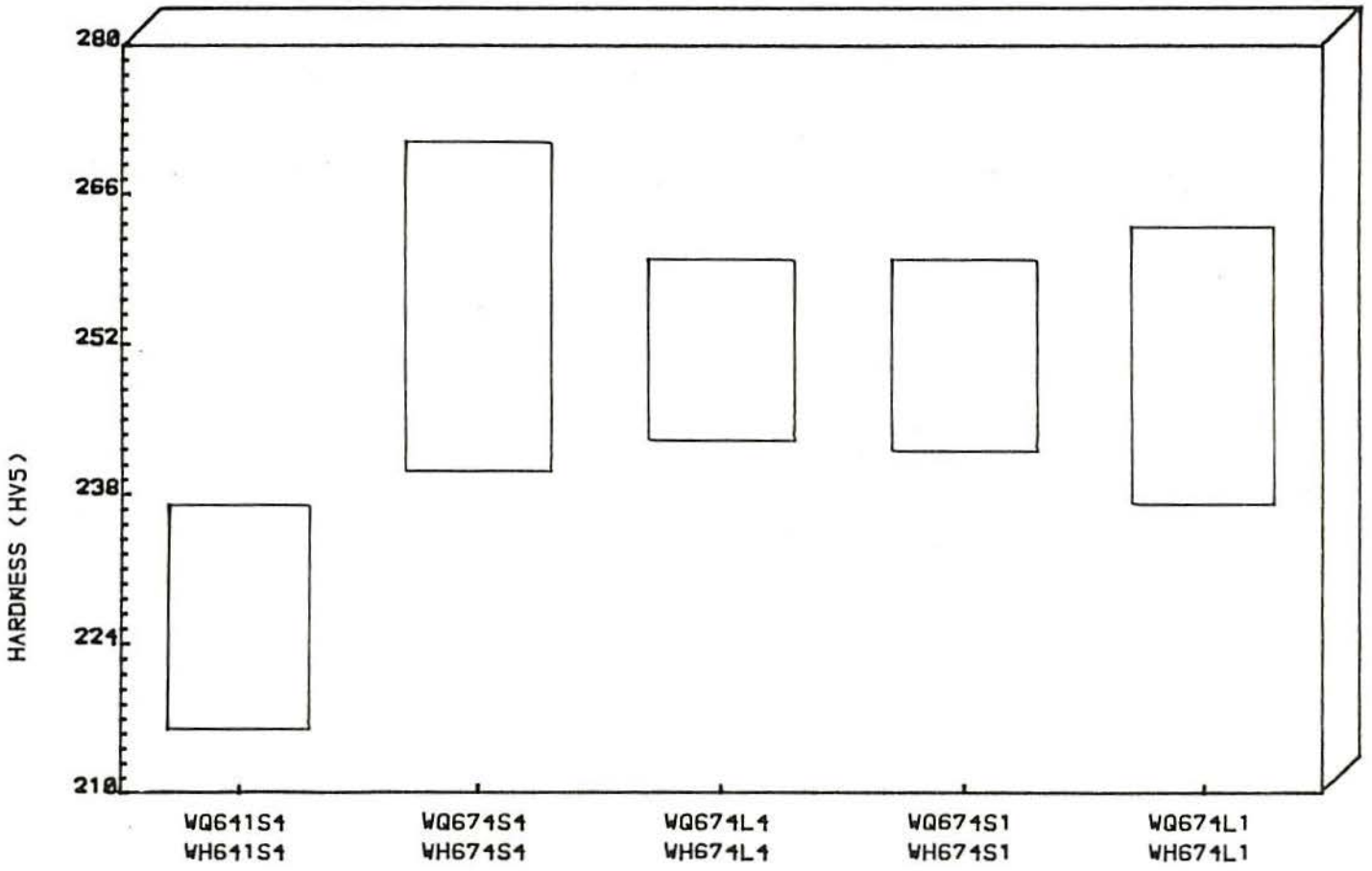

FIGURE 7.8(e)-HARDNESS RANGE FOR ALL WELD METALS

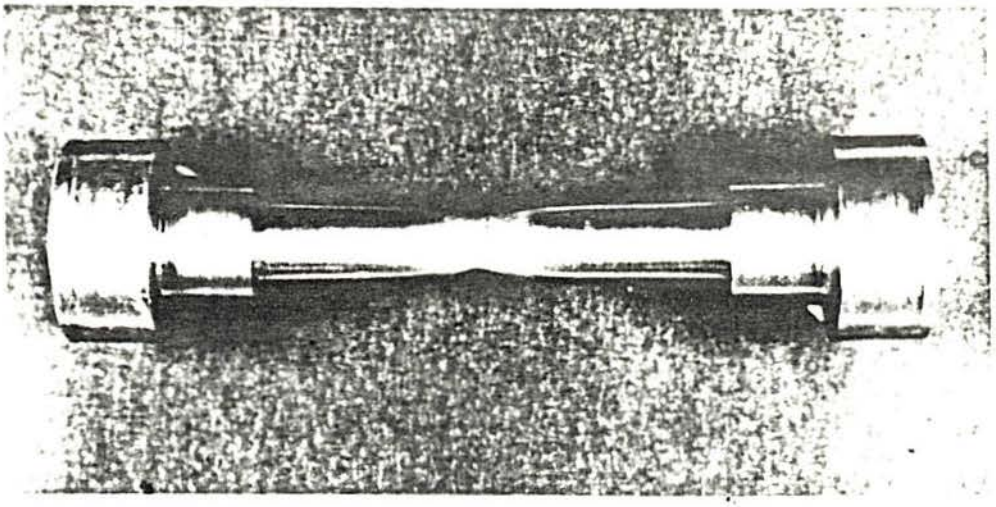

FIG. 7.9(a) All Weld Metal Tensile Specimen Pieces Assembled After Test. X 1.

FIG. 7.9(b) 'Cup' and 'Cone' Fracture Surfaces Macrophotograph. X 1.4

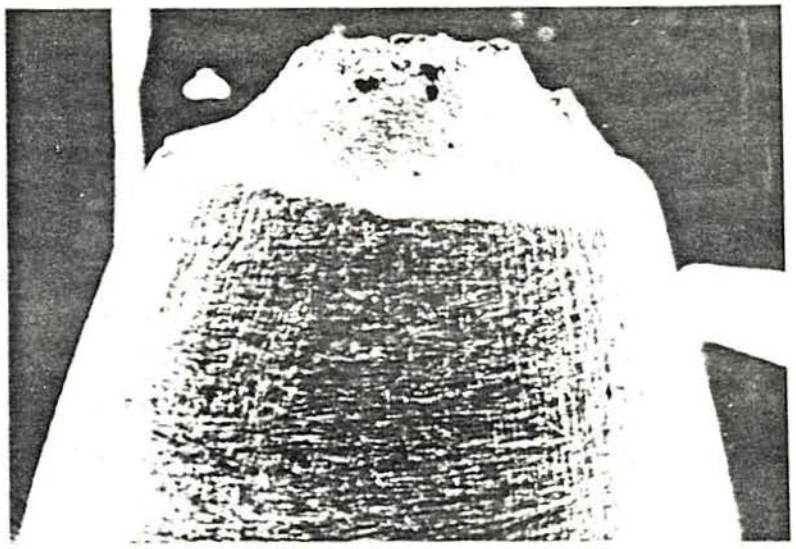

FIG. 7.10(a) SEM View of the 'Cone' part. Tensile Specimen. X 20.

FIG. 7.10(b) SEM View of the 'Cup' part. Tensile Specimen. X 20.

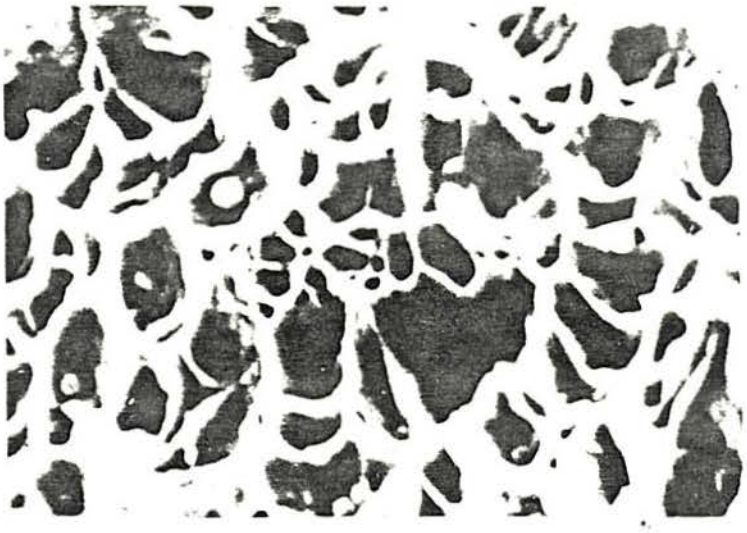

HG. 7.10(c) Micro-Voids on the 'Cup' Surface Fractured Tensile Specimen. The Particles Which Initiated the Voids are Visible. SEM, X 5K.

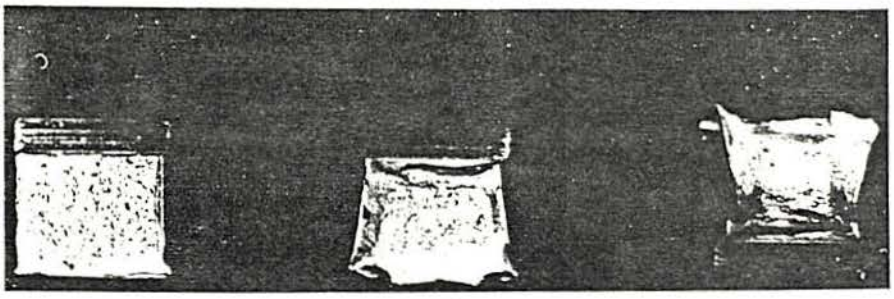

$-80^{o}C$ $-40^{o}C$ $20^{o}C$

FIG. 7.13 Examples of Fracture Surface Degree of Crystallinity for Charpy Specimens Tested at 20, -40 and -80 ^{o}C. X 2.

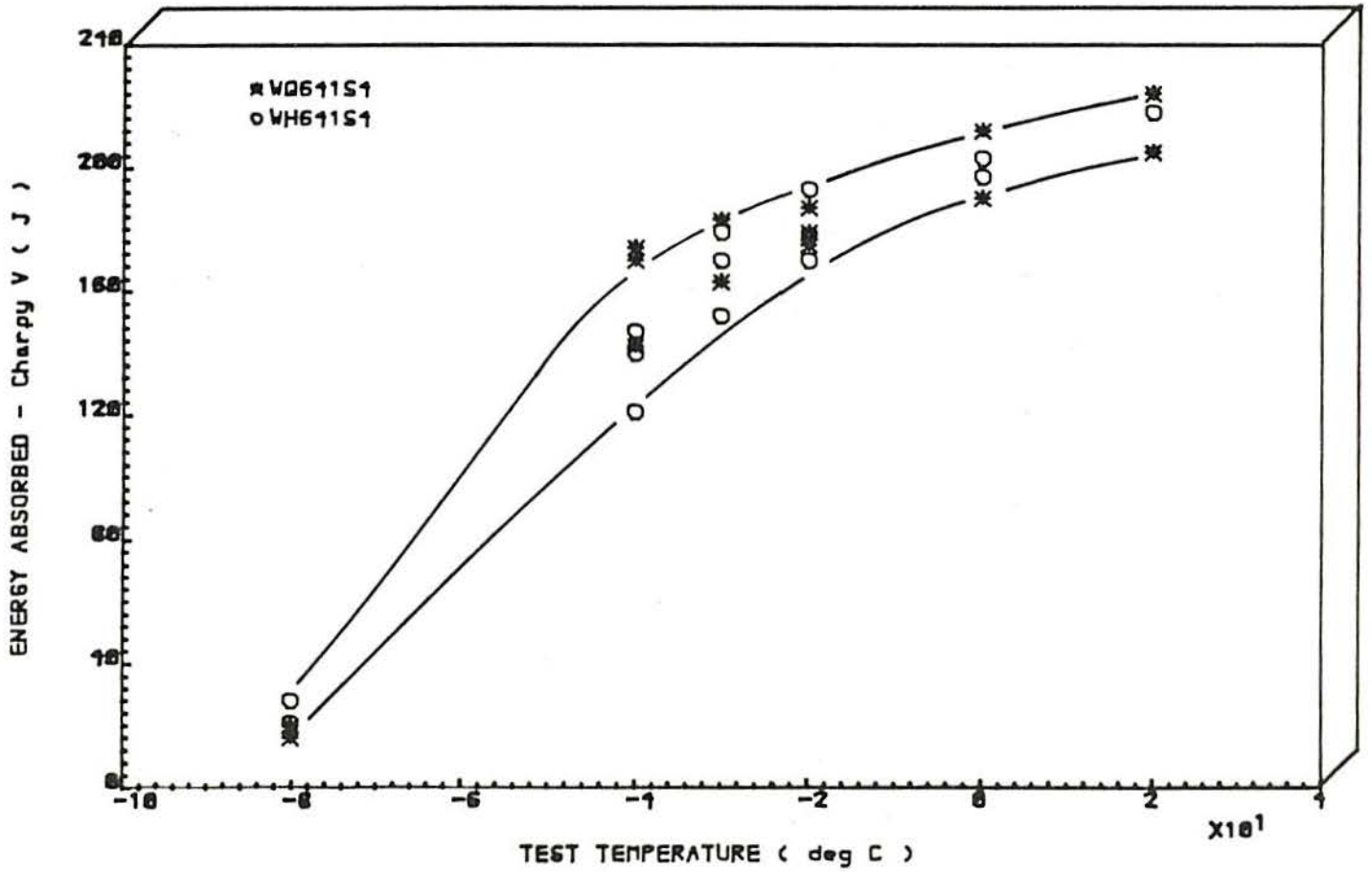

FIGURE 7.11(a) -CHARPY V-NOTCH TRANSITION CURVES FOR WELD METALS DEPOSITED UNDER SAME CONDITIONS ON Q2N AND HY 100 STEELS

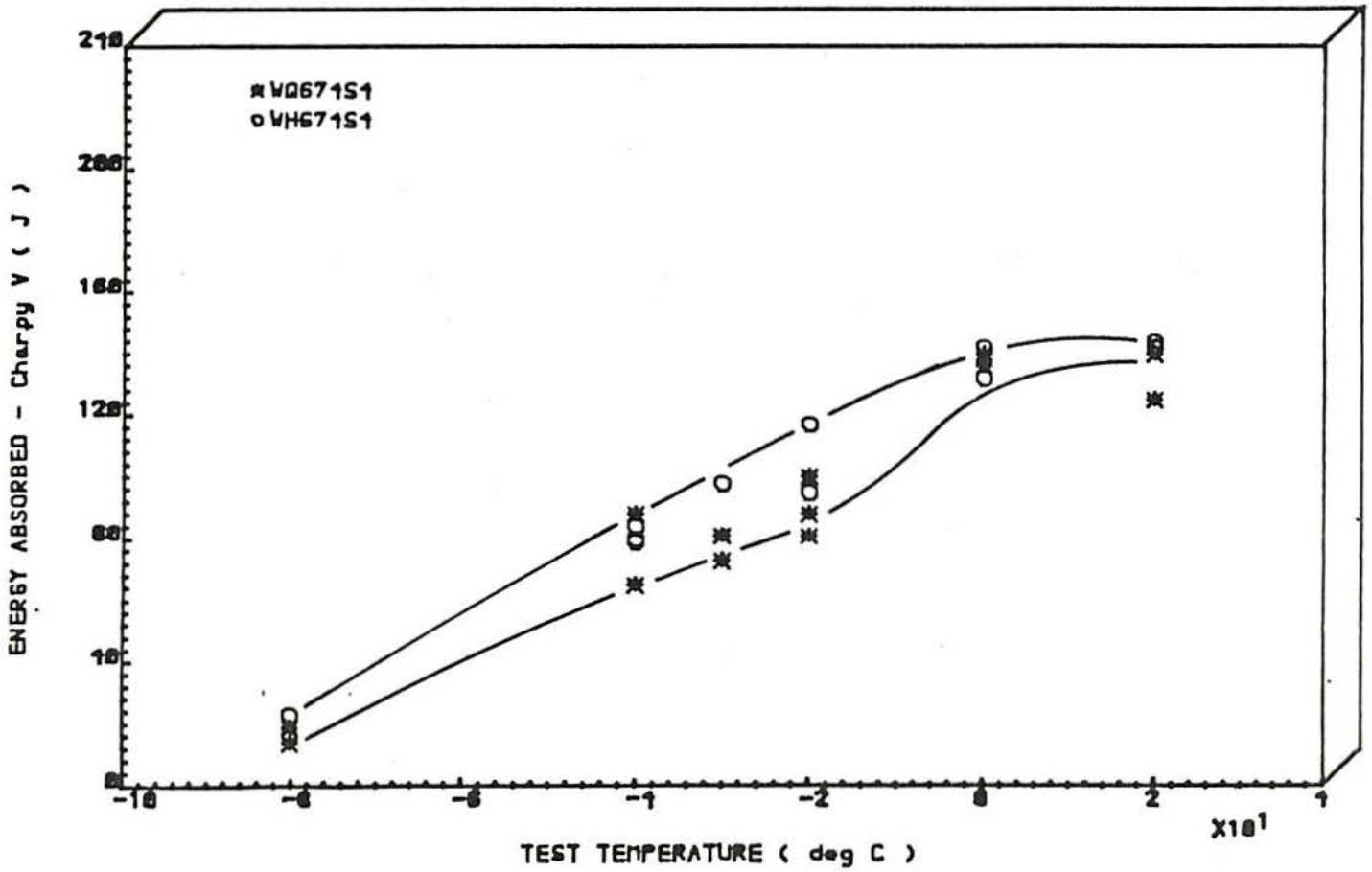

FIGURE 7.11(b)- CHARPY V-NOTCH TRANSITION CURVES FOR WELD METALS DEPOSITED UNDER SAME CONDITIONS ON Q2N AND HY 100 STEELS

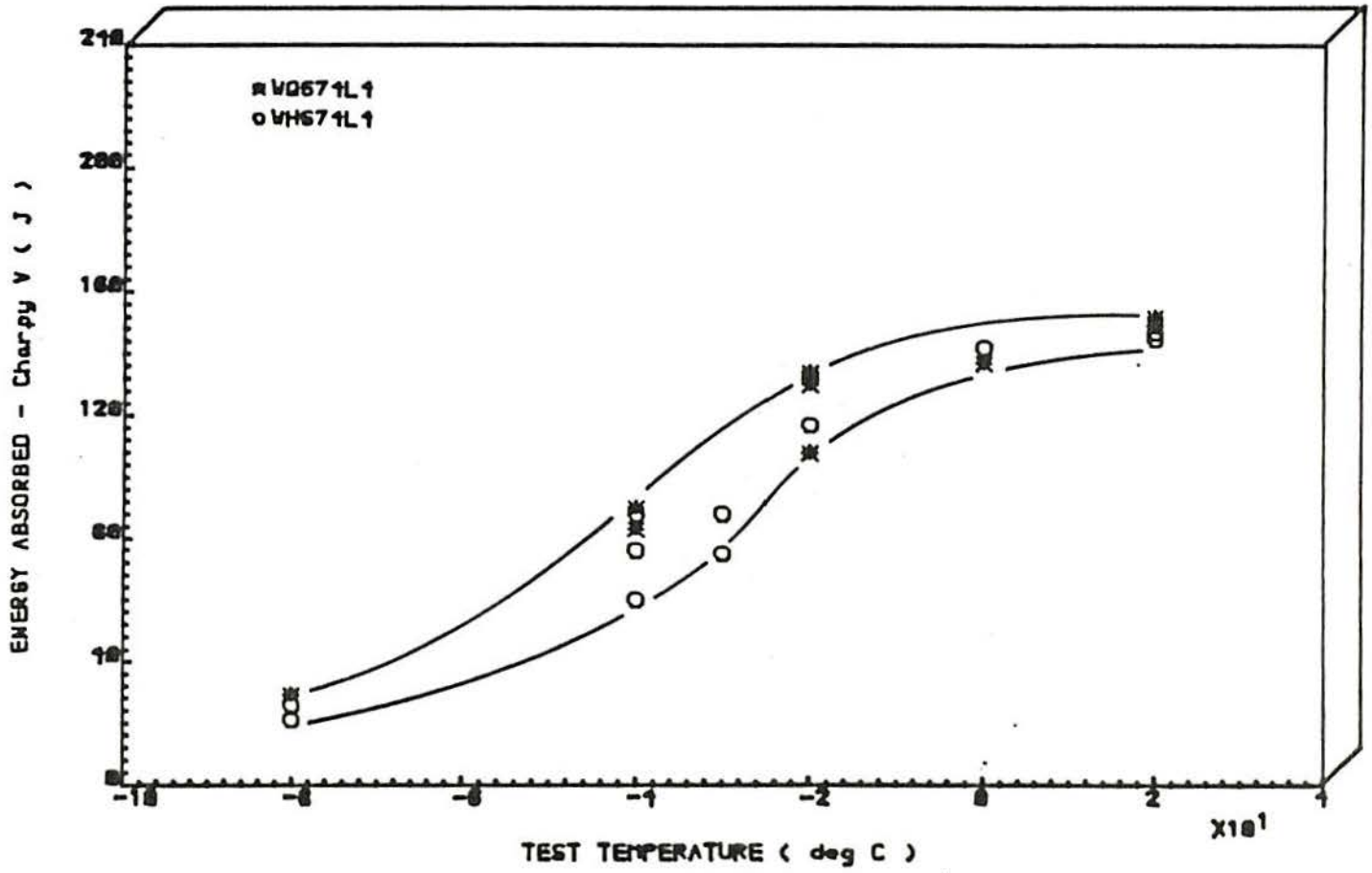

FIGURE 7.11(c)- CHARPY V-NOTCH TRANSITION CURVES FOR WELD METALS DEPOSITED UNDER SAME CONDITIONS ON Q2N AND HY 100 STEELS

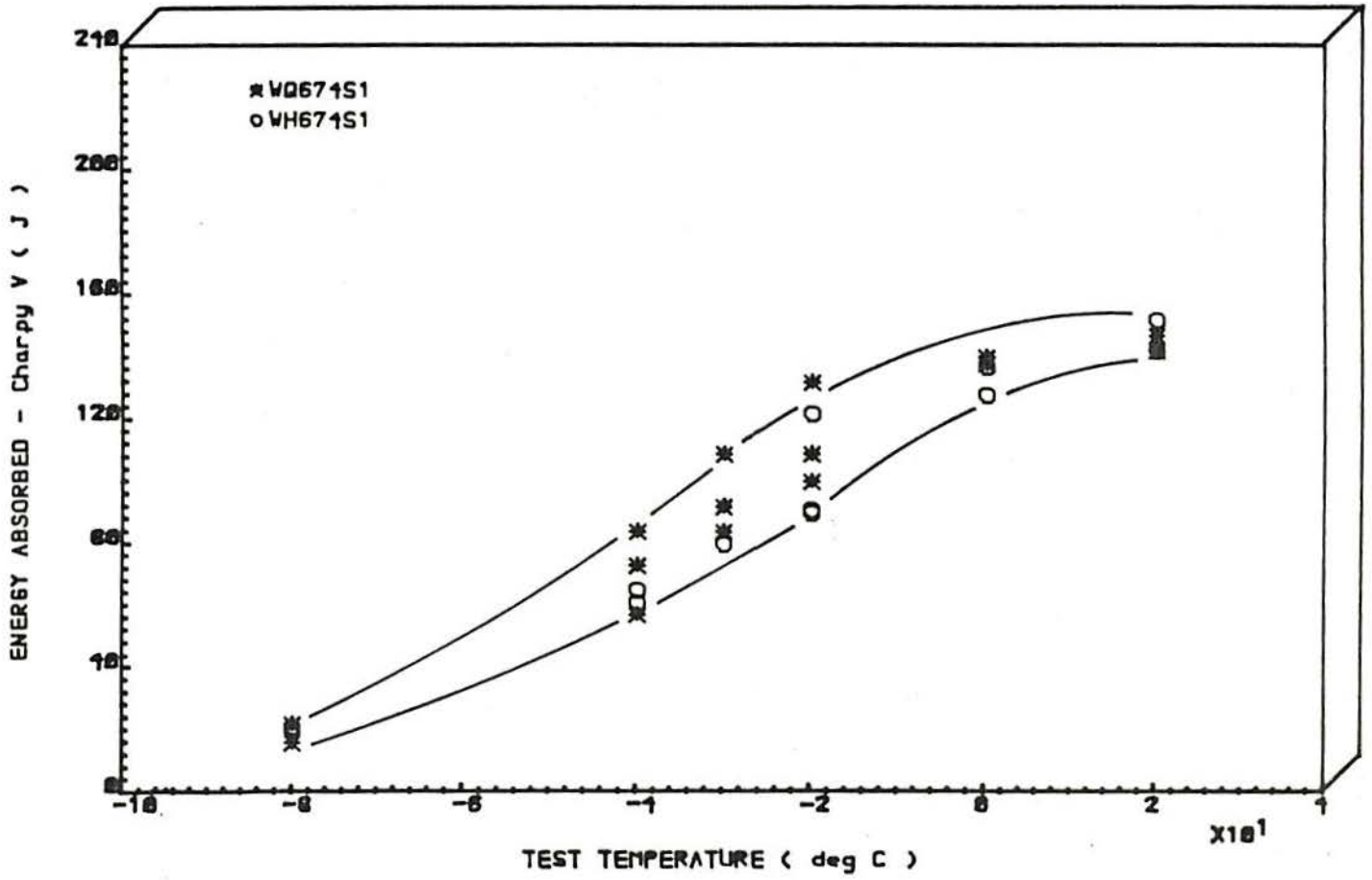

FIGURE 7.11(d)- CHARPY V-NOTCH TRANSITION CURVES FOR WELD METALS DEPOSITED UNDER SAME CONDITIONS ON Q2N AND HY 100 STEELS

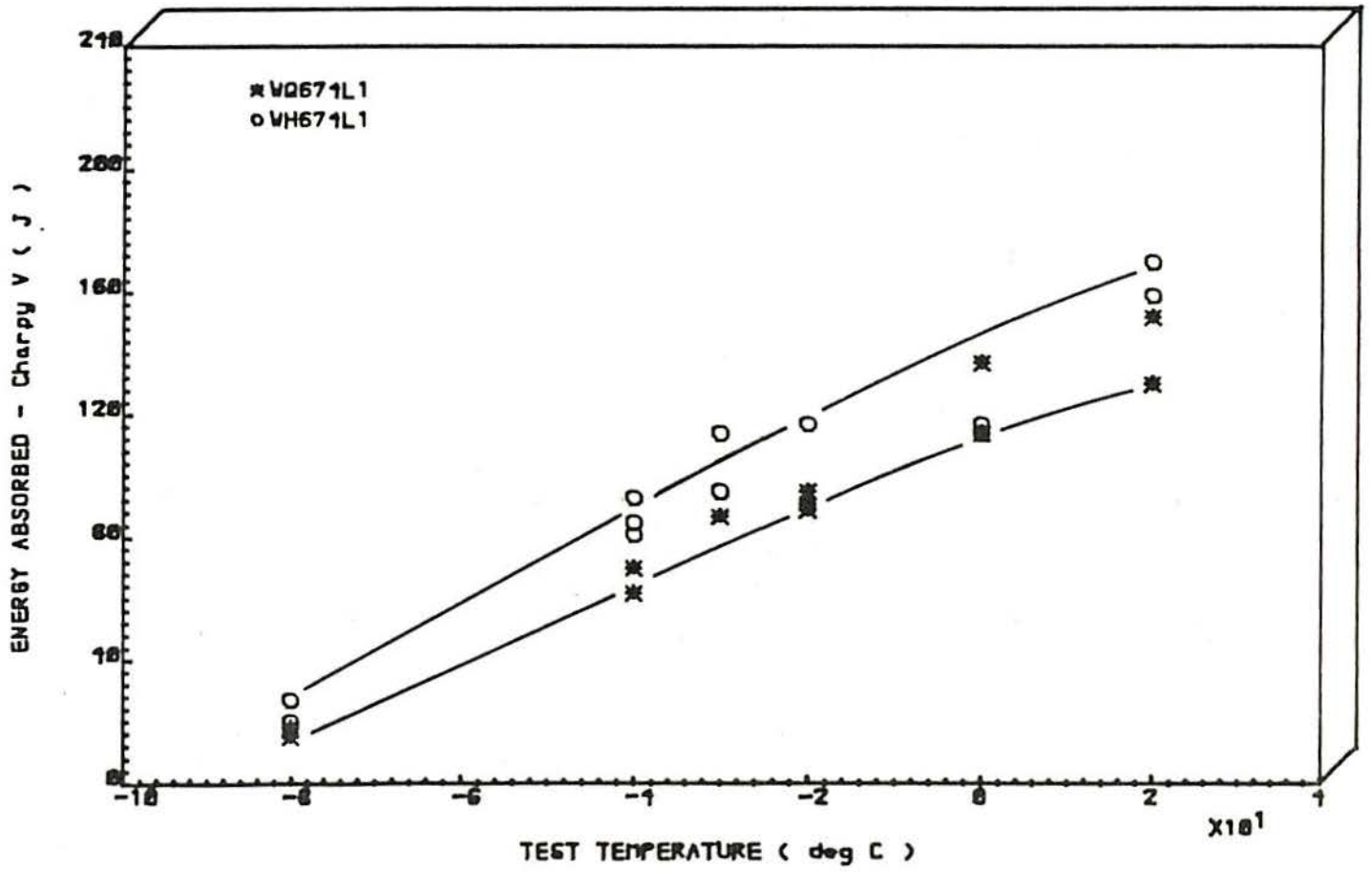

FIGURE 7.11(e)- CHARPY V-NOTCH TRANSITION CURVES FOR WELD METALS DEPOSITED UNDER SAME CONDITIONS ON Q2N AND HY 100 STEELS

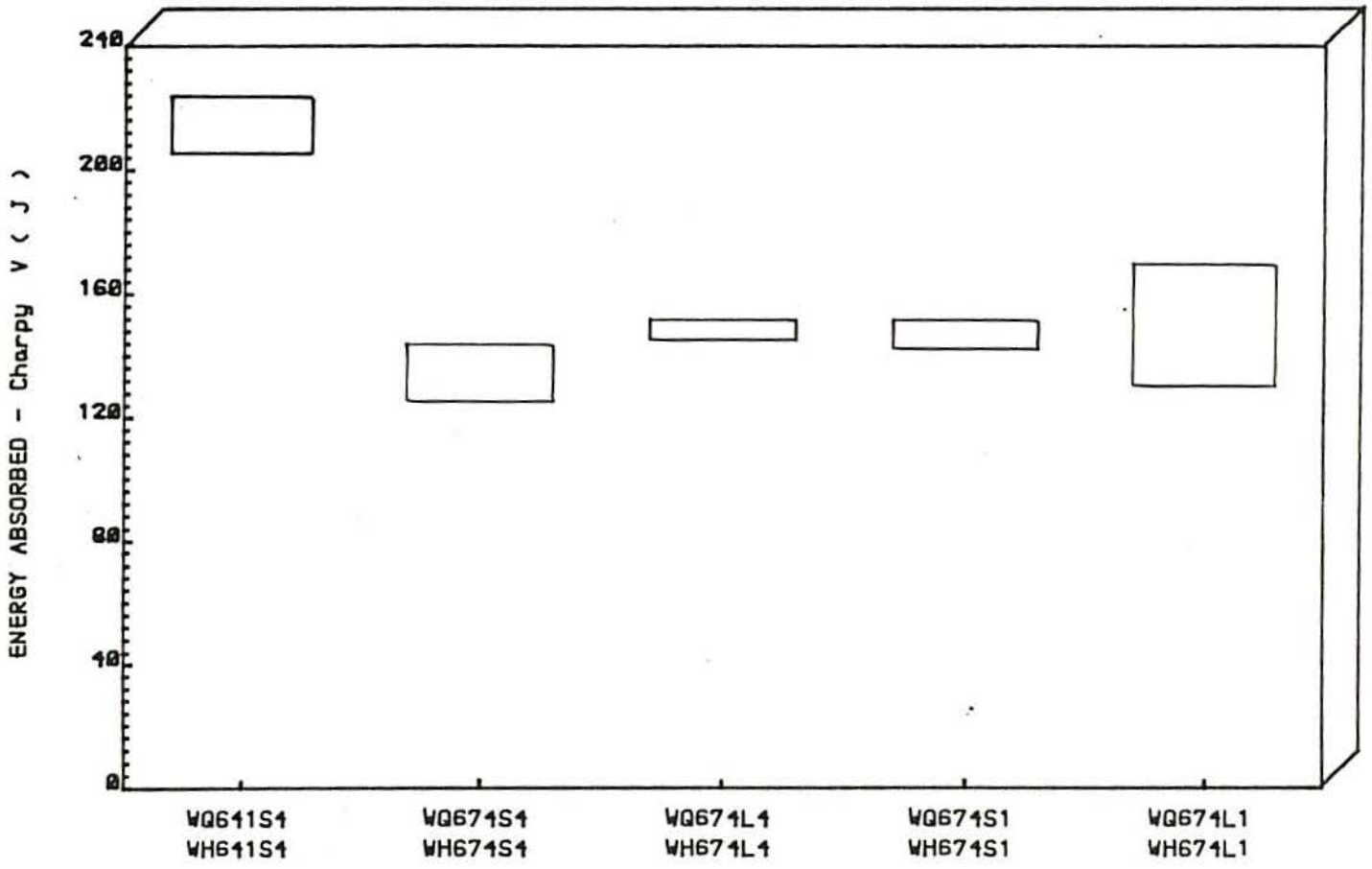

FIGURE 7.12(a) CHARPY V-NOTCH ENERGY ABSORBED RANGE FOR ALL WELD METALS AT 20 deg Celsius

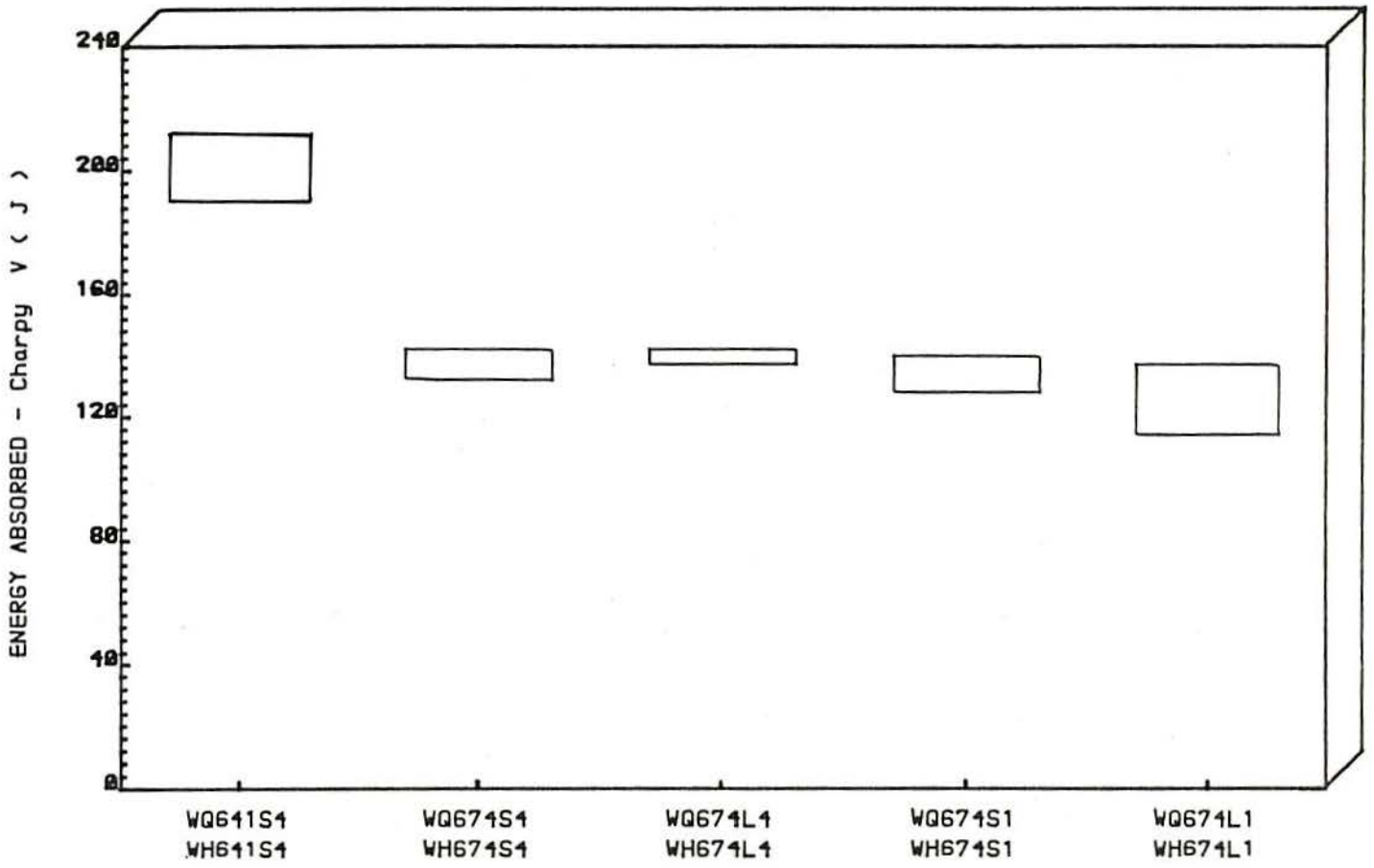

FIGURE 7.12(b)-CHARPY V-NOTCH ENERGY ABSORBED RANGE FOR ALL WELD METALS AT 0 deg Celsius

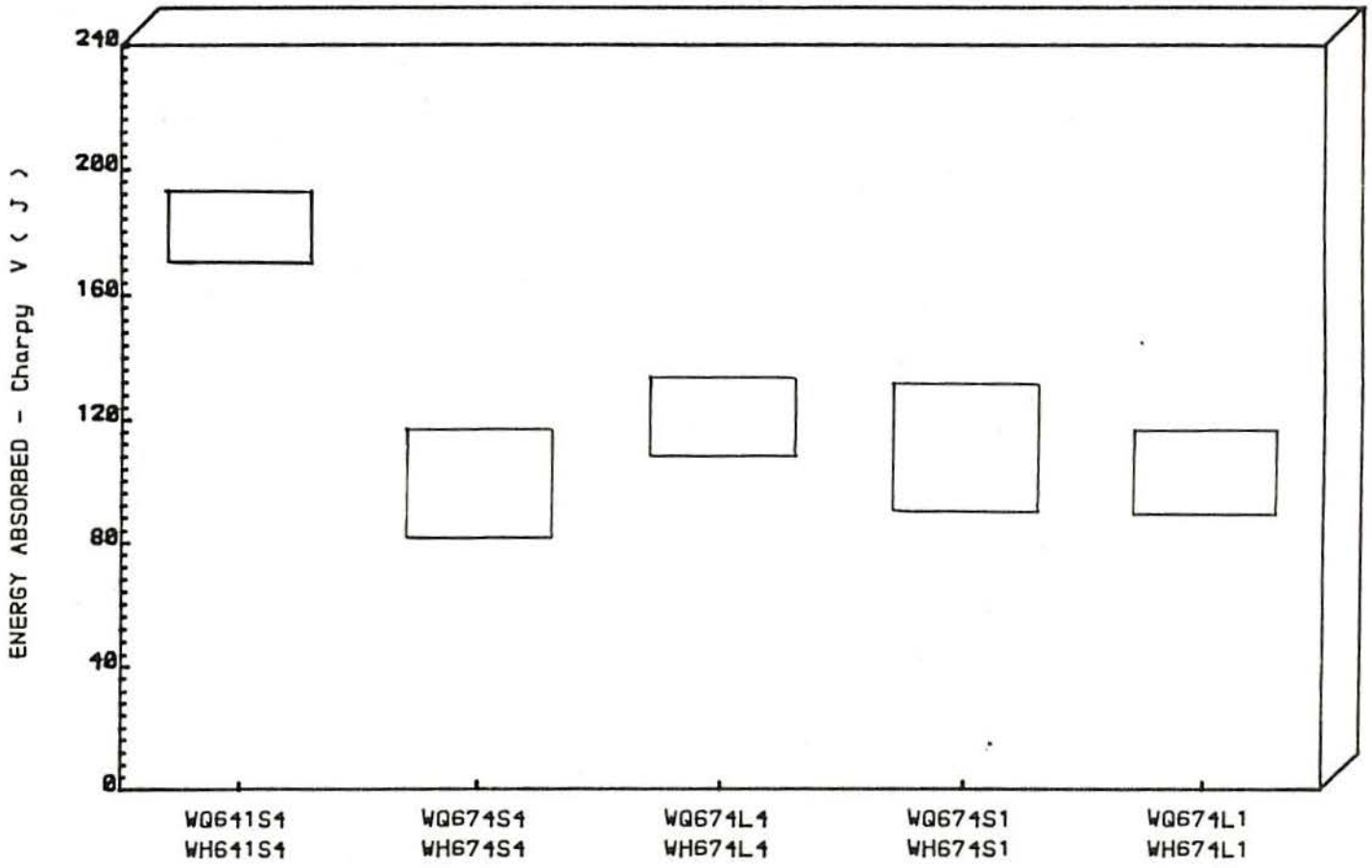

FIGURE 7.12(c)CHARPY V-NOTCH ENERGY ABSORBED RANGE FOR ALL WELD METALS AT -20 deg Celsius

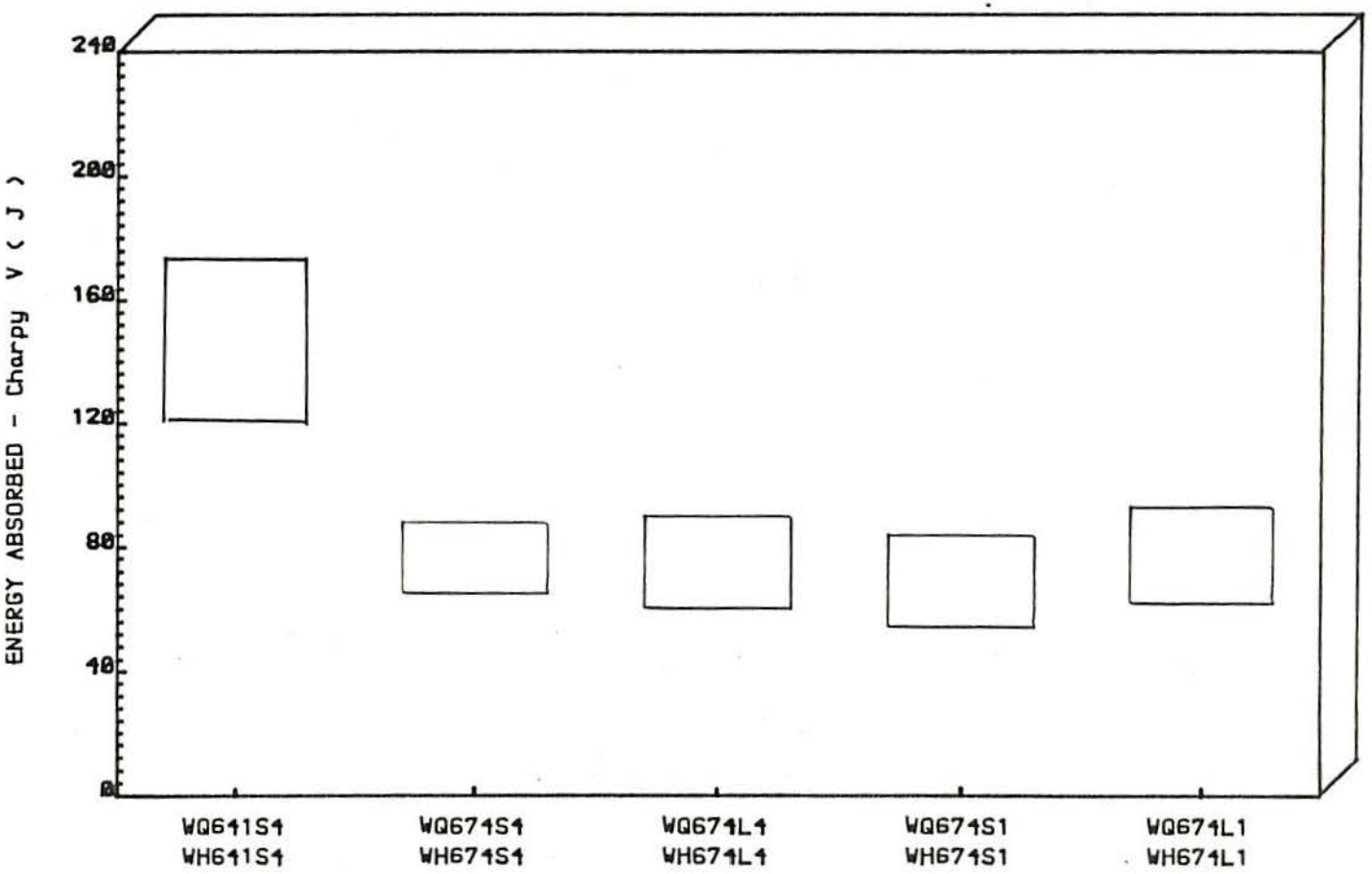

FIGURE 7.12(d)CHARPY V-NOTCH ENERGY ABSORBED RANGE FOR ALL WELD METALS AT -40 deg Celsius

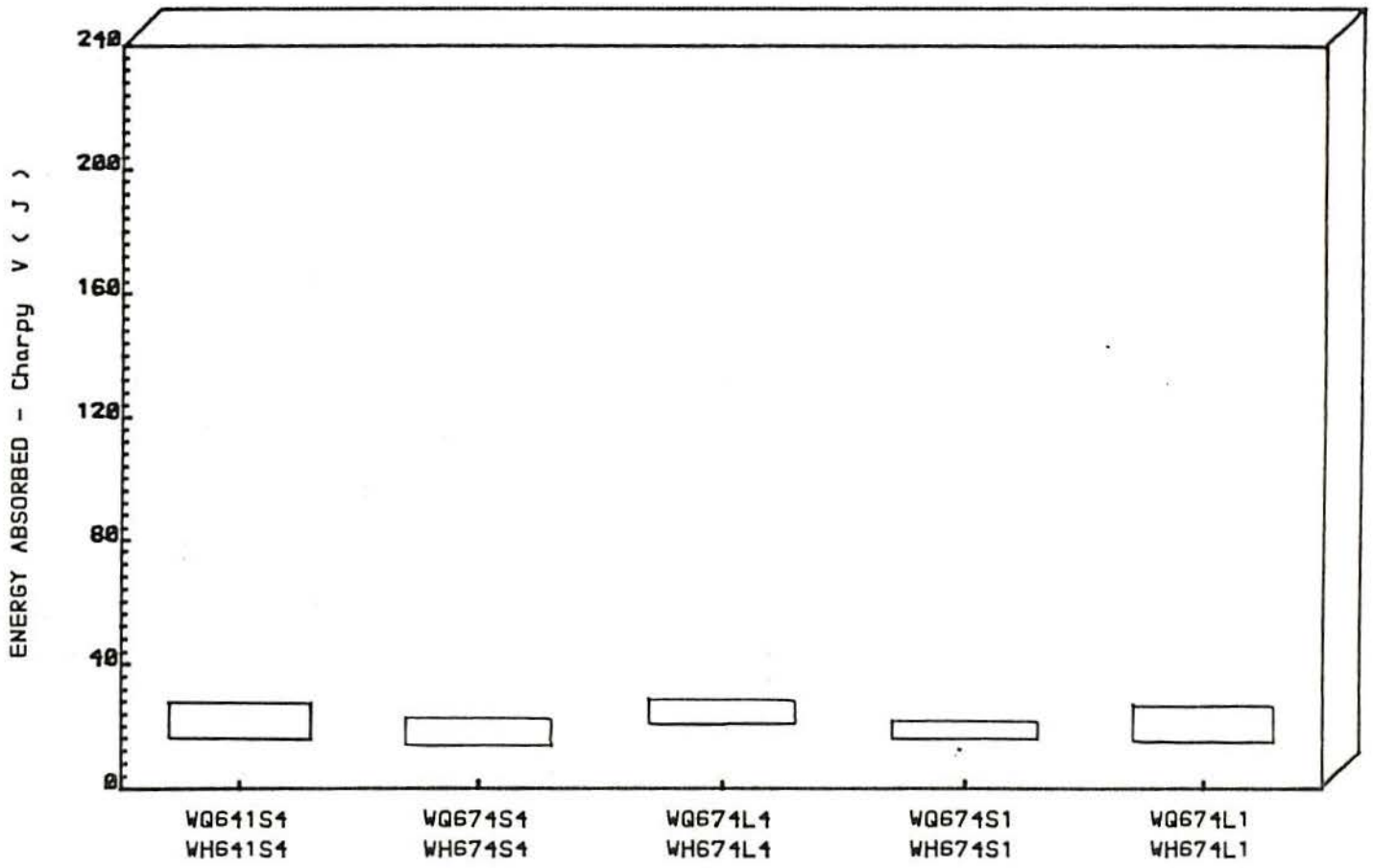

FIGURE 7.12(e)CHARPY V-NOTCH ENERGY ABSORBED RANGE FOR ALL WELD METALS AT -80 deg Celsius

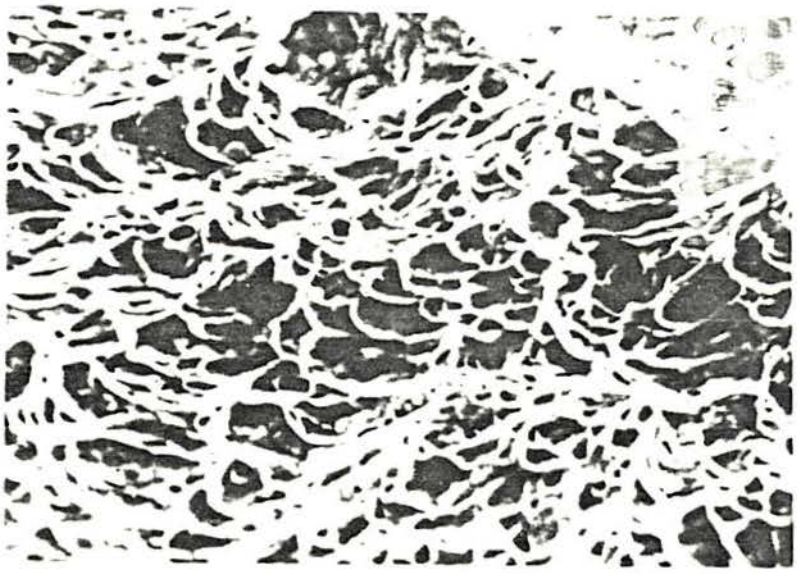

(a)

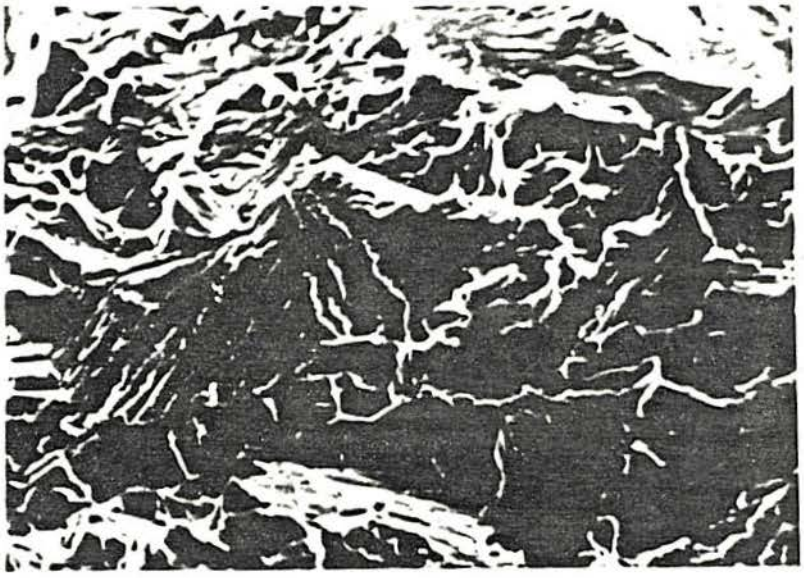

(b)

FIG. 7.14 General Fracture Mode for Charpy Specimens SEM, X 2K. Tested at: (a) 20°C . Micro - -Void Coalescence Type. (b) -80°C. Quasi - cleavage, with ill-defined cleavage Facets.

8. WELD METAL SOLIDIFICATION CRACKING TESTS

8.1 Welding conditions and coding

To investigate root run weld metal solidification cracking susceptibility, a series of single pass submerged arc welds was made. All fluxes, wires and base metals described in Chapter 6 were combined and used at different welding parameters.

The weld specimen geometry selection was not straightforward. The main aims were to: obtain repeatable geometry; induce consistent and reproducible weld metal cracking; have some similarity with practical conditions. Furthermore, it was desirable (as always it is) to obtain these conditions without excessive expenditure of money or labour. Therefore, the proper choice involves technical and economic considerations.

The literature lists many weldability tests / 244, 245 /, for example.

After a critical analysis, however, we conclude that they are directed to very specific conditions, or base metal study only / 202 /, and in general not suitable for submerged arc process due to operational problems.

Therefore, we had to design our own test specimen and after some initial trials investigating hydrogen induced cracking (Chapter 1) we decided on the geometry seen in Figure 8.1. It almost entirely satisfies our conditions. The high restraint is provided by the anchor (MMA and MIG) welds and stiffeners, whilst the 60° groove angle seems to intensify this restraint (Chapter 9) and it is used in the wellknown NRL keyhole test.

Handling is another point to be considered, and in spite of the final specimen relatively heavy weight (36 Kg), it is still manageable by one man.

To have a constant amount and shape of flux, a special asbestos container was always placed on the specimen during welding. It was a rectangular box, with a special geometry to allow the run off/on tabs covering as well. Its (inside) dimensions were 70 mm x 500 mm and variable height, from 25 mm on the base plate to 35 mm at the run off/on tabs. The optimum flux height was established as 20 mm above the plate level. This gives an approximate volume of 800 cm^3 and weight of 1.7 Kg of flux inside the box.

The complete set-up is shown in Figure 8.2. It must be noticed that connected to the welding head there is a small component, which is not part of the normal system for submerged arc weld. This is the mechanism for wire oscillation and it will be explained in Chapter 9. It can also be seen that the welding head is rotated 90° from the position the welds in the present study were made. Again, this rotation was necessary to make the longitudinal (welding direction) oscillation and will be justified and explained in Chapter 9.

Based on practical considerations, gap widths (nomiaally 2.0 mm) were only accepted within the range 1.7 - 2.2 mm, being not realistic a narrow range. The numbers of rejected specimens due to this (assembly) problem were relatively low (5 specimens), and they were

used after repair. The number of discarded specimens due to operational error or welding problems was also relatively small (6 specimens).

The chosen welding conditions are shown in Table 8.1. For easy reference to each one, a special coding was developed, similar (but extended) to that used in Chapter 7. The reading of this chapter will be less hard if this code is understood. Therefore, consider an example weld coded Q or H VAE XF:

- 'H' or 'Q' means welding on HY100 or Q2N steel, respectively
- 'V' means welding speed (it can be given by one or two digits)

  6 = 6.3 mm/s

  9 = 9.5 mm/s

  13 = 13.8 mm/s

- 'A' means welding current:

  4 = 400 A

  6 = 600 A

  7 = 770 A

- 'E' means energy input:

  1 = 1.9 KJ/mm

  2 = 2.8 KJ/mm

  4 = 4.1 KJ/mm

- 'X' means wire type:

  L = LINDE 95

  S = OERLIKON S3

- 'F' means flux type:

  1 = OP121TT

  4 = OP41TT

Therefore, if there are seven digits in the code, the speed will be 13.8 mm/s (13), otherwise the speed is a single digit and will be 6.3 (6) or 9.5 mm/s (9). So, for example:

- H 641 L1 is a weld on HY100 (H), and welding conditions: 6.3 mm/s (6); 400 A (4); 1.9 KJ/mm (1); wire LINDE 95 (L); flux OP121TT (1).

- Q 1371 S4 is a weld on Q2N (Q), and welding conditions: 13.8 mm/s (13); 770 A (7); 1.9 KJ/mm (1); wire OERLIKON S3 (S); flux OP41TT (4).

To assure hydrogen induced cracking free welds, all specimens were preheated to 120° using the system and control explained in Section 6.1.2, and the fluxes were baked for 2 hs at 450°C. Section 6.1.2 also describes the groove cutting and cleaning. The contact tip-workpiece distance was 30 mm.

The lowest energy input of 1.9 KJ/mm was chosen because it is within the recommended range to weld this class of steel / 246 / and it is largely used in practice. The 2.8 and 4.1 KJ/mm energy inputs are justifiable, for little information is available on their use. It is necessary to know the behaviour of the present weld metals at higher energy inputs, for they are not used on this class of steels due to the HAZ toughness degradation only. As a consequence, relatively little work was done up to date on this subject.

The wire/flux 'L4' (LINDE 95 and OP41TT) combination was used in the experiments covering all possible variations among current and speed chosen. Therefore, there are three welds at different (increasing) current at constant speed (Q/H - 641, 662, 674 - L4); three welds made at different (increasing) speed at constant current (Q/H - 674, 972, 1371 - L4); and three welds at different combinations of current and speed, but keeping to the same energy input (Q/H - 641, 961, 1371 - L4).

The other wire/flux combination 'S4' (OERLIKON S3 andOP41TT), 'L1' (LINDE 95 and OP121TT), and 'S1' (OERLIKON S3 and OP121TT) were used in the same way, but not with welding parameters '961' (9.5 mm/s; 600 A; 1.9 KJ/mm) or '972' (9.5 mm/s; 770 A; 2.8 KJ/mm), as can be seen in Table 8.1.

Thus, as we always had to weld two base steels (Q2N and HY100), there were 18 (welding conditions) x 2 (steels) = 36 welds to analyse.

8.2 Cracking and bead measurement

From each weld bead were sectioned nine transverse sections to search for defects, geometrical measurements,dilution, metallography and hardness, as Figure 8.3 illustrates. As can be seen in this figure, sections were taken from the 165 mm central length of the weld bead, the rest being discarded. Also from these transverse sections a number was cut in a plane parallel to the welding direction (longitudinal section at the weld centreline), and in a plane parallel to the plate surface (plan section). Metallography was carried out in sections 'L', 'C' or 'P'.

The cracking quantification was done on centreline crack type, measuring the crack length (height) in each transverse section (taking the average), or on the weld bead surface, when it occurs. Those cracks which did not show a characteristic centreline shape were not quantified, being here called 'transverse' and the results denoted by a 'T'.

To allow cracking susceptibility comparison between welds made by distinct welding conditions, we had to relate the crack size with some bead dimensions. In other words, we had to normalize the measured averages. A natural choice was the weld bead height for the transverse measurements, and the total bead length for the surface cracks. Therefore, in this work when we say that one specimen is more susceptible to

cracking than another, we are comparing how much percent of their true (actual) weld bead height is cracked, and unless otherwise stated, this refers to the transverse section, for few welds had surface cracking.

We tried to characterise in a most complete way the weld bead shape as summarised in Figure 8.3 and Table 8.2. The 'conventional weld bead height' (H) has been shown / 247 / to be more meaningfully related to the solidification cracking problem than the actual bead height (X). Therefore, it was used for the other relationships. Theoretical considerations were applied using actual dimensions to monitor the weld bead area (WH/2), bead external perimeter (P) and the ratio between them. The width (W) and conventional height (H) product had shown to be a good way to characterise weld bead dimensions. The weld bead ripple surface lag (r) seems to have some correlation with the weld metal solidification process / 77 /, and therefore it also might have influence on solidification cracking.

Dilution, primary (solidification) and secondary metallographic analysis, microsegregation, SEM on the crack surface and hardness were performed on the specimens, as explained in Chapter 6. Also was recorded the amount of fused flux for each experiment. All obtained data will be analysed in the following section.

8.3 Cracking identification and tendency: results

8.3.1 Definite solidification cracking

The first natural step in this investigation was to be sure about the test specimen and welding conditions suitability to induce weld solidification cracking (and only this type of cracking). In fact, the following metallographic evidences will show that the induced defect was always solidification cracking.

In Figures 8.4 (a-c) are shown typical weld bead transverse sections and also can be seen the general centreline cracking shape for three different welding conditions using wire/flux 'L4' (LINDE 95 and OP41TT).

Figures 8.5 (a,b) show transverse and plan sections of characteristic centreline solidification cracking and its unmistakable relationship to the weld solidification macrostructure. The interdendritic path is evident and even dendrite secondary arms are visible.

Cracks like the latter one were opened up just after welding to expose their internal faces. Figures 8.6(a,b) illustrate two typical aspects of (dendritic) cracking surfaces. Notice that the dendrites show a very smooth surface, free of corrosion or any other visible phase forming a 'film' or layer on or in between the dendrites. In Figure 8.6 (b) it is seen a classic 'bridge', which grew up almost perpendicular to the surface and would contact the opposite face if cracking had not occurred.

8.3.2 Cracking size, bead geometry and chemical analysis

The second step is to monitor solidification cracking behaviour with changes in welding conditions. At this point our approach to the problem diverges from the way it is generally attacked. Our aim was not to seek only for relationships between cracking tendency and welding

parameters. This is because we understand that welding parameters are just agents in the process, not the fundamental cause. Hold the welding parameters but change, for example, groove angle, or flux, or wire diameter etc., and another system was created, different from the first. As each researcher inevitably has his (her) preset conditions, another way must be found to correlate the findings.

The assessment of bead dimensions, flux usage, and chemical analysis, together with the knowledge of welding parameters, better characterises the experiments. They provide a basic set of data, which can then be related to cracking susceptibility. Therefore, the following results on solidification cracking tendency will be given together with those factors. Essential information on solidification (primary) microstructures are in the next sections, and the effect of base plate mechanical properties is discussed in Section 8.6.1.

Tables 8.3 (a,b) show up all bead dimensions and Tables 8.4 (a,b) the related cracking tendency together with other parameters. In Table 8.1 the welding conditions are shown, whilst Table 8.2 and Figure 8.3 summarise and explain some symbols used. It must be noticed in Tables 8.4 (a,b) that each welding condition refers to welds on HY100 (H) and Q2N (Q) steels, and the values given under columns 'l_c' and 'h_c' are the cracked height percentage. When cracking is absent its value is 'zero' (there is no cracking) or there are transverse cracking and this is denoted by a 'T'.

The summary of all cracking tendency data is given as a histogram in Figure 8.7. There is shown the centreline cracking in section in the upper block, and below it the presence of transverse cracking.

It is striking that the LINDE 95 wire and OP41TT flux combination show up to be the most crack susceptible to welding parameter changes. Figures 8.8 and 8.9 show transverse sections taken from welds on Q2N and HY100 steels, respectively, made using all welding parameters (Table 8.1). In both figures all specimens in the same rows show welds made at constant welding speed but increasing current; in the same columns: constant current but increasing speed; in the same diagonals; different speed and current, but same energy input. As can be seen, the change in weld shape is very large between extremes. The other wire/flux combinations were not used with all these welding parameters. Nevertheless, they did not show such high cracking susceptibility, and the reasons will be discussed later.

The available weld chemical analyses are in Tables 8.5 (a-d). It can be seen that all welds using OP41TT flux and LINDE 95 wire were analysed. However, only one weld (6.3 mm/s; 770 A; 4.1 KJ/mm) from each other wire/flux combination was analysed.

These data were sufficient to assess the influence of change in: all welding parameters; base metals; wire and flux. The following sections will show that this really was possible.

Tables 8.5 (a,b) also show the expected (EXP) composition of the weld, together with the difference (DIF) which is the analysed minus the expected value, and the respective analysis error. The expected composition is calculated taking 100% nickel recovery and no losses

for the considered element. Therefore, the difference is a good indication of the degree of oxidation and reduction, or flux influence on the metallurgical process. In Appendix A it is fully explained together with the analysis error which is based on the chemical analysis standard deviation for each element (Section 6.1.5).

8.4 Dendrite size and growth direction

Dendrite size has been measured for all welding conditions on a longitudinal section (plane parallel to the welding direction) at half bead height (X/2, Figure 8.3). As explained in Section 6.1.1. the specimens were etched with SASPA and the mean lineal intercept method was used for the measurements (1 mm line length) made at 100 x. Not less than 200 interceptions were counted in each weld.

As it seems that there is not yet a standard procedure to measure this important factor, we hope the methodology here employed can help to establish one. This would allow a complete figure of weld solidification to be compared, between welds made at different places and/or using different processes.

After the results had been assembled, it was noticed their total independence from base metal, flux or wire, within the experimental error limits and welding conditions. The dendrite size was found to be strongly dependent on welding parameters, as the theory foresees (Chapter 3), and probably on other factors, as it (the theory) does not.

Figures 8.10 (a-d) show how the dendrite size is influenced by welding parameters, and this is a typical example, common to all other conditions. From Figures 8.10 (a) to (c) the speed was kept constant (6.3 mm/s) and the current increased (from 400 to 770 A). Comparing Figures 8.10 (c) and (d) it can be seen the speed effect, for it was raised from 6.3 to 13.8 mm/s at constant current (770 A). Even without any kind of measurement it is clear, for example, that Figure 8.10 (a) shows a larger dendrite size than Figure 8.10 (b). Thus, we could conclude that between welds made at same energy input (1.9 KJ/mm) but different welding speeds (6.3 mm/s in Figure 8.10 (a) and 13.8 mm/s in Figure 8.10 (b)),the dendrite size is the smallest for that with the highest speed. In Figure 8.10 'WC' means welding conditions.

Now, Figure 8.10 (a-d) do not reflect, however, the true dendrite size behaviour. This is because we have to introduce another component present in the dendrite size measurements - the dendrite growth direction.

Figure 8.11 (a) shows a schematic view of a weld bead transverse section and dendrites growing from the fusion zone. In this transverse section the angle ('α') between the dendrite growth direction and the weld bead symmetry line characterises the dendrite growth direction. This angle was measured on the same specimens used for dendrite size above referred to, using the same SASPA etchant at 50 x, in an anticlockwise direction, at half bead height.

The dendrite size had been measured on a longitudinal section (plane orthogonal to the paper and containing AA') at half bead height (X/2). Figure 8.11 (b) schematically shows that when a dendrite is

cut through section AA', the section actually seen and photographed is CE, which size is 'Z'. Therefore, 'Z' is the 'apparent' dendrite size. Due to the very small distances involved, it is a good approximation to take lines BC parallel to ED, and BE parallel to CD, for rectangle BCDE can be treated as being infinitesimal.

It is a simple matter to prove that the actual dendrite size is 'DS' and that it is related to 'Z' (the apparent size) through the following relationship:

$$DS = Z\ (90 - \alpha)$$

Table 8.6 shows the average dendrite growth angle ('α'), the 'apparent' dendrite size and its 'actual' value, after the above correlation can be applied. Also is shown in that table the welding parameters and the related weld codes, which are given without reference to base plate, flux or wire because, as already said, it was not detected any effect from them.

Therefore, although Figures 8.10 (a-d) show examples of dendrite size, they must be seen as partially true. The current increasing (at constant speed) does make the dendrite size larger but at a different rate from that shown when comparing Figures 8.10 (a-c). The speeding up at constant current does decrease the dendrite size, but again, not exactly in the amount seen in Figures 8.10 (c,d). The largest and easily made mistake probably happens when Figures 8.10 (a) and (d) are compared. Actually, for our welding conditions, the dendrite size of welds made at same energy input, but different welding speeds is greatest for that with the highest speed. At this point caution must be taken, for different welding conditions can induce different results. In fact, it is easy to show that an essentially two-dimensional heat flow welding should always have the smallest dendrite size for the highest speed, when comparing welds made at same energy input. However, higher speeds might lead to better arc efficiency and, therefore, to higher energy input than the nominal value, and this can complicate the analysis.

The results suggest that the widely accepted view that dendrite size is unequivocally related to energy input / 248 / is disputable. Physically speaking, dendrite size should be related to welding parameters and preheat, but now it is clear that factors like weld bead shape or groove angle might have an effect on it. This is because a factor like the weld bead height-to-width ratio (H/W) has an influence on the welding heat flow, at least during the weld freezing time, which is the one of interest. Being so, many factors that have effect on heat flow and growth rate will have an effect on dendrite size, certainly in a complex way.

Bearing this in mind we found, through multiple linear regression analysis of results given in Table 8.6, that there is at least one way to correlate the 'actual' dendrite size with welding parameters, at constant preheat, and weld bead dimensions. One equation that correlates welding voltage (U), current (I), speed (V) and weld bead height-to-width ratio (H/W) with dendrite size is:

$$DS(U,I,V,H/W) = 1.348 \times 10^{-1} - 2.744 \times 10^{-3} \times U + 2.248 \times 10^{-4} \times I - 5.031 \times 10^{-3} \times V - 9.017 \times 10^{-2} \times (H/W) \quad (mm)$$

Despite the highly significant 100% correlation coefficient of the above equation, the important point, we think, is not the particular values for the coefficients in it. These coefficients might change for another set of welding conditions, but the way these factors can affect dendrite size should remain.

However, the most striking relationship is held between dendrite size and weld bead area-to-perimeter ratio (Tables 8.3 (a,b) and 8.6). Figure 8.12 shows the linear correlation between these factors.

The wellknown CHVORINOV's rule / 25 / relates solidification time with the volume-to-external area ratio of the castings. In foundry practice it is usual to take the external area-to-perimeter ratio of the castings (and risers, or feeding system), because it is easier to get them from the drawings than the volume. Invariably the casting, or parts of it, which shows the highest external area-to-perimeter ratio (called 'modulus' in the foundry jargon) solidifies later.

Therefore, due to the strong relationship shown between weld bead external area-to-perimeter ratio and dendrite size (Figure 8.12), it is justifiable to think that this ratio influences the weld solidification rate. Being so, much more attention should be given to the weld geometry effect, instead of trying to explain solidification time through welding parameters only.

Another interesting result given in Table 8.6 is the relationship between angle 'α' and power input (UxI). At the constant 6.3 mm/s welding speed it is strongly affected by the power input increasing (welding parameters '641', '662' and '674'). However, for the same power input (26180 W) increasing welding speed (from 6.3 mm/s to 13.8 mm/s) has little effect on this angle (welding parameters '674', '972' and '1371').

8.5 Weld pool retention time

The slag metal reactions are sometimes related to welding parameters as for example, the work of VALETTE / 216 / using OP41TT flux shows.

We think, however, that an important factor is missing using the above approach, for the time available for the reactions is not considered. It is easy to prove that different welding parameter combinations can produce welds with same solidification time / 248, p.88, for example /. This time, therefore, must be known, or at least estimated, if a better understanding of the problem is intended.

The time available for reactions between the slag metal system and surrounding atmosphere is given / 66 / and successfully used / 249 / as the weld crater length-to-welding speed ratio. The ripple surface lag is of direct access on any weld and its measurement is simpler than the pool crater. Furthermore, the length of both parameters is proportional.

Therefore, we define (an approximate) weld pool retention time as the weld bead ripple lag-to-welding speed ratio.

Table 8.7 summarises values of weld bead ripple lag (Tables 8.3

(a,b)),fused slag-to-weld length ratio (SWL - Tables 8.4 (a,b)) and correlates then with welding conditions (Table 8.1) and weld pool retention time. As can be seen, Table 8.7 is divided in four main quarters, depending on wire (LINDE 95 or OERLIKON S3) and flux (OP41TT or OP121TT). Each main quarter is sub-divided in nine boxes, each one related to a specific combination of welding speed and current. As the factors shown in Table 8.7 are independent of base metal, the values are averages of two experiments. Therefore, each welding condition is unequivocally characterised. Thus, H or Q 662 S1, for example, is found in the main quarter defined by OERLIKON S3 wire and OP121TT flux ('S' and '1' in the weld code, respectively). The 600 A current and 6.3 mm/s speed identifies the box, which shows that welds made using these conditions have: 21 mm of weld bead ripple lag; approximate 3.3 s of weld pool retention time; and 173 x 10^{-3} g/mm fused slag-to-weld length ratio.

A quick inspection of Table 8.7 reveals that weld pool retention time should show itself as a good indicator for fused slag yielding. In fact, Figures 8.13 and 8.14 illustrate the behaviour for OP41TT and OP121TT fluxes, respectively. As can be seen, there is a definite trend for greater amounts of fused slag as weld pool retention time increases, even if we do not consider the difficulties reported to measure ripple lag (and the error introduced), to take out (without great losses) fused slag from the bead, and the approximation taken.

The previous results are important not only under the obvious economics aspect, and its effect on welding optimisation. With greater weld pool retention time there is more time available for chemical reactions to develop. Based on the difference between the analysed and expected content of certain elements (see Tables 8.5 (a,b) and Section 8.3.2) it is possible to detect that element carbon does not show any variation with weld pool retention time, within the limits of our experience. However, deoxidants like silicon and manganese show good correlation with the latter factor, as Figures 8.15 and 8.16 illustrate. These figures show only results for OP41TT flux because for it alone we have chemical analyses for a complete series of welding parameters.

8.6 Factors which are not totally quantifiable

8.6.1 The weld stress

To isolate welding parameters effects on weld metal solidification cracking is not a straightforward task. At first glance it is sufficient to maintain constant all other conditions and to make changes only to them. However, what everybody does not realise is that when different parameters are tried, weld metal primary micro/macrostructure morphology, weld bead dimensions, and stress fields within and around the weld pool are altered, all at the same time. The worst is that these factors are inter-correlated, making it even more difficult to isolate an effect due exclusively to one of them. As we have seen (Chapter 4), there is a growing interest on weld restraint and stress. One of the most important workers in this field is MASUBUCHI and his book / 131 / summarises the extensive work done up to now. However, the work of CHIHOSKI / 193, 194 /, also reviewed in Chapter 4, gives a better insight into the effect of stress fields, immediately around the weld pool, on solidification cracking. Nevertheless, everywhere the empirical methodology to measure weld pool stresses still is in its

infancy, mainly when the problem involves welding of thick base metals. Therefore it is out of the question to carry it on here.

In general, high H/W ratio indicates great susceptibility to centre-line solidification cracking, as already seen in Chapter 4. This is not always true, however, and comparing weld H/Q 674 L4 and H/Q 1371 L4 (Table 8.3 (a)), their H/W ratios are 1.6 and 1.4 respectively. We should conclude that the former welds would show greater cracking tendency than the latter ones. Nevertheless, Table 8.4 (a) shows that the percentage of cracking in sections is much larger for H/Q 1371 L4 than for H/Q 674 L4.

The same reasoning applies to other welding conditions using different wire/flux combinations, Therefore, other factors are involved and H/W ratio is not the strongest. Just to reinforce the point that different stress fields do exist between our welds, and to have an idea about the temperature fields distribution around the weld pool, Figures 8.17 (a-c) were computed. They were calculated in the middle of the plate, and the number besides each isotherm is the related temperature, in degrees Celsius (Figure 8.17 (b)),with corresponding lines in the other figures. It is not the intention to say that those isotherms are the true temperature distribution around the pools. This model represents only the tendency of those energy fields. These isotherms were done using, basically, the wellknown ROSENTHAL's three dimensional theory on heat distribution / 250 /, as improved by MYERS et al / 251 / for more realistic situations. The computation block diagram is in Appendix B, and it is a trivial problem.

When comparing welds made at the same speed but different current (energy inputs) as Figures 8.17 (a,b) show, it is clear that the isotherms are much wider in the highest energy input case, Figure 8.17(b). The pool is larger at 4.1 KJ/mm and its length is nearly twice that at 1.9 KJ/mm, Figure 8.17 (a). While the 700°C isotherm, for example, in the 1.9 KJ/mm case reaches a maximum half width of around 7 mm, the corresponding isotherm for the 4.1 KJ/mm is around 11 mm, Figure 8.17 (b). On the other hand, comparing welds made with the same current, but different speed (Figures 8.17 (b,c)) the isotherms lengths are not so different, but their widths are. Finally, Figures 8.17 (a,c) can be compared for they both have the same energy input (1.9 KJ/mm), but different welding parameters. A quick inspection shows that these welds are completely different as far as the isothermic pattern is concerned.

There is another important point to be considered as regards weld stress, even if we cannot quantify it. In Chapter 4 we have seen that solidification cracking can be highly affected by the base metal stress condition (heat treatment and strength). Thus, we decide to verify if this concept could be applied to both base metals used in this investigation.

Plates in sufficient number to make three specimen tests (one for Q2N and two for HY100 steel) had the grooves cut, and before assembly they were placed into a furnace at 200°C. The heating rate was 67°C/h and the plates were kept inside the furnace at 650°C for 2.5 hs. After this time had passed, the furnace was switched off and the plates taken from it only when the temperature dropped to 150°C.

Small samples were taken from the plates to carry on a metallographic analysis. No differences in microstructure between the heat treated and the as received material could be observed.

The plates were then assembled in three 'standard' specimens (Section 8.1).

It was decided to weld these specimens using OP41TT flux and LINDE 95 wire, for they had shown a well defined centreline solidification cracking for conditions H/Q 1371 L4 and H 674 L4 (Table 8.4 (a)),which were the chosen. Therefore, we obtained one weld on Q2N steel coded Q 1371 L4 T and two welds on HY100 steel coded H 1371 L4 T and H 674 L4 T respectively. These welds are completely similar to those welds in Table 8.4 (a) without 'T' in the code (standing for 'treated'), but the base metals were heat treated.

The results obtained are shown below and comparison is made between welds from heat treated and as received base metals:

Heat treated base metal	Centreline solidification cracking (%)
H 674 L4 T	Zero (transverse cracking only)
H 1371 L4 T	36
Q 1371 L4 T	28
As received base metal	
H 674 L4	31
H 1371 L4	68
Q 1371 L4	51

As can be seen, the centreline solidification cracking for the worst case ('1371') was reduced to half, and the H 674 L4 welding condition had just small transverse cracking, probably due to another kind of problem, which will be analysed in the following sections.

Therefore, as we did not alter the welds chemical composition, these results can only be interpreted as a result of stress relief of the base plates, which reduced their (negative) effect of solidification cracking.

Thus, the stress/strain fields developed are different, because they are temperature dependent. The weld pools are also different, by theoretical and practical considerations (Section 8.5). We cannot say, however, which one is the worst as regards centreline solidification cracking. Therefore, we do not know the actual stress field values for our welds, and geometrical factors like H/W ratio have shown to be only part of the problem, which is still more complicated by the effects of base metal mechanical action. Thus we have to study weld metal primary micro/macrostructure and microsegregation, extracting as much as possible information from them, to resolve the puzzle.

8.6.2 The primary macrostructure morphology

Two works already tried to establish a general notation for weld metal centreline primary macrostructure types / 252, 253 /. Unfortunately, both were on thin ferrous alloy sheets with two-dimensional heat flow, and the metallographic studies were mainly based on sections parallel to the plate surface (plan section). We shall try here to follow the proposed nomenclature, rather than to define new terms, which would come only to complicate even more the situation. The metallographic plan sections are prejudiced in our welds by obvious reasons. Therefore, unless otherwise stated, the metallographic sections that follow were taken from a plane transverse to the welding direction.

The terminology question must be cleared first of all. Primary microstructure is here understood as those described in Chapter 3: planar, cellular, cellular-dendritic, dendritic, and equiaxed. The morphological aspect at the weld centreline or around it is the primary macrostructure, which sometimes can take their name from the microstructures, for they represent one particular type, or they can have different forms and names.

In the present investigation, the primary macrostructure of welds on Q2N and HY100 base metals, and those using different wires (but same flux) have shown the same morphology, for equivalent welding parameters.

Therefore, Figures 8.18 (a-c) illustrate the influence of welding parameters on primary macrostructure morphology, using OP41TT flux. Figure 8.18 (a) (sp.H 641 L4 : 6.3 mm/s; 1.9 KJ/mm) shows the weld centreline (at the picture centre), just below the existing centreline solidification cracking in this specimen, and the crack tip is visible in the upper part of the picture. It is clear that the dendrites do not meet in a well defined line at the centre and the angle ('α' - Section 8.4) they have with it is small. This macrostructure can be approximately defined as "stray", for the dendrites from each other side of the pool change orientation near the weld centreline, and compete with each other in the growing process. Using the OP41TT flux this welding parameter shows vertically growing dendrites around the crack tip. In Figure 8.18 (b) (sp.H 674 L4: 6.3 mm/s; 4.1 KJ/mm) it can be seen that as current increases (at constant speed), the weld centreline macrostructure changes to an essentially "competitive columnar" type, and the angle ('α') between the dendrites and the centreline grows (compare with Figure 8.18 (a). In this case, the dendrites grow continuously from the fusion boundaries, but compete at the centreline, making it to be in a zigzag. With the rise in speed, maintaining constant current as in H 674 L4, Figure 8.18 (c) (sp.H 1371 L4: 13.8 mm/s; 1.9 KJ/mm) shows that the macrostructure turns to an almost "centreline" type, but retains much of the "competitive columnar" type. The dendrite trend is to meet at the weld centre in a well defined line, not totally accomplished here.

It is worth mentioning that near the crack tip in Figure 8.18 (b) there are few equiaxed dendrites trying to develop.

Details at higher magnification are shown in Figures 8.19 (a-c) for similar welds. In Figure 8.19 (a) can be seen the vertically

growing dendrites around the crack tip, like in Figure 8.18 (a). Notice that these welds were not made on the same base metal. Nevertheless, the macrostructure is similar and Figure 8.19 (a) is shown just to emphasise this point, with the weld centreline arrowed in these figures.

The effect of change to OP121TT flux on centreline primary macrostructure is only noticeable for the 6.3 mm/s welding speed. This is illustrated in Figures 8.20 (a,b), which show the centreline macrostructure for welding parameters similar to Figures 8.19 (a,b), with the same wire (LINDE 95). Figure 8.20 (a) shows the same "stray" macrostructure of 8.19 (a), but there are neither vertically growing dendrites nor centreline solidification cracking. For the other base metal (Q2N) and wire (OERLIKON S3) the same morphology is obtained, if OP121TT flux is used. In Figure 8.20 (a) can be seen at the left upper corner (arrowed) part of an existing transverse crack, not common for all welds using these conditions. Figure 8.20 (b) shows the best example of macrostructure morphology alteration due to the use of OP121TT flux, for a great number of equiaxed dendrites are induced to grow along almost all weld centrelines. This specimen (H 674 L1) has shown a small centreline solidification cracking (Table 8.4 (b), which seems to be arrested at the beginning of the equiaxed macrostructure. There is no doubt that the previous structure is equiaxed, for all welds here discussed had their longitudinal section examined, and this particular case can be seen at Figure 8.10 (c).

Finally, another aspect of the macrostructure and solidification cracking relationship is seen in Figures 8.5 (a,b) (already shown) and Figure 8.21. The former figures show two views of the same cracking (plan and transverse). Only at this relatively high welding speed (13.8 mm/s) the plan section has shown dendrites near parallel to this section. The welds made at lower speeds tend to have them almost perpendicular to this plane, probably due to heat flow characteristics.

Figure 8.21 shows the solidification microstructures from the fusion zone to near the weld centreline. It also shows a transverse cracking, which grew up perpendicular to the bands (there is a discussion on banding phenomenon in Chapter 3). It is interesting to notice that after the crack meets the first band it notably decreases in width, being apparently arrested at the third one. On the other hand, this figure permits us to observe the change in size and in type of the microstructures from the fusion zone inwards, as foreseen and illustrated in Chapter 3.

Therefore, primary (solidification) macrostructures prone to centreline solidification cracking seem to be those showing vertically growing dendrites and dendrites meeting in line at the weld centre. Use of OP121TT flux seems to reduce this tendency and, up to a point, promote formation of equiaxed structure. At higher welding speeds a change in flux (from OP41TT to OP121TT) has little or not effect. This, perhaps, can be explained through very basic weld solidification theory, for now it is much more likely for the macrostructure to follow heat flow, due to the weld pool shape and heat balance that must be satisfied. Therefore, relatively weak external actions are much less effective. However, strong external mechanical actions like arc oscillation or cold wire injection do affect welding conditions and solidification cracking tendency, as will be shown in Chapter 9.

8.6.3 The microsegregation

The previous section has shown what the weld solidification macrostructure looks like and how they change, as welding conditions are changed. We have seen that some morphologies are, probably, less resistant to solidification cracking, because mechanical action on them (trying to tear off the centreline) is easily carried on. However, similar mechanical actions will be less or more effective depending on which material they are acting on. By analogy, suppose that a beam practically free of defects of a very strong and tough material is tensioned. A very high tension will be applied before the structure fails. Now, if we substitute this beam by another one of the same material and shape, but containing a very high number of internal defects dangerously positioned, the tension applied to rupture is much less than in the former case.

Therefore, shape and general qualities are not sufficient data. Distribution and, if possible, identification of the defects are highly desirable.

In welds, the detection and analysis of microsegregation is not straightforward. As distinct from conventional casting, the interdendritic spaces are very narrow and the level of segregation is small. These two factors help to make this a difficult technique.

In general, only the major alloying elements are traced, as have been shown by FRASER and METZBOWER / 254 /. These authors, working on similar steels (HY100) used in the present investigation, detected only the elements nickel, manganese and chromium. The work of RUSSEL / 255 / also illustrated the problem, for he had no success at all in tracing any segregating element, with a similar instrument in use here at Cranfield.

We had the same problem with our welds, for neither the Cranfield dispersive X-ray microanalyser nor two different instruments tried in other research organisations were successful in detecting microsegregation.

Obviously this fact does not mean that the welds in this study were segregation free. Very basic solidification principle rules (Chapter 3) that in any alloy,containing at least two elements with different distribution coefficients, there is segregation.

Beam size and detection limits of the instruments used (among other factors) naturally decide the effectiveness of analysis. Therefore, we can conclude that what happened was that the equipment used had not sufficient qualities to resolve the interdendritic phases. Nevertheless, segregation sensitive etchants can help us look for this very important factor. The following microphotographs show and confirm the existence of segregation in the welds, disclosed through the use of ammonium persulphate / 254 /.

Figures 8.22 (a-f) compare segregation lines in welds made on HY100 (a-c) and Q2N (d-f) steels, for different welding parameters, using LINDE 95 wire and OP41TT flux. All welds, but Q 641 L4, have shown centreline solidification cracking, and the microphotographs

were taken just below the crack tip. The white lines and solute pools indicate segregation of some elements. The wide white area around some crack tips are not segregation, but staining due to alien substances flowing from the cracking (likely liquid paraffin used for polishing).

Thus, for each welding parameter, welds made on different steels can be compared. The most striking differences are noticed in Figures 8.22 (b,e) and (a,d). A well defined centreline segregation is visible in Figure 8.22 (b) whilst in counterpart it does not exist in Figure 8.22 (e). The welds made on Q2N steel using the welding parameters 6.3 mm/s and 1.9 KJ/mm never have shown cracking, under any conditions. In fact, Figure 8.22 (a) when compared to Figure 8.22 (d) shows much more segregation.

Therefore, welds in HY100 steel seem to segregate at the centreline more than in Q2N steels.

Having seen the general segregation tendencies of welds made on different steels, we now look how wire or flux seems to affect this factor. The welding parameter chosen for these comparisons was 6.3 mm/s, 770 A, and 4.1 KJ/mm, for it chemical analysis is available at all combinations of wire/flux.

Thus, the flux effect can be assessed comparing Figure 8.23 (a) with Figure 8.22 (e), and Figure 8.23 (b) with Figure 8.23 (c).

The first two figures (8.23 (a) and 8.22 (e)) do not show clear centreline segregation, but the weld Q 674 L4 (Figure 8.22 (e))has centreline solidification cracking, whilst the Q 674 L1 has not (Tables 8.4 (a,b)). This apparently puzzling result cannot be explained through chemical composition (or microsegregation). This behaviour seems to be a result of the, likely, different thermal flow both fluxes induce on the welds (Section 6.3.2), combined with the reactions taken place within the weld pool retention time (Section 8.5). In this case, the primary macrostructure seems to affect the weld resistance to solidification cracking more than the microsegregation. This was seen in Figure 8.20 (b), for the OP121TT flux induced a centreline equiaxed morphology to form, whilst the OP41TT flux did not.

Welds Q 674 S1 and Q 674 S4 (Figures 8.23 (b) and (c), respectively) do not show continuous centreline solidification cracking (Tables 8.4 (a,b)). In those welds made with OP121TT flux only small purely transverse cracks are found. However, welds using OP41TT flux do show, as well as transverse cracking, small amounts of intermittent centreline solidification cracking, following a segregation line (Figure 8.23 (c)). The same reasoning previously applied to Figures 8.23 (a) and 8.22 (e) applies here, and the primary macrostructure seems to determine the cracking tendency.

On the other hand, the wire effect can be assessed comparing Figure 8.22 (e) with Figure 8.23 (c), and Figure 8.23 (a) with Figure 8.23 (b). The change to OERLIKON S3 wire, illustrated in the two first figures seems to include a slightly higher resistance to centreline solidification cracking. The weld Q 674 L4 (Figure 8.22 (e)) shows a measurable tendency to have it, whilst the Q 674 S4 (Figure 8.23 (c)) has only a small tendency. The difference is not, however,

conclusive. When both welds exhibit centreline equiaxed macrostructure (likely) induced by OP121TT flux, that using LINDE 95 wire does not show any sign of cracking. However, the weld made with OERLIKON S3 wire does show small transverse cracks.

8.7 Related secondary phase transformations: results and discussion

In a solidification cracking investigation it is not usual to include studies on secondary phase transformation. We think this almost standard procedure inhibits at least two possible sources of further knowledge on the subject, viz: the detection of possible phenomena developing from solidification cracking, and the understanding of the complete weld defect cycle.

Therefore, we feel that weld metal cooling rate (solid state) and the resultant microstructure and hardness, for a particular chemical composition, must be considered. Firstly it follows our own theoretical approach, which tries to interpret weld solidification cracking through all possible ways, and secondly, because it is possible that these solid state transformations give some indication about what happened at higher temperatures. Finally, for completeness' sake, a weldability study must be as informative as possible about the materials involved, and because weld metals of this type, welded in this range of energy inputs are not so common; it is interesting to have their behaviour monitored.

8.7.1 Thermal analysis and hardness

Weld thermal analyses were performed as described in Section 6.1.3. Although we did not get cooling curves for all welding conditions, due to the experimental problems described in Section 6.1.3, a significant number of welds were recorded, and they allowed us to verify some immediate points. Using the present instrumentation, both fluxes had the same detectable influence on weld cooling rate (solid state), but in spite of this fact, Section 8.7.2.2 will show that welds made with OP121TT flux seem to have finer columnar (secondary) microstructures than welds using OP41TT flux. Furthermore, in Section 6.3.2 we had seen the results of gas released from both fluxes, which lead us to think that, at higher temperatures, the flux might have an influence on the weld metal thermal behaviour. The difference in the amounts of major alloying elements for the same welding parameters, but different wires, were so small (see Tables 8.5 (a-d)) due to the high dilution that it was impossible to detect any variation in factors such as phase transformation temperatures.

In Section 7.2.1 the meaning of each curve in the thermal analysis graphics was explained. Figures 8.24 to 8.29 show typical cooling curves and their first derivative, together with cooling rates and cooling times for temperature ranges of interest. The Retention Time above 1000°C (RT(1000)) is also given, being here the time the weld metal spends in the range 1400-1000°C. Table 8.1 shows welding conditions and their respective codes used throughout this work. Thus, we have to bear in mind that they are valid for all welds made with the same welding parameters. For example, Figure 8.24 shows weld metal thermal analysis for weldment Q 641 S1 (6.3 mm/s; 1.9 KJ/mm).

It is also valid for weldments H 641 S1, H/Q 641 L4, H/Q 641 S4 and H/Q 641 L1, which have either different base metal, or electrode, or flux, but the same welding parameters.

An immediate deduction from the analysis of those figures is that, in spite of weldments in Figures 8.24, 8.28 and 8.29 having the same energy input (1.9 KJ/mm), they show a small different in cooling rates, mainly in the ranges 1100/800°C and 800/500°C (the same with the two 2.8 KJ/mm energy input welds, Figures 8.25 and 8.27). These differences can be partially explained by differences in the thermocouple positioning and partially by heat flow theory /i.e. 250, 251 /. However, as will be seen in Section 8.7.2.2 the first and second transformation temperatures (start) correlate extremely well with cooling times in both ranges (1100/800°C and 800/500°C). Therefore, we think that the possibility of error due to bad thermocouple positioning is excluded.

Tables 8.8 (a,b) show the average weld metal hardness and the peak value in the coarse grained Heat Affected Zone (HAZ) for all welds. The welds were grouped by energy input value, and sub-grouped by average cooling time. There is a consistent trend for higher values of hardness in welds on HY100 steel than on Q2N steel. This can be due to the chemical composition effect (Tables 8.5 (a-d)),and differences in shape and size of carbonitrides, as shown in Section 6.2.2.

Table 8.9 shows clearly, we think, the effects of energy input, wire and flux. This table is divided into four main quarters, depending on wire (LINDE 95 or OERLIKON S3, Table 6.2 and Section 6.3.1) and flux (OP41TT and OP121TT, Table 6.3 and Section 6.3.2) combinations used. Each main quarter is sub-divided into nine boxes, each one related to a specific combination of welding speed (6.3, 9.5 or 13.8 mm/s) and current (400, 600 or 770 A). Inside each box, the first line shows weld metal carbon equivalent (CE) in wt% x 10^{-2}, when available; the second and third lines show average weld metal hardness for Q2N and HY100 steels, respectively. Thus, each welding condition is unequivocally characterised. For example, Q 641 L4 (upper-left box) has 0.66% CE and 392 HV5; H 674 S1 (extreme right column, third row from bottom) has 0.73% CE and 327 HV5.

Even a relatively quick inspection of Tables 8.8 (a,b) and Table 8.9 permits the following conclusions:

- For all wire/flux combinations, longer cooling times lead to softer weld metal;
- Welds made with the same parameters and wire, but different flux, show no significant change in weld metal hardness, observing the 'standard deviation' for each element;
- Welds made with the same parameters and flux, but different wires, show the highest hardness for those using LINDE 95 wire;
- In general, due to high dilution, the difference in carbon equivalent among welds within each main quarter

or even among welds from different quarters, is small, particularly if we take into account standard deviation of the analysis. We have already seen that for CE (Section 6.2.1) this shows a 'SD' of 0.02%. This means, for example, that CEs of 0.64 and 0.68% cannot be taken as different; they probably are equivalent.

- For welds under study, no immediate relationship can be taken from CE alone and weld metal hardness.

- Welds on HY100 steel have shown higher hardness in the weld metal and coarse HAZ than those on Q2N steel, for the same welding conditions. In spite of the small difference in CE, it must be noticed that for all available weld metal chemical analyses, carbon is higher in HY100 welds than in Q2N ones.

8.7.2 Microstructures

8.7.2.1 The heat affected zone

Measurements were made on welds in order to assess their largest HAZ width (in the 'bay' region when it was present). As far as the accuracy of a light microscope measurement can be, both steels were found to be equally sensitive to thermal cycles, in terms of width. The 1.9 KJ/mm energy input welds have the coarse HAZ width≃ 1.0 mm, while the total HAZ width is ≃1.8 mm. The 4.1 KJ/mm welds have ≃2.8mm and ≃4.9 mm, respectively.

Figure 8.30 (a) shows the dendrite size dependence on the HAZ grain size, in a longitudinal (parallel to welding direction) section, near the weld root, for a 2.8 KJ/mm weld. Epitaxial growth can clearly be seen. Considering the three dimensional aspects of this weld (and heat flow), this section was only obtained after many trials.

Figure 8.30 (b) discloses the martensitic microstructure as seen in the 'bay' region of a 4.1 KJ/mm weld, which was etched by Ammonium Persulphate followed by Nital. This double etch allows a better definition of the microconstituents at low magnification.

Two coarse HAZ close-ups are shown in Figures 8.30 (c,d) for welds on Q2N and HY100 steels, respectively. At the bottom of the latter can be seen what probably is a complex inclusion colony. We did not notice any cracking propagating from there, but the possibility is obvious, for it can originate either 'cold' / 256, 257 / or liquation cracks / 258 /. This fact also indicates that HY100 is a less clean steel than Q2N.

Therefore both steels show a similar HAZ microstructure, in spite of the fact that HY100 has its coarse region ≃ 30 HV5 harder than Q2N.

8.7.2.2 The weld metal

All welds had their transverse sections examined in a light microscope, and some of them through Scanning Electron Microscope (SEM) and Transmission Electron Microscope (TEM). For equipment description, see Section 6.1.

As we have seen in Chapters 2 and 3, weld metals with the chemical composition of the present ones should solidify as δ (delta) - ferrite.

The transformation from δ-ferrite to austenite can be only indirectly assessed, but the literature indicates / 259 / that the primary (solidification) and the secondary structures do not follow the same path. However, COCHRANE / 96 / suggests that in submerged arc weld deposits made under acid fluxes the δ -dendrite and the austenitic (γ- gamma) boundaries coincide, whilst using basic fluxes the latter boundary is much larger than the δ -dendrite spacing.

To disclose the relationship held between the primary and secondary structures of the welds made in this investigation (using basic fluxes), a special etching technique was developed. Firstly, we heavily etched a previously polished specimen using SASPA. After drying it, a slight polishing (1/4 micron diamond paste) and a Nital etching was performed. Figures 8.31 (a,b) show the result at two different magnifications, as seen under SEM. It is important to use SEM, for the light microscope does not provide the necessary depth of focus.

In Figure 8.31 (a) the δ-ferrite preferred growth direction is indicated (DF). The dark points result from the SASPA etching by pitting. In Figure 8.31 (b) can be seen acicular ferrite grains crossing over the δ-ferrite boundaries, with corresponding positions arrowed in both figures.

Due to the relatively high magnification, these figures do not show the γ-boundaries. Thus, as the acicular ferrites cross over the boundaries marked δ-ferrite, they surely are not γ -boundaries and therefore they really are δ-ferrites.

Then, these metallographic evidences permit us to think that COCHRANE's suggestion / 96 / is right for the welds here investigated.

The following investigation was to give a qualitative assessment of microconstituents, which have been indicated using the ABSON and DOLBY / 242 / proposed notation (light microscopy), and to search for a possible link between secondary microstructure and solidification cracking path.

(i) Microstructure coarseness

Firstly, as regards energy input influence, the coarseness of the microstructure can be evaluated for 4.1 KJ/mm and 1.9 KJ/mm welds in Figures 8.32 (a,b) respectively. Incidentally, Figure 8.32 (a) shows transverse cracking (sp. Q 674 S1) following approximately the columnar boundary. Figures 8.32 (b-d) show the columnar microstructure for the same energy input welds (1.9 KJ/mm). In Figures 8.32 (b,c) are seen the columnar microstructures for the same flux (OP121TT) but different wire (OERLIKON S3 and LINDE 95, respectively). No obvious difference between them can readily be noticed, but a less defined grain boundary in Figure 8.32 (b) is clear. When comparing Figures 8.32 (c,d) a difference is seen in columnar microstructure coarseness between welds using OP121TT and OP41TT fluxes. The former flux seems to induce a finer columnar microstructure than the latter.

welds on HY80, HY100 and HY 130, FRASER and METZBOWER / 254 / found similar structures, which they said to be 'solute pools' with increased amounts of all major elements, as compared with the surrounding matrix. At the centre of these pools they detected very high levels of nickel and sometimes chromium and manganese.

Figures 8.36 (a,b) show in a SEM image acicular ferrite and a much coarser lath structure (the same position is arrowed in both figures) for 4.1 KJ/mm welds (compare with Figures 8.34 (a,b) taken at the same magnification). Figures 8.36 (c-g) show another TEM series of micro-photographs that resemble microstructures already quoted for 1.0 KJ/mm energy input welds. The main differences seem to be that they are coarser than the 1.9 KJ/mm and their relative amounts of microconstituents differ. However, as no quantitative analysis was performed, these are only suggestions.

Figures 8.36 (a-d) and Figures 8.36 (e-g) show microstructures of welds using OP41TT and OP121TT fluxes, respectively. In Figure 8.36 (c) the (austenitic) grain boundary (AGB) and ferrite with aligned M-A-C (AC) are readily visible. This boundary is shown at higher magnification on another specimen in Figure 8.36 (d). The carbides (c) distributed over the ferrite matrix are again seen, and Figures 8.36 (e,f) show good examples of the autotempering occurring in these welds.

Figure 8.36 (g) shows an uncommon situation, for a ferrite island can be seen at the boundary, being therefore a grain boundary ferrite (arrowed). This fact, however, seems to happen very seldom.

8.7.3 Phases: order of appearance and thermal cycles

From the work of LEVINE and HILL / 220 / and CHOI and HILL / 221 / we know that the microstructural phase of order of appearance as the temperature decreases is: Grain Boundary Ferrite; Ferrite with aligned M-A-C; Acicular Ferrite; Bainitic lath structure; after that and some intermediary structures, Martensite is certaily the last microstructure. The transformation temperatures are extremely variable and cannot be generalised. This fact is corroborated by COCHRANE / 261 / who stated that: "in more highly alloyed composition, e.g. containing substantial nickel and molybdenum additions, transformation temperatures are lowered and as a result more complex structures can be developed." In the work of CHRISTENSEN and SIMONSEN / 262 /, too, it is clear that deposits containing 2.25% Ni and 1.0% Ni - - 0.5% Mo had lower transformation temperatures than C-Mn deposits, and that higher cooling rates (shorter cooling times) increase the start and end of transformations. Furthermore, there is a role played by oxygen content on the microstructure, which is highlighted by ABSON, DOLBY and HART / 225 / and COCHRANE and KIRKWOOD / 226 /, already examined in Chapter 5.

Table 8.10 shows the estimated phase transformation temperatures and average cooling times, collected from weld thermal analysis (Figures 8.24 to 8.29). In this table are data from two welding conditions (WH 641 S4 and WQ 674 L4) used for All-Weld Metal Mechanical Tests, as stated in Chapter 7. The analysis of this table shows a very consistent trend between Average Cooling Times (1100/800, 800/500 and 1100/500°C) and Transformation Temperatures (first and second) and

they are shown in Figures 8.37, 8.38 and 8.39, respectively. Highly significant correlation factors of 96% and 96.5% were obtained for the range of 1100/800°C and the first and second (start) transformation temperatures, respectively. For the range 800/500°C the correlation is almost as good (94%) for the first (start) transformation temperature, whilst for the range 1100/500°C it is 95%.

In line with the current approach to the classification of weld metal microstructures / 242 /, we can say that the single pass welds made in this investigation are composed mainly af Acicular Ferrite, Ferrite with aligned M-A-C (ferrite containing Martensite-Austenite or Carbide phases), and Martensite. Therefore, in Table 8.10 the first and second Transformation Temperatures should correspond to Ferrite with aligned M-A-C and Acicular Ferrite, respectively.

It must be recognised, however, that the weld metal secondary microstructure classification is not well defined. Proof of this is the relatively recent 'Robin Round No.3'/ 263 /, in which the author participates. The exercise has demonstrated that there is still not a broad consensus on microstructure morphology definition.

In counterpart, the 'Robin Round No.2', exercise, in which the author did not participate but close followed the solution, showed up another important point about quantitative metallography. Among three relatively experienced people in the science (art) of metallography, we were witness that two quantified a same metallographic constituent (ferrite with aligned M-A-C) in a same photomicrograph, with a difference of $\simeq 30\%$ in their results. These facts, of course, do not increase the author's confidence on the present weld metal quantitative metallography 'state-of-the-art'.

8.8 Solidification cracking and secondary microstructure connexion

The opportunity to analyse the solid state path followed by solidification cracking might have been unnoticed in Section 8.7.2.2 (i) and (ii), when Figures 8.32 (a) and 8.33 (d) were shown. In these figures it is clearly seen that the solidification cracking follows the same direction of the (lath) boundary. Figures 8.40 (a-c) show other aspects of this correspondence, which were common for all welding conditions with this defect. Figure 8.40 (c) is a detail examined under SEM of Figure 8.40 (b). They show that the crack tip follows a line of (likely) carbides, just besides the ferrite with aligned M-A-C microconstituent. As we have shown in Section 8.7.2.2 the welds investigated have the δ-dendrites confined in the γ-boundaries. As the cracks are of the solidification type (demonstrated throughout this work and specially in Section 8.3.1), we can only deduce that in the previous examples a δ-dendrite was beside the γ-boundary.

Mainly from Figure 8.40 (c) can be deduced the possibility of 'cold' cracking developing prior to solidification cracking. In fact, in Section 8.3.1 we have indicated that Figure 8.5 (a) has an important feature. It shows that at the crack tip (the last stage in its formation) some dendrites bend upwards, perhaps due to the build-up of thermal stresses. The important point is seen after the end of the clearly inter-dendritic centreline cracking. There initiates a thin one, which seems to cross many dendrite secondary arms. Thus, this thin cracking could have had origins at temperatures below the solidification point and to be either of the 'cold' or high temperature (not solidification) type.

The evidences are small but relevant, and we can deduce that solidification cracking can give origins to the 'cold' type, due perhaps, only to mechanical forces build-up at the crack tip, which acts as a stress concentration factor.

8.9 General discussion on solidification cracking and its relationship with secondary microstructure

8.9.1 Test specimen geometry and cracking

From a critical compilation of weldability tests done by the author some years ago / 264 / it could be inferred that two kinds of criticisms were made on this subject: that coming from individuals with no R & D experience, stating that these tests are useless; the other, made by people with no production experience, claiming that these tests are ideal.

We think that those with some experience in both environments would agree that the following points on the objectives of a weldability test are closer to the truth: (a) a high degree of simulation can be reached, permitting predictions to be made, but it is not a substitute of actual production, the final and definitive test: (b) on several occasions the researcher is not at all interested to repeat the actual welding conditions found in a production shop, for the objective is to monitor and to investigate the origins and/or progress of a particular phenomenon, unlike to allow such a systematic observation outside the conditions offered by a laboratory; (c) it is much more sensible to spend a few thousand pounds to get right the general tendency of the material when welded, than to lose millions of pounds directly welding, in a completely wrong way, the actual structure.

The design of the specimen used throughout this investigation was rightly chosen, for it fulfilled the conditions assigned to it in Section 8.1, viz: repeatable geometry; consistent and reproducible weld metal cracking; some similarity with practical conditions. After repeating four times one welding condition (H 674 L4), the average cracking size was the same $\pm$ 10%, a deviation considered good. The geometry was kept within the limits described in Section 8.1 and the latter condition was at least partially achieved, for in submarines, for example, we know that stiffeners are placed on the plates in a similar way they were here, (albeit with larger distances between them). Furthermore, to approach the temperature distribution of a plate of infinite width, the specimen half-width should be around / 265 / ten times the average weld bead width. This was practically accomplished for all welding conditions. The same amount of flux over the plates, together with the above conditions created an approximate constant environment for the weld pool, other parameters being the same.

The cracking quantification through its size measurement is a widely accepted practice to assess the defect tendency, as shown, for example, in the works of HOULDCROFT / 266 /, SAVAGE and LUNDIN / 202 /, GARLAND and BAILEY / 154 /, and in the comprehensive review on weldability tests done by BORLAND / 244 /.

In this work the cracking susceptibility could be compared between welds through both their cracked bead percentage and also the crack-no-crack concept.

8.9.2 Analysis of results

In Tables 8.11 (a,b) it can be seen all the results as regards solidification cracking tendency for base steels Q2N and HY100, respectively. In each box is the cracked bead percentage or an indication if it contains transverse cracking, for each welding condition. A crack-free specimen is indicated in the box through a zero.

First of all we would like to compare both tables seeking different results given by the base steels.

(a) As regards freedom from centreline solidification cracking, the welds made on Q2N and HY100 steels have shown 10 and 7 specimens, respectively;

(b) Completely crack-free specimens (5) were obtained only in the Q2N steel;

(c) Welding parameters of 6.3 mm/s, 400 A, 1.9 KJ/mm were always crack-free for welds on Q2N steel, whilst those welds on HY100 steel were always cracked;

(d) The welds made on Q2N have always shown less cracking tendency, for each welding condition.

Thus, the results have shown the Q2N as the less susceptible steel to solidification cracking. Reasons for this behaviour are found below. It must be recognised, however, that several phenomena can be explained through indirect observation only, and this seems to be the case.

In Chapter 6 we have seen that both steels have a very similar chemical composition. However, the HY100 steel showed up as the more potentially susceptible to solidification cracking, when both steels were compared through the use of the empirical formulae based on the chemical elements combined effect on this defect (Sections 4.3.2 and 6.2.3). At that stage we cautioned the reader about the applicability of these formulae, but it is important to notice that in general they agree that carbide forming elements have a favourable influence in reducing the steel susceptibility to solidification cracking. We also must point out that there is seven times more vanadium in the Q2N than in the HY100 steel (Table 6.1) and that, as a consequence, the welds on the former steel have this element at least five times more than in the welds on the latter steel (Table 8.5 (c)).

Therefore, we cannot completely disregard the indication given by those formulae simply because there is not (yet) a total explanation (theoretically based) on the principles involved in their action. At least for base steels, welded under exactly the same conditions, it is significant that the difference in behaviour showed up by them agrees well with the results obtained.

The base steels metallographic analysis (Chapter 6) has shown that despite the apparent larger inclusion colonies found in the HY100, they have similar microstructure, but only at light microscopy level (Figures 6.1 and 6.2). The examination of these steels under TEM disclosed that their carbides are different, at least in shape, size and distrib-

ution over the matrix (Figures 6.5 (a-e) and Section 6.2.3).

In Section 4.4 (Chapter 4) there is a lengthy discussion on base metal high (transient) temperature mechanical influence on solidification cracking tendency. There it also was seen how relatively small difference in chemical composition and/or heat treatment can make the base steel behave in a completely different way,as far as solidification cracking is concerned. Thus, both steels could have, at high temperature, different mechanical response to thermal stress/strain. This fact could make one of them (Q2N) relieve more than the other metal around the weld pool, leaving less strain to be absorbed by the weld metal in the 'mushy' state. In fact, a simple experiment with heat treatment in specimens from both steels (Section 8.6.1) have shown that this reduces solidification cracking in welds made on them.

Another point of interest is that welds on HY100 have shown more centreline segregation than those made on Q2N steel (Section 8.6.3).

Therefore, we are compelled to believe that two possible origins for the greater solidification cracking tendency shown by the HY100 are: (1) high temperature mechanical properties, inducing the steel to relieve less the metal around the weld pool and (2) unfavourable chemical composition balance.

The above arguments, we think, can explain the observed phenomenon on the base steels behaviour side. The following discussion will concentrate on solidification cracking tendency induced by welding parameters, fluxes and wires. It will also disclose chemical difference, brought up by the base metals.

Firstly, we would like to introduce five tables which have some facts to add to the discussion. Tables 8.12 to 8.16 show different aspects of chemical analysis and how they can influence the solidification cracking tendency. Table 8.12 is an evaluation of the WILKINSON, COTTRELL and HUXLEY formula / 133 / for all the available weld chemical analysis. In each box (each welding condition), the first and the second lines are the result of this formula for welds in Q2N and HY100 steels, respectively. The last line in the box indicates which weld is more susceptible to solidification cracking. It is important to remember that the higher this value, the higher is the predicted solidification cracking tendency. As can be seen, all welds on HY100 steel have larger values than in Q2N steel. However, there is not a corresponding increase or decrease in solidification cracking tendency for welds made in the same steel, but at different welding parameters. This might be an indication that welding parameters changes cause stronger effects than the difference in chemical balance (at this level.)

In Table 8.13 the available carbon and sulphur analysis for welds made on both steels were collected for each welding condition. Again, as a consequence of base steel, carbon and sulphur are higher in all welds on HY100 steel, with only one exception (6.3 mm/s, 1.9 KJ/mm), with sulphur slightly higher in the Q2N steel.

Low manganese-to-silicon ratio has been shown (Chapter 4) to increase solidification cracking severity. In Table 8.14 this fact is

confirmed, for all the welds on HY100 show it lower than the welds on Q2N steel. We are not stating, of course, that this is the unique factor, but it seems to be a relevant one.

Relatively high carbon equivalent for solidification cracking -CE(SC), together with phosphorus is a other factor, and it is a dangerous combination, as seen in Chapter 4 (works of NAKAGAWA et al / 134, 140 - 144 /). The same authors have also shown that Mn^5/S is a better ratio to indicate solidification cracking tendency in the class of steels here discussed. Tables 8.15 and 8.16 show these factors. It can be seen that the combination of highest CE(SC) and phosphorus are found in welds on HY100 steel (Table 8.15), whilst the lowest Mn^5/S ratio is also found in welds on this steel (Table 8.16).

Therefore we think that the data contained in these tables reinforced the point of chemical balance influence on solidification cracking, as stated before.

In both Tables 8.11 (a,b) it is striking that welds using LINDE 95 wire and OP41TT flux were the most affected by centreline solidification cracking, for all welding parameters. As seen in Figures 8.8 and 8.9, welds made using LINDE 95 wire and OP41TT flux show a definite progression of this defect when the current increases at constant speed, or as it increases at constant speed. Using 6.3 mm/s and increasing the current (from 400 A to 770 A), the weld bead height-to-width ratio (H/W, Table 8.3 (a)) increases from 1.1 to 1.6 and this could be one explanation for the increase in solidification cracking tendency. However, using 770 A and increasing the speed (from 6.3 to 13.8 mm/s), the H/W ratio slightly decreases, but the cracking tendency strongly increases. As there is not any sign of change in chemical composition, this increase in solidification cracking susceptibility may be caused by different stress fields (Section 8.6.1), but we have not direct evidence to show. However, the primary macrostructure morphology (Section 8.6.2) might explain both behaviour. Firstly, with the increase of current at constant speed, the centreline changes from 'stray' to 'competitive columnar' type, competing at the centreline in zigzag, as shown in Figures 8.18 (a,b), respectively. Together with the change in morphology, the angle ('α' -Section 8.4) between the dendrite and the centreline rapidly increases. Also, the dendrite size increases more than three times in this range of welding parameters (see Table 8.6 for both factors).

As speed increases at constant current, the centreline changes from that already shown in Figure 8.18 (b) to an almost perfect 'centreline' type in Figure 8.18 (c), with the dendrites meeting at the weld centre in a well-defined straight line. The angle 'α' practically does not change (it slightly increases), and the dendrite is reduced to little less than half from its original size.

As we have seen in Chapter 3, in front of the solidification interface there is a solute build-up. When the dendrites meet at the weld centreline the amount of low melting point elements increases, as well as the constitutional supercooling extent. This effect is much more enhanced with the dendrites increasing in size, and with the angle 'α', for it is a component in the determination of centreline structure forming as a straight line. Also, both factors act together increasing the solute concentration at the weld centre. Another

point is the formation of vertically growing dendrites at the centre-line, as found in welds using the LINDE 95/OP41TT wire/flux combination (Section 8.6.2), which seems to offer to the stress their weakest resistant section.

The change in flux from OP41TT to OP121TT has a beneficial effect on those welds made at 6.3 mm/s welding speed. This fact can be seen in Tables 8.11 (a,b) and it was illustrated in Section 8.6.2 through comparison of Figures 8.19 (a,b) and 8.20 (a,b). The OP121TT flux seems to induce the formation of equiaxed dendrites at the weld centre-line, being perhaps an effect of the apparent different characteristics of this flux. In Section 6.3.2 we have shown that the amount of gas(es) released by the OP121TT flux is more than twice that realised by the OP41TT flux, and this may be one factor in the process. The effect is noticeable only at 6.3 mm/s welding speed, as said before. At higher welding speeds the heat balance and weld pool shape seem to dominate the microstructure, as we have seen in Section 8.6.2. The microsegregation is also affected by the flux type, as shown in Section 8.6.3, and welds made with OP121TT have less centreline microsegregation. Thus, at least two factors cooperate to induce better resistance to solidification cracking in welds made using OP121TT flux: a tendency to have equiaxed dendrites at the centreline, and (perhaps as a consequence of this) less segregation at this region in the weld metal.

The effect of wire change can also be assessed from Tables 8.11 (a,b). The OERLIKON S3 leads to a large reduction in centreline solidification cracking, and only the 13.8 mm/s welding speed welds have it. As shown in Table 8.14, the OERLIKON S3 wire has the best manganese-to-silicon ratio, much higher than using LINDE 95 wire. In Section 8.6.3 it was also seen that the OERLIKON S3 wire produces less centrellne segregation. Therefore, it seems that these factors combine to give a better resistance to solidification cracking.

In Tables 8.11 (a,b) it can be seen that either the change in flux to OP121TT, or wire, to OERLIKON S3, leads to a general improvement in the resistance to solidification cracking. However, for some welding conditions, the centreline cracking is replaced by the transverse type. The only explanation we can give for this phenomenon follows. Changing flux or wire does not practically alter the stress field around or within the weld pool. As the OERLIKON S3 wire or OP121TT flux induced less centreline segregation or a macrostructure less prone to centreline solidification cracking, or both, some welds simply could not tear any more along the centreline and had cracks along the interdendritic spaces in the transverse areas. In other words, the stress effect (the cracking) simply was transferred to regions of lower resistance to it.

As concluding remarks, we still have to point out two factors indirectly related to this phenomenon. The weld pool retention time (Section 8.5) has also an effect on the solidification cracking tendency, at least through the change in chemical composition and amount of fused slag. In this work, as seen in Figures 8.15 and 8.16 the elements silicon and manganese have shown a change in the bulk analysis. The effect on microsegregation, however, is unknown and it might be higher than the overall one. On the other hand, the flux takes heat from the arc to melt, leaving less to the weld metal, and different amounts of fused slag around the weld pool can modify the balance among the

surface tensions involved in the process during welding, as we have seen in Chapter 3.

The dendrite growth direction behaviour with welding parameters change is also an important factor. As we have seen in Section 8.4, current is the most significant parameter related to it (Table 8.6), within the limits of our experiments. The explanation might be that, as the current increases there is a consequent increase in penetration, leading to a geometrical change in the weld bead. The heat (mainly at the weld centre) tends to flow almost parallel to the base plate and the angle between the dendrites and the weld centreline increases.

Thus, follows a summary of the most important factors thought to affect solidification cracking tendency. This list is certainly not complete and must be followed by the 'unknown' factors:

(a) Factors thought to enhance the solidification cracking tendency:

- Ferrite stabiliser elements
- Large solidification range
- Macrostructure forming at the weld centreline a low stress resistant structure (centreline etc.)
- Metal around the weld pool does not relieve strain at high temperature
- Low Mn^k/S ratio (where k = 1, 3 or 5)
- Low Mn/Si ratio
- Great liquid film thickness between the solidified faces
- Unfavourable joint and weld bead geometry such as high H/W ratio and groove angle around 60^o
- Large dendrite size
- High dendrite growth direction angle
- Combined effects of elements such as carbon, nickel and phosphorus etc.

(b) Factors thought to decrease the solidification cracking tendency:

- Carbide forming elements
- Short solidification range
- Macrostructure forming at the weld centreline a high stress resistant structure (equiaxed etc.)
- Metal around the pool relieving strain at high temperature
- High Mn^k/S ratio
- High Mn/Si ratio
- Small liquid film thickness between the solidified faces

- Favourable joint and weld bead geometry such as low H/W ratio and groove angle around 0^{o} or 120^{o}
- Small dendrite size
- Low dendrite growth direction angle

Furthermore, a factor such the weld pool retention time can have double effect through its action on the formation of slag and chemical recovery. Also have double effect factors such as flux physical properties on the weld metal geometry or microstructure, or its influence on the elements recovery.

From the studies on weld metal microstructure, we think that one of the most significant factors there disclosed was the possibility to have 'cold' or high temperature (not solidification) cracking originating from existing solidification cracking. As seen in Section 8.8, it is quite possible that the crack tip shown in Figure 8.5 (a) might have originated a low temperature crack. If this is the case, we believe that the mechanical forces building up at the crack tip, which acts as a stress concentration factor, should be blamed for this crack propagation.

Another interesting possibility, disclosed principally in Figure 8.40 (c), is the association of the solidification cracking path with (likely) carbides. This would confirm the segregation either of solid carbides during solidification, or carbide former elements, as advanced in Chapter 3, and would call for special attention as regards their homogenisation. However, it is not clear whether this segregation is beneficial or not.

8.10 Summary

In this chapter experiments were successfully made in order, principally, to study the weld metal solidification cracking origins and tendencies of two High Yield Strength Quenched and Tempered Steels (HY100 and Q2N), two different wires (LINDE 95 and OERLIKON S3), and two different fluxes (OP41TT and OP121TT). As additional information, the secondary weld metal microstructure was monitored, as well as hardness and thermal cycles.

The cracking occurring in the tests was unmistakably identified as of solidification type, through inspection of its (dendritic) faces in the SEM and special etchants under light microscopy.

The cracking susceptibility assessment was done through the concepts of cracking size, crack-no-crack and presence of transverse cracking. Together with these parameters, all major weld bead dimensions were measured. Also the amount of fused flux for each welding condition was evaluated and weld bead ripple lag measured.

The dendrite size was measured for all welds and found to be related to change in welding parameters and weld bead geometry. As these measurements were done in a longitudinal section, a 'correction' component for the dendrite size had to be introduced. This was the angle between the dendrite growth direction and the weld bead symmetry line, as seen in the transverse section. Thus, the dendrite size

changes with welding parameters at different rates from those seen in the cutting section. Furthermore, there is a strong correlation between the actual dendrite size, welding parameters and weld bead height-to-width ratio, and with the weld bead external area-to-perimeter ratio. Also, it was noticed that the dendrite growth direction angle is strongly influenced by the power input (U x I) and changes very little with welding speed, within the limits of our experiments.

An approximate weld pool retention time has been also proposed, calculated through the weld bead ripple lag-to-welding speed ratio. This parameter correlates well with fused slag amount. Also, its effect on deoxidants like silicon and manganese was observed, and there is a decrease in their recovery, with longer weld pool retention time.

Stress relieving the two different base steels led to an increase in weld metal resistance to solidification cracking. As there was not change in chemical composition, this must be resultant from the (probable) decrease of the base metals stress level through this stress relief. Consideration was given to the stress fields within and around the weld pool. The weld bead height-to-width ratio did not give a reasonable correlation with cracking tendency, and has not shown to be the strongest factor involved in this process. Different chemical composition balance and carbides between both steels was pointed out and, as a consequence, the possibility of different mechanical responses at high (transient) temperatures.

The primary (solidification) macrostructure morphology and its (likely) influence on cracking tendency was analysed. In the weld bead transverse section at least four types of solidification macrostructure were notices: stray; competitive columnar; centreline; equiaxed.

The welding parameters influence on the primary macrostructure was monitored. For the lowest welding speed and energy input (6.3mm/s; 1.9 KJ/mm) and usimg OP41TT flux, it is 'stray', with some vertically growing dendrites at the weld centre. As the current increases it changes to 'competitive columnar'. Keeping the highest current (770A) and increasing the speed, the macrostructure is 'centreline' at 13.8 mm/s.

Changing the flux to OP121TT has an effect on the weld solidification macrostructure at 6.3 mm/s welding speed only. The 'stray' macrostructure is maintained, but without vertically growing dendrites, and any existing centreline cracking disappears. Increasing the current using OP121TT flux leads to the formation of some equiaxed structure.

Microsegregation was detected through metallographic means. Welds made on HY100 had the tendency to show higher microsegregation. The OP121 flux seems to decrease the microsegregation concentration, perhaps working through its influence on solidification macrostructure. The change in wire had no conclusive effect on the microsegregation, but the OERLIKON S3 seems to induce less at the centreline.

The general results have shown that the welds least susceptible to solidification cracking were those made using Q2N base steel, OP121TT flux and OERLIKON S3 or LINDE 95 wire. Based on all the data disclosed during this study, explanations were given to each case, being a complex interaction between chemical composition balance and

high temperature properties of both steels, microsegregation, primary (solidification) macrostructure morphology and welding parameters.

The weld secondary microstructure, hardness and thermal cycles were monitored as complementary information on the subject. The hardness progression with cooling time was analysed. The highest hardness for each welding parameter was obtained for welds using LINDE 95 wire.

Both steels have shown the same sensitivity to thermal cycles, as regards HAZ width and microstructure (light microscopy), which was essentially martensitic. The HY100 steel showed up some complex inclusion colonies within the coarse HAZ.

The weld microstructure was analysed for high (4.1 KJ/mm) and low (1.9 KJ/mm) energy input welds through three different techniques: light microscope; SEM; TEM.

The OP41TT flux seems to induce a coarser microstructure than the OP121TT, but no measurements were made to confirm this point. Also, no metallographic differences were noticed between the two wires.

At light microscopy level, areas of martensite, acicular ferrite and an unresolved lath structure were detected. Only the use of TEM resolved the lath microstructure, which showed up to be ferrite with aligned M-A-C and autotempered martensite.

During this investigation, 'islands' were found in the weld metal, with hardness well above that of the surrounding matrix.

Thus, considering the expected phases order of appearance and the measured thermal cycles, the welds under study are composed mainly of: ferrite with aligned M-A-C, acicular ferrite, and autotempered martensite, phases which should have formed in this order.

Evidence was found of 'cold' and/or high temperature (not solidification) cracking formation from existing solidification cracking. Also, it was disclosed a possible carbide segregation following the solidification cracking path.

Table 8.1 - Welding Conditions for each Parent Steel Plate

Specimens *	Welding Speed (mm/s)	Arc Current (A)	Arc Voltage (V)	Energy Input (Kj/mm)
H641 or L4,S4,L1,S1 Q641	6.3	400	30	1.9
H662 or L4,S4,L1,S1 Q662	6.3	600	30	2.8
H674 or L4,S4,L1,S1 Q674	6.3	770	34	4.1
H961 or L4 Q961	9.5	600	30	1.9
H972 or L4 Q972	9.5	770	34	2.8
H1371 or L4,S4,L1,S1 Q1371	13.8	770	34	1.9

Note: L4,S4,L1,S1 Refers to the following Wire/Flux Combination

L4 = LINDE 95-A/OP41TT S4 = OER S3-Ni Mo1/OP41TT
L1 = LINDE 95-A/OP121TT S1 = OER S3-Ni Mo1/OP121TT
*All Specimens were Welded with 120°C Preheat Temperature and Flux Baked two hours at 450°C

TABLE 8.2 - SOME SYMBOLS FROM TABLES 8.3(a,b) AND 8.4(a,b) AND THEIR MEANINGS (SEE FIG. 8.3)

H/W: Weld Bead Height/Width Ratio

r/W: Weld Bead Ripple Lag/Width Ratio

WH/2 (mm^2): Theoretical Weld Bead Area Considering it as a Perfect Isosceles Triangle (But W and H are actual measurements)

P (mm): Theoretical Weld Bead Perimeter, Considering it as a Perfect Isosceles Triangle (= $(4H^2 + W^2)^{\frac{1}{2}} + W$)

WH/2P: Theoretical Weld Bead Area/Perimeter Ratio

D (%): Dilution (= AP/AT x 100)

GAE (Kj): Net Gross Arc Energy Input (= E x Weld Length)

SWL (g/mm): Fused Slag/Weld Length Ratio

SWT (g/s): Fused Slag/Weld Time Ratio

SWL/AT ($g/mm.mm^2$): Ratio Giving the Approximate Amount of Fused Slag per Volume of Fused Weld Metal, but Intentionally not in Units of g/mm^3

TABLE 8.3(a)- WELDING CONDITIONS AND BEAD GEOMETRY FOR EACH WIRE/FLUX COMBINATION
MEASUREMENTS X10^{-1}. APPROXIMATE ERRORS: LINES=5% ; AREAS=6%

	W (mm)	X (mm)	H (mm)	d (mm)	H/W	r (mm)	r/W	WH/2 (mm^2)	P (mm)	WH/2P (mm)	
641L4	100	80	110	90	11	190	19	550	340	16.2	641L4
662L4	130	140	180	110	14	220	19	1170	510	22.9	662L4
674L4	140	190	220	120	16	250	18	1540	600	25.7	674L4
961L4	100	110	150	100	15	240	24	750	420	17.8	961L4
972L4	110	150	180	110	16	310	28	990	490	20.2	972L4
1371L4	100	120	140	100	14	370	37	700	400	17.5	1371L4
641S4	99	80	102	91	10	170	17	500	330	15.1	641S4
662S4	135	131	165	107	12	210	16	1080	490	22.0	662S4
674S4	138	185	205	129	15	240	17	1410	570	24.7	674S4
1371S4	88	113	125	106	14	350	40	550	350	15.7	1371S4

TABLE 8.3(b)- WELDING CONDITIONS AND BEAD GEOMETRY FOR EACH WIRE/FLUX COMBINATION
MEASUREMENTS $X10^{-1}$. APPROXIMATE ERRORS: LINES=5% ; AREAS=6%

	W (mm)	X (mm)	H (mm)	d (mm)	H/W	r (mm)	r/W	WH/2 (mm^2)	P (mm)	WH/2P (mm)	
641L1	108	82	107	89	9.9	210	19	580	350	16.6	641L1
662L1	127	127	162	109	12.7	230	18	1030	470	21.9	662L1
674L1	141	194	215	127	15.2	270	19	1520	590	25.8	674L1
1371L1	97	126	140	108	14.4	350	36	680	390	17.4	1371L1
641S1	106	76	103	91	9.7	180	17	550	340	16.2	641S1
662S1	122	127	162	103	13.3	210	17	990	470	21.1	662S1
674S1	135	195	211	127	15.6	250	19	1420	580	24.5	674S1
1371S1	87	112	124	106	14.2	340	39	540	350	15.4	1371S1

TABLE 8.4(a) - WELDING CONDITIONS, CRACKING SIZE, DILUTION, AND FUSED SLAG (FUNCTIONS) FOR EACH WIRE/FLUX COMBINATION

	l_c (%)	h_c (%)	AT (mm^2)	AD (mm^2)	AP (mm^2)	D SD (%)	GAE (KJ)	SWL ($X10^{-3}$) (g/mm)	SWT ($X10^{-3}$) (g/s)	SWL/AT ($X10^{-6}$) (g/mm.mm^2)	
641L4	Q-0 H-0	Q-0 H-24	95	39	56	70* (3)	570	150	945	1579	641L4
662L4	Q-0 H-0	Q-11 H-25	157	61	96	73* (3)	840	183	1155	1166	662L4
674L4	Q-0 H-0	Q-13 H-31	233	82	151	76* (3)	1230	227	1428	974	674L4
961L4	Q-0 H-100	Q-28 H-50	112	43	69	80* (3)	570	117	1108	1045	961L4
972L4	Q-0 H-100	Q-32 H-59	170	57	113	78* (3)	840	153	1457	900	972L4
1371L4	Q-38 H-100	Q-51 H-68	97	35	62	82* (3)	570	103	1426	1062	1371L4
641S4	Q-0 H-0	Q-0 H-13	75	32	42	57	570	180	1134	2400	641S4
662S4	Q-0 H-0	Q-T+ H-T	141	55	87	62	840	183	1239	1298	662S4
674S4	Q-0 H-0	Q-T H-T	220	72	147	69* (2)	1230	250	1575	1136	674S4
1371S4	Q-100 H-100	Q-35 H-68	107	35	72	67	570	123	1702	1150	1371S4

TABLE 8.4(b) - WELDING CONDITIONS, CRACKING SIZE, DILUTION, AND FUSED SLAG (FUNCTIONS) FOR EACH WIRE/FLUX COMBINATION

	l_c (%)	h_c (%)	AT (mm^2)	AD (mm^2)	AP (mm^2)	D SD (%)	GAE (KJ)	SWL ($X10^{-3}$) (g/mm)	SWT ($X10^{-3}$) (g/s)	SWL/AT ($X10^{-6}$) (g/mm.mm^2)	
641L1	Q-0 H-0	Q-0 H-T	91	40	51	56	570	146	924	1604	641L1
662L1	Q-0 H-0	Q-T H-T	150	-	-	-	840	177	1113	1180	662L1
674L1	Q-0 H-0	Q-0 H-17	252	86	166	78* (3)	1230	230	1449	913	674L1
1371L1	Q-54 H-100	Q-54 H-80	118	40	78	66	570	150	2070	1271	1371L1
641S1	Q-0 H-0	Q-0 H-T	72	30	42	58	570	150	945	2083	641S1
662S1	Q-0 H-0	Q-T H-T	140	-	-	-	840	173	1092	1236	662S1
674S1	Q-0 H-0	Q-T H-T	205	70	135	77* (2)	1230	213	1344	1039	674S1
1371S1	Q-0 H-100	Q-39 H-51	105	-	-	-	570	113	1564	1076	1371S1

* Obtained from Chemical Analysis (Ni Recovery of 100% - See Text).

TABLE 8.5(a) – WELD METALS CHEMICAL ANALYSES (wt% x 10^{-2}): VALUES ANALYSED (ANA), EXPECTED (EXP), DIFFERENCE (DIF), AND THEIR RESPECTIVE ERRORS (±E)

	C			Si			Mn			Cr			Mo			
	ANA	EXP (E)	DIF (E)	ANA	EXP (E)	DIF (E)	ANA	EXP (E)	DIF (E)	ANA	EXP (E)	DIF (E)	ANA	EXP (E)	DIF (E)	
Q641L4	15	13 (2)	2 (3)	30	26 (1)	4 (1)	84	78 (2)	6 (0)	89	101 (6)	-12 (8)	42	45 (5)	-3 (7)	Q641L4
H641L4	17	16 (2)	1 (3)	33	30 (1)	3 (1)	81	72 (3)	9 (1)	96	113 (7)	-17 (9)	39	41 (5)	-2 (7)	H641L4
Q662L4	12	13 (2)	-1 (3)	27	25 (1)	2 (1)	76	72 (2)	3 (0)	91	107 (7)	-16 (9)	44	45 (5)	-1 (7)	Q662L4
H662L4	16	16 (2)	0 (3)	32	30 (1)	2 (1)	79	70 (3)	9 (1)	104	116 (7)	-12 (9)	37	42 (5)	-5 (7)	H662L4
Q674L4	12	13 (2)	-1 (3)	28	24 (1)	4 (1)	78	70 (2)	8 (0)	100	110 (7)	-10 (9)	41	46 (5)	-5 (7)	Q674L4
H674L4	17	17 (3)	0 (4)	30	29 (1)	1 (1)	71	66 (3)	5 (1)	105	120 (7)	-15 (9)	41	42 (5)	-1 (7)	H674L4
Q961L4	16	14 (3)	2 (4)	31	23 (1)	8 (1)	81	64 (3)	17 (1)	103	116 (7)	-13 (9)	44	47 (5)	-3 (7)	Q961L4
Q972L4	15	14 (3)	1 (4)	30	23 (1)	7 (1)	78	64 (3)	14 (9)	107	117 (7)	-10 (9)	43	47 (5)	-4 (7)	Q972L4
H972L4	17	17 (3)	0 (4)	32	29 (1)	3 (1)	71	66 (3)	5 (1)	111	120 (7)	-9 (9)	40	42 (5)	-2 (07)	H972L4

TABLE 8.5(b) – WELD METALS CHEMICAL ANALYSES (wt% × 10^{-2}): VALUES ANALYSED (ANA), EXPECTED (EXP), DIFFERENCE (DIF), AND THEIR RESPECTIVE ERRORS (±E)

	C			Si			Mn			Cr			Mo			
	ANA	EXP (E)	DIF (E)	ANA	EXP (E)	DIF (E)	ANA	EXP (E)	DIF (E)	ANA	EXP (E)	DIF (E)	ANA	EXP (E)	DIF (E)	
Q1371L4	14	14 (3)	0 (4)	28	23 (1)	5 (1)	72	63 (3)	9 (1)	103	118 (7)	-15 (9)	42	47 (5)	-5 (7)	Q1371L4
H1371L4	19	18 (3)	1 (4)	31	27 (1)	4 (1)	69	59 (3)	10 (1)	111	129 (8)	-18 (10)	38	43 (5)	-5 (7)	H1371L4
Q674L1	15	13 (2)	2 (3)	28	25 (1)	3 (1)	83	74 (2)	9 (0)	96	105 (7)	-9 (9)	45	45 (5)	0 (7)	Q674L1
H674L1	16	18 (3)	-2 (4)	31	27 (1)	4 (1)	75	57 (3)	18 (1)	112	131 (8)	-19 (10)	44	43 (5)	1 (7)	H674L1
Q674S4	16	15 (2)	1 (3)	20	17 (1)	3 (1)	78	81 (2)	-3 (0)	97	100 (6)	-3 (8)	54	52 (1)	2 (1)	Q674S4
H674S4	18	18 (2)	0 (3)	22	21 (5)	1 (7)	77	80 (2)	-3 (0)	105	107 (6)	-2 (8)	51	49 (1)	2 (1)	H674S4
Q674S1	13	16 (2)	-3 (3)	20	17 (1)	3 (1)	81	71 (2)	10 (0)	96	110 (6)	-14 (8)	52	52 (1)	0 (1)	Q674S1
H674S1	17	19 (2)	-2 (3)	24	22 (5)	2 (7)	82	69 (2)	13 (0)	107	119 (6)	-12 (8)	52	48 (1)	4 (1)	H674S1

TABLE 8.5(c) – WELD METALS CHEMICAL ANALYSES (wt% x 10^{-2}): VALUES ANALYSED

	Ni	Al	Cu	Nb	Ti	V	W	
Q641L4	293	4	6	1	< 1	5	2	Q641L4
H641L4	282	2	7	1	< 1	1	2	H641L4
Q662L4	301	3	5	< 1	1	5	< 2	Q662L4
H662L4	285	3	7	1	< 1	1	2	H662L4
Q674L4	305	3	6	1	< 1	5	2	Q674L4
H674L4	290	2	7	< 1	< 1	1	< 2	H674L4
Q961L4	314	4	7	1	< 1	5	2	Q961L4
Q972L4	315	5	7	1	< 1	6	2	Q972L4
H972L4	290	3	8	1	< 1	1	2	H972L4
Q1371L4	316	3	6	1	< 1	5	2	Q1371L4
H1371L4	300	2	8	1	< 1	1	2	H1371L4
Q674L1	299	3	7	–	< 1	5	–	Q674L1
H674L1	302	2	7	–	< 1	1	–	H674L1
Q674S4	274	4	6	–	< 1	5	–	Q674S4
H674S4	256	6	7	–	< 1	1	–	H674S4
Q674S1	292	3	6	–	< 1	5	–	Q674S1
H674S1	274	2	8	–	< 1	1	–	H674S1

TABLE 8.5(d) – WELD METALS CHEMICAL ANALYSES (wt% x 10^{-3}): VALUES ANALYSED

	P	S	B	Co	Sn	Ø	N	
Q641L4	11	4	1	13	3	21	15	Q641L4
H641L4	13	4	1	13	4	23	-	H641L4
Q662L4	10	5	< 1	16	< 10	-	-	Q662L4
H662L4	11	4	1	14	4	-	-	H662L4
Q674L4	9	3	1	13	3	21	15	Q674L4
H674L4	12	6	< 1	18	< 10	-	-	H674L4
Q961L4	12	4	1	14	4	-	-	Q961L4
Q972L4	10	4	1	13	3	-	-	Q972L4
H972L4	12	5	1	14	4	-	-	H972L4
Q1371L4	9	3	1	13	2	-	-	Q1371L4
H1371L4	11	4	1	14	4	-	-	H1371L4
Q674L1	12	7	-	12	10	20	13	Q674L1
H674L1	14	7	-	13	10	21	-	H674L1
Q674S4	13	10	-	11	10	24	-	Q674S4
H674S4	13	8	-	12	10	19	-	H674S4
Q674S1	10	7	-	12	10	24	-	Q674S1
H674S1	14	8	-	12	10	22	-	H674S1

TABLE 8.6 - SOLIDIFICATION CRACKING TESTS (SINGLE RUN): RELATIONSHIP BETWEEN WELDING CONDITIONS, DENDRITE GROWTH DIRECTION ANGLE, AND DENDRITE SIZE (APPARENT AND ACTUAL).

Weld Code	Welding Parameters				Angle (*)	Dendrite Size (**)	
	U (V)	I (A)	V (mm/s)	UxI (W)	α (^{o})	Apparent (mm x 10^{-3})	Actual (mm x 10^{-3})
641	30	400	6.3	12000	30	23	11.5
662	30	600	6.3	18000	60	34	29.4
674	34	770	6.3	26180	75	40	38.6
972	34	770	9.5	26180	70	24	22.5
1371	34	770	13.8	26180	85	19	18.9

(*) Average Standard Deviation = ± 10%

(**) Average Standard Deviation = ± 12%

TABLE 8.7 - SOLIDIFCATION CRACKING TEST (SINGLE RUN): RELATIONSHIP BETWEEN WELDING CONDITIONS, WELD BEAD RIPPLE LAG, WELD POOL RETENTION TIME, AND FUSED SLAG/WELD LENGTH RATIO.

FLUX \ WIRE	CURRENT / SPEED	LINDE 95			OERLIKON S3		
		400	600	770	400	600	770
OP	6·3	19 3.0 150	22 3.5 183	25 4.0 227	17 2.7 180	21 3.3 183	24 3.8 250
41	9·5	-	24 2.5 117	31 3.3 153	-	-	-
TT	13·8	-	-	37 2.7 103	-	-	35 2.5 123
OP	6·3	21 3.3 146	23 3.6 177	27 4.3 230	18 2.9 150	21 3.3 173	25 4.0 213
121	9·5	-	-	-	-	-	-
TT	13·8	-	-	35 2.5 150	-	-	34 2.5 113

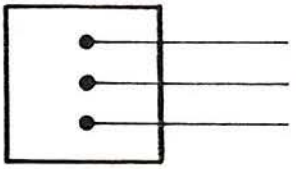

WELD BEAD RIPPLE LAG (mm) - (r)
WELD POOL RETENTION TIME (S) - (r/V)
FUSED SLAG/WELD LENGTH RATIO ($g/mm \times 10^{-3}$) - (SWL)

TABLE 8.8(a) SOLIDIFICATION CRACKING TESTS (SINGLE RUN): WELD METAL HARDNESS AND COOLING TIME

ENERGY INPUT: 1.9kJ/mm

AVERAGE COOLING TIME
1100-800°C: 3.4
800-500°C: 14.1

COARSE HAZ HARDNESS (PEAK)
Q2N: 437 (HV5)
HY100: 476

Weld Code	HARDNESS (HV5)	Weld Code	HARDNESS (HV5)
Q641L4	392 ±10	H641L4	407 ± 7
Q641L1	401 ±4	H641L1	404 ± 3
Q641S4	352 ±6	H641S4	371 ± 5
Q641S1	328 ±4	H641S1	357 ± 9

AVERAGE COOLING TIME
1100-800°C: 4.1S
800-500°C: 15.1S

COARSE HAZ HARDNESS (PEAK)
Q2N: 405 (HV5)
HY100: 442

Weld Code	HARDNESS (HV5)	Weld Code	HARDNESS (HV5)
Q961L4	405 ± 9	H961L4	442 ± 13

AVERAGE COOLING TIME
1100-800°C: 3.3S
800-500°C: 13.0S

COARSE HAZ HARDNESS (PEAK)
Q2N: 463 (HV5)
HY100: 487

Weld Code	HARDNESS (HV5)	Weld Code	HARDNESS (HV5)
Q1371L4	424 ± 7	H1371L4	417 ± 8
Q1371L1	406 ± 6	H1371L1	398 ± 6
Q1371S4	388 ± 6	H1371S4	407 ± 5
Q1371S1	355 ± 8	H1371S1	395 ± 10

TABLE 8.8(b) SOLIDIFICATION CRACKING TEST (SINGLE RUN): WELD METAL HARDNESS AND COOLING TIME

ENERGY INPUT: 2.8kJ/mm

AVERAGE COOLING TIME

1100-800°C: 6.4S

800-500°C: 27.1S

COARSE HAZ HARDNESS (PEAK)

Q2N: 432 (HV5)

HY100: 470

Weld Code	HARDNESS (HV5)	Weld Code	HARDNESS (HV5)
Q662L4	339 ± 8	H662L4	354 ± 11
Q662L1	320 ± 4	H662L1	334 ± 9
Q662S4	320 ± 3	H662S4	361 ± 7
Q662S1	321 ± 4	H662S1	332 ± 8

AVERAGE COOLING TIME

1100-800°C: 4.5S

800-500°C: 24:4S

COARSE HAZ HARDNESS (PEAK)

Q2N: 439 (HV5)

HY100: 461

Weld Code	HARDNESS (HV5)	Weld Code	HARDNESS (HV5)
Q972L4	381 ± 13	H972L4	373 ± 8

ENERGY INPUT: 4.1kJ/mm

AVERAGE COOLING TIME

1100-800°C: 10.7S

800-500°C: 49.5S

COARSE HAZ HARDNESS (PEAK)

Q2N: 437 (HV5)

HY100: 463

Weld Code	HARDNESS (HV5)	Weld Code	HARDNESS (HV5)
Q674L4	337 ± 9	H674L4	349 ± 7
Q674L1	339 ± 3	H674L1	352 ± 5
Q674S4	315 ± 6	H674S4	349 ± 6
Q674S1	320 ± 5	H674S1	327 ± 6

TABLE 8.9 - SOLIDIFICATION CRACKING TESTS (SINGLE RUN): RELATIONSHIP BETWEEN WELDING CONDITIONS, CARBON EQUIVALENT AND WELD METAL HARDNESS (HV 5).

FLUX \ WIRE	CURRENT / SPEED	LINDE 95			OERLIKON S3		
		400	600	770	400	600	770
OP 41	6·3	66/68 392 407	62/68 339 354	64/68 337 349	- 352 371	- 320 361	69/72 315 349
	9·5	-	70/- 405 442	69/70 381 373	-	-	-
TT	13·8	-	-	66/71 424 417	-	-	- 388 407
OP 121	6·3	- 401 404	- 320 334	68/71 339 352	- 328 357	- 321 332	67/73 320 327
	9·5	-	-	-	-	-	-
TT	13·8	-	-	- 406 398	-	-	- 355 395

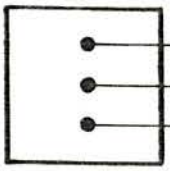

CARBON EQUIVALENT (x 10^{-2}): Q2N/HY100 WELDS

AVERAGE WELD METAL HARDNESS: Q2N STEEL

AVERAGE WELD METAL HARDNESS: HY100 STEEL

TABLE 8.10 - ESTIMATED PHASE TRANSFORMATION TEMPERATURES AND AVERAGE COOLING TIMES

WELD CODE	ENERGY INPUT (kJ/mm)	AVERAGE COOLING TIMES (S) 1100/800 °C	800/500 °C	FIRST TRANSFORMATION (°C) START	FINISH	SECOND TRANSFORMATION (°C) START	FINISH
Q641S1	1.9	3.4	14.1	490	420*	420*	380*
H662S4	2.8	6.4	27.1	630	530	530	480
Q674S1	4.1	10.7	49.5	810	680*	680*	630*
Q972L4	2.8	4.5	24.4	530	490	490	440
H1371S4	1.9	3.3	13.0	480	420	420	390
H961L4	1.9	4.1	15.1	520	470	470	440
WH641S4	1.9	5.9	20.5	600	510*	510*	470*
WQ674L4	4.1	10.4	45.9	690	600	600	540

(*) NOT CLEARLY DEFINED.

TABLE 8.11(a) - SOLIDIFICATION CRACKING TESTS (SINGLE RUN) ON Q2N STEEL: RELATIONSHIP BETWEEN WELDING CONDITIONS AND CRACKING TENDENCY

FLUX \ WIRE	CURRENT / SPEED	LINDE 95			OERLIKON S3			SPECIMENS	
		400	600	770	400	600	770	CL-SC* FREE	CRACK FREE
OP 41 TT	6·3	0	11	13	0	0 T (+)	0 T	4	2
	9·5	-	28	32	-	-	-	0	0
	13·8	-	-	51	-	-	35	0	0
OP 121 TT	6·3	0	0 T	0	0	0 T	0 T	6	3
	9·5	-	-	-	-	-	-	-	-
	13·8	-	-	54	-	-	39	0	0
SPECIMENS	CL-SC* FREE	2	1	1	2	2	2	10	
	CRACK FREE	2	0	1	2	0	0		5

(*) CL-SC: CENTRE LINE - SOLIDIFICATION CRACKING.

(+) T: TRANSVERSE SOLIDIFICATION CRACKING (PRESENCE)

TABLE 8.11(b) - SOLIDIFICATION CRACKING TESTS (SINGLE RUN) ON HY100 STEEL: RELATIONSHIP BETWEEN WELDING CONDITIONS AND CRACKING TENDENCY.

FLUX \ WIRE	CURRENT / SPEED	LINDE 95			OERLIKON S3			SPECIMENS	
		400	600	770	400	600	770	CL-SC* FREE	CRACK FREE
OP 41 TT	6·3	24	25	31	13	O T(+)	O T	2	0
	9·5	-	50	59	-	-	-	0	0
	13·8	-	-	68	-	-	68	0	0
OP 121 TT	6·3	O T	O T	17	O T	O T	O T	5	0
	9·5	-	-	-	-	-	-	-	-
	13·8	-	-	80	-	-	51	0	0
SPECIMENS	CL-SC* FREE	1	1	0	1	2	2	7	
	CRACK FREE	0	0	0	0	0	0		0

(*) CL-SC: CENTRE LINE - SOLIDIFICATION CRACKING.

(+) T: TRANSVERSE SOLIDIFICATION CRACKING (PRESENCE)

TABLE 8.12 - SOLIDIFICATION CRACKING TESTS (SINGLE RUN): RELATIONSHIP BETWEEN WELDING CONDITIONS, CHEMICAL COMPOSTION BALANCE AND SOLIDIFICATION CRACKING (SC) TENDENCY FOR HY100 AND Q2N STEELS.

FLUX \ WIRE	CURRENT / SPEED	LINDE 95			OERLIKON S3		
		400	600	770	400	600	770
OP	6·3	2.18 2.62 H>Q	1.82 2.38 H>Q	1.70 2.79 H>Q	-	-	2.40 2.57 H=Q(*)
41	9·5	-	2.42 - H>Q	2.21 2.74 H>Q	-	-	-
TT	13·8	-	-	2.10 3.05 H>Q	-	-	-
OP	6·3	-	-	2.28 2.66 H>Q	-	-	1.78 2.47 H=Q(*)
121	9·5	-	-	-	-	-	-
TT	13·8	-	-	-	-	-	-

WELDING ON Q2N STEEL } EVALUATION OF WILKINSON COTTRELL
WELDING ON HY100 STEEL } AND HUXLEY FORMULA

SC TENDENCY IN HY100 STEEL WELDS (H) IS GREATER (>), EQUAL (=), OR LESS (<), THAN SC TENDENCY IN Q2N STEEL WELDS (Q).

(*) BOTH WELDS SHOW TRANSVERSE SOLIDIFICATION CRACKING ONLY (NOT QUANTIFIABLE IN THIS WORK).

TABLE 8.13 SOLIDIFICATION CRACKING TESTS (SINGLE RUN): RELATIONSHIP BETWEEN WELDING CONDITIONS, CARBON, SULPHUR AND SOLIDIFICATION CRACKING (SC) TENDENCY FOR HY100 AND Q2N STEELS.

FLUX \ WIRE	CURRENT / SPEED	LINDE 95			OERLIKON S3		
		400	600	770	400	600	770
OP	6·3	15/17 4/4 H>Q	12/16 5/4 H>Q	12/17 3/6 H>Q	-	-	16/18 10/8 H=Q(*)
41	9·5	-	16/- 4/- H>Q	15/17 4/5 H>Q	-	-	-
TT	13·8	-	-	14/19 3/4 H>Q	-	-	-
OP	6·3	-	-	15/16 7/7 H>Q	-	-	13/17 7/8 H=Q(*)
121	9·5	-	-	-	-	-	-
TT	13·8	-	-	-	-	-	-

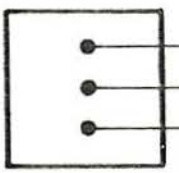

CARBON (x 10^{-2}): Q2N/HY100 WELDS.

SULPHUR (x 10^{-3}): Q2N/HY100 WELDS.

SC TENDENCY IN HY100 STEEL WELDS (H) IS GREATER (>), EQUAL (=), OR LESS (<) THAN SC TENDENCY IN Q2N STEEL WELDS (Q).

(*) BOTH WELDS SHOW TRANSVERSE SOLIDIFICATION CRACKING ONLY (NOT QUANTIFIABLE IN THIS WORK).

TABLE 8.14 - SOLIDIFICATION CRACKING TESTS (SINGLE RUN): RELATIONSHIP BETWEEN WELDING CONDITIONS, Mn/Si RATIO, AND SOLIDIFICATION CRACKING (SC) TENDENCY FOR HY100 AND Q2N STEELS.

FLUX \ WIRE	CURRENT / SPEED	LINDE 95			OERLIKON S3		
		400	600	770	400	600	770
OP 41	6·3	2.80 2.45 H>Q	2.81 2.47 H>Q	2.78 2.37 H>Q	-	-	3.90 3.50 H=Q (*)
	9·5	-	2.61 - H>Q	2.60 2.22 H>Q	-	-	-
TT	13·8	-	-	2.57 2.22 H>Q	-	-	-
OP 121	6·3	-	-	2.96 2.42 H>Q	-	-	4.05 3.42 H=Q (*)
	9·5	-	-	-	-	-	-
TT	13·8	-	-	-	-	-	-

Mn/Si RATIO - WELDING ON Q2N STEEL

Mn/Si RATIO - WELDING ON HY100 STEEL

SC TENDENCY IN HY100 STEEL WELDS (H) IS GREATER (>), EQUAL (=), OR LESS (<) THAN SC TENDENCY IN Q2N STEEL WELDS (Q)

(*) BOTH WELDS SHOW TRANSVERSE SOLIDIFICATION CRACKING ONLY (NOT QUANTIFIABLE IN THIS WORK).

TABLE 8.15 - SOLIDIFICATION CRACKING TESTS (SINGLE RUN): RELATIONSHIP BETWEEN WELDING CONDITIONS, CARBON EQUIVALENT (FOR SC - SEE TEXT), AND PHOSPHORUS CONTENTS FOR Q2N AND HY100 STEELS.

FLUX \ WIRE	CURRENT / SPEED	LINDE 95			OERLIKON S3		
		400	600	770	400	600	770
OP	6·3	28/29 11/13 H>Q	25/28 10/11 H>Q	25/30 9/12 H>Q	-	-	28/29 13/13 H=Q(*)
41	9·5	-	30/- 12/- H>Q	29/30 10/12 H>Q	-	-	-
TT	13·8	-	-	28/32 9/11 H>Q	-	-	-
OP	6·3	-	-	28/29 12/14 H>Q	-	-	26/29 10/14 H=Q(*)
121	9·5	-	-	-	-	-	-
TT	13·8	-	-	-	-	-	-

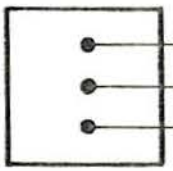

CARBON EQUIVALENT (SC) x 10^{-2}: Q2N/HY100 WELDS.
PHOSPHORUS (Wt % x 10^{-3}): Q2N /HY100 WELDS.
SC TENDENCY IN HY100 STEEL WELDS (H) IS GREATER (>), EQUAL (=), OR LESS (<) THAN IN Q2N STEEL WELDS (Q).

(*) TRANSVERSE CRACKING ONLY (NOT QUANTIFIABLE IN THIS WORK).

TABLE 8.16 - SOLIDIFICATION CRACKING TESTS (SINGLE RUN): RELATIONSHIP BETWEEN WELDING CONDITIONS, Mn^5/s RATIO, AND SOLIDIFICATION CRACKING (SC) TENDENCY FOR HY100 AND Q2N STEELS.

FLUX \ WIRE	CURRENT / SPEED	LINDE 95			OERLIKON S3		
		400	600	770	400	600	770
OP	6·3	104 87 H>Q	51 77 H>Q	96 30 H>Q	-	-	29 34 H=Q (*)
41	9·5	-	87 - H>Q	72 36 H>Q	-	-	-
TT	13·8	-	-	64 39 H>Q			
OP	6·3	-	-	56 34 H>Q	-	-	50 46 H=Q (*)
121	9·5	-	-	-	-	-	-
TT	13·8	-	-	-	-	-	-

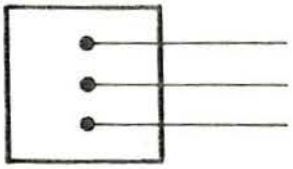

Mn^5/S - WELDING ON Q2N STEEL.
Mn^5/S - WELDING ON HY100 STEEL.
SC TENDENCY IN HY100 STEEL WELDS (H) IS GREATER (>), EQUAL (=), OR LESS (<) THAN IN Q2N STEEL WELDS (Q).

(*) TRANSVERSE CRACKING ONLY (NOT QUANTIFIABLE IN THIS WORK).

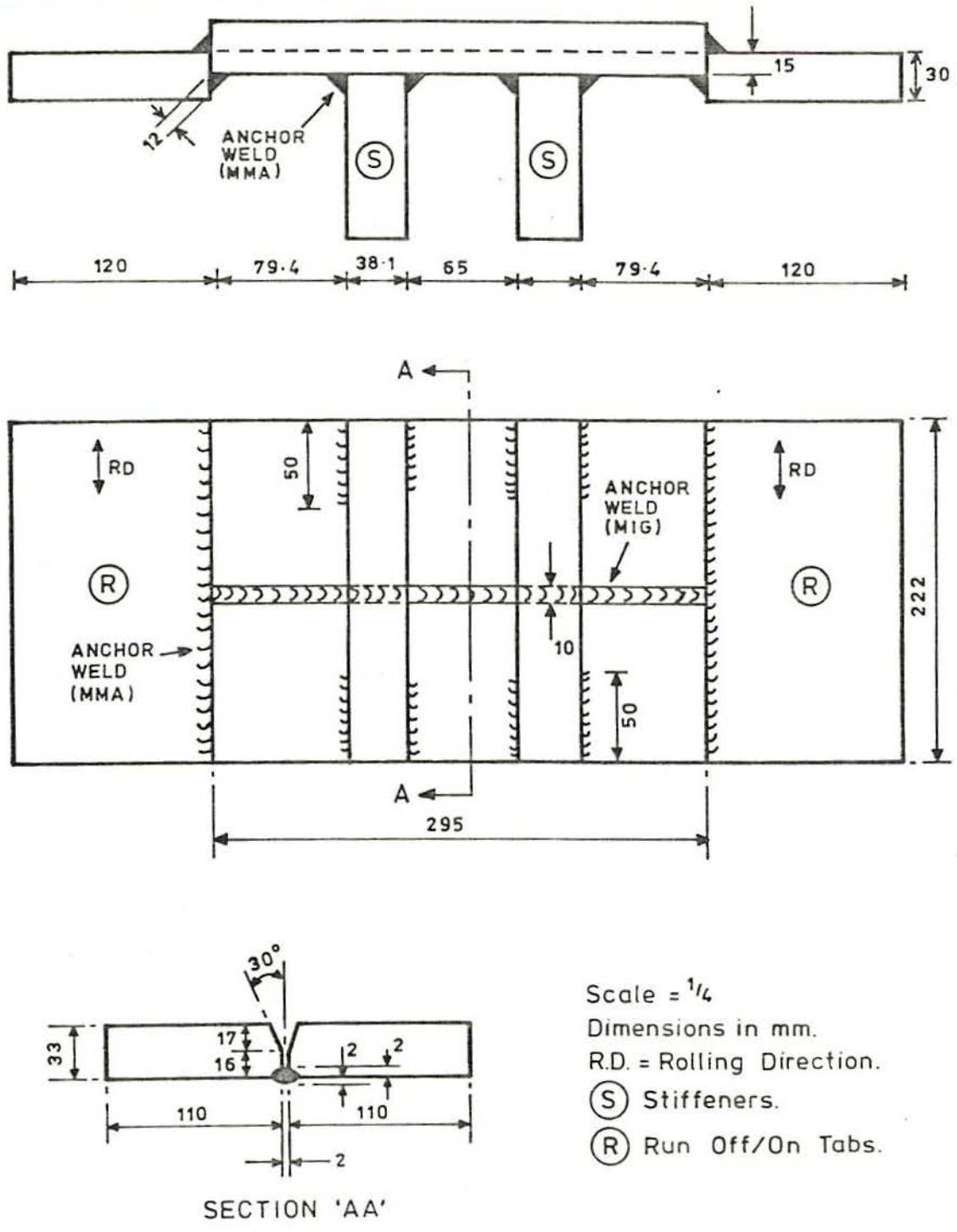

FIGURE 8.1 SPECIMEN CONFIGURATION FOR SUBMERGED ARC WELD TESTS.

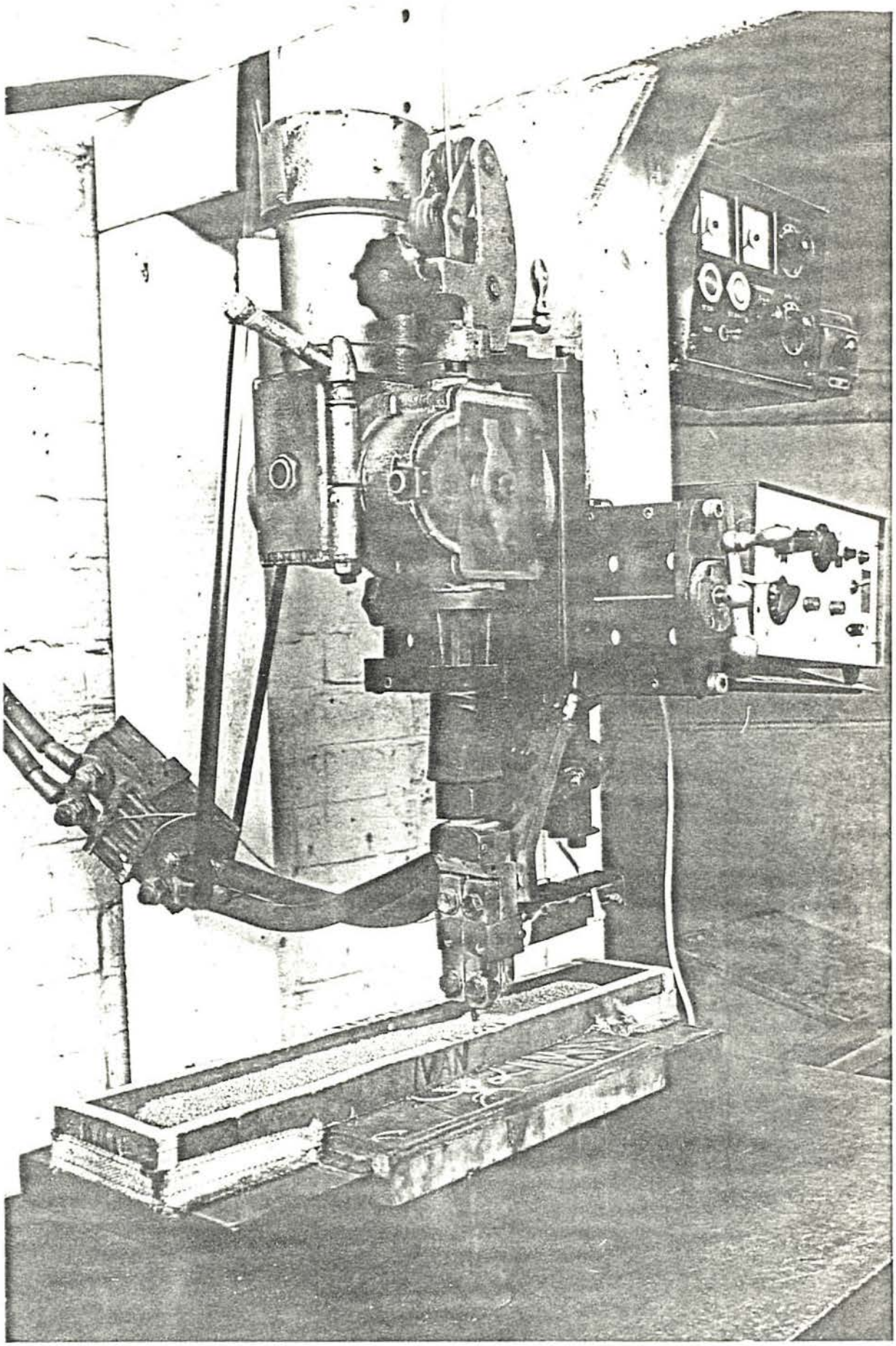

FIG. 8.2 - Welding Setting Up for Standard Submerged Arc Welding and for Arc Oscillation.

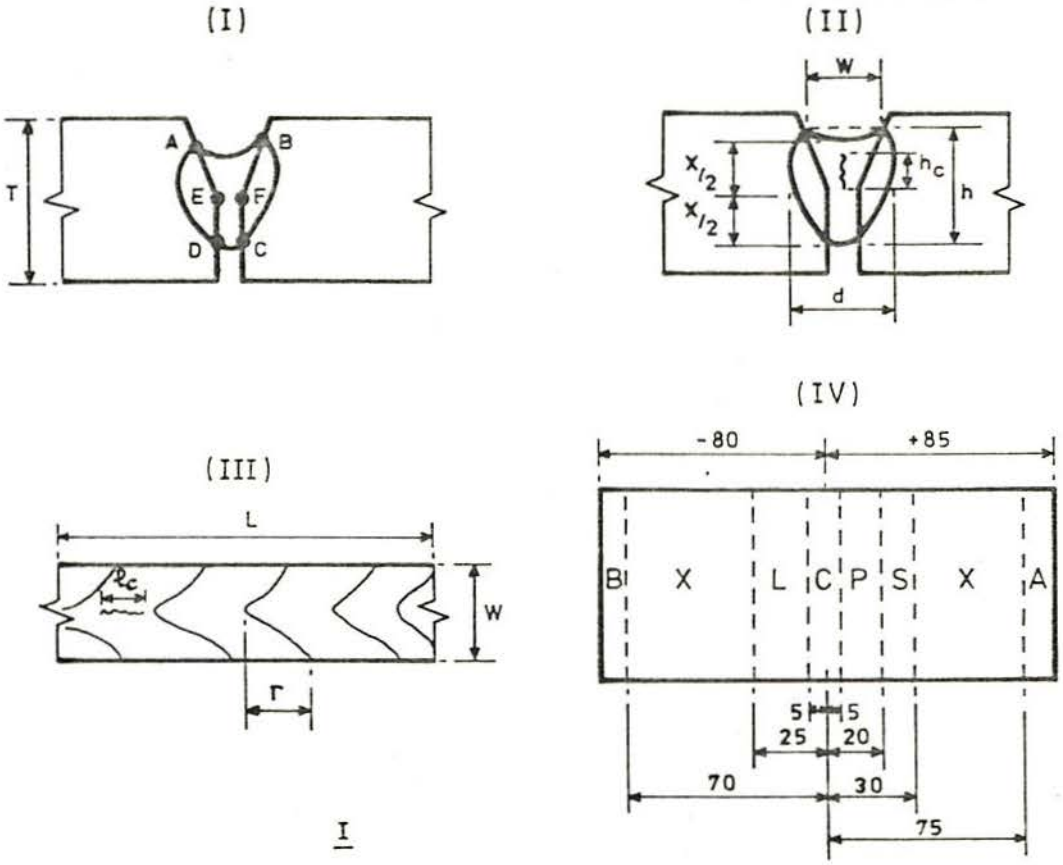

I

AT = ABCDA = Total transverse weld bead area
AD = ABFCDEA = Deposited filler metal area
AP = AT-AD = AEDA + BCFB = Parent melted metal area
T = Plate thickness

II

W = Weld bead width
X = True weld bead height
h = Conventional weld bead height (also effective penetration)
h_c = Solidification cracking height in the transverse section.
d = Average weld bead width (measured at X/2)

III

L = Weld bead length
l_c = Surface (visible) solidification cracking length
r = Ripple lag

IV

Approximate locations from where the analysed sections in the present work were taken.

FIGURE 8.3 BEAD GEOMETRY AREAS AND DEFECTS GLOSSARY.

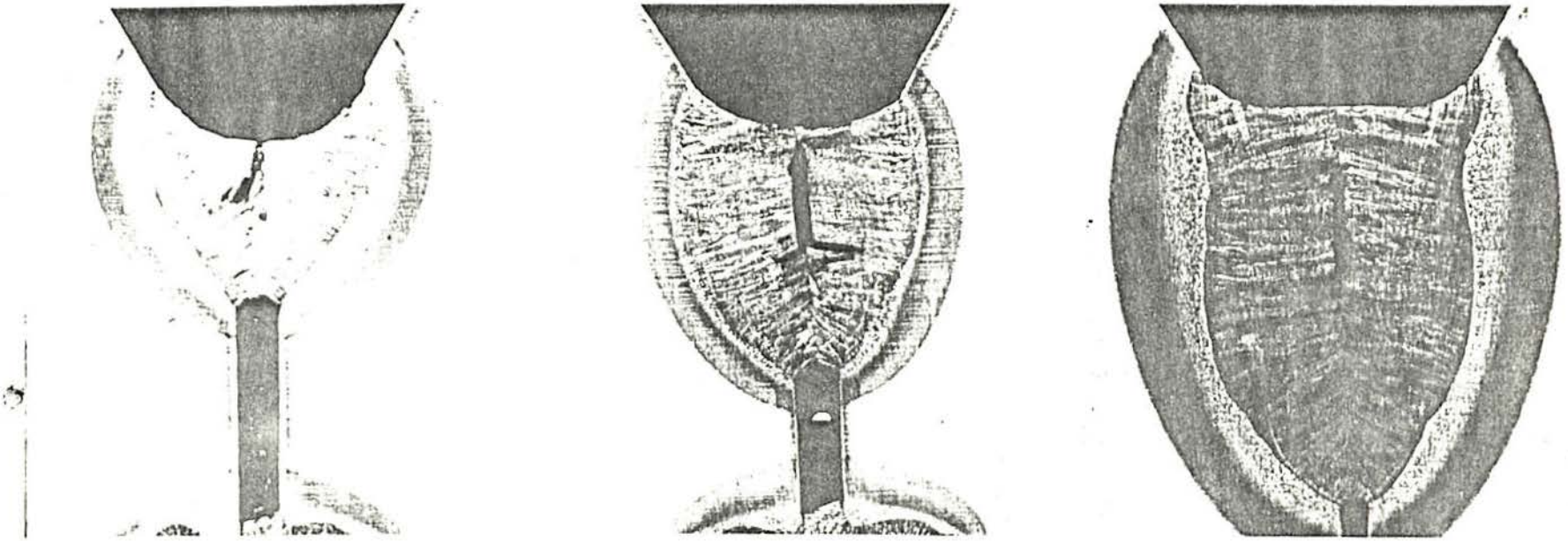

(a) Sp. H 641 L4

(b) Sp. Q 1371 L4

(c) Sp. H 674 L4

FIG. 8.4 Typical Weld Bead Transverse Sections. Nital, X 3.

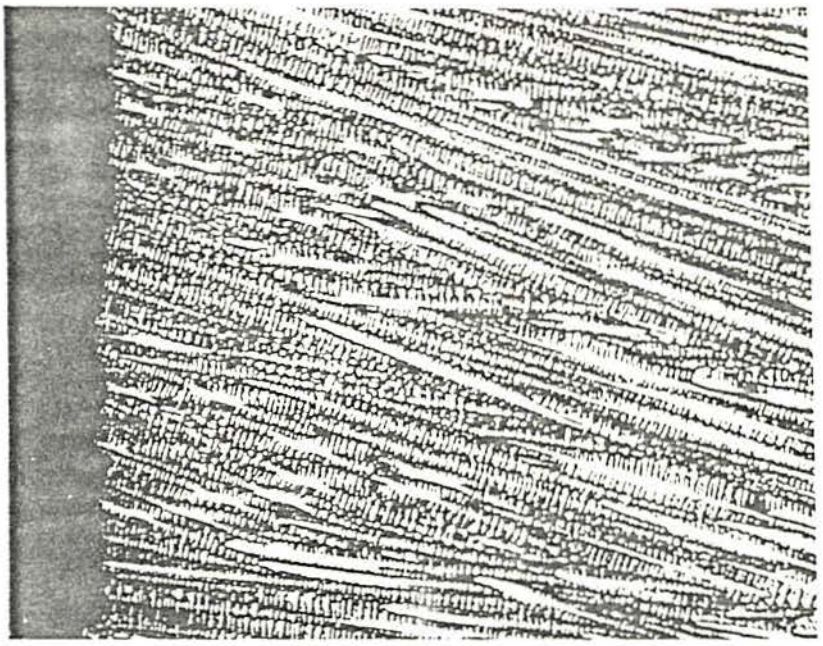

FIG. 8.5 - (b) Ibid. Plan Section. SASPA, x 50

FIG. 8.5 - (a) SP.H1371L1 (13.8 mm/s, 1.9 KJ/mm) Transverse Section Showing a Centre-Line SC. SASPA, x 100

(a)

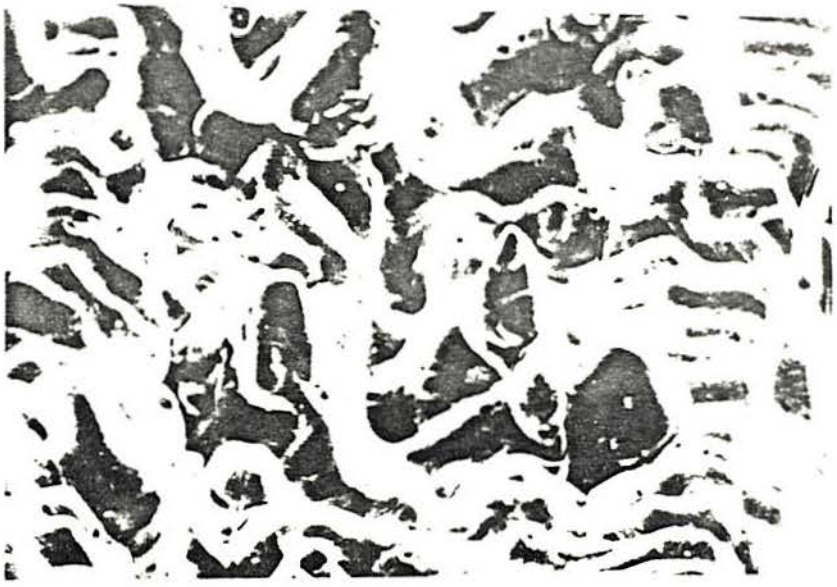

(b)

FIG. 8.6(a,b) Two Typical Aspects of (Dendritic) Solidification Cracking Surface, SEM. X 1K

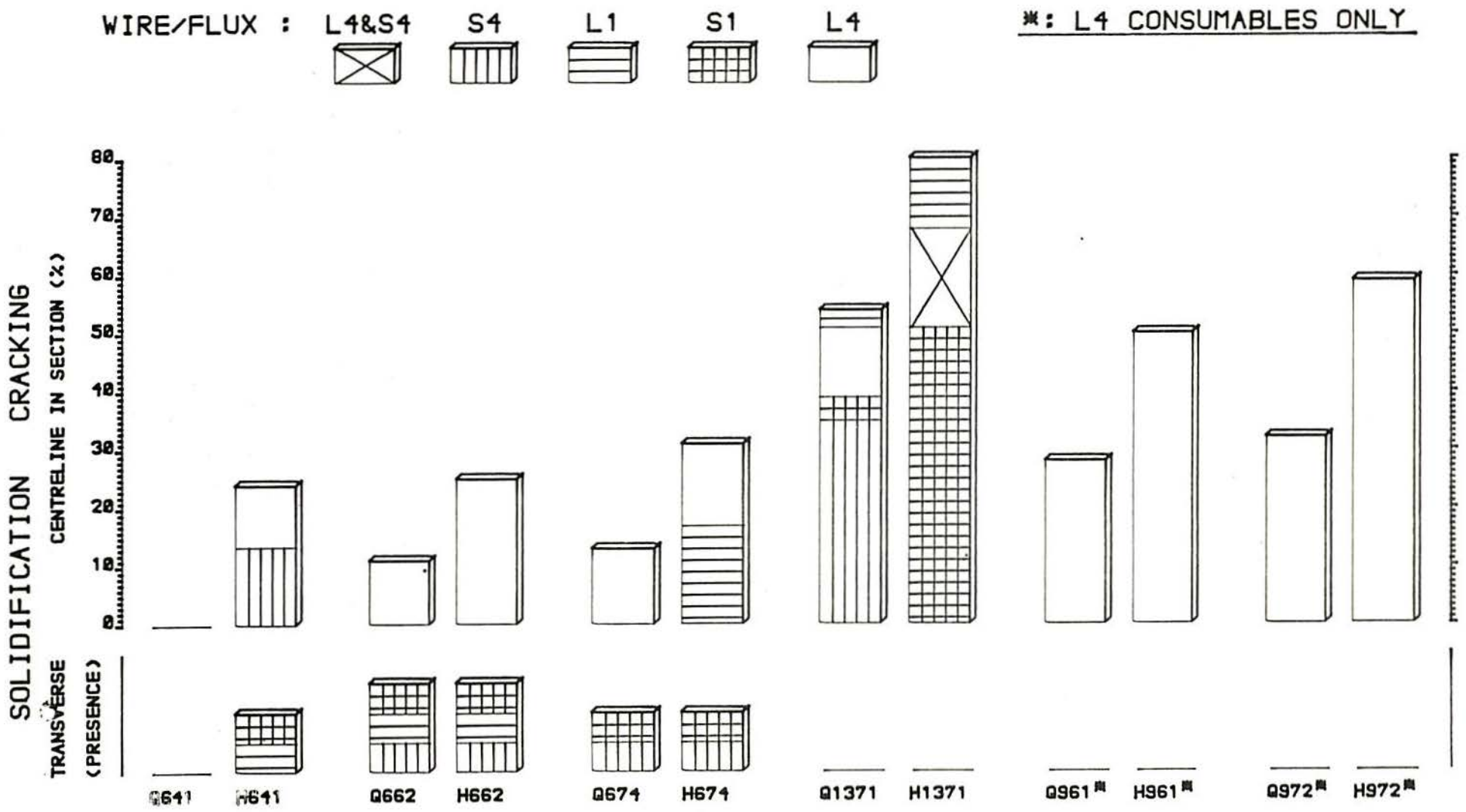

FIGURE 8.7 - RELATIONSHIP AMONGST WELDING CONDITIONS, PERCENTAGE OF CENTRELINE SOLIDIFICATION CRACKING IN SECTION (AVERAGE), AND PRESENCE OR ABSENCE OF TRANSVERSE CRACKING (cold wire addition or wire oscillation results not shown)

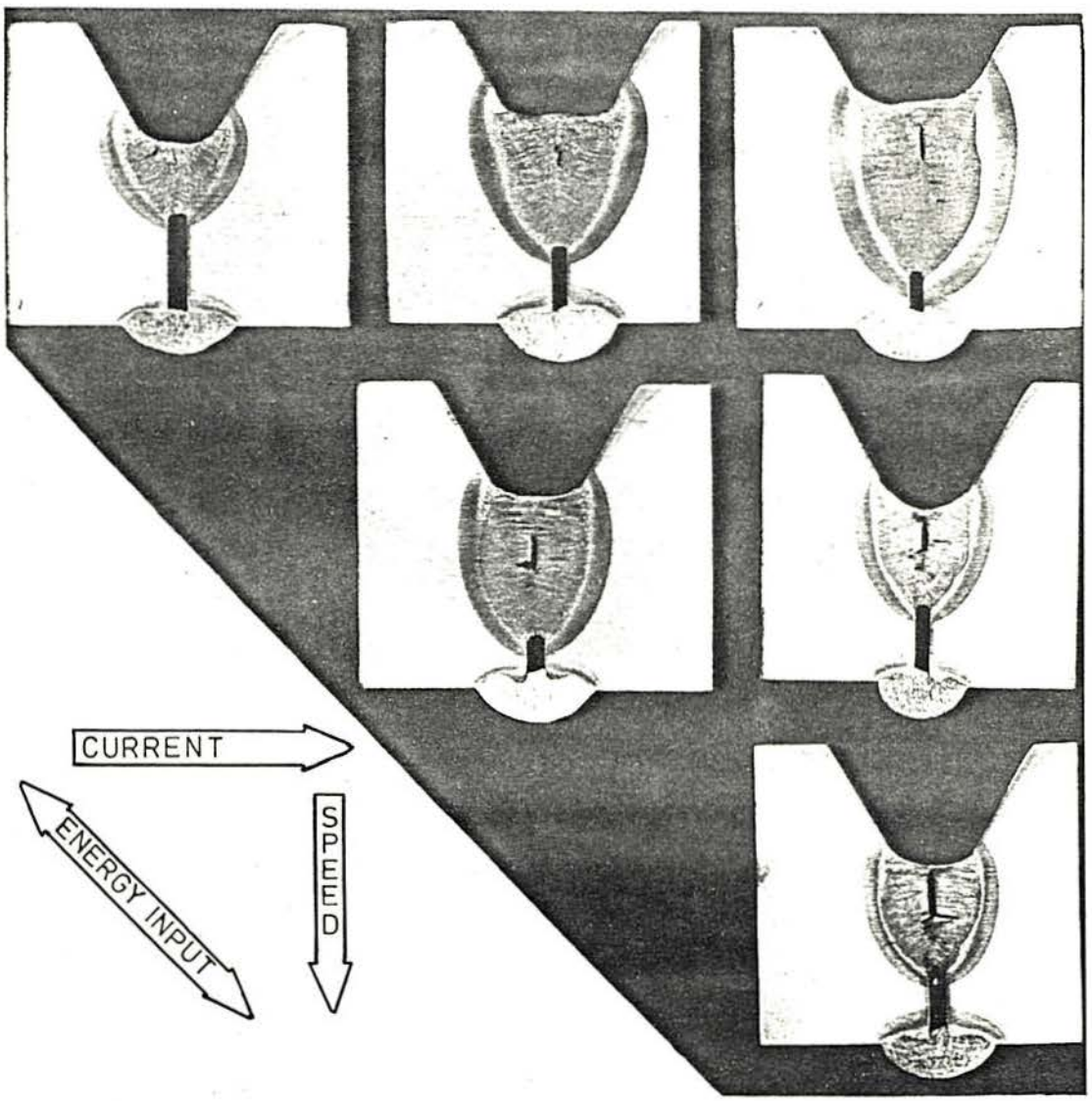

FIGURE 8.8 – Q2N WELDMENTS.
LINDE 95 WIRE AND OP41TT FLUX.

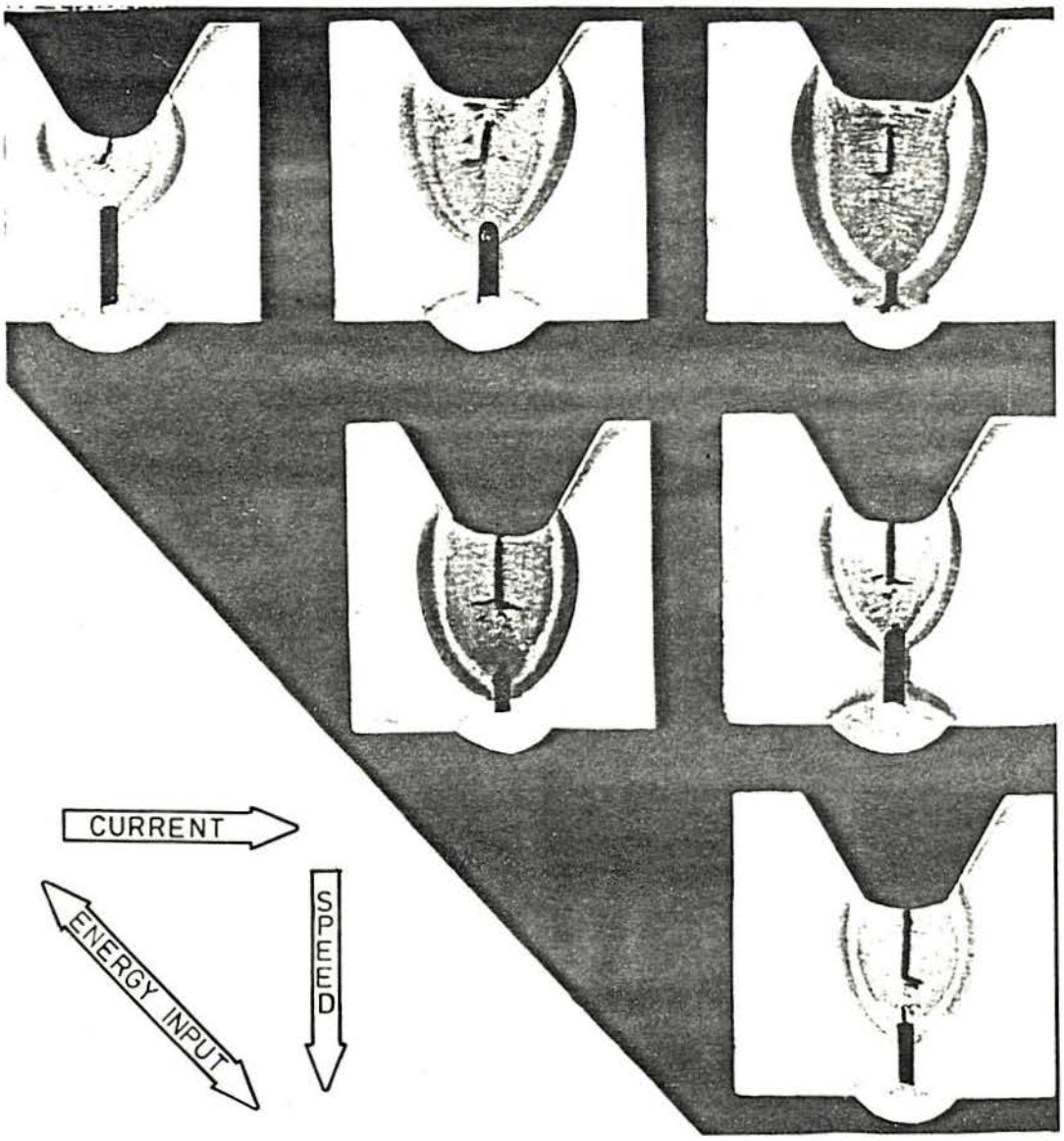

FIGURE 8.9 - HY 100 WELDMENTS.
LINDE 95 WIRE AND OP41TT FLUX.

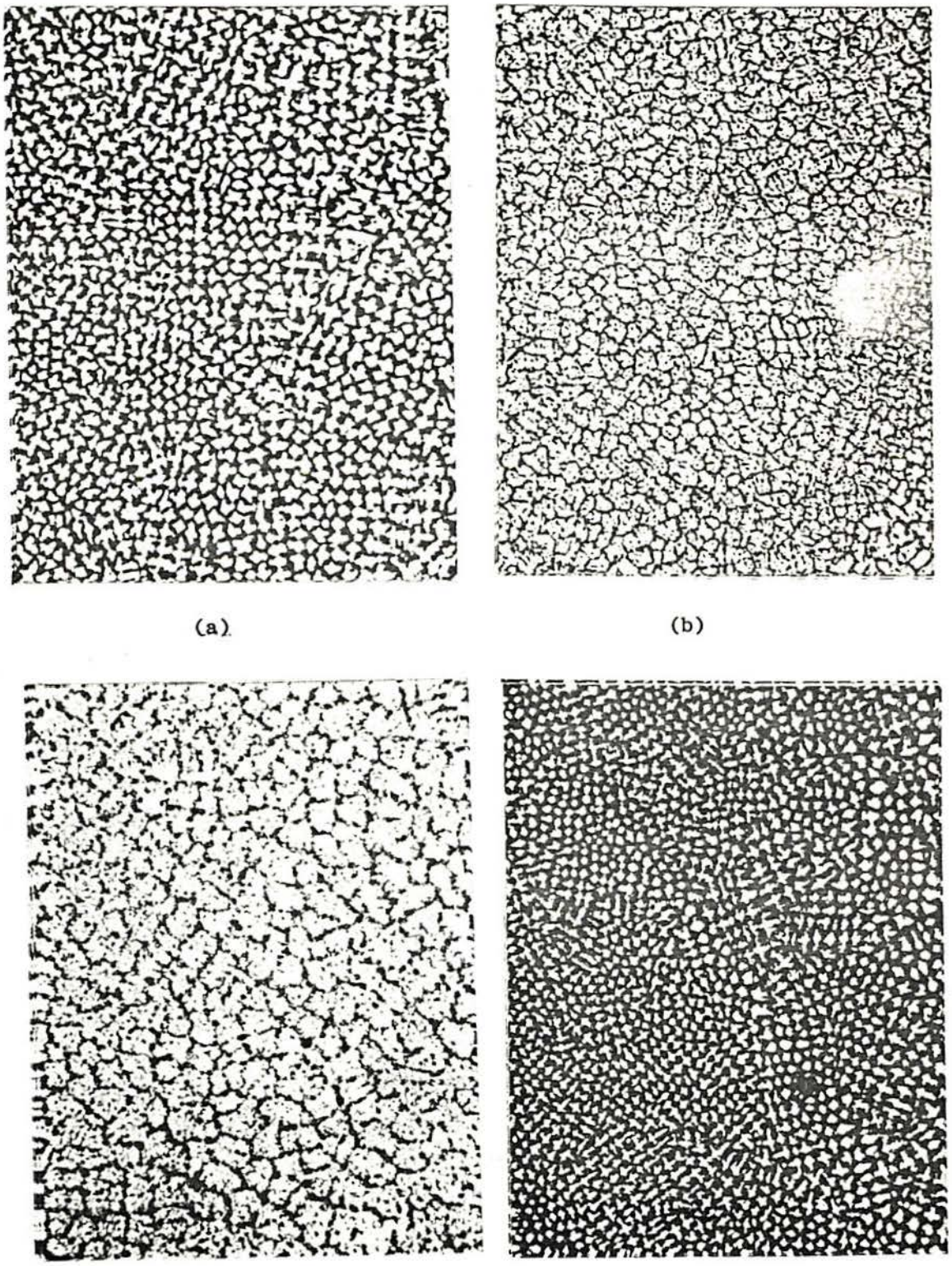

(a) (b)

(c) (d)

Figure 8.10 - Dendrites as seen in a Longitudinal Weld Bead Section.
(a) WC 641, (b) WC 662, (c) WC 674, (d) WC 1371.
SASPA X100

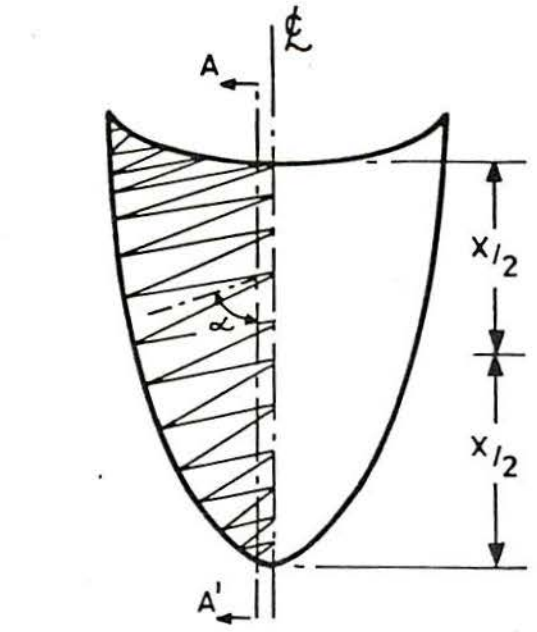

(a)

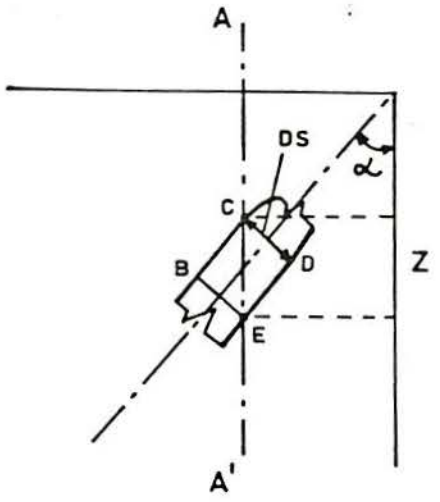

$DS = Z \cos(90 - \alpha)$

(b)

FIGURE 8.11 RELATIONSHIP BETWEEN THE APPARENT (Z) AND ACTUAL (DS) DENDRITE SIZE AND ITS DEPENDENCE ON THE DENDRITE GROWTH ANGLE (α)

(a.) SCHEMATIC DENDRITE GROWTH DIRECTION ON A WELD TRANSVERSE SECTION.

(b.) GEOMETRICAL RELATIONSHIP BETWEEN Z AND "DS"

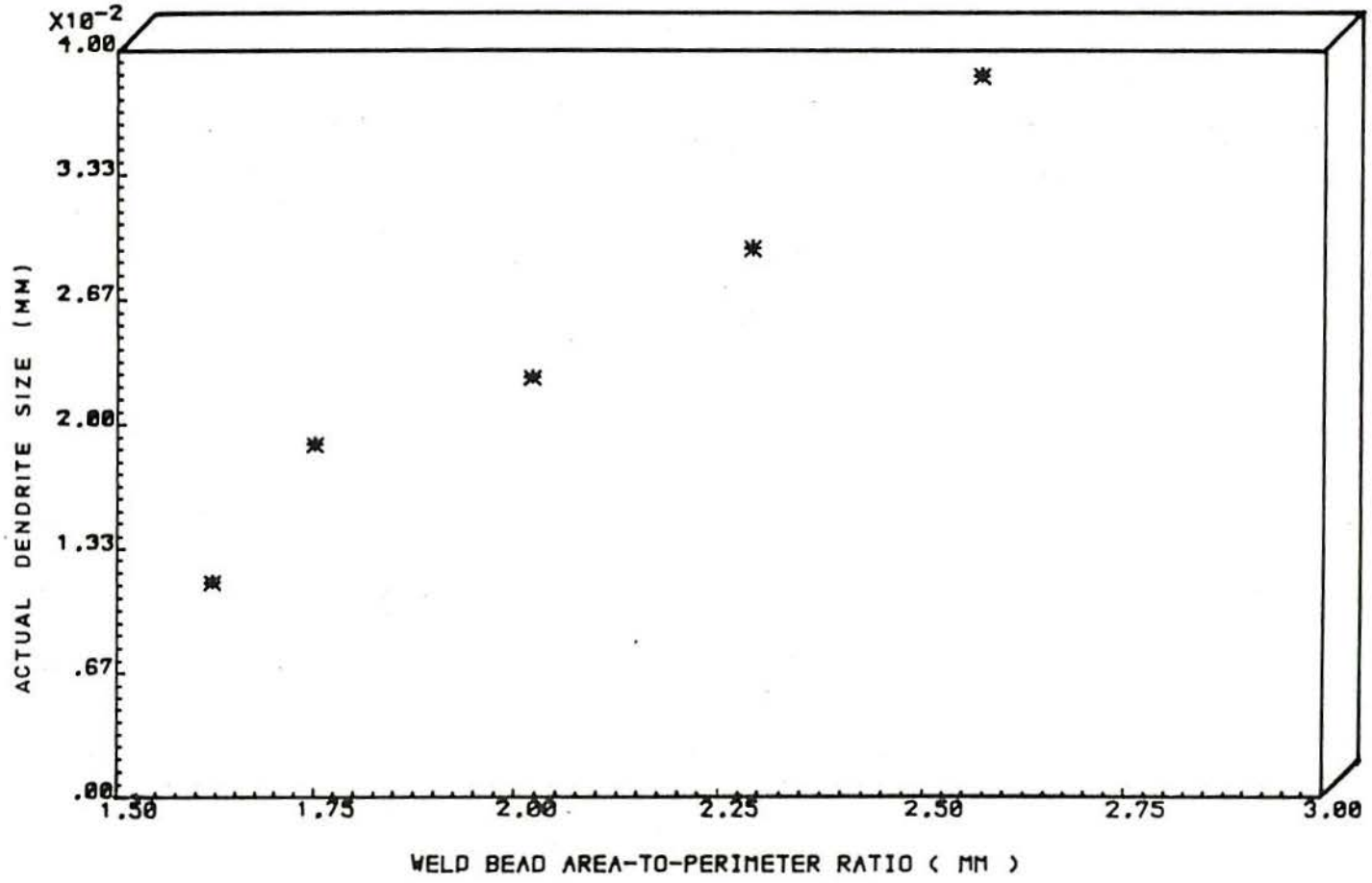

FIGURE 8.12 - RELATIONSHIP BETWEEN WELD BEAD AREA-TO-PERIMETER RATIO AND ACTUAL DENDRITE SIZE

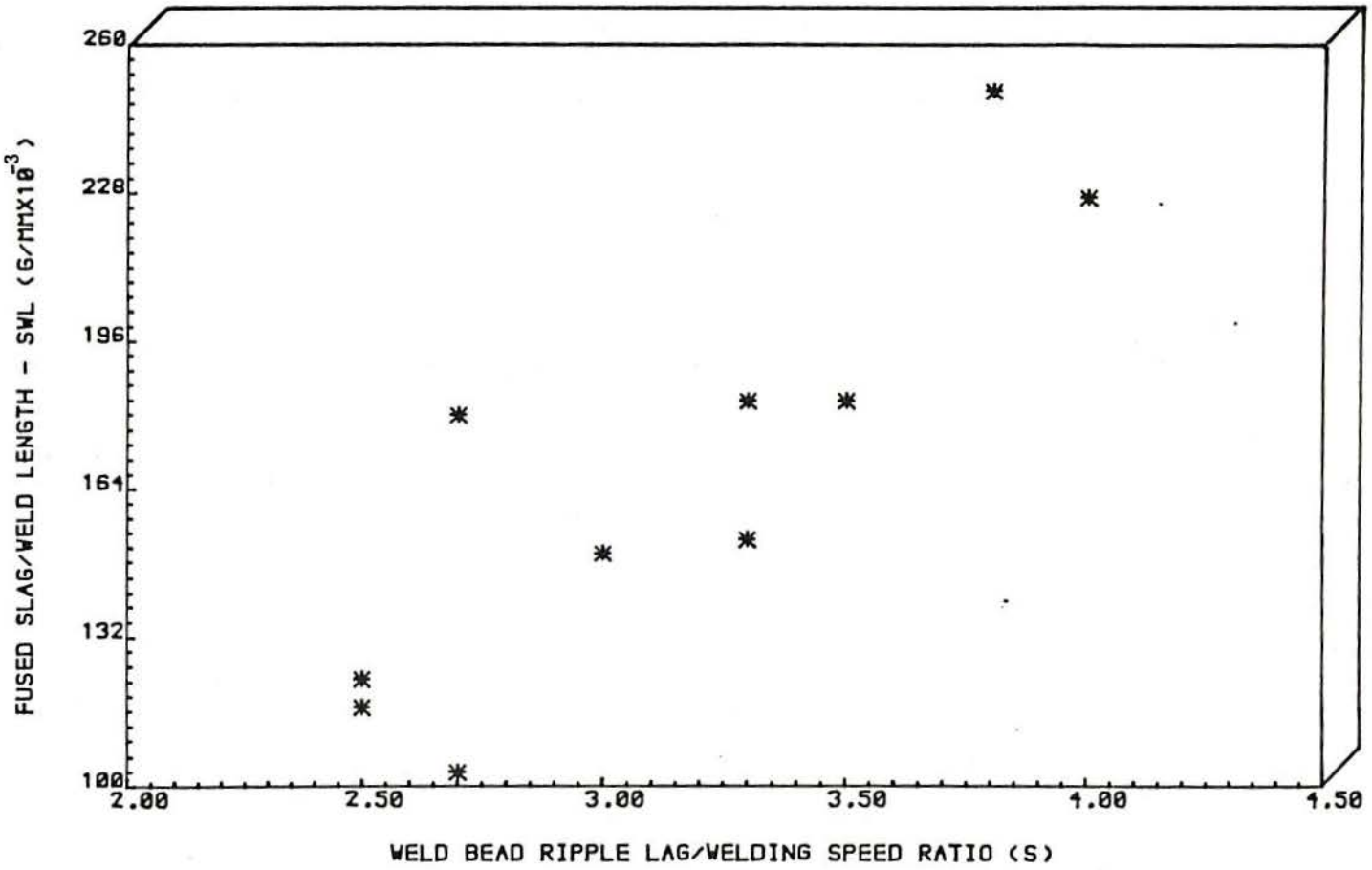

FIGURE 8.13 - RELATIONSHIP BETWEEN WELD POOL REACTION TIME (APPROXIMATE-SEE TEXT) AND FUSED SLAG (OP41TT FLUX)

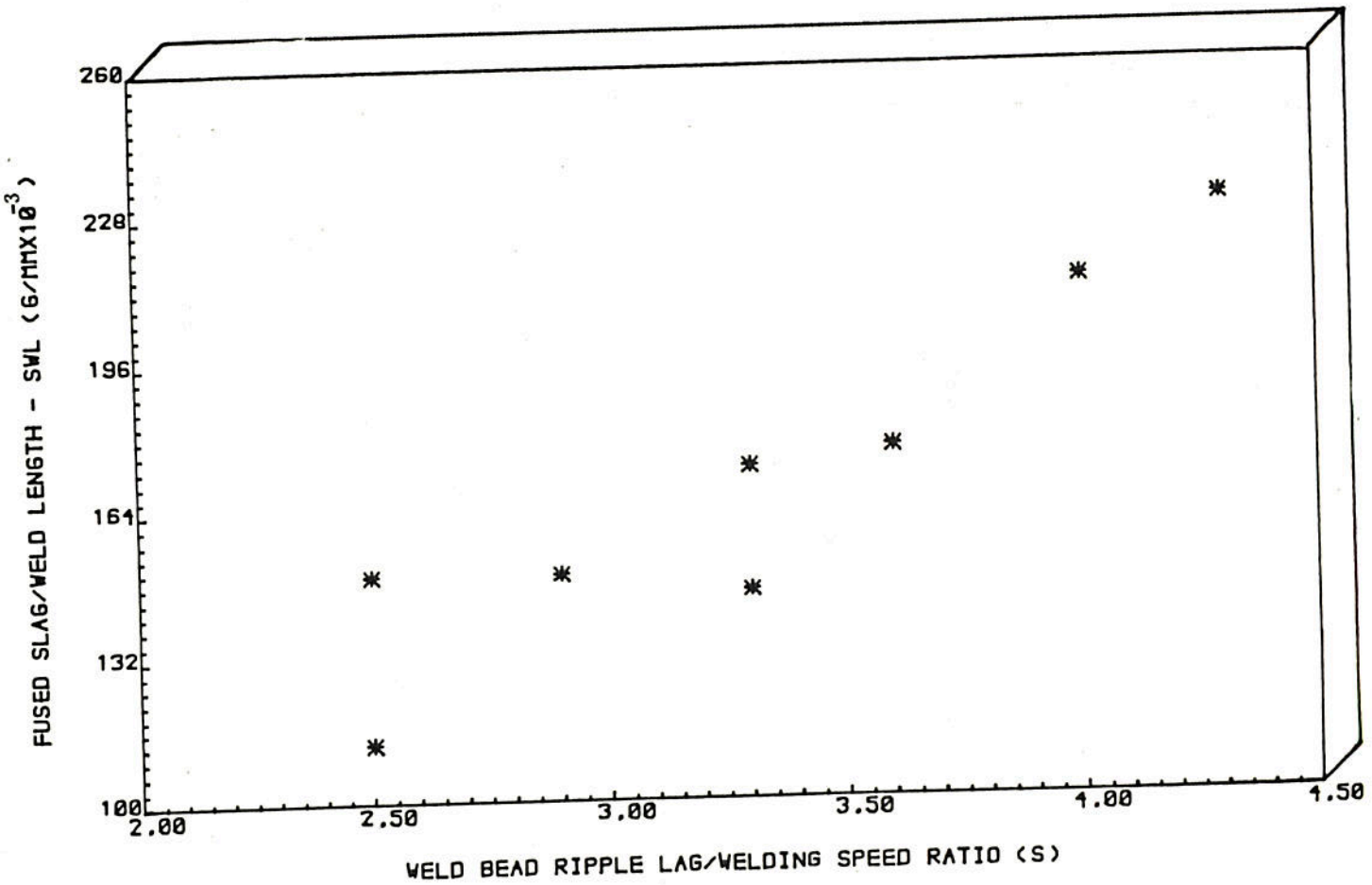

FIGURE 8.14 - RELATIONSHIP BETWEEN WELD POOL REACTION TIME (APPROXIMATE-SEE TEXT) AND FUSED SLAG (OP121TT FLUX)

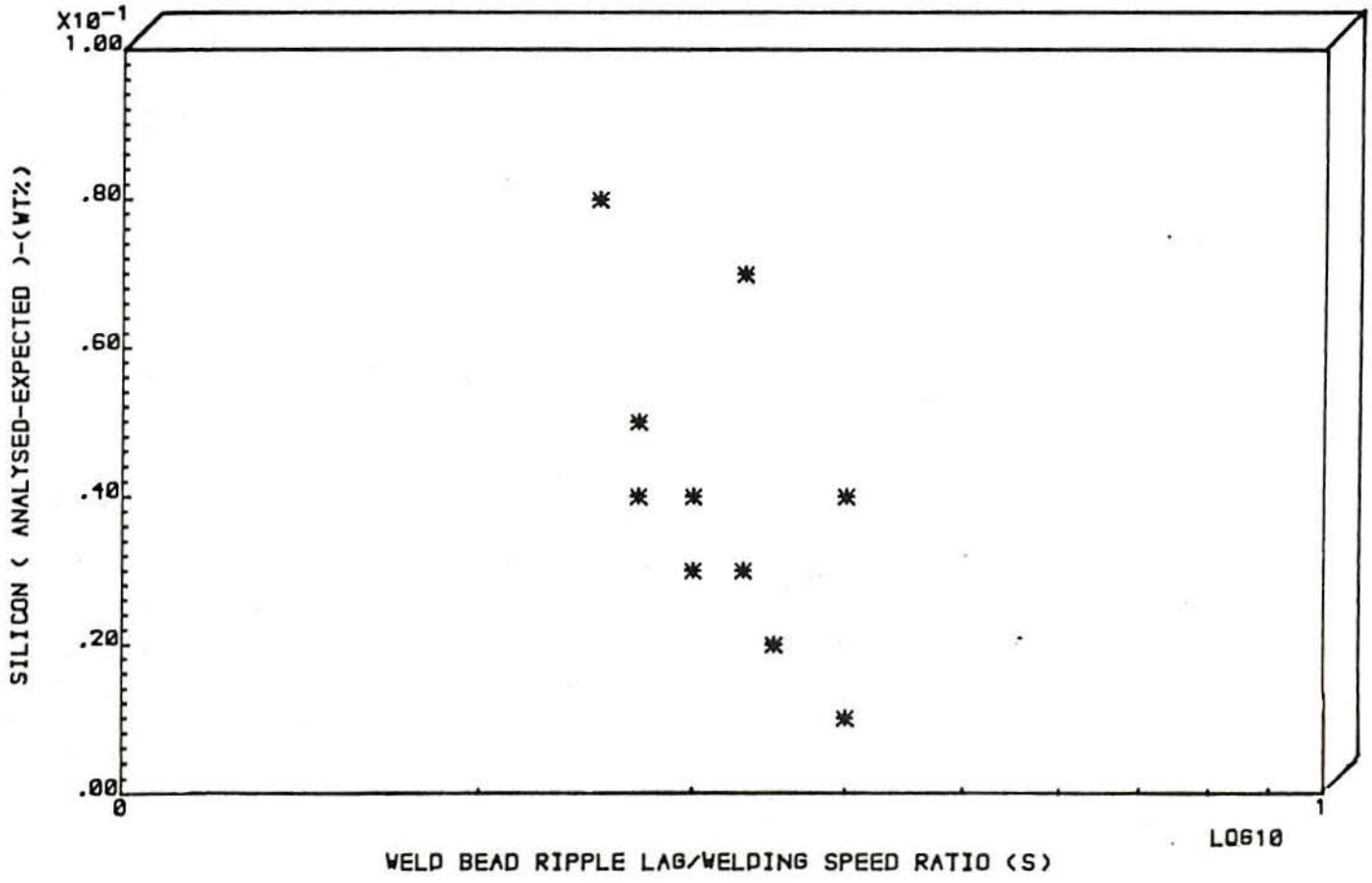

FIGURE 8.15 - RELATIONSHIP BETWEEN WELD POOL REACTION TIME (APPROXIMATE-SEE TEXT) AND SILICON DIFFERENCE (OP41TT FLUX)

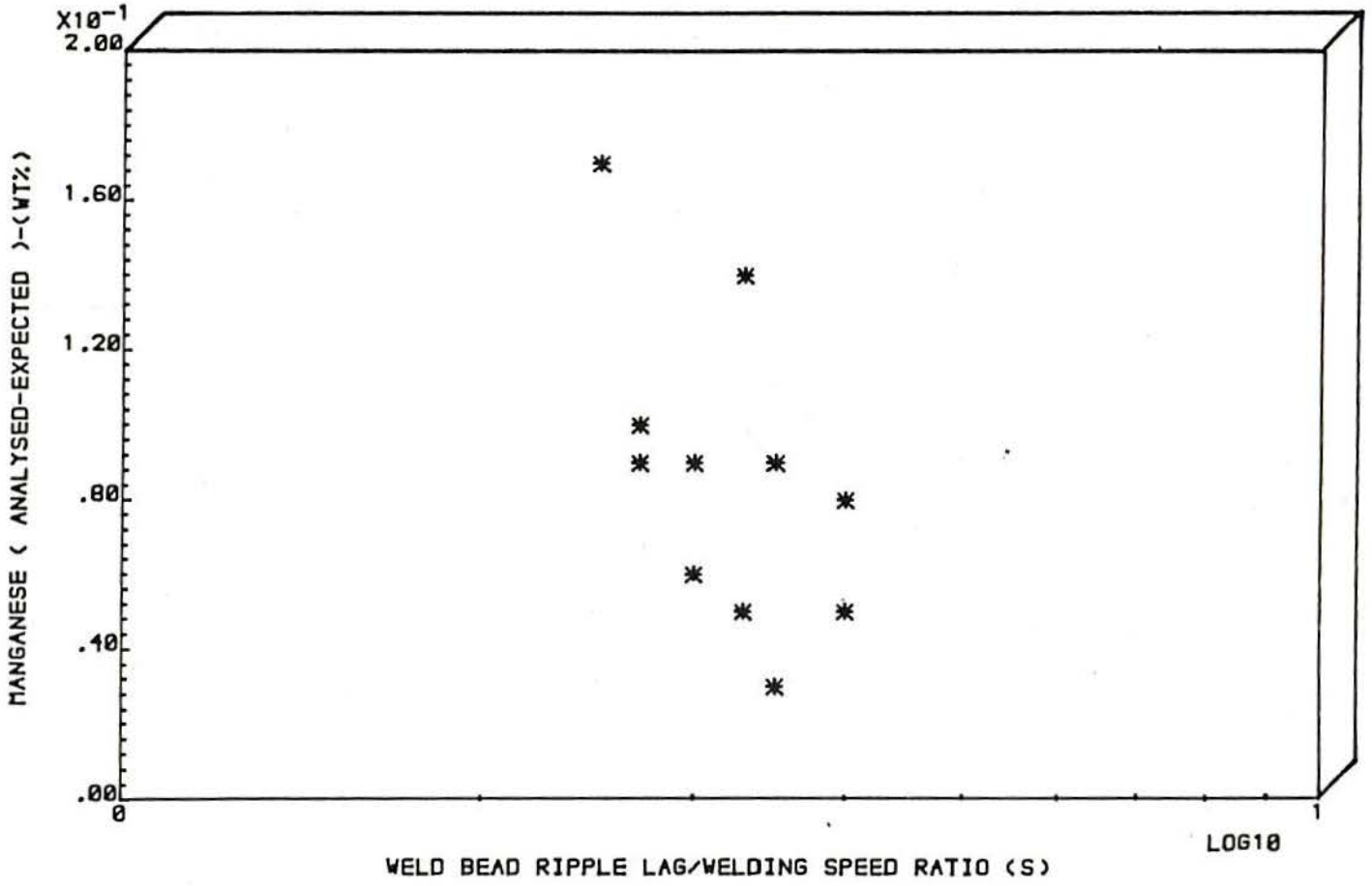

FIGURE 8.16 - RELATIONSHIP BETWEEN WELD POOL REACTION TIME (APPROXIMATE-SEE TEXT) AND MANGANESE DIFFERENCE (OP41TT FLUX)

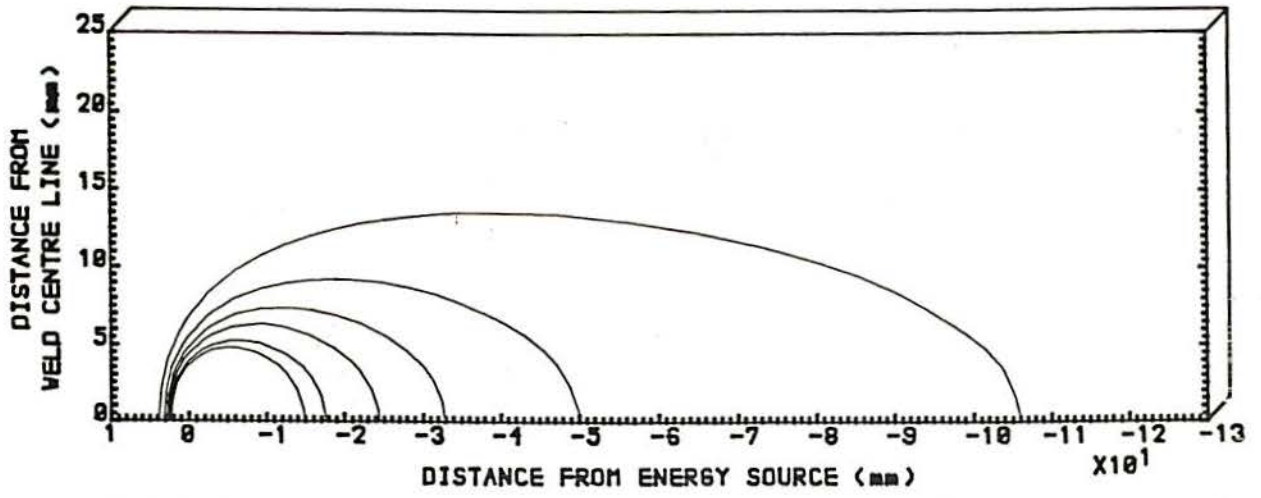

(a)- Welding Parameters: 1.9 KJ/mm , 30 V , 100 A , 6.3 mm/s

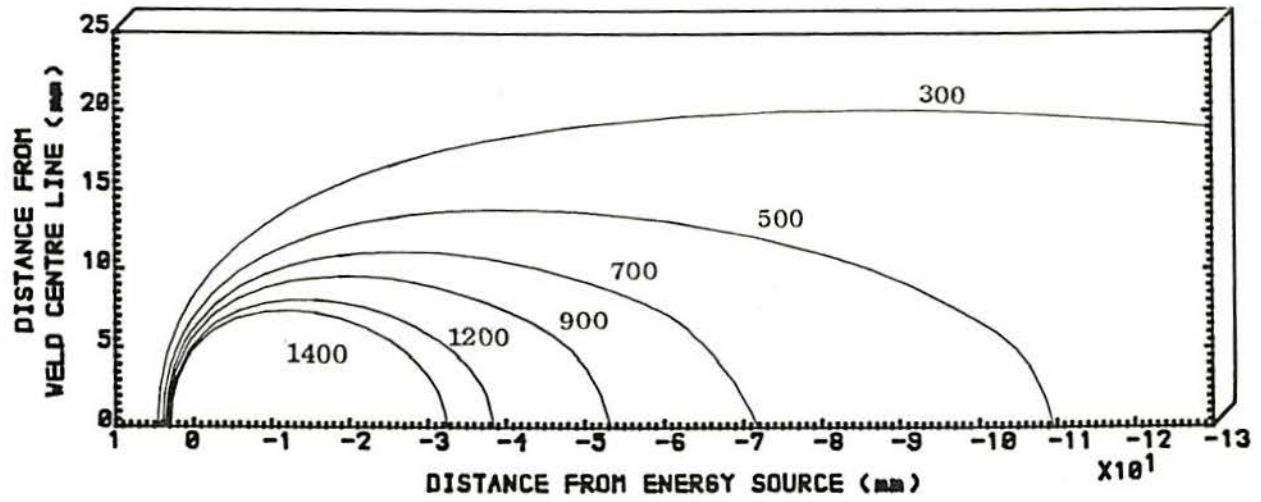

(b)- Welding Parameters: 1.1 KJ/mm , 34 V , 770 A , 6.3 mm/s

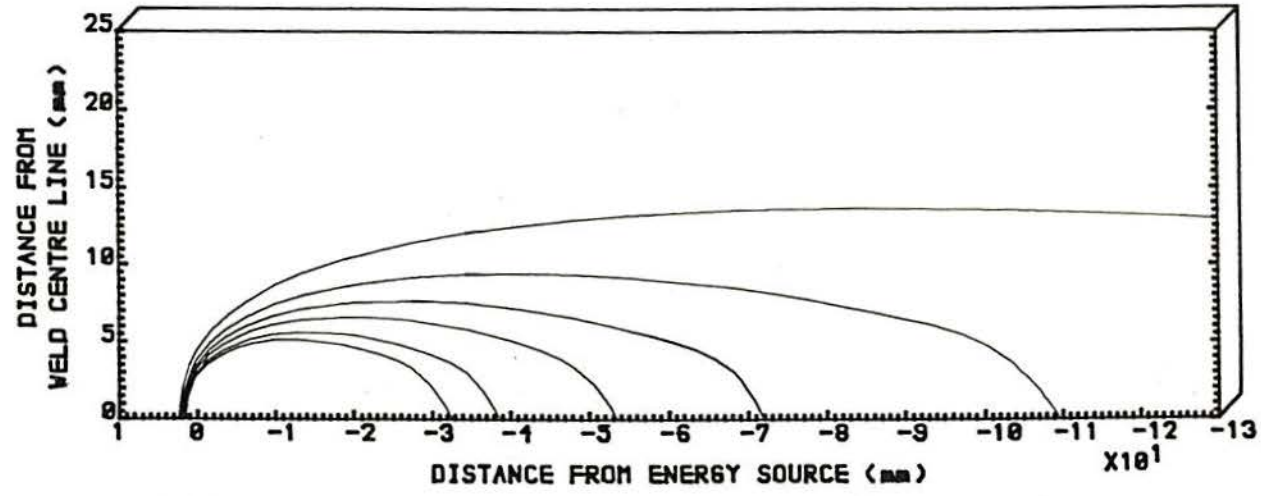

(c)- Welding Parameters: 1.9 KJ/mm , 30 V , 770 A , 13.8 mm/s

FIGURE 8.17 - COMPUTED ISOTHERMIC PATTERN FOR THREE DIFFERENT WELDING CONDITIONS (120 deg C PREHEAT) ON THE X-Y PLANE AND Z=0 (HALF THICKNESS OF A 33mm STEEL PLATE).

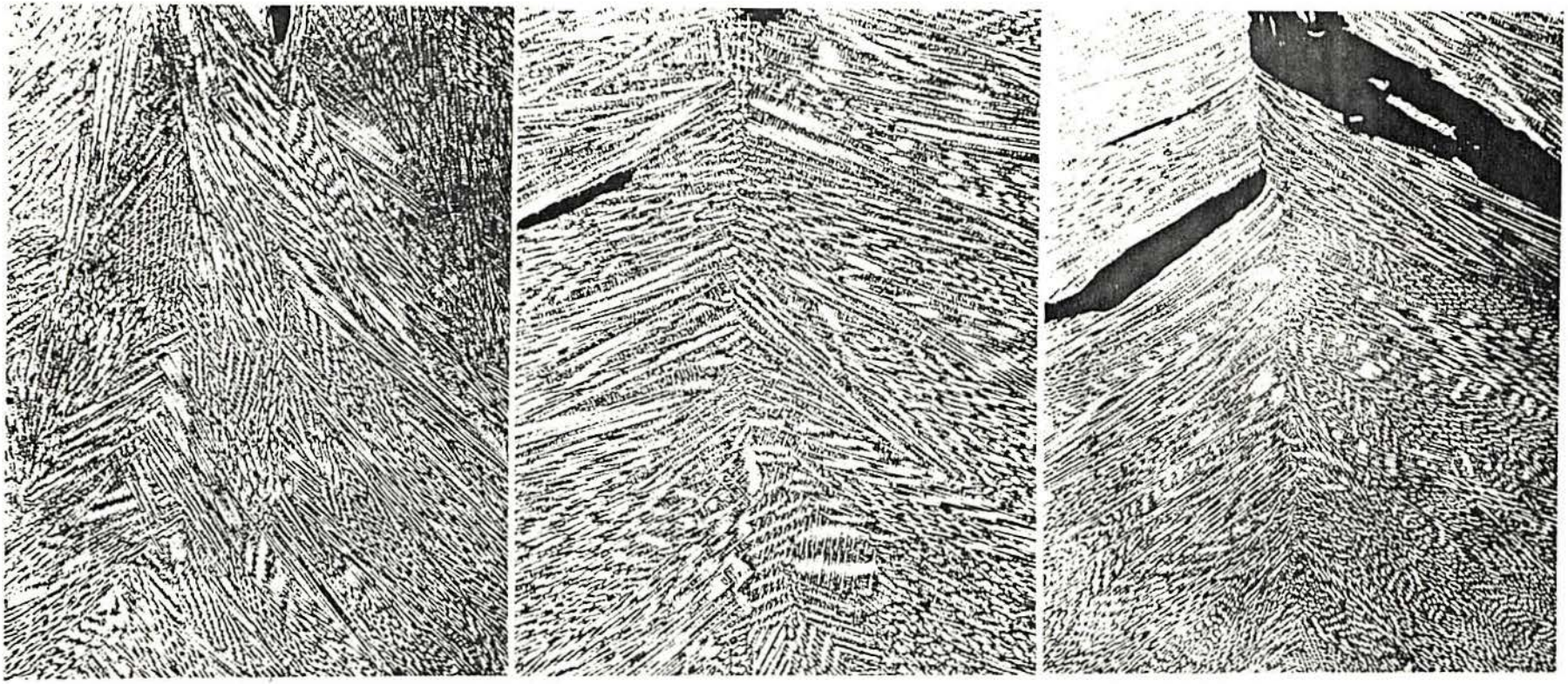

(a) SP.H641L4 (6.3. mm/s, 1.9 KJ/mm). Stray Macrostructure. Some vertically growing dendrites around crack tip.

(b) SP.H674L4 (6.3 mm/s, 4.1 KJ/mm). Competitive columnar macrostructure. Weld centre-line in zigzag. Some equiaxed dendrites just below crack tip.

(c) SP.H1371L4 (13.8 mm/s, 1.9 KJ/mm). Near centre-line macrostructures (holding much of the competitive columnar type). Dendrites meet at weld centre in a better defined line than (b).

FIG. 8.18 Primary (solidification) Macrostructure at Weld Centre-Line Using OP41TT Flux. SASPA, x 25

CL

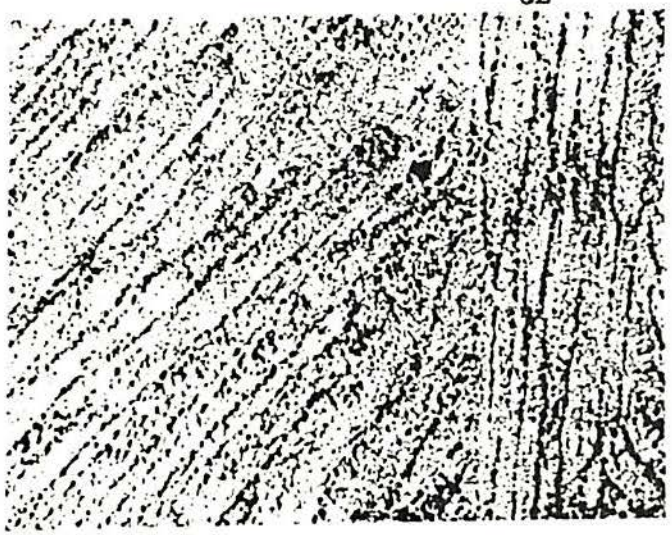

(a) SP.Q641L4
(6.3 mm/s, 1.9 KJ/mm)
Vertically growing dendrites.

CL

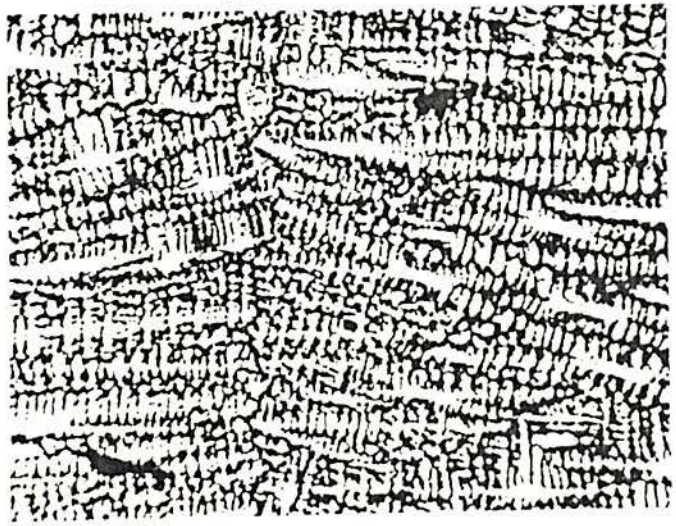

(b) SP.H674L4
(6.3 mm/s, 4.1 KJ/mm)
Zigzag centre-line.

CL

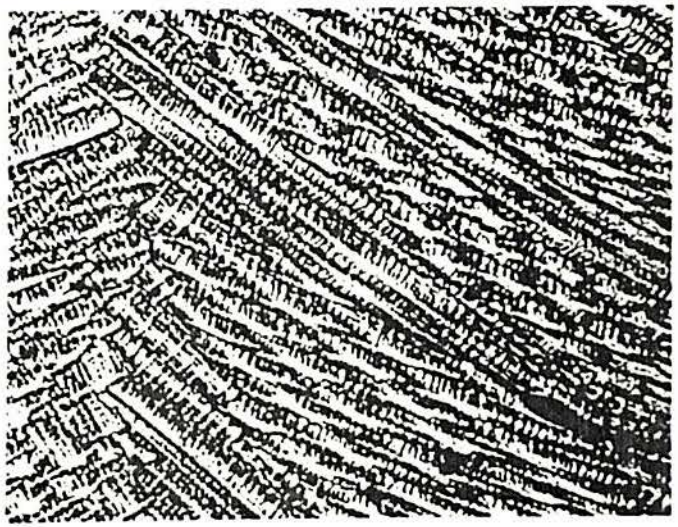

(c) SP.Q1371L4 (13.8 mm/s, 1.8 KJ/mm)
Well defined centre-line, just below centre-line SC crack tip.

FIG. 8.19 Primary macrostructure. Details from weld centre-line (Figs. 8.18 (a-c). SASPA, x 100.

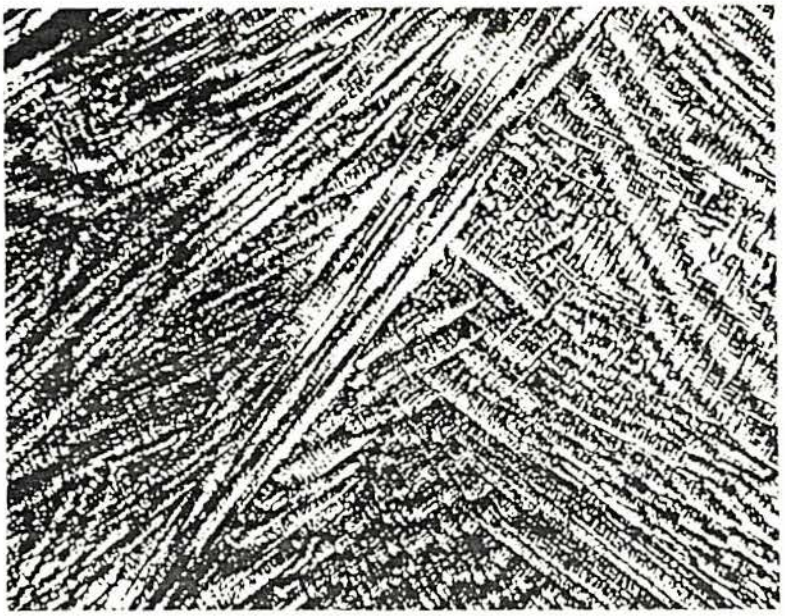

(a) SP.H641L1 (6.3 mm/s, 1.9 KJ/mm). Stray. There are no vertically growing dendrites and no centre-line SC. Transverse cracking is visible.

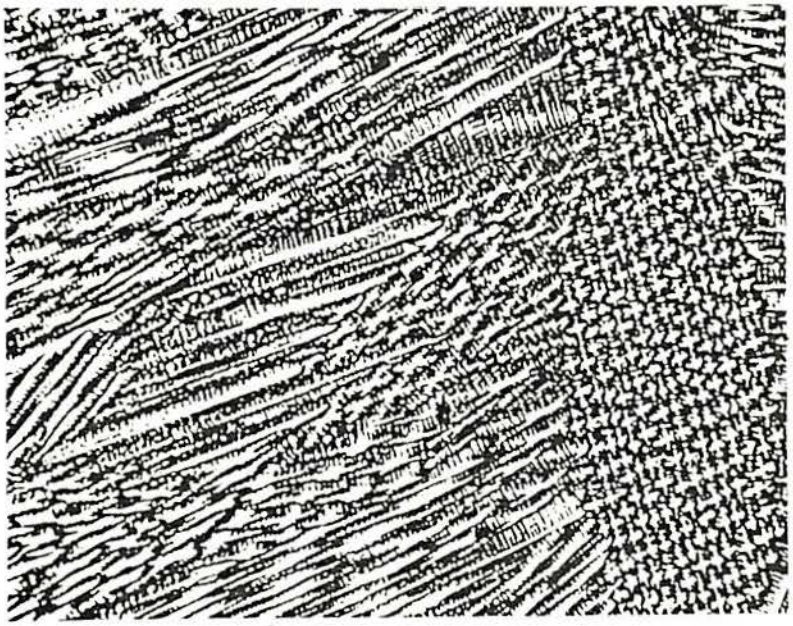

(b) SP.H674L1 (6.3 mm/s. 4.1 KJ/mm). Equiaxed dendrites just below small centre-line SC crack tip.

FIG. 8.20 Primary macrostructure at weld centre-line using OP121TT flux. SASPA, x 50

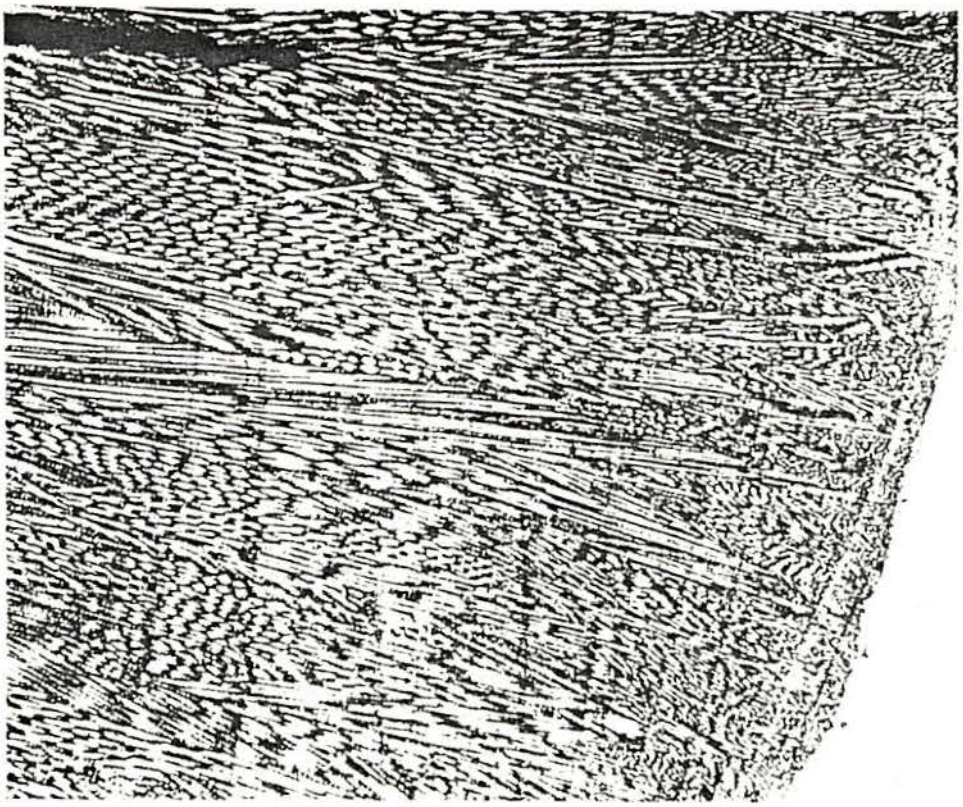

FIG. 8.21- SP.H662L1 (6.3 mm/s, 2.8 KJ/mm). Transverse Cracking Being Apparently Arrested at one Weld Band.

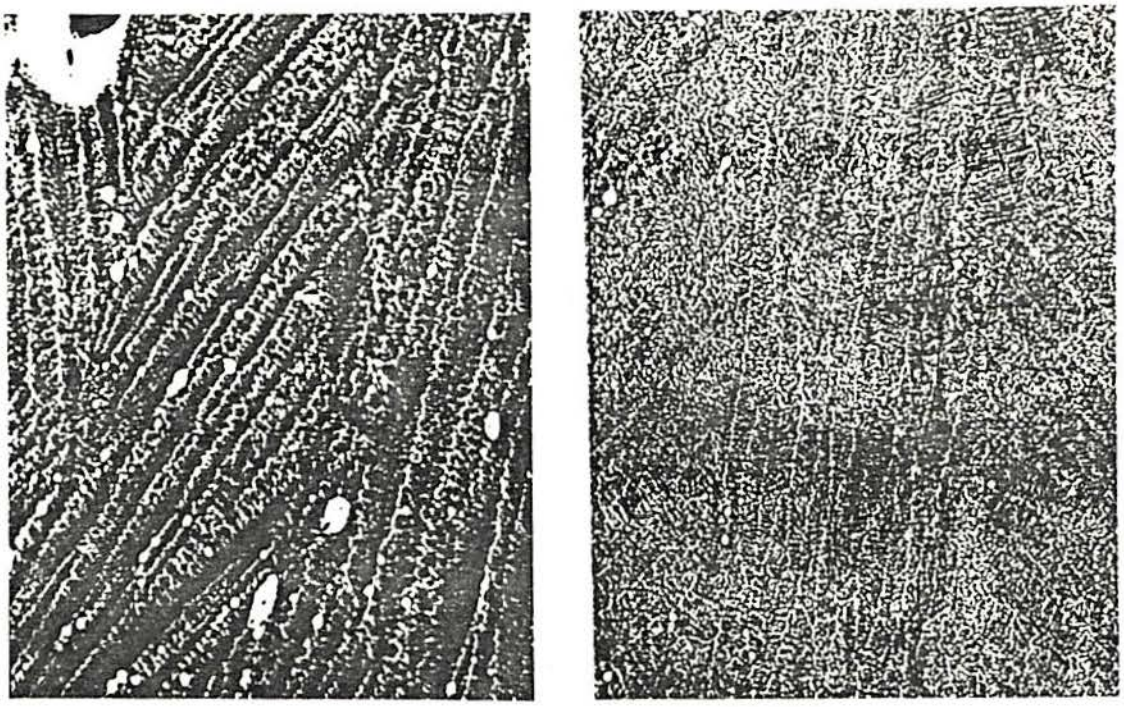

(a) SP.H641L4 (6.3 mm/s, 1.9 KJ/mm) (d) SP.Q641L4. (6.3 mm/s, 1.9 KJ/mm)

FIG. 8.22 -Segregation Lines in Welds on HY10Q (a-c) and Q2N (d-f) Base Metals, using LINDE 95 and OP41TT flux. Ammonium Persulphate, x 100

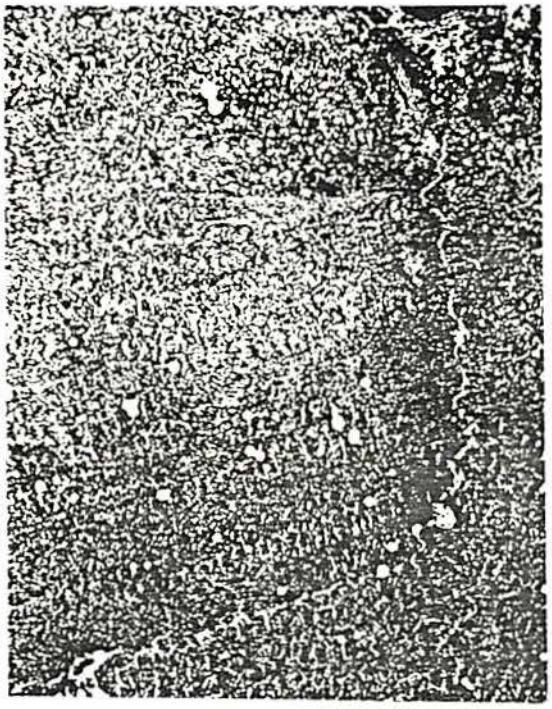

(b) SP.H674L4 (6.3 mm/s, 4.1 KJ/mm)

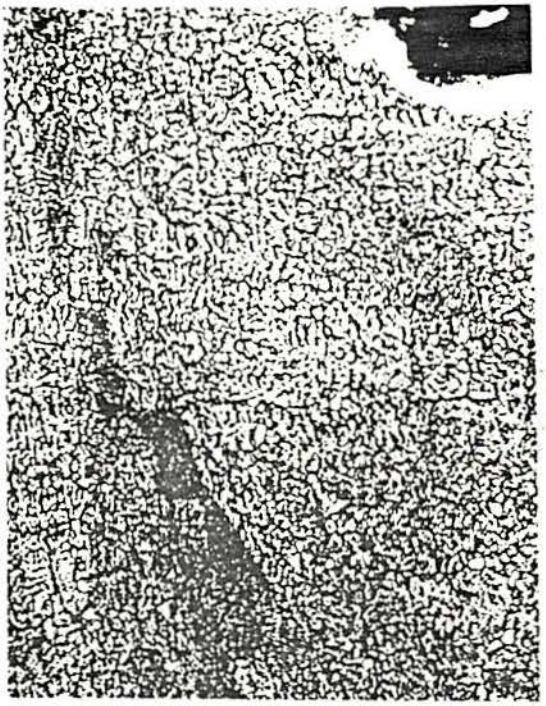

(e) SP.Q674L4 (6.3 mm/s, 4.1 KJ/mm)

(c) SP.H1371L4 (13.8 mm/s, 1.9 KJ/mm)

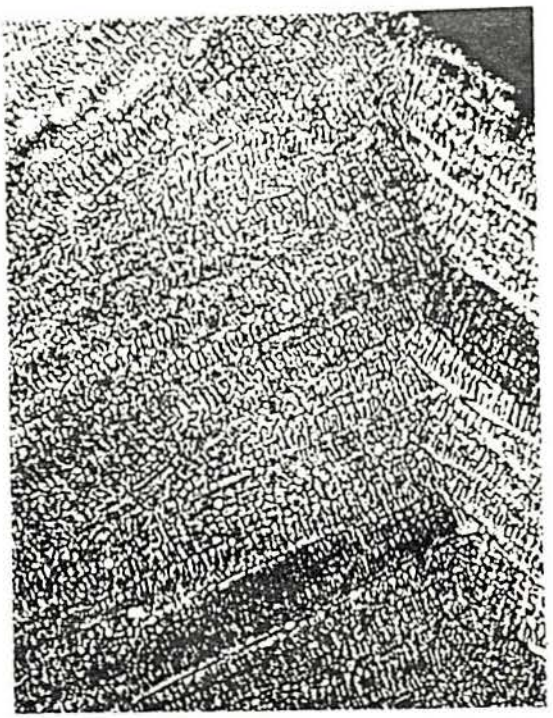

(f) Q1371L4 (13.8 mm/s, 1.9 KJ/mm)

FIG. 8.22 - (cont.)

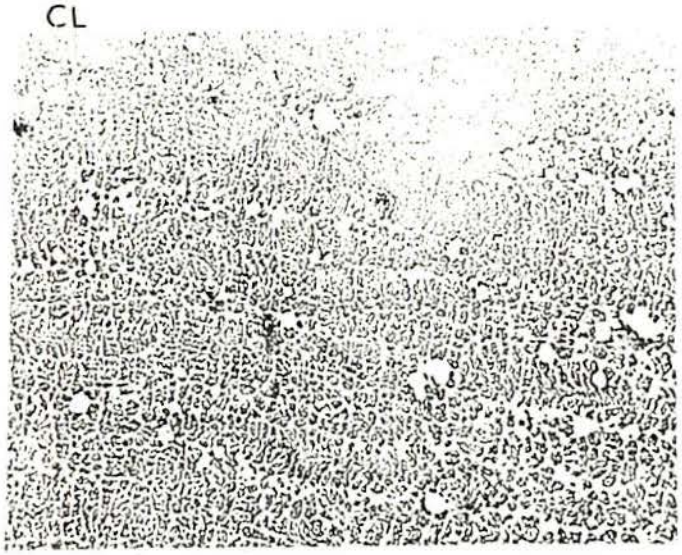

(a) SP.Q674L1. (LINDE 95 Wire, PO121TT flux).

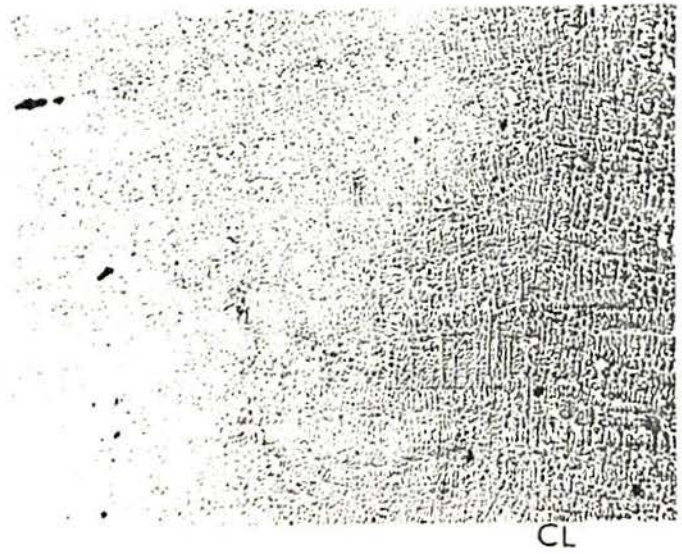

(b) SP.Q674S1 (OERLIKON S3 Wire, OP121TT flux).

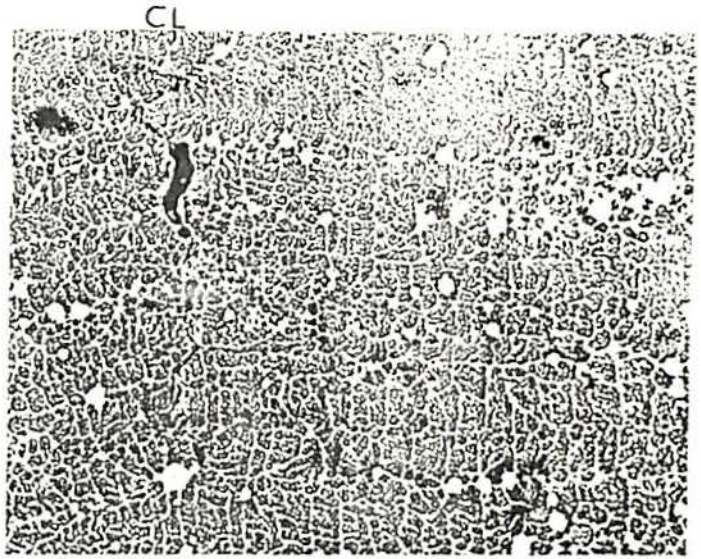

(c) SP.Q674S4 (OERLIKON S3 Wire, OP41TT flux).

FIG. 8.23 - Weld Segregation Lines (6.3 mm/s, 4.1 KJ/mm). Ammonium Persulphate, x 50.

Temperature range (deg C)	Average Cooling Rate (deg C/s)	Average Cooling Time (s)
RT(1000)	--	3.3
1100- 800	-89.12	3.4
800- 500	-21.06	14.1

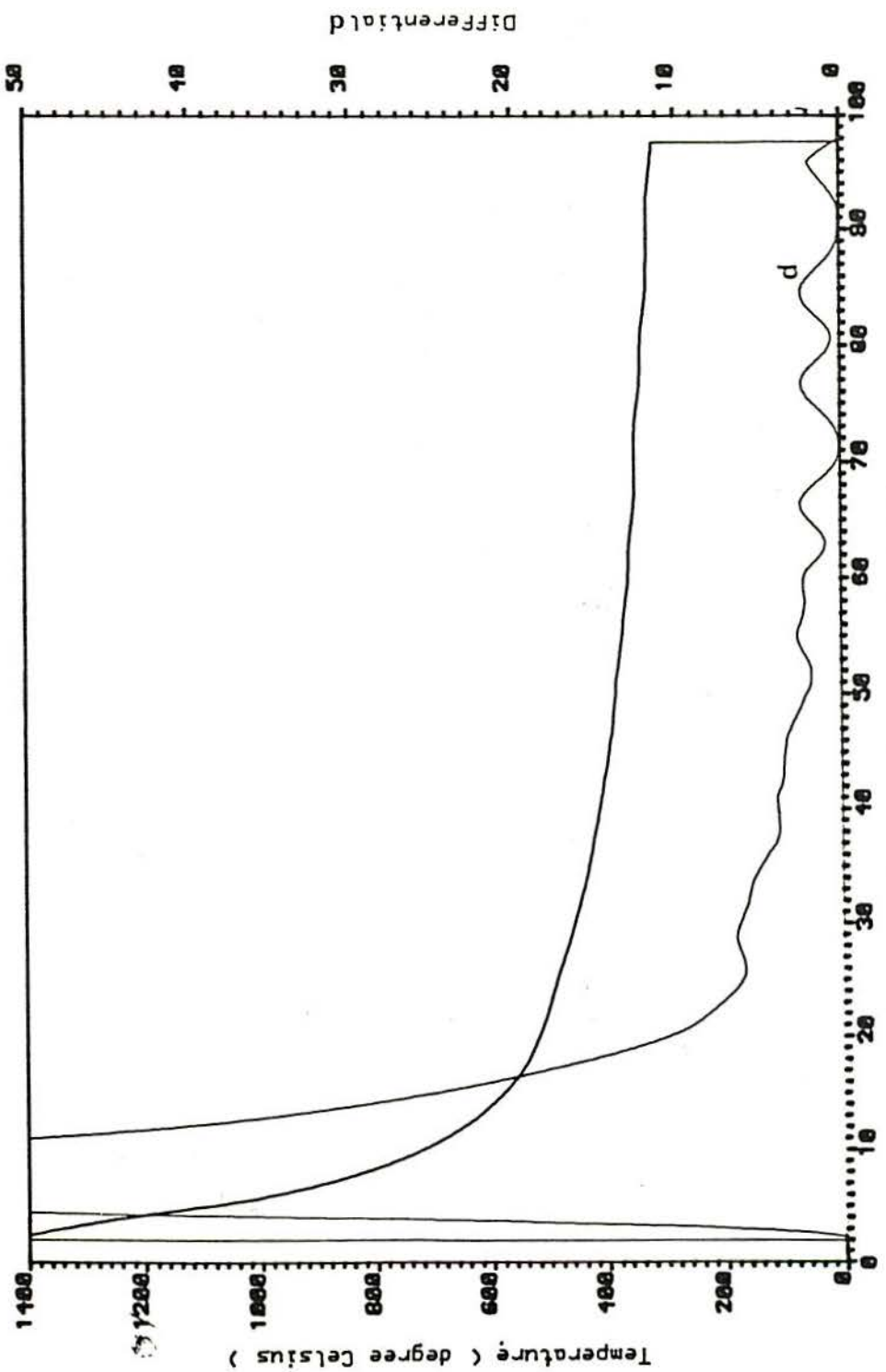

FIGURE 8.24 - WELD METAL THERMAL ANALYSIS - WELDMENT: Q641S1

Temperature range (deg C)	Average Cooling Rate (deg C/s)	Average Cooling Time (s)
RT(1000)	--	1.5
1100- 800	-15.78	6.4
800- 500	-11.07	27.1

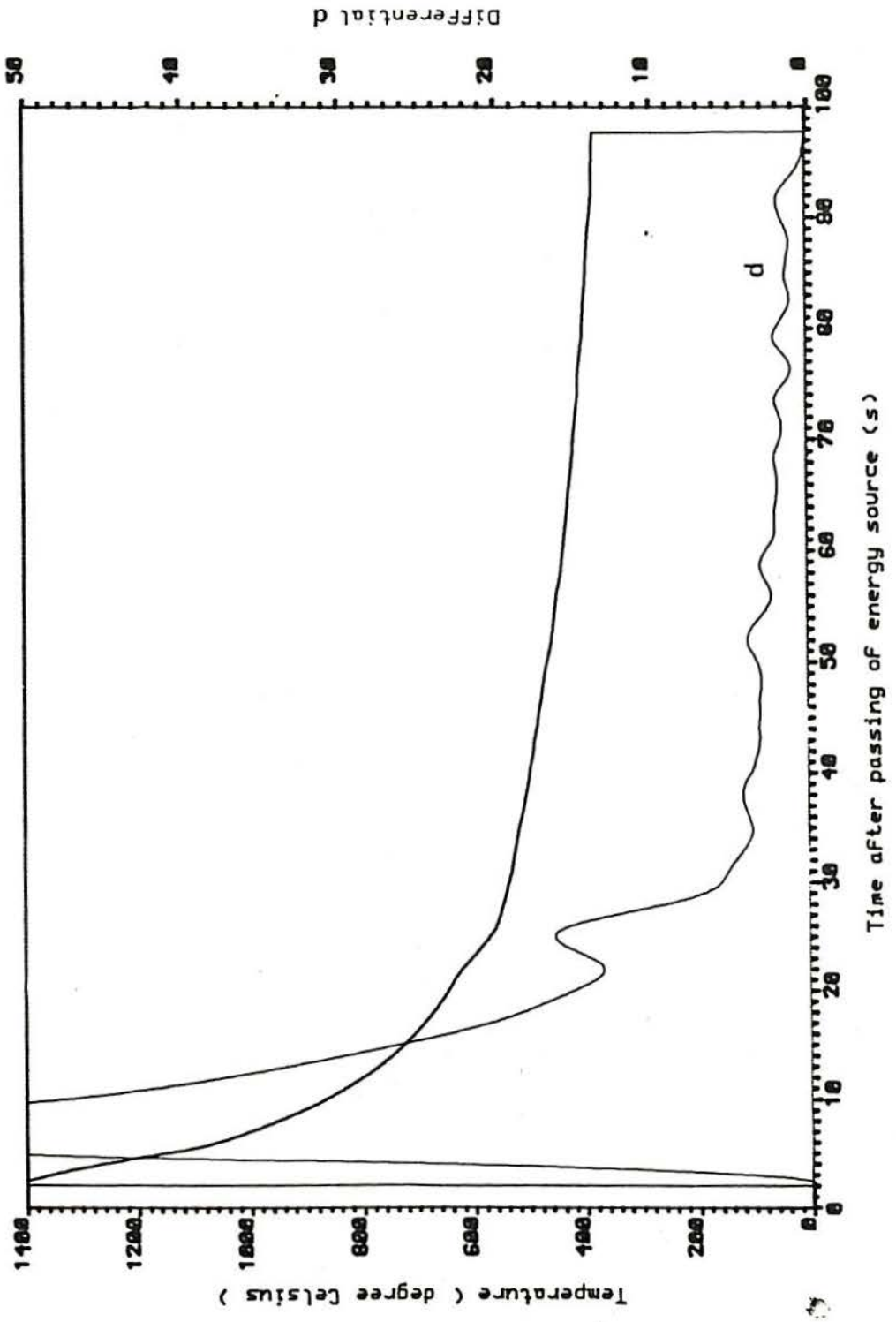

FIGURE 8.25 - WELD METAL THERMAL ANALYSIS - WELDMENT: H662S4

Temperature range (deg C)	Average Cooling Rate (deg C/s)	Average Cooling Time (s)
RT(1000)	--	7.9
1100- 800	-27.94	10.7
800- 500	-6.06	49.5

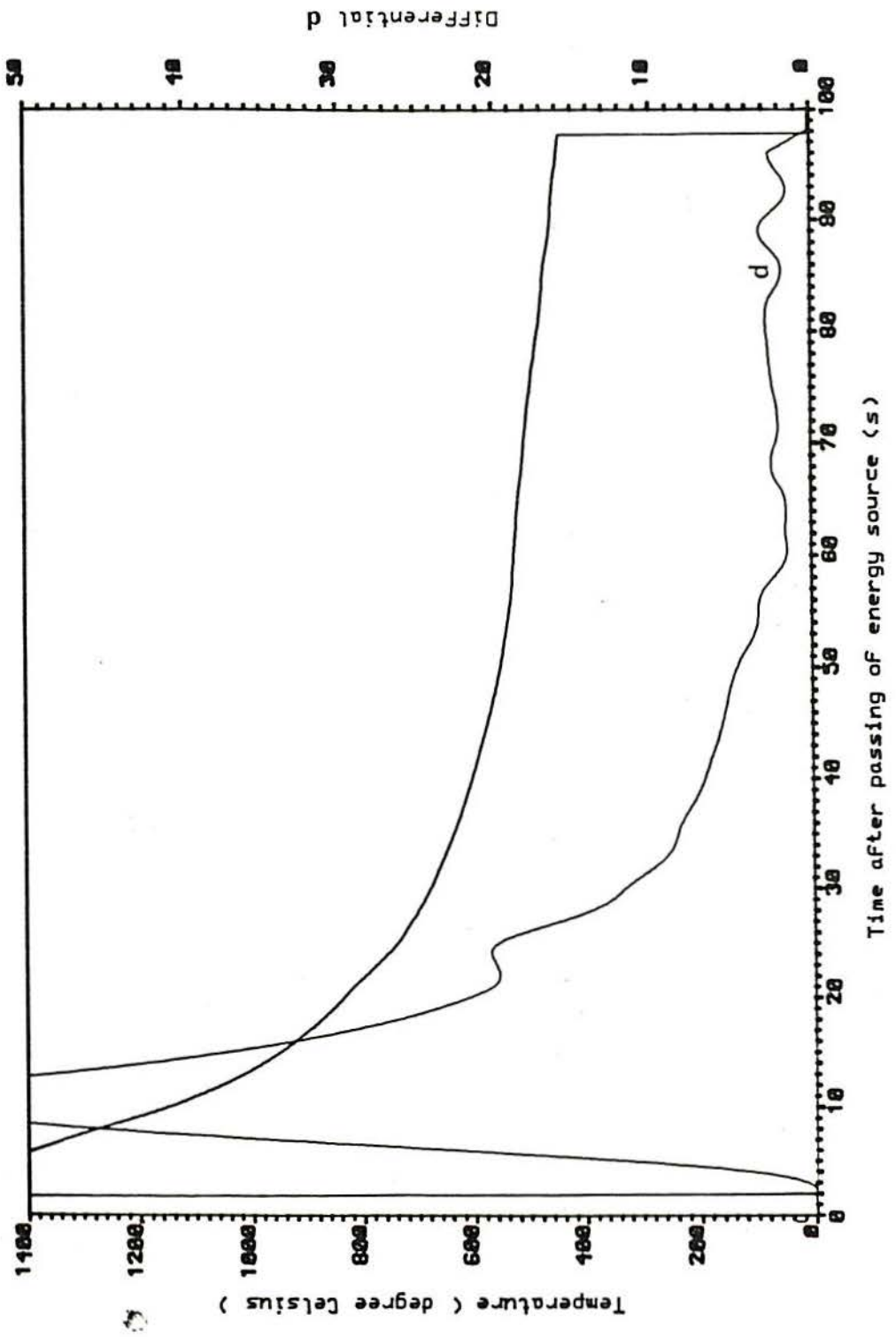

FIGURE 8.26 - WELD METAL THERMAL ANALYSIS - WELDMENT: Q674S1

Temperature range (deg C)	Average Cooling Rate (deg C/s)	Average Cooling Time (s)
RT(1000)	--	3.8
1100- 800	-65.33	4.5
800- 500	-12.21	24.4

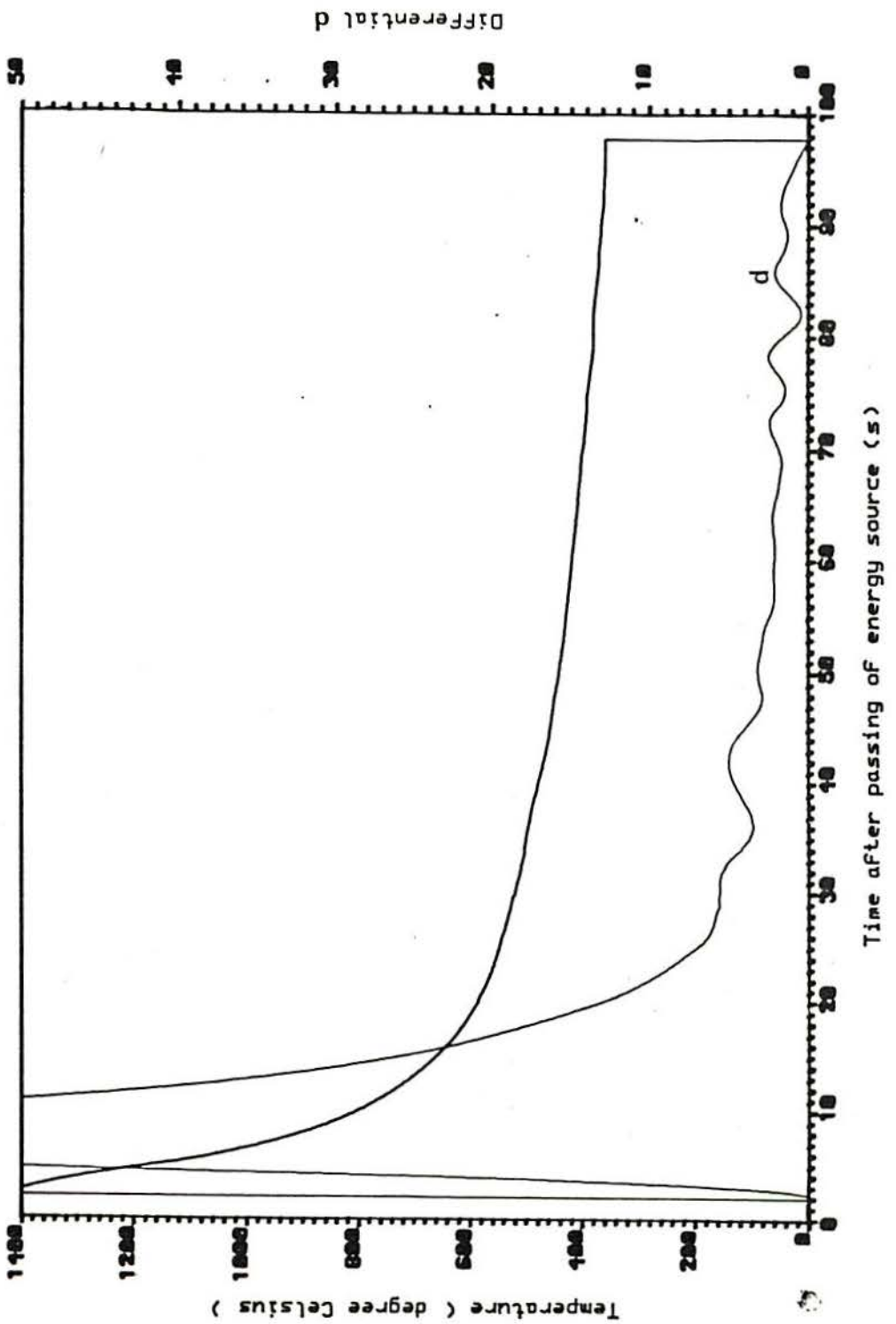

FIGURE 8.27 - WELD METAL THERMAL ANALYSIS - WELDMENT: Q972L4

Temperature range (deg C)	Average Cooling Rate (deg C/s)	Average Cooling Time (s)
RT(1000)	--	3.8
1100- 800	-72.20	4.1
800- 500	-19.80	15.1

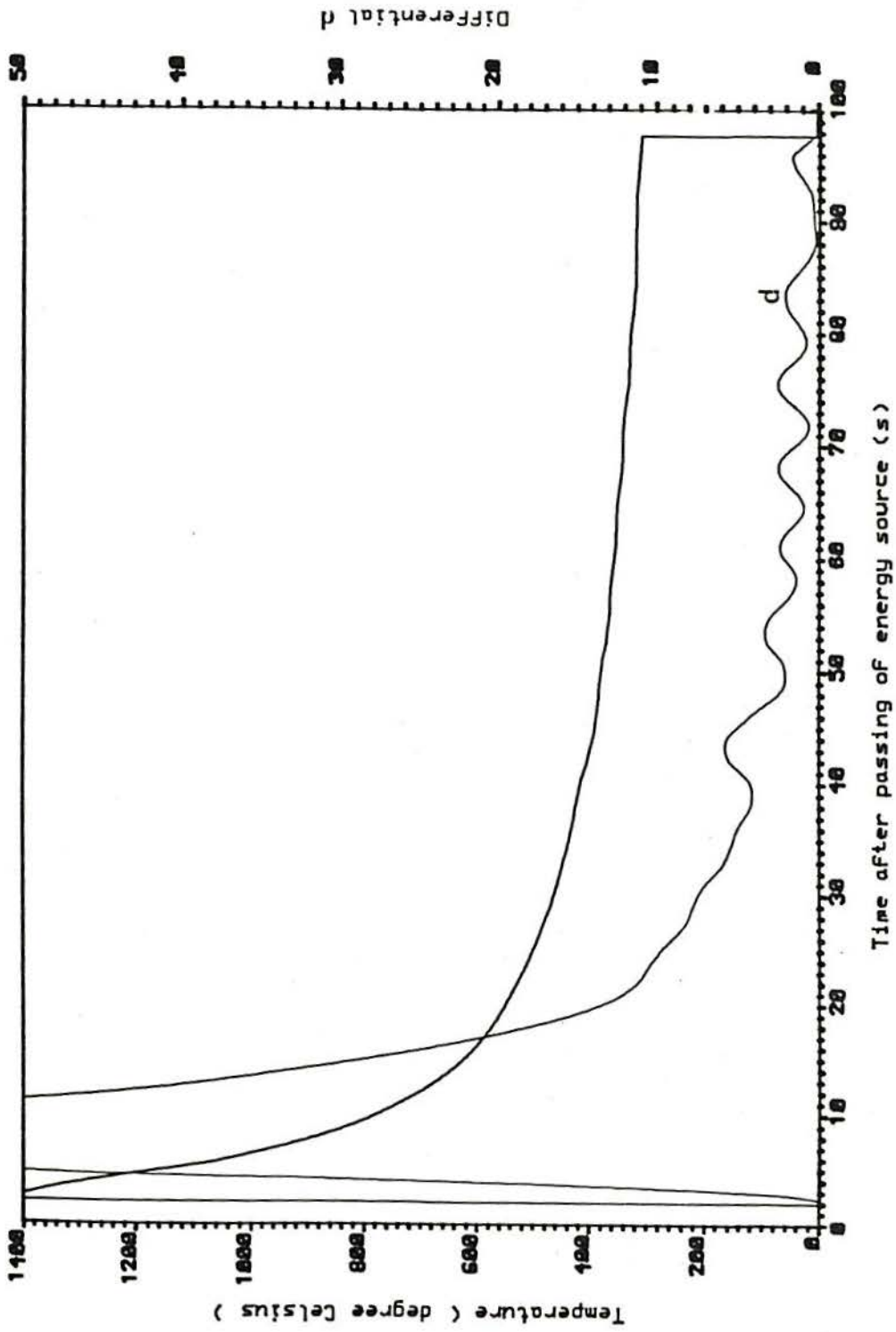

FIGURE 8.28 - WELD METAL THERMAL ANALYSIS - WELDMENT: H961L4

Temperature range (deg C)	Average Cooling Rate (deg C/s)	Average Cooling Time (s)
RT(1000)	--	3.1
1100- 800	-91.21	3.3
800- 500	-22.85	13.0

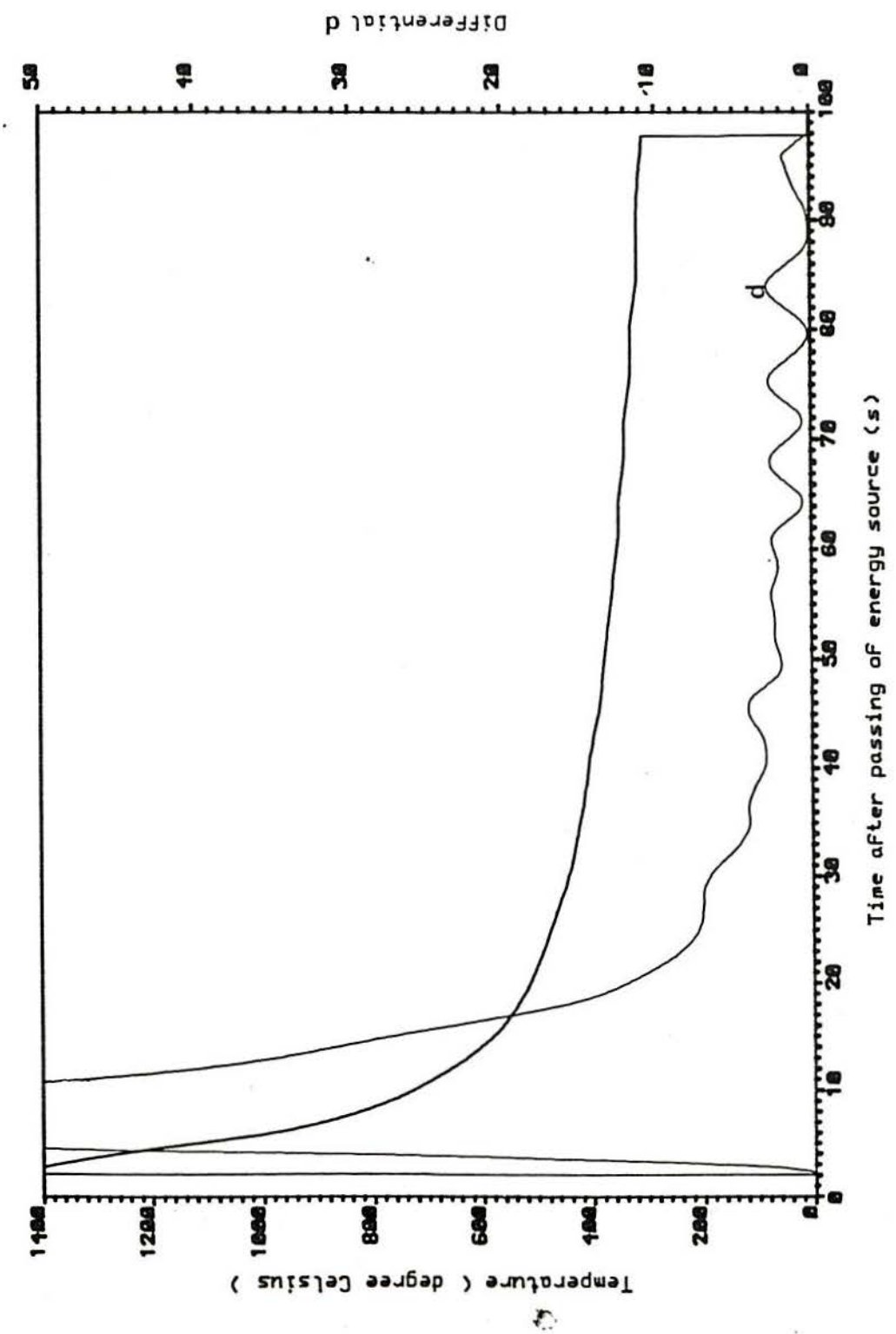

FIGURE 8.29 - WELD METAL THERMAL ANALYSIS - WELDMENT: H1371S4

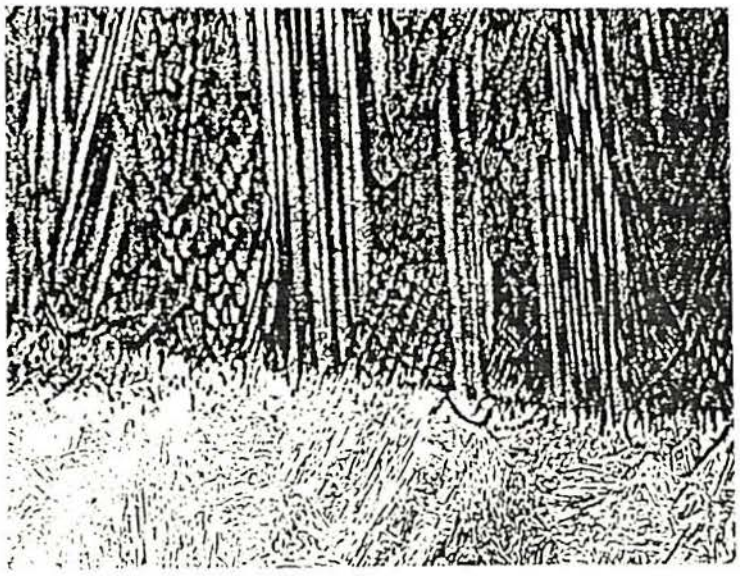

FIG. 8.30(a)- Dendrite Growing Into Weld Metal from the HAZ. Notice the Dependence on Base Metal Grain Size. Specimen Q662L4 (2.8 KJ/mm). SASPA, x100.

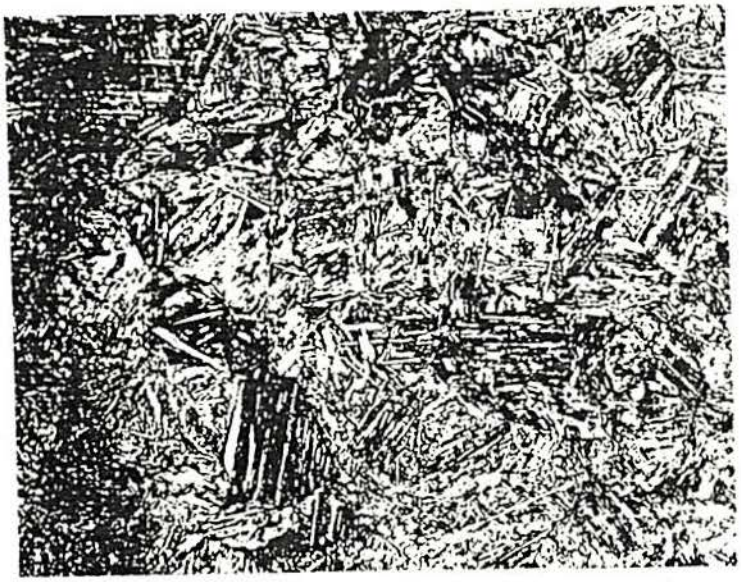

FIG. 8.30(b)- Martensitic Microstructure in the Bay Region. Specimen Q674L1 (4.1 KJ/mm). Ammonium Persulphate + Nital, x100

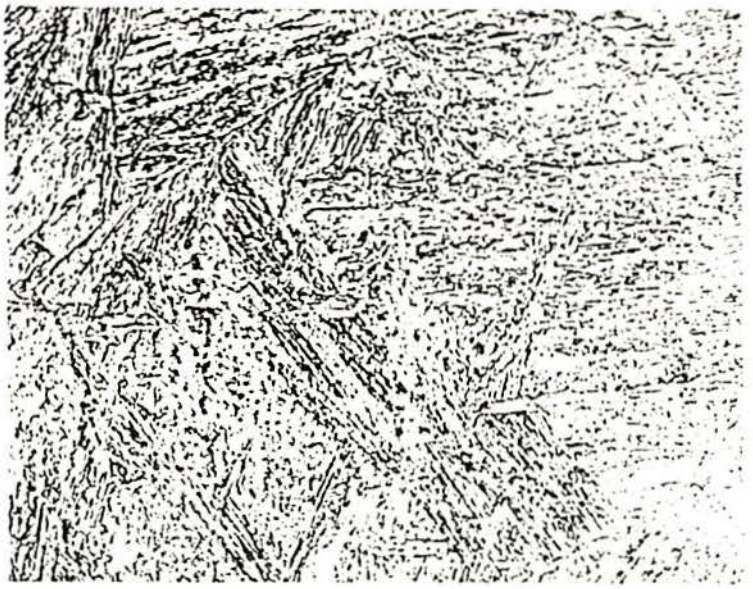

FIG. 8.30(c)- Detail of Coarse HAZ for 4.1 KJ/mm. Specimen Q674L1. Nital, x 500

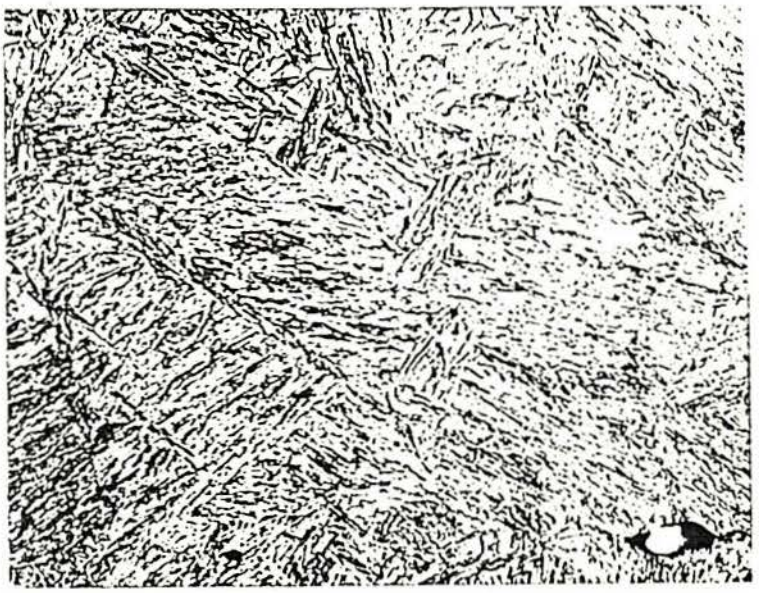

FIG. 8.30(d)- Detail of Coarse HAZ for 4.1 KJ/mm. Specimen H674L1. Nital, x 500

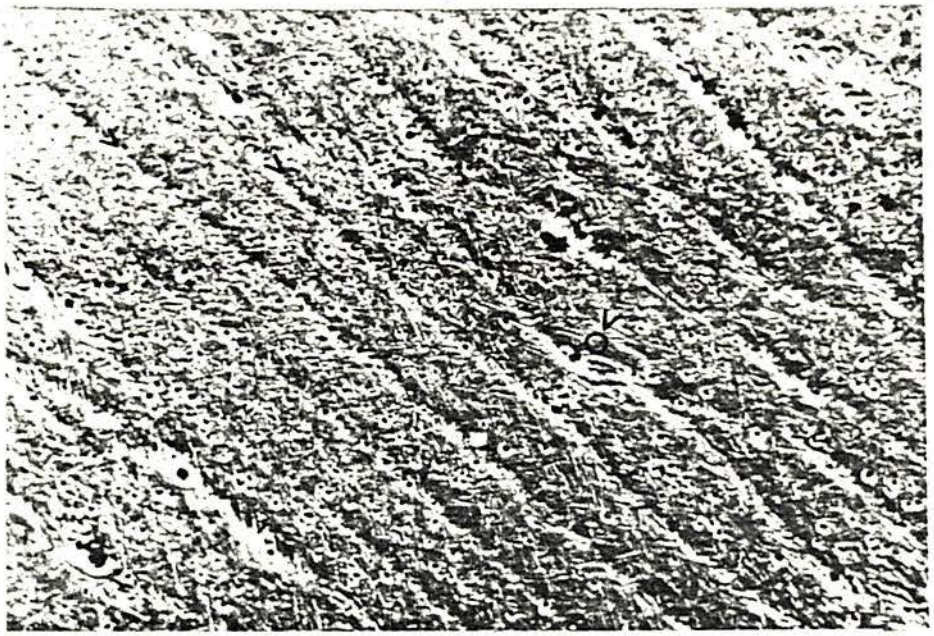

(a) Position Arrowed Corresponds to that in (b). X 1K.

(b) X 5K.

FIG. 8.31 Delta Ferrite (DF) and Secondary Microstructure. SEM, Nital+SASPA.

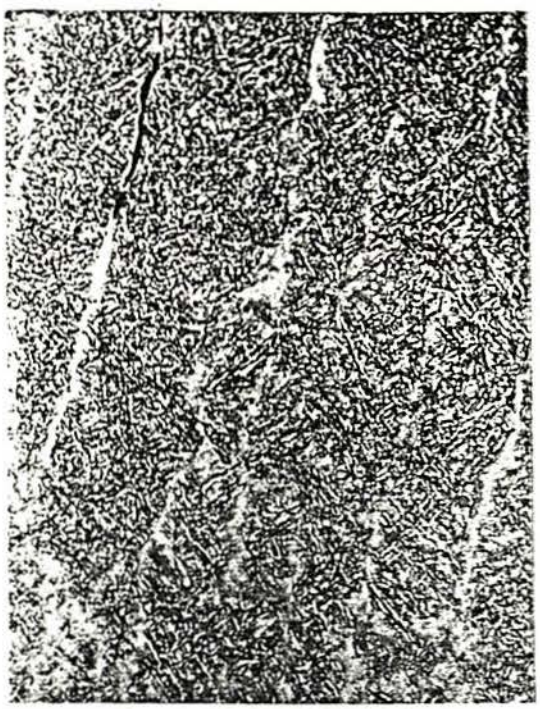

(a) SP.Q674S1, 4.1 KJ/mm

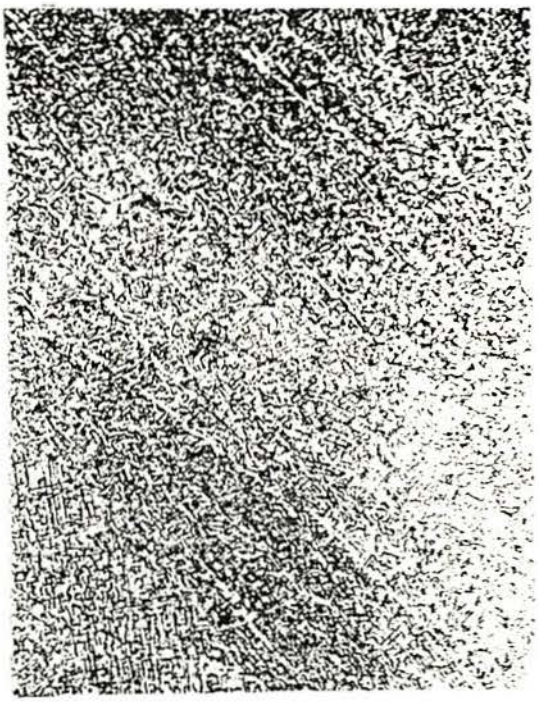

(b) SP.Q641S1, 1.9 KJ/mm

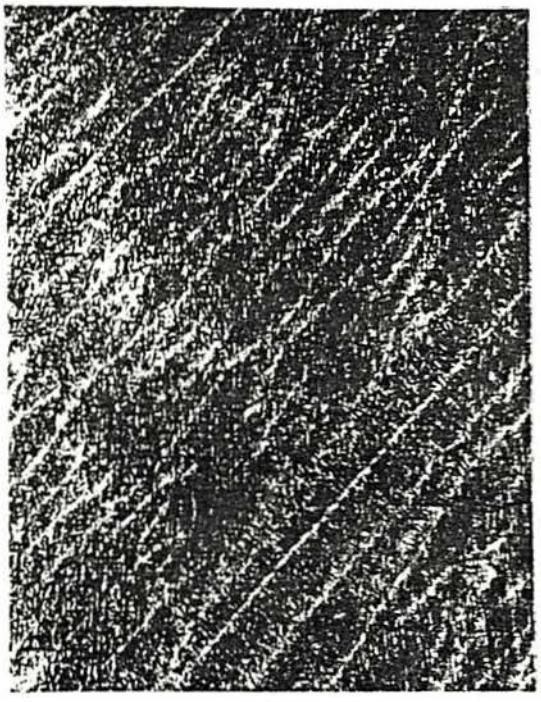

(c) SP.Q641L1, 1.9 KJ/mm

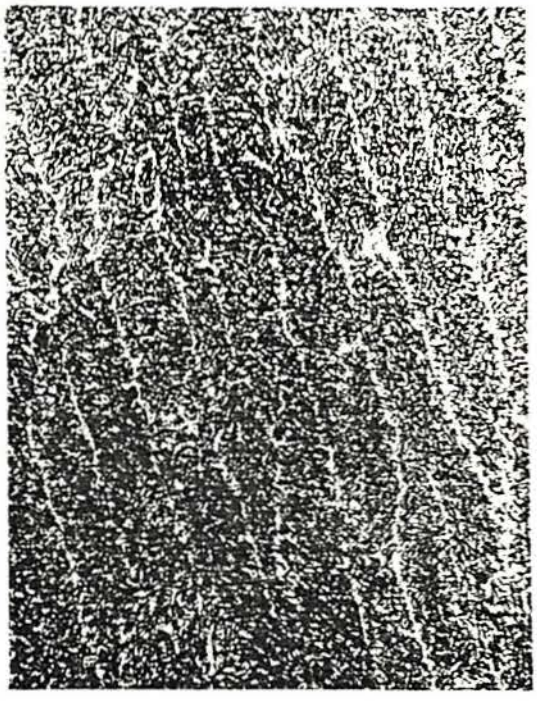

(d) SP.Q641L4, 1.9 KJ/mm

FIG. 8.32 Weld Metal Columnar Secondary Microstructure. Nital, x 200

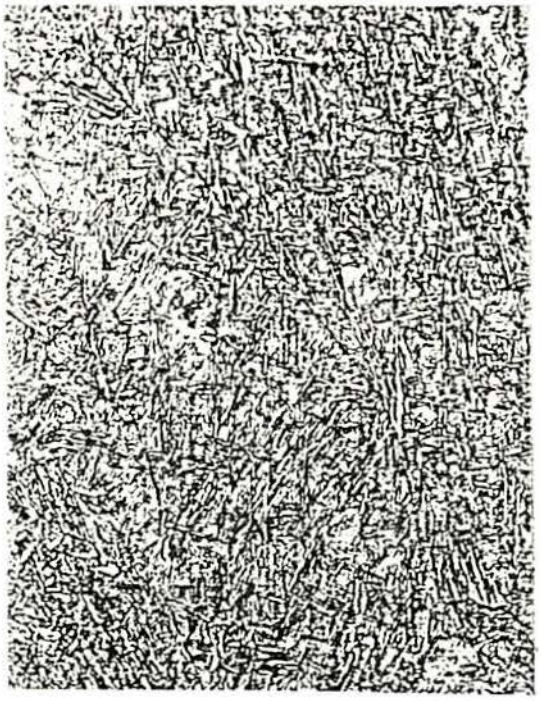

(a) SP.Q641L4, Nital, x 500

(b) SP.H641L1, Nital, x 500

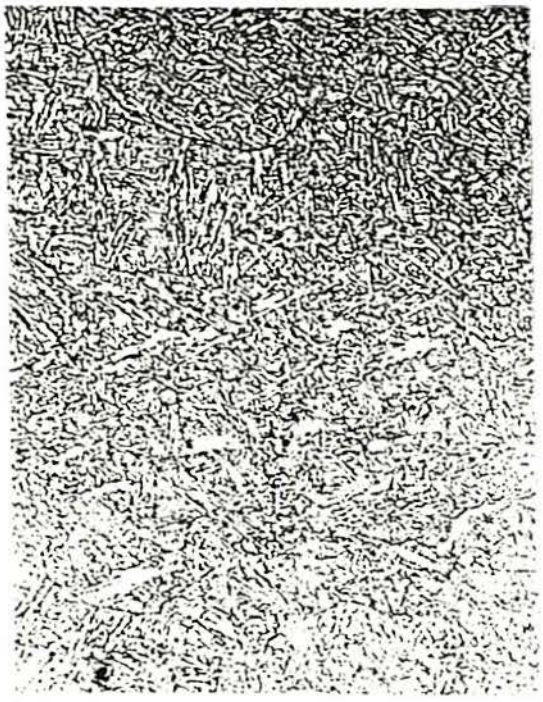

(c) SP.Q641S1, Nital, x 500

(d) SP.H641L1, Nital, x 1000

FIG.8.33 Weld Metal Secondary Microstructure of 1.9 KJ/mm Energy Input Welds.

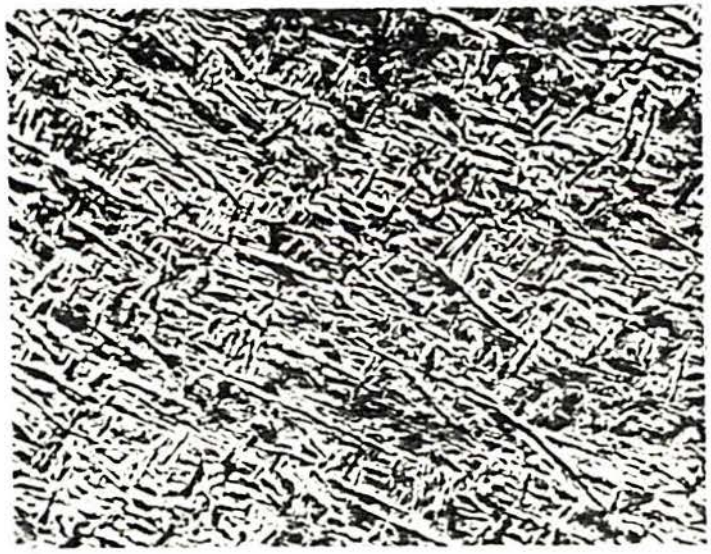

(a) SP.H641L4. SEM, x 2000

(b) SP.H641L4. SEM, x 5000

FIG. 8.34 - Weld Metal Secondary Microstructure of 1.9 KJ/mm Energy Input Welds. Nital.

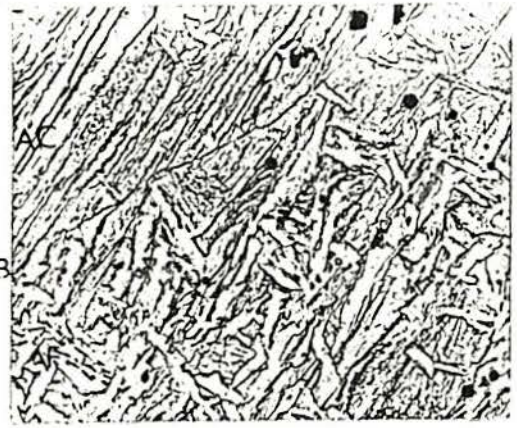

(c) SP.H641L1. TEM, x 2000

(d) SP.Q641L1. TEM x 4000

(e) SP.Q641L1. TEM x 5000

(f) SP.Q641L4. TEM, x 4000

(g) SP.Q641L4. TEM x 7000

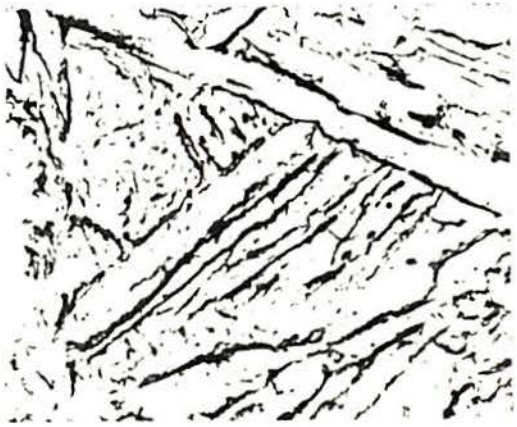

(h) SP.Q641L1. TEM x 8000

FIG.8.34 (cont.) -

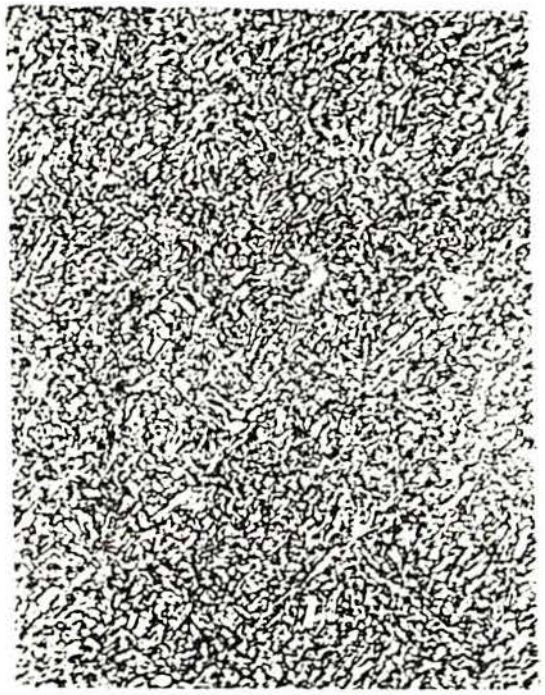

(a) SP.Q674L4. Nital, x 500

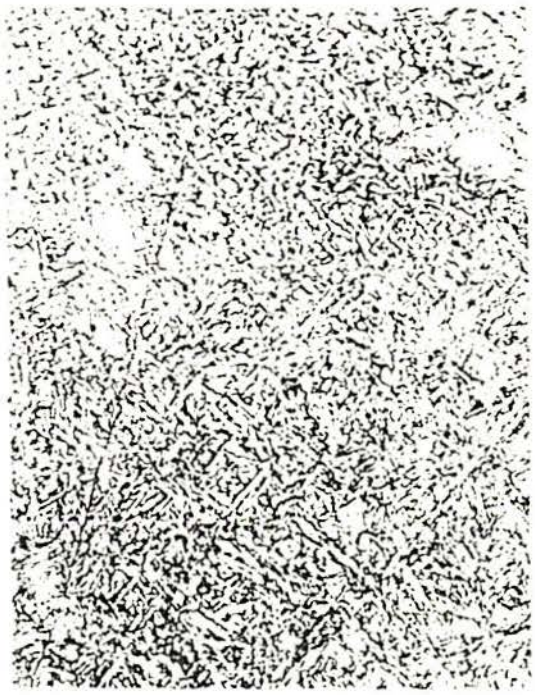

(b) SP.H674L1. Nital, x 500

(c) SP.Q674S1. Nital, x 500

(d) SP.H674L4. Nital + Sodium Bisulfite, x 1000

FIG.8.35 - Weld Metal Secondary Microstructure of 4.1 KJ/mm Energy Input Welds.

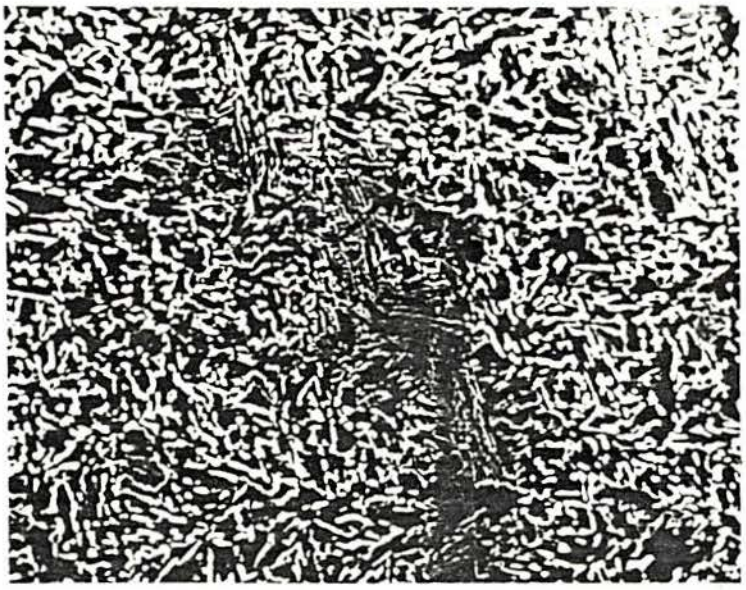

(a) SP.Q674L4. SEM, x 2000

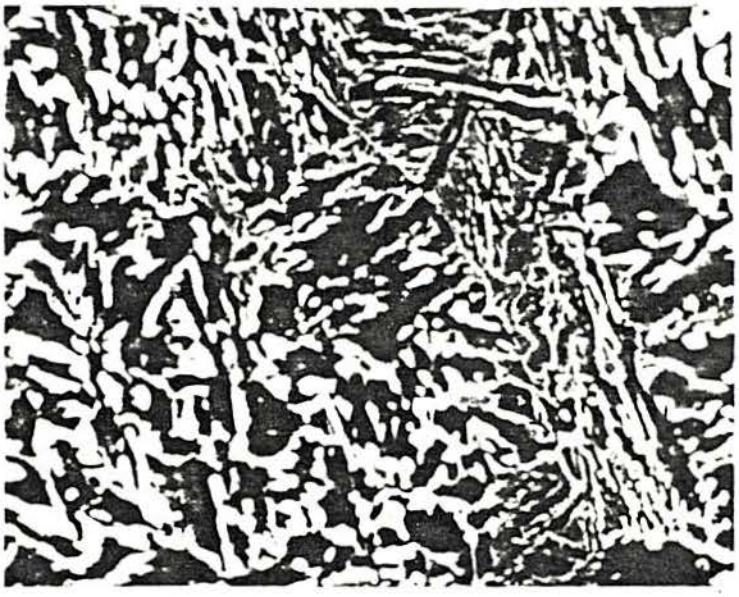

(b) SP.Q674L4. SEM, x 5000

FIG. 8.36 - Weld Metal Secondary Microstructure of 4.1 KJ/mm Energy Input Welds. Nital.

(c) SP.H674L4. TEM, x 4000

(d) SP.Q674L4. TEM, x 7200

(e) SP.Q674L1. TEM, x 4000

(f) SP.Q674L1. TEM x 7000

(g) SP.Q674L1. TEM, x 4000

FIG. 8.36 - (cont.).

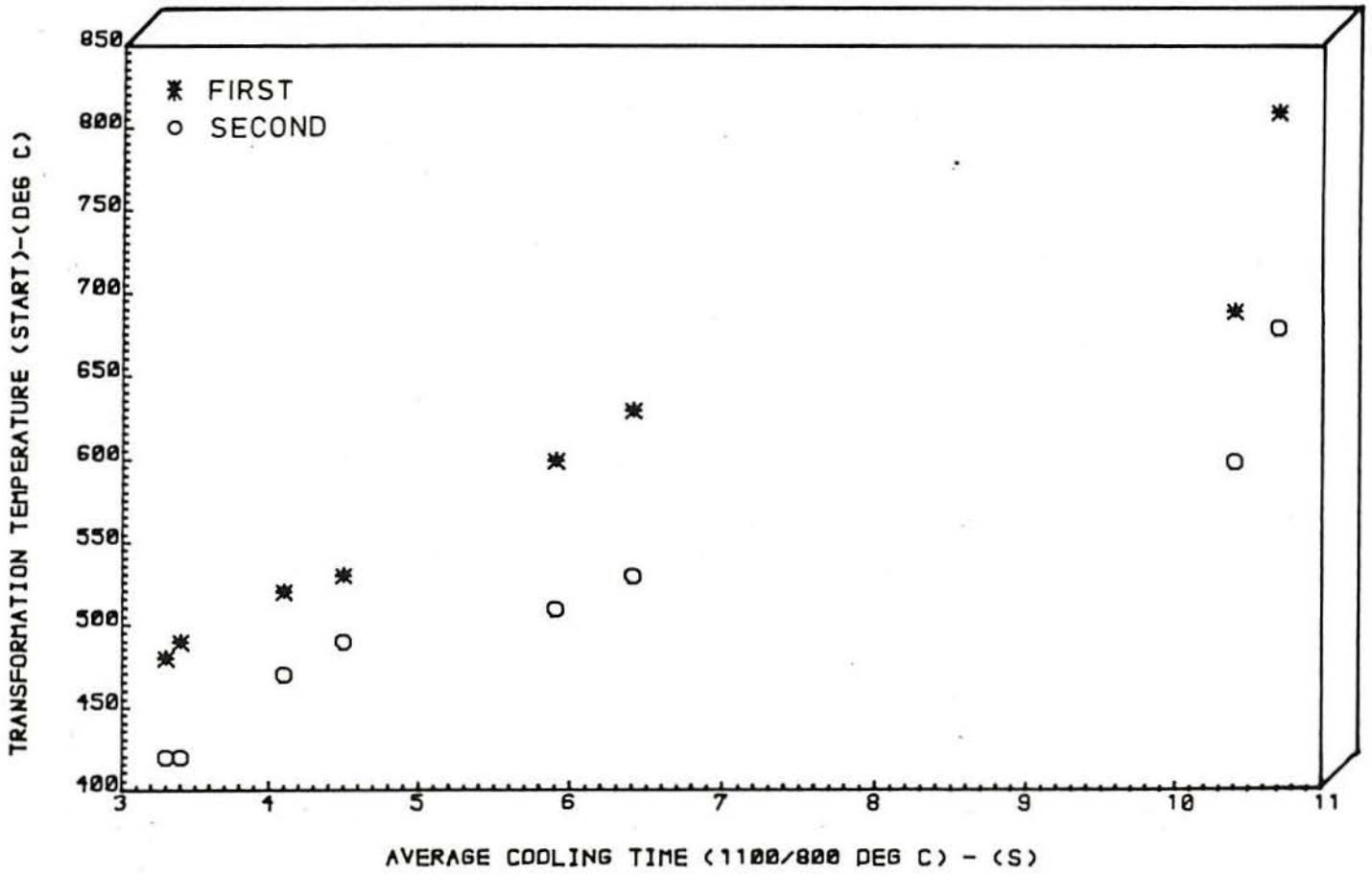

FIGURE 8.37 - RELATIONSHIP BETWEEN FIRST AND SECOND TRANSFORMATION TEMPERATURES (START), AND COOLING TIME (1100/800 DEG C)

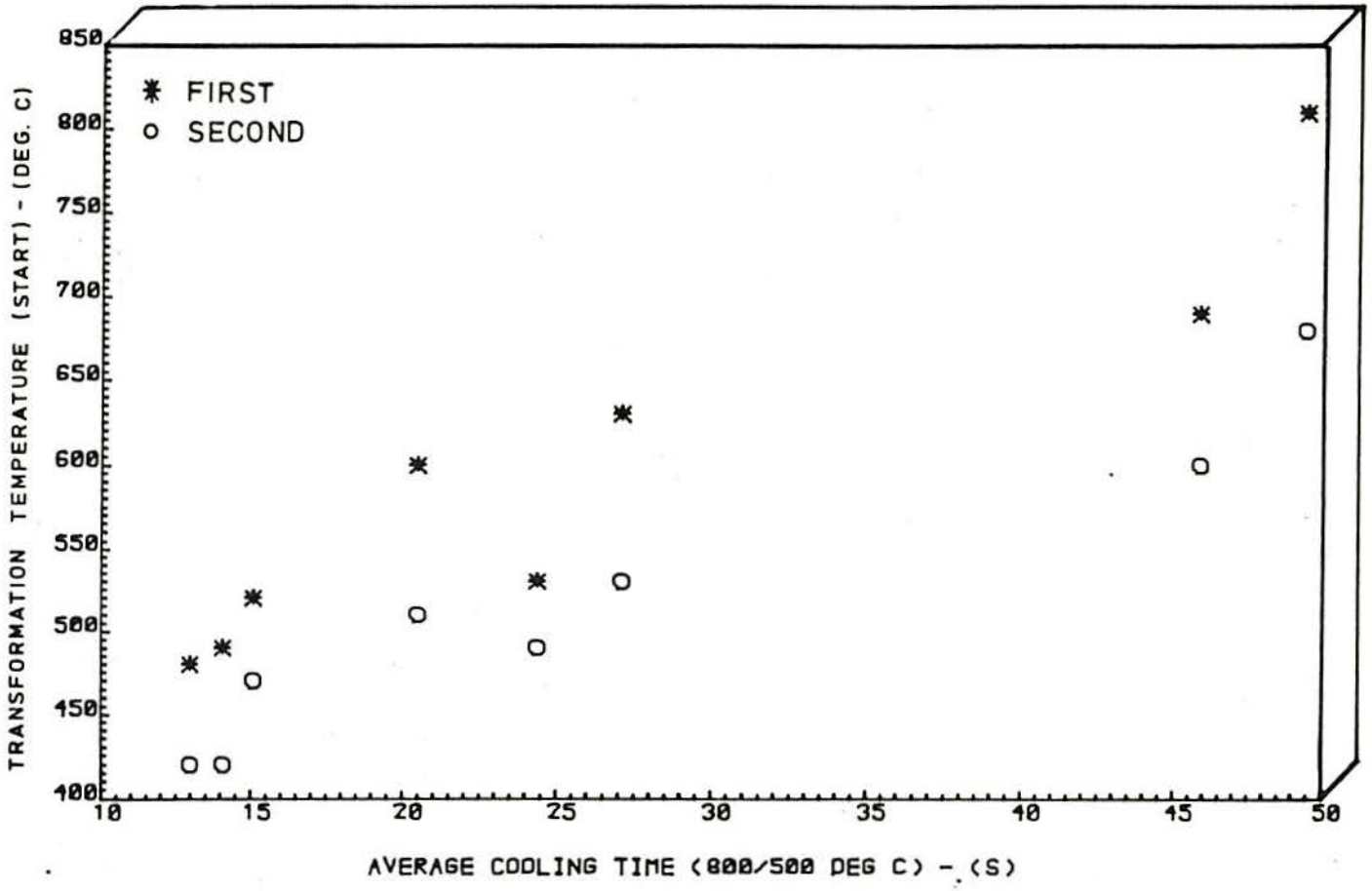

FIGURE 8.38 - RELATIONSHIP BETWEEN FIRST AND SECOND TRANSFORMATION TEMPERATURES (START), AND COOLING TIME (800/500 DEG C)

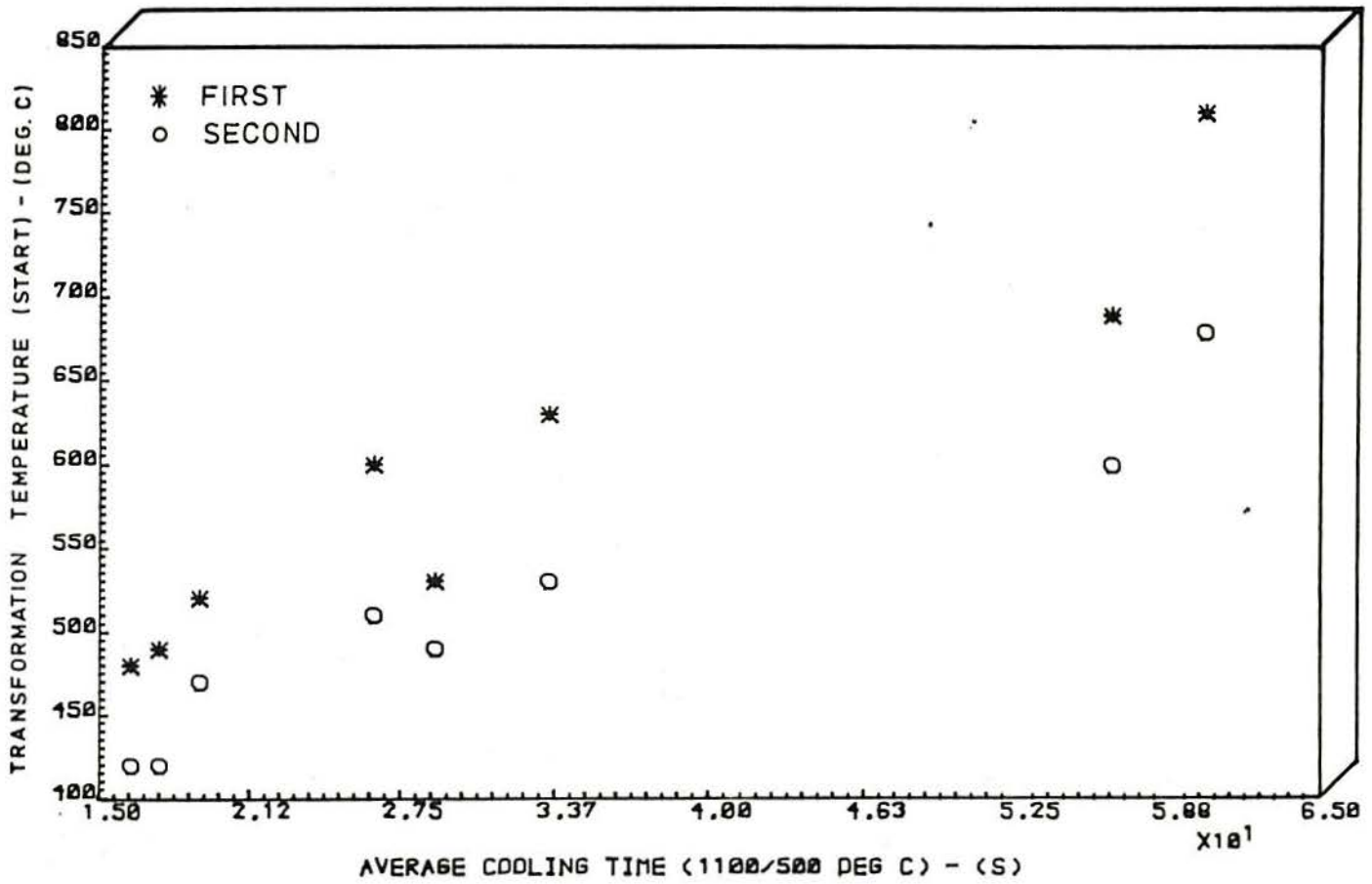

FIGURE 8.39 - RELATIONSHIP BETWEEN FIRST AND SECOND TRANSFORMATION TEMPERATURES (START), AND COOLING TIME (1100/500 DEG C)

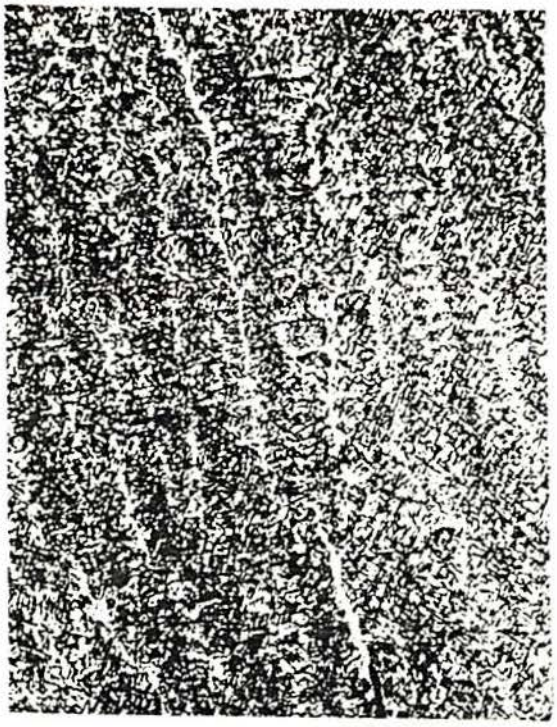

(a) SP.Q1371L4 (1.9 KJ/mm) x 200

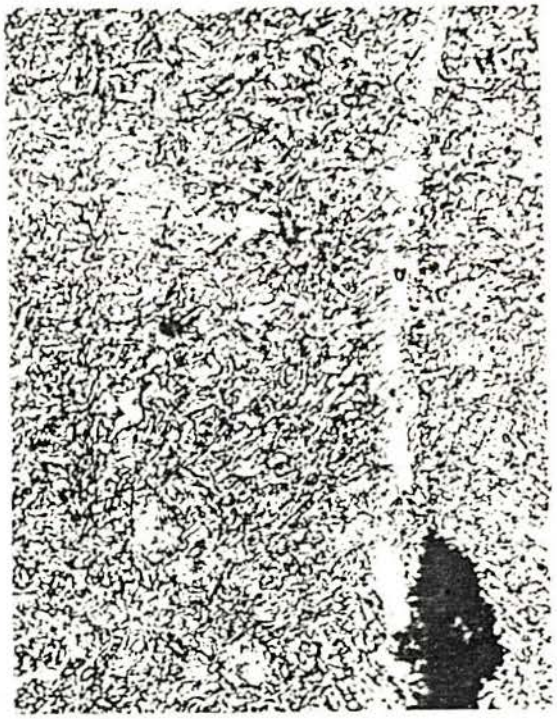

(b) SP.H674L4 (4.1 KJ/mm) x 500

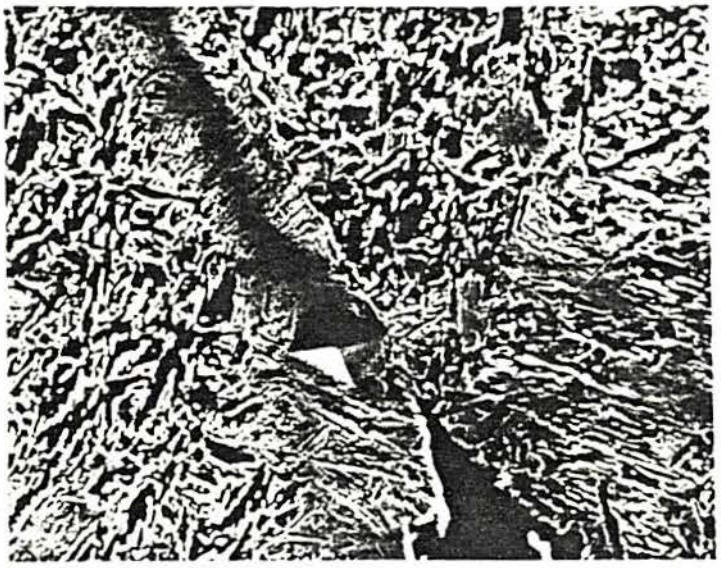

(c) SP.H674L4 (4.1 KJ/mm), SEM, x 2000

FIG. 8.40 - Weld Metal Solidification Cracking Path Related to Secondary Microstructure. Nital.

9. PROCEDURE TECHNIQUES TO REDUCE SOLIDIFICATION CRACKING TENDENCY

9.1 Introduction

In the previous chapter a highly restrained weld test was used to investigate root run solidification cracking progression and origins.

Structures with a high degree of restraint are also found in welding practice. If solidification cracking is a problem and base metal and consumables cannot be changed, the first action is to change welding parameters, within the allowed limits. However, often such a change in welding parameters does not help and the problem persists.

In Chapters 3 and 4 we reviewed techniques that can be used in this case. They either are complicated and expensive, or alter the weld metal chemical composition through alloying or deoxidation, such that the mechanical properties have to be reviewed. Therefore a completely different system for wire oscillation was devised, and simple concepts were put in practice, like groove angle change and cold wire addition.

We also tried to apply the idea given by BORLAND / 107 /, heating the weld pool tail as a measure to decrease stress and thus cracking. For the submerged arc process this system is difficult to use. Firstly, because if the heating is through a flame, the gases blow off the flux and the pool is displaced to one side of the bead. Even with the use of a multi-nozzle torch the problem was not solved. Second, in a relatively large pool (and thick plate) the flame energy input must be sufficiently high to be effective. This increases the problem with the pool dislocation and with the flux that is covering the not yet solidified part of the pool, leading to metallurgical reactions of the melted alloy without proper protection. Therefore, after initial trials we did not proceed with the mentioned idea / 107 /.

Instead, we stuck to the three techniques previously referred to, which have been shown to be simple and inexpensive, and can be employed at any laboratory or production shop.

The welding procedures here applied are equivalent to those of Chapter 8, as regards plate preheat, preparation, welding parameters, etc. The only difference is the technique added, which is explained in the proper section. The welding condition '674', (6.3 mm/s; 770 A; 4.1 KJ/mm) was largely employed, for in Chapter 8 it was used as 'standard' for comparison among different conditions. In all cases the LINDE 95 and OP41TT wire/flux combination was preferred, for they have been shown to induce more centreline solidification cracking than any other combination (see Chapter 8).

Thus, the main objective was to prove the viability of the methods as regards their effectiveness to eliminate or reduce solidification cracking.

Investigation on possible side effects, like changes in mechanical properties, was not considered at this stage, but could be subject of future research.

9.2 Wire oscillation technique

If an experienced welder knows that a centreline solidification cracking usually forms under a specific welding condition (using MMA), he (she) can manage to 'push back' the electrode each time the weaving is done. Following very closely and carefully such operations, it is possible to see that the previous pool is completely deformed by the electrode tip. Furthermore, even the low temperature (probably 'mushy') area of the pool is mechanically shaken. Depending on not yet determined conditions, this technique works very well and the weld bead is free of defects.

This idea was employed here using the same automatic submerged arc equipment previously described (Chapters 6 and 8).

Instead of oscillating all the welding head as it is usually done (Chapters 3 and 4), we preferred to use an equipment able to oscillate just the wire (electrode). Such an oscillation has a number of advantages, among them simplicity of operation and low cost.

In Figure 9.1 can be seen the schematic oscillation system. Two main controls on it are the oscillation frequency and the actuating time (mark/space ratio), which determine the generated square wave. The solid state relay switches on or off the actuating solenoid, depending on the chosen frequency and mark/space ratio. The solenoid then oscillates the wire.

A standard shoe at the welding head would not allow, of course, the necessary wire movement. Therefore, a special shoe was designed and it can be seen in Figure 9.2. There are some differences between it and the standard one: a hole made near the middle height (as indicated in the front view of Figure 9.2) to allow the solenoid actuation; and the elliptical conduct for the wire, as seen in the section through the centre and top face, allowing its oscillation.

The wire used was 4.0 mm diameter. After some trials it was determined that it could still maintain good electrical contact with the shoe if the larger diameter of the ellipse was 6.0 mm, as indicated in Figure 9.2 oscillation amplitude of the electrode tip was constant and ~ 1.5 mm (exactly 1.4 mm).

Before the system actually works, however, there is a small but important detail to be explained. Obviously, the oscillation is done in one direction only. The solenoid actuates pushing the wire up to the maximum allowed amplitude and then retracts. At this stage the wire is left on its own, and only will retract if it acts like a spring. This can be obtained through a suitable positioning of the wire reel in relation to the wire feed system.

This is one inconvenience of this set, and it was recognised right at the beginning. As we already managed to overcome the problem using the spring effect of the wire, we did not try to improve it. However, it is sufficient to insert a pair of arms connected to the solenoid to bring back the wire when it retracts. Also it was noticed that a voltage variation of ~ 10% around the nominal value, was due to oscillation.

The welding set-up for wire oscillation can be seen in Figure 8.2. The white box with some control switches contains the electric circuitry. The actuating solenoid is attached to the welding head.

Initial trials have shown that oscillation was only effective in the welding direction, and this explains why the welding head is in the position seen in Figure 8.2.

The range of available oscillation frequencies was 0 to ~ 25 Hz. The welding coding employed was similar to that in Chapter 8. The difference is that two digits were added at the end: '0' standing for 'oscillation'; the second digit ('1' or '2') standing for 10 or 7 Hz (oscillation frequency), respectively.

9.3 Other techniques

9.3.1 Cold wire addition

This technique is not new. However, it is generally applied, as far as we know, with different objectives than to reduce solidification cracking tendency.

The welding procedure was similar to that described in Chapter 8. A 1.2 mm diameter wire electrically neutral (thus the name 'cold wire') was additioned from a guide placed behind the welding head.

This cold wire has a similar chemical composition to the main wire. In fact, as Table 6.2 shows (Chapter 6), both wires have the same designation (LINDE 95), and the digits 'A' or 'B' were added simply for our convenience.

The general procedure was to inject the cold wire into the weld pool just after the arc had passed. As the wire's mass is small, it should melt, modifying the weld pool solidification and also causing some mechanical movement in the almost 'mushy' metal. These combined actions are thought to reduce solidification cracking tendency, because they shall provide nuclei which have a good change to survive, for there is a reduction in the pool temperature as well, enhancing the growth rate. Also, as the 'cold' wire melts, it provides fresh metal to fill in any eventual forming crack.

The weld coding follows that of Chapter 8,adding two digits at the end of it. The first, a 'C' stands for 'cold wire addition'; the second can be a '3', '5' or '7', and indicates the rate of wire injection viz: 0.34, 0.50, 0.73 g/s respectively.

9.3.2 Groove angle change

This is not properly a 'technique'. Rather, the groove angle is a factor that should be decided at the welding design stage and not at the production shop, due to technical and economic reasons. For example, the groove angle change from 30° to 90° leads to en increase in deposited weld metal of ~ 3.7 times.

However, supposing it is feasible, it can significantly reduce the solidification cracking tendency, as will be shown and explained below (Section 9.4 (i)).

As the weld specimens used for solidification cracking tests (Chapter 8) had a 60° groove angle, we decided to test the same welding condition with 0° and 120°. The weld coding follows that of Chapter 8, but two digits were added at its end. An 'A' stands for 'groove angle change' and a '0' or '1' for 0° and 120° respectively.

9.4 Results and discussion

In Table 9.1 can be seen results for groove angle change, cold wire addition and wire oscillation. The following lines suggest explanations for them:

(i) Groove angle change

In Table 9.1 the three first welds coded H 674 L4 A0, H 674 L4 A1 and Q 674 L4 A1 have shown 'zero' centreline solidification cracking. Comparing these welds with those equivalent (H or Q 674 L4) in Table 8.4 (a), it can be seen that H 674 L4 and Q 674 L4 have shown 31% and 13% of centreline solidification cracking, respectively.

These results show that groove angle change is very effective against the solidification cracking problem within the limits of the experiments.

As the welding conditions (except, of course, groove angle) were exactly the same as those used in Chapter 8, the groove was the agent acting to change the welds susceptibility to solidification cracking. Two explanations for this behaviour were found. One is that these welds have a completely different stress field acting on them, and the other is the interrelationship of this factor with the different centreline structure noticed. This new stress field was either less intense or acting at different places than that of Chapter 8 for equivalent welding conditions. It can readily be seen that the H/W ratios in this case are nearly half of the tests shown in Table 8.4 (a).

We can elaborate still more this explanation. Let us suppose, in a recognisable simplistic view, that there are only two forces acting horizontally on the weld centreline. The action force 'F', orthogonal to the groove face, and the reaction 'R' which tries to maintain the centreline integrity and is horizontal. Thus:

$$R/F = \cos (ANG/2)$$

where

'ANG' is the groove angle

For 'ANG' in the range 30 to 120°, for example, the R/F ratio will stay between 0.96 and 0.5 respectively. This means that the necessary reaction force 'R' to maintain the centreline integrity at ANG = 120° is half of the acting force 'F' at Ang = 30°. The ANG = 0° case cannot, however, be directly compared to the other groove angles. This is because it leaves below the bead a much larger resistant section that opposes itself to the plate's bending. Therefore 'R' should be smaller than the expected.

Now, looking to Figures 9.3 (a,b) and comparing them with Figure 8.18 (b) and Figure 8.19 (b) it can be seen that both (0° and 120° groove angle) centreline are different from those made at 60° groove angle.

Therefore, our theory is that with change in groove angle the weld heat flow was changed (Chapter 8). As a consequence, both the thermal stress and the solidification macrostructure changed as well. For this particular welding condition the changes increased the weld metal resistance to solidification cracking.

(ii) Cold wire addition

The next block of welds in Table 9.1 refers to those made using cold wire addition. Comparing with Table 8.4 (a) it can be seen that there was an overall reduction in cracking tendency. However, no totally crack-free welds were obtained, with the transverse type persisting to exist.

The cold wire feeding rates in Table 9.1 are those which give the best results against solidification cracking tendency, within the limits of our experiments. It is clear that the wire addition rate is limited by the weld pool ability to melt it. For 13.8 mm/s, 770 A, 1.9 KJ/mm or weld code H 1371 L4 C7, this maximum (and in this case the most effective) rate was 0.73 g/s (43.8 g/min) and for this welding condition without cold wire addition (H 1371 L4 in Table 8.4 (a)) the reduction in centreline solidification cracking was not too encouraging (from 68% to 40%).

Comparing welding conditions H 641 L4, H 674 L4 and Q 674 L4 with H 641 L4 C3, H 674 L4 C5 and Q 674 L4 C3 or Q 674 L4 C5, respectively, it can be seen that a good improvement was achieved, for the centreline cracking completely disappeared. Thus, it seems that cold wire addition is an effective way to eliminate centreline solidification cracking, but its action is almost nil against the transverse type. One possible interpretation to what is happening follows.

It is known (Chapter 4), that, among other factors, the greater the alloy solidification range the greater the danger to solidification cracking. The cold wire injection acts in two ways. First, as this wire needs heat to melt, it lowers the weld pool solidification time. Thus, there is less time to low melting point films to form at the centreline, being also disrupted the overall pattern in which impurities and alloying elements segregate. Second, at least in the weld centreline, the 'normal' solidification mode is altered, as Figure 9.4 shows. In this figure the (arrowed) weld centreline is not defined, and it can be seen dendrites crossing from one 'side' of the centre to the other.

Thus it seems to be clear that those two factors alter the degree of constitutional supercooling (Chapter 3), through the temperature gradient and the equilibrium liquidus temperature distribution, which is a function of solidification rate.

(iii) Wire oscillation

The first trials using wire oscillation have shown that frequencies outside the range 7 to 10 Hz and/or oscillation transverse to the welding direction had no effect at all on solidification cracking tendency, within the limits of our experiments. Also a mark/space ratio of 1/7 has shown to be the best, holding some kind of relationship with

the inherent inertia of the system. Firstly, bead on plate (BOP) welds were made (including 5 Hz frequency) just to assess the oscillation frequency effect on weld bead dimensions, dilution and deposition rate.

Table 9.2 and the accompanying schematic figure of a BOP weld on a 33 mm thick base plate, shows the related dimensions as oscillation frequency changes. Four sections were cut from each weld bead, the dimensions were measured and the averages shown in this table.

Comparing welds made with wire oscillation to that in which it did not oscillate (BOP 1), it is striking that: there is a reduction in dilution (D), bead height (X) and penetration (P): there is an increase in weld bead width (W): the over-filling (R) is not affected, while the overall deposition rate increased ~10%.

The third block of welds in Table 9.1 shows the best reduction obtained in solidification cracking tendency when wire oscillation is applied. So, comparing this table with Table 8.4 (a) it can be seen that there is a clear tendency to crack free welds. Specimens H 641 L4, H 674 L4 and Q 674 L4 can be compared with H 641 L4 01, H 674 L4 01, and Q 674 L4 01, respectively. There is a good improvement, for welds which previously had shown centreline solidification cracking are now either crack free (H 641 L4 01, Q 674 L4 01) or have only transverse type cracking (H 674 L4 01). This result is important, for attention is drawn to the fact that welding condition H 641 L4 always had shown cracking, for all wire/flux combinations (see Tables 8.4 (a, b)).

For the worst welding condition in Chapter 8 (Q/H 1371 L4) there is also a significant reduction in centreline cracking tendency (Q 1371 L4 02).

As could be seen, this technique seems to be very effective against centreline and transverse solidification cracking. It is quite right to believe that more effective results can be obtained after some adjustments (previously pointed out) in the system, and conditions (mark/space ratio and frequency) optimisation.

In the search for explanation(s) of the results, the first evidence to be noticed is the profound alteration in primary macrostructure caused by wire oscillation. Figures 9.5 (a-c) show the solidification macrostructure of weld Q 674 L4 01, which was taken as a general example. Comparing Figure 9.5 (a) with 8.18 (b) it is readily seen that welds made with wire oscillation: have a much finer solidification macrostructure; the weld centreline is not defined (is not 'in line'), being rather equiaxed; there are no dendrites growing straight from the fusion zone to the weld centreline (in the paper place) as it happens in Figure 8.18 (b).

Figures 9.5 (b,c) illustrate another two aspects of the same weld, in transverse and longitudinal sections, respectively. The transverse section clearly shows the macrostructure formed at the centreline (arrowed). In the longitudinal section (parallel to the welding direction) there is a sudden change in solidification macrostructure, for near the fusion zone (bottom of the figure) there is a cellular-dendritic growth and then it becomes completely disorientated. What we are seeing at the middle of this figure might be exactly the border between the region affected by the wire oscillation and that which grows under 'normal' solidification process.

The theoretical explanation for the weld solidification macrostructure change is controversial and not completely understood, as we have seen in Chapters 3 and 4. However, the wire oscillation technique seems to affect, at the same time, two of the main mechanisms thought to affect weld pool solidification mode.

It alters the extent of constitutional supercooling (Chapter 3) of the solidifying weld metal, for its mechanical action causes stirring in the pool. This pool movement, much more intense than the electromagnetic Lorentz forces (Chapters 3 and 4), reduces the thermal gradient and detaches solid particles. In general, under 'normal' solidification process these particles could not survive and growth, due to the very high temperatures found in the pool (Chapter 3). As there is a fall in temperature due to the stirring, the particles act as muclei and increase the growth rate.

In Chapter 3 we have seen that decreasing temperature gradient and increasing growth rate tend to produce equiaxed dendrites (Figure 3.7). Furthermore, higher growth rate means more dendrite boundaries for the same volume of solid metal, or finer dendrite size. In fact, the previous microphotographs.confirm this tendency (Figures 9.3 (a-c)).

Therefore, the effect of primary macrostructure change on solidification cracking can be explained through the decreasing in dendrite size, the formation of equiaxed dendrite and the overall reduction in the thermal gradient. Also there is the mechanical wire action, which throws fresh liquid metal over regions of the pool in the 'mushy' state.

Thus, many mechanisms cooperate to reduce the weld sensitivity to solidification cracking. Finer dendrite size means less chance to large low melting point films formation. Equiaxed dendrite is a solidification macrostructure much more resistant to cracking (Chapter 8) than, for example, centreline type. The decreasing in thermal gradient shorter the weld pool solidification range and, at the same time, gives the right environment to nuclei, which will survive and grow, increasing the growth rate. Finally, fresh liquid moved by the wire can fill up large centreline solidification cracking.

9.5 Summary

In this chapter we have seen that simple and inexpensive techniques to reduce solidification cracking tendency can be successfully employed.

Initial experiments have shown that the flame heating of the weld pool tail is almost impracticable when submerged arc process is used.

Three other techniques were effectively employed, viz: cold wire addition, groove angle change and wire oscillation.

The groove angle change might reduce the solidification cracking tendency under certain welding conditions. The theory proposed to explain why it has beneficial action is based on the possibly different stress fields created by different groove angles, together with the modification in weld centreline macrostructure. This change in groove angle depends, however, on economics and technical considerations and cannot always be employed.

Shortening the alloy solidification range and disrupting the pattern in which impurities and alloys segregate can be an effective way of reducing solidification cracking. The injection of cold wire at the weld pool tail gives good results, for it causes alteration in the temperature gradient and fill up (when it melts) centreline type cracking. For transverse type cracking, however, it did not show to be so effective.

Complex but powerful mechanisms act cooperatively through the wire oscillation technique, which reduces centreline and transverse solidification cracking tendency. Theoretically, supercooling and nuclei growth seem to be the basic metallurgical agents. The process is conducted through reduction in dendrite size, equiaxed dendrite formation, and decreasing in the overall pool thermal gradient. Also, due to the stirring, fresh liquid fills centreline solidification cracking once it had formed.

TABLE 9.1 - SOLIDIFICATION CRACKING TESTS (NON-STANDARD WELDINGS): WELDING CONDITIONS, WELD BEAD DIMENSIONS AND WELD DEFECTS

Weld Code	W (mm)	H (mm)	X (mm)	d (mm)	H/W	CL-SC(*) (%)	Remarks
H674L4Aϕ	22.0	15.3	18.1	12.6	0.7	0	Groove angle (GA) 0^{o}
H674L4A1	20.5	17.3	17.3	12.6	0.8	0	GA 120^{o}
Q674L4A1	19.3	19.0	18.8	12.8	1.0	0	GA 120^{o}
H641L4C3	10.2	10.0	9.1	9.8	1.0	0_T (+)	Cold Wire Addition (CWA) ∿ 0.34g/s
H674L4C5	13.9	19.9	19.4	12.6	1.4	0_T	CWA ∿ 0.50g/s
H1371L4C7	9.1	12.2	11.9	10.3	1.3	40	CWA ∿ 0.73g/s
Q674L4C3	14.5	20.0	17.4	12.1	1.4	0_T	CWA ∿ 0.34g/s
Q674L4C5	14.4	20.6	19.4	12.6	1.4	0_T	CWA ∿ 0.50g/s
H641L401	11.8	10.1	7.2	9.0	0.9	0	Oscillation (OSC) ∿ 10Hz
H674L401	15.9	20.1	16.5	12.7	1.3	0_T	OSC ∿ 10Hz
Q674L401	15.5	20.8	16.7	12.0	1.3	0	OSC ∿ 10Hz
Q1371L401	9.4	11.9	10.2	10.0	1.3	36	OSC ∿ 10Hz
Q1371L402	9.9	13.3	11.0	10.1	1.3	28	OSC ∿ 7.1Hz

(*) Centre-Line Solidification Cracking (% in section)

(+) Transverse SC (presence)

TABLE 9.2 - OSCILLATION TESTS: WELD DIMENSIONS OF BEAD ON PLATE (BOP) WELDINGS

Weld Code	W (	X mm	R	P)	D (%)	Oscillation Frequency (Hz)
BOP1	20	19.1	4.7	14.5	71	No*
BOP2	23.9	14.2	4.7	9.5	59	5.0
BOP3	26.2	14.2	4.2	10.0	61	7.1
BOP4	24.3	16.0	5.0	11.0	59	10.0

* No: No Oscillation

Note: Welding conditions were 34V, 770A, 6.3mm/s. (4.1kJ/mm)

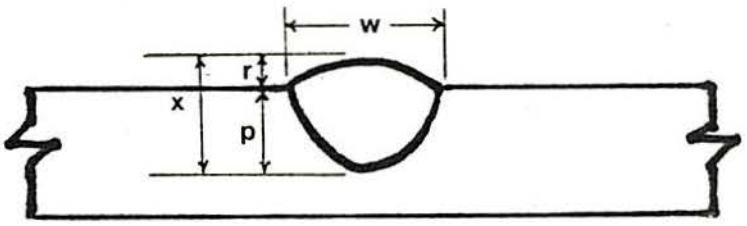

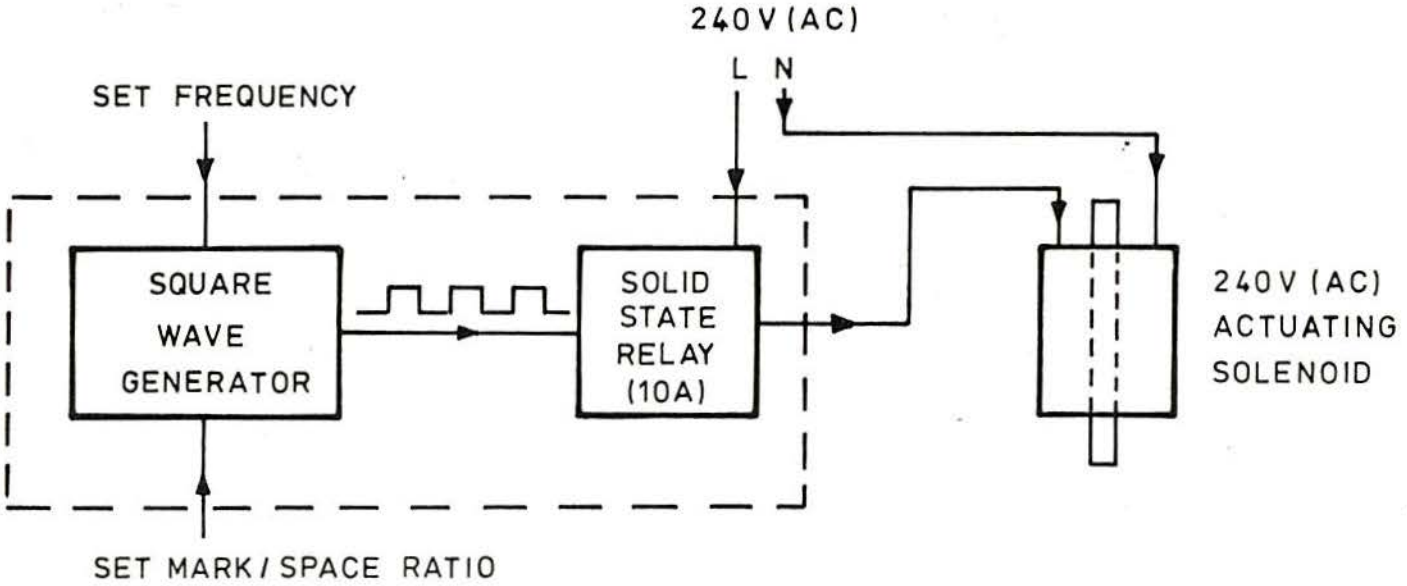

FIGURE 9.1 - OSCILLATION SET (SCHEMATIC). THE SOLENOID ACTUATES ON THE WELDING WIRE.

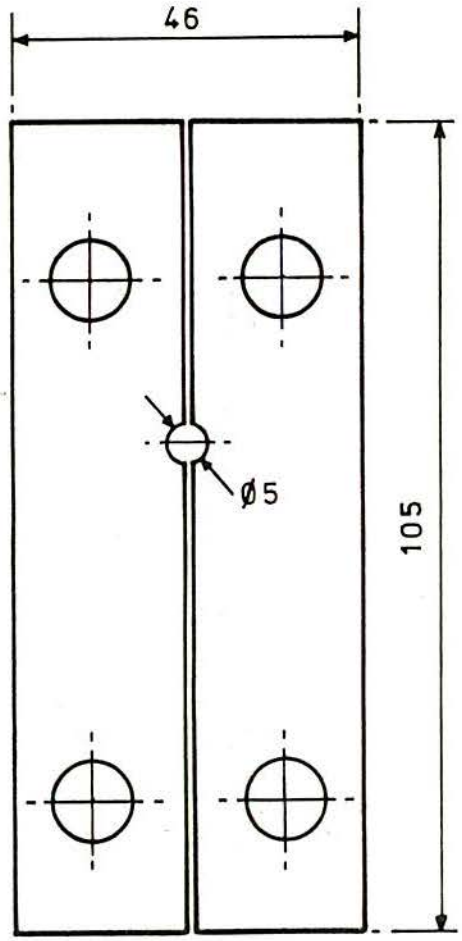

FRONT VIEW

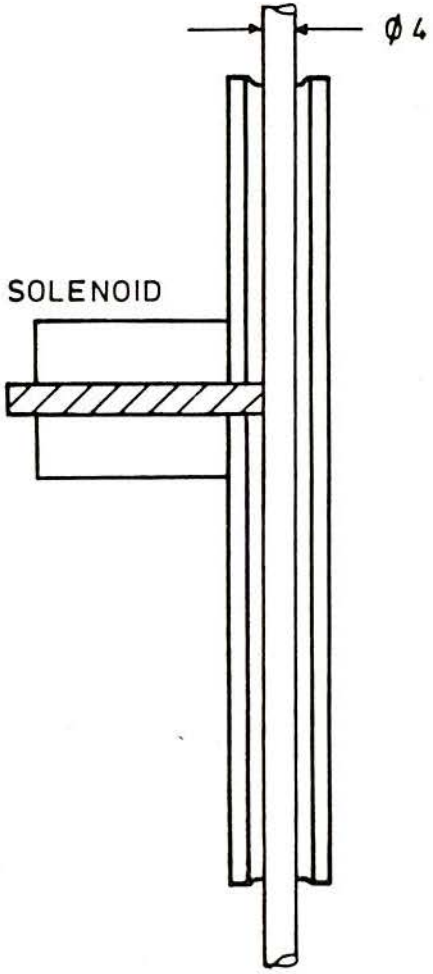

CUT THROUGH CENTRE

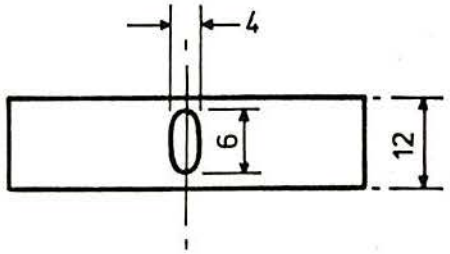

TOP FACE

FIGURE 9.2 – SPECIAL SHOE FOR THE OSCILLATION SET. SEE FIGURE 9.1

(a) 0^{o} Groove Angle

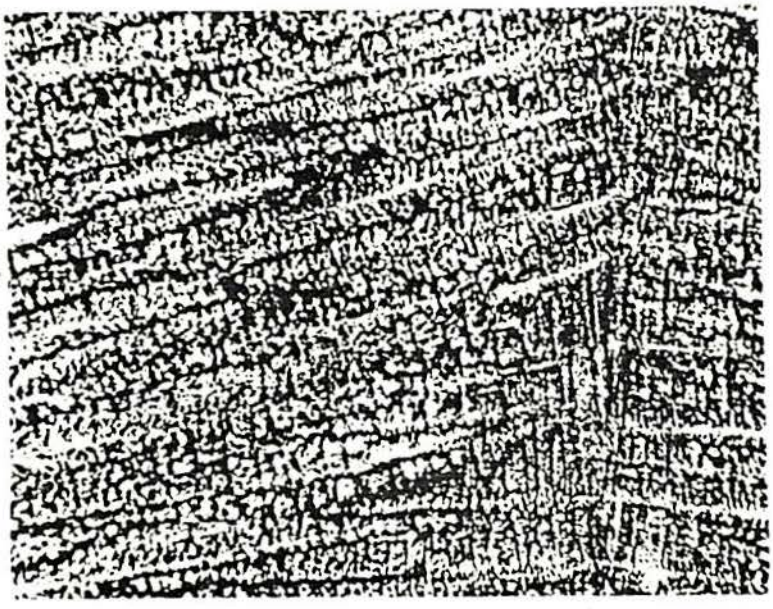

(b) 120^{o} Groove Angle

FIG. 9.3 Solidification Macrostructure (Centreline) with Change in Groove Angle. SASPA, X 50.

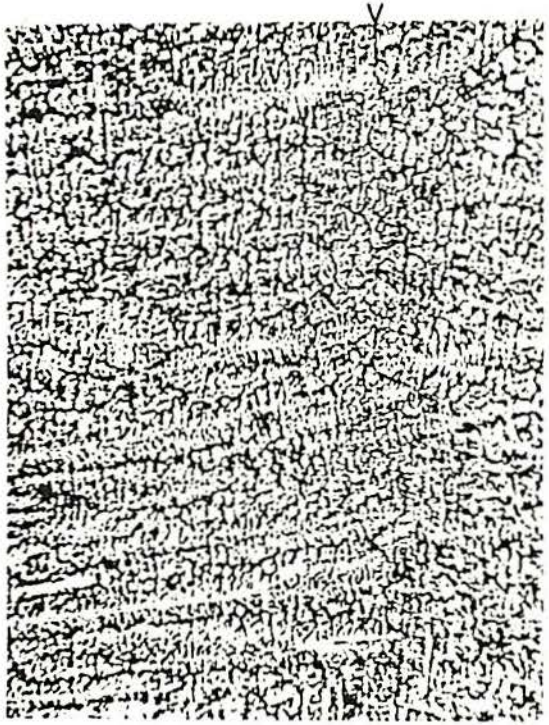

FIG. 9.4 Solidification Macrostructure (Centreline)
Sp. Q 674 S4 C5, Cold Wire Addition.SASPA,
X 50.

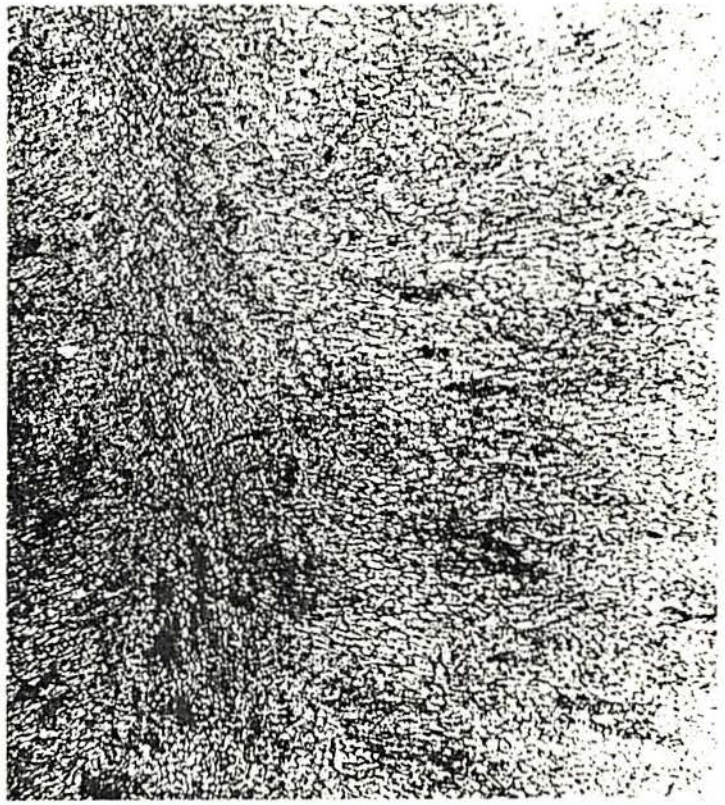

(a) Transverse Section, X 25

FIG. 9.5 Solidification Macrostructure. Sp.
Q 674 S4 01. Wire Oscillation.
SASPA.

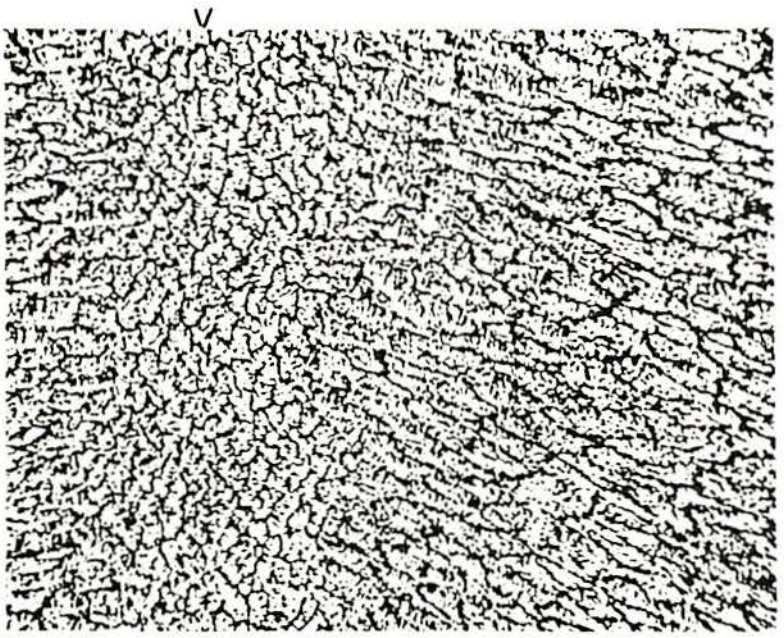

FIG. 9.5(b) Transverse Section. X 50.

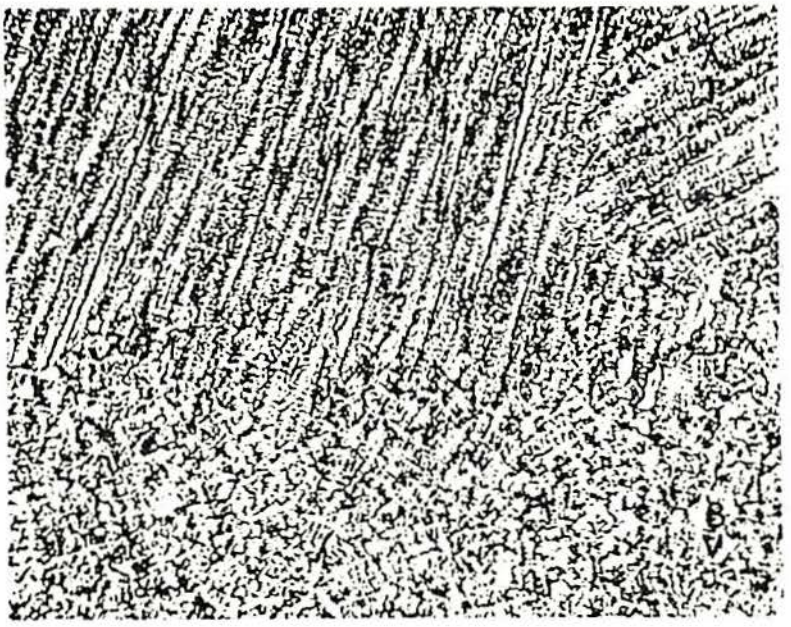

FIG. 9.5(c) Longitudinal Section, X 50.
T-Top. B-Bottom.

10. CONCLUSIONS

10.1 Solidification cracking

It was one of the main concerns of this work to point out the complexity involved in the weld metal solidification cracking phenomenon, for most of the previous studies have neglected the existing interactions among the welding conditions. As we have seen, in general, there is neither only one explanation for each fact, nor only one result being unequivocally related to a cause.

Thus, the following general conclusions are derived considering the base metal specimen test, welding parameters, fluxes and wires batches used, level and acuity of analysis employed and developed throughout this research program.

10.1.1 Compositional factors

Chemical composition showed up as one of the most important factors deciding solidification cracking tendency. Two main origins for the welds different chemical analyses were found to be the base steels and the wires.

The influence of steel type on the weld chemical composition is not obvious, and it is only understood when the inherited balance between carbide-to-ferrite elements forming ratio is analysed. As we have seen, all the empirical formulae, which basically used this ratio predicted the HY100 as the most susceptible steel to solidification cracking, because it always showed the lowest ratio. Furthermore, the metallurgical investigation carried out on both steels suggested that their production follows different steelmaking practice, with the Q2N showing to be a cleaner steel than the HY100.

Therefore, the welds made on each steel approximately held the same carbide-to-ferrite elements forming ratio, and those on Q2N also showed five times more vanadium than those on the HY100 steel.

The wire chemical analyses show a much clearer difference, which was naturally reflected in the welds made with each one of them. The OERLIKON S3 wire has significantly more carbon and molybdenum content than the LINDE 95, whilst the latter has more silicon, chromium and nickel than the former. The most striking difference, however, is that the Mn/Si ratio in the OERLIKON S3 is approximately three times greater than in the LINDE 95.

Thus, the base metal and wire chemical composition combined and those welds with the following characteristics were the most crack susceptible: the lowest carbide-to-ferrite elements forming ratio; the highest carbon plus nickel contents together with the highest phosphorus and sulphur contents; the lowest Mn/Si ratio.

Having the best characteristics, the welds using Q2N base steel and OERLIKON S3 wire showed up as the most resistant to solidification cracking.

10.1.2 Solidification macrostructure and microsegregation factors

The solidification macrostructure shows up through its size, type and growth direction. The weld metal dendrite size was found to be primarily dependent on welding parameters and weld bead geometry, principally the external area-to-perimeter ratio. However, when it is measured on the weld bead longitudinal section, the measured value must be corrected by the angle between the dendrite growth direction and the weld symmetry line, measured on the transverse section. So, the actual rate of change in dendrite size with welding parameters is not that observed through metallographic analysis. As it was seen, the increase in welding current at a constant speed has much more effect on the actual dendrite size than the increase of the latter welding parameter at a constant current.

The dendrite size relevance to solidification cracking is understood through its reduction of large microsegation planes, and thus higher resistance to stress in the solidifying stage. The 1.9 KJ/mm (6.3 mm/s; 400 A) welding condition showed up as the most resistant to this defect in both steels, and also as having the smallest dendrite size.

Four types of centreline solidification macrostructure were identified, viz: stray, competitive columnar, centreline and equiaxed. The former three macrostructures have a strong relationship with changes in welding parameters. The stray structure is associated with the lowest energy input and welding speed. Increasing current and keeping constant other parameters induced a transition to competitive columnar structure. At the highest energy input and current, an increase in speed led to a transition to centreline type.

Some equiaxed structures formed only at the highest energy input and lowest speed using the OP121TT flux. This flux has been shown to release twice as much gas(es) than the OP41TT, and this might be one of the reasons of this behaviour.

Thus, when analysed on their own, the solidification macrostructures which showed the least tendency to solidification cracking were the stray and the equiaxed types. Therefore, welds made either at 1.9 KJ/mm (6.3 mm/s welding speed) or at 4.1 KJ/mm (6.3 mm/s) and using the OP121TT flux have shown greater resistance to this defect.

Cold wire addition reduced centreline solidification cracking, but had no effect on the transverse type. Thus, it has a short range effect, filling the central cracking as it melts and also shortening the weld pool solidification time. This latter factor induces the formation of smaller dendrite size.

The specially designed wire oscillation device was extremely useful in reducing solidification cracking tendency both, centreline and transverse. The low oscillation frequencies (below 10 Hz) in the welding direction promoted the formation of a non-oriented structure from the middle weld bead upwards, enhancing the weld resistance to this defect.

The microsegregation was found to be closely related to chemical composition and solidification macrostructure type. The use of Q2N base steel and OERLIKON S3 wire induced less centreline microsegregation, probably due to the differences in chemical composition pointed out in the previous section. The solidification macrostructure effect on centreline microsegregation was clearly demonstrated, with stray and equiaxed macrostructure showing less segregation.

Thus, stray or equiaxed solidification macrostructures are the most resistant to this defect. These structures together with less microsegregation were obtained through the use of the following elements: Q2N base steel; OERLIKON S3 wire; OP121TT flux and 4.1 KJ/mm (at 6.3 mm/s); 1.9 KJ/mm (at 6.3 mm/s); cold wire addition; wire oscillation.

10.1.3 Stress field factor

Stress relieving both base steels before welding has shown a reduction in the weld solidification cracking tendency. This illustrates the evidence brought up in the literature review on the importance of base metal strength and high temperature properties on this defect, albeit not quantified for both steels.

Factors such as the weld bead height-to-width ratio, weld bead size etc., have shown not to be, in this work, a sure guide to predict the weld solidification cracking susceptibility. However, we cannot exclude the possibility of some kind of overlapping effect due to chemical composition, solidification macrostructure or microsegregation.

On the other hand, change in the specimen groove angle to 0^{o} or 120^{o} reduced the defect tendency, and this may be attributed to the change in the stress fields. Also, cold wire addition and wire oscillation might affect the stress fields, at least within the weld pool, through their effects on the welding heat flow.

It was shown that the greater the weld ripple lag-to-welding speed ratio, the greater the amount of fused slag. As this influences the interfacial tensions equilibrium along the weld pool, the stress fields within the weld pool might also be affected.

10.1.4 Concluding remarks

From the previous sections it can be concluded, therefore, that the most resistant welds to solidification cracking are those having: (a) the highest carbide-to-ferrite elements forming ratio; (b) the highest Mn/Si ratio; (c) the lowest carbon plus nickel contents together with the lowest phosphorus and sulphur contents; (d) stray or equiaxed solidification macrostructures type; (e) small or nil centreline microsegregation; (f) base metals with the lowest possible residual stress; (g) the smallest actual dendrite size; (h) minimum stress fields within or around the weld pool.

The above conditions may be fulfilled through the rational use of the following measures, at least: (a) appropriated selection of base metal and consumables chemical composition, attempting not only to the individual element contents but, principally (in the welding of these steels), to their resultant combined action; (b) stress

relieved base metal; (c) correct welding parameters choice, e.g. those inducing the formation of stray macrostructure and the smallest dendrite size; (d) fluxes with relatively high amount of gas release, for this induces equiaxed dendrite formation at high current and, consequently, less microsegregation at the weld centreline; (e) if the problem is centreline cracking only, the addition of cold wire might be very effective to reduce it; (f) for centreline and transverse cracking, the wire oscillation technique is a powerful way to reduce or eliminate it; (g) the largest possible groove angle.

Thus, the root run welds made in this study have shown that, as regards solidification cracking tendency, the best results are obtained with Q2N base steel, OERLIKON S3 NiMo 1 wire and OP121 TT flux, independently of welding parameters.

10.2 Secondary microstructure

Both base steels were found to be equally sensitive to thermal cycles in terms of HAZ width and microstructure, which consists essentially of martensite. The HY100 showed some inclusion colonies within the HAZ and to be about 30 HV5 harder than the Q2N steel in the coarse region.

As regards weld metal microstructure, no major distinction brought by wire/flux could be assessed. Again, the most influential factor seems to have been the energy input, through the change in microstructure size. For all weld metals the increase in cooling rate was followed by increase in hardness.

The complete microstructure characterisation could be made using the TEM only, for a 'lath' microconstituent did not resolve under the light microscope or SEM. Thus, the welds under study are composed mainly of ferrite with aligned M-A-C, acicular ferrite and autotempered martensite. It was also detected an unidentified white material, distributed in 'islands' surrounded by the matrix, perhaps contributing to the weld metal embrittlement.

From the obtained weld metal thermal cycles, the ferrite with aligned M-A-C should have formed about 490°C for the 1.9 KJ/mm welds, and about 810°C for the 4.1 KJ/mm energy input welds. The acicular ferrite should have formed about 420°C for the 1.9 KJ/mm welds and about 680°C for the 4.1 KJ/mm welds.

A good agreement has been found between first and second transformation temperatures with cooling time.

Evidence was shown relating the solidification cracking with 'cold' or high temperature (not solidification) cracking, and this is a matter that can rouse some concern. The mechanism thought to explain this fact is the solidification cracking tip acting as a stress concentration factor. Thus, the crack propagation as the stress increases with the decrease in temperature.

It also was pointed out a possible association between carbonitrides segregation and solidification cracking path.

10.3 All-weld metal mechanical properties

The submerged arc all-weld metal tests have shown that the major microstructural difference is brought up by the increase in size of the microconstituents when the energy input is raised from 1.9 KJ/mm to 4.1 KJ/mm.

The highest yield strength, tensile strength and hardness values were obtained at 4.1 KJ/mm energy input welds. The 1.9 KJ/mm welds have shown the best values for elongation, reduction in area and Charpy V-notch energy absorbed in all test temperatures.

Comparison between the use of different fluxes or wires could be made at 4.1 KJ/mm energy input welds only. They have shown relatively little practical difference in the resulting properties, and it is possible that the energy input effect has been overlapping the effects brought about by the change in the consumables.

In any case the properties were considered very good when analysed together, relatively surprisingly being the obtaining of weld metals with yield strength over 600 N/mm^2, more than 68% reduction in area, more than 30% elongation and impact resistance over 200 J at room temperature or an average of 80 J at -40°C, and transition to quasicleavage fracture mode between -40°C and -80°C.

10.4 Suggestions for future research

(1) Study on high (transient) temperature mechanical properties of High Yield Strength Q & T steels. Do the Q2N and HY100 actually have such different properties?

(2) Detailed study of base materials residual stress and/or heat treatment effects on solidification cracking.

(3) Careful monitoring of the carbide and ferrite element forming effects on weld metal solidification cracking. Also, study of the effects of residual on the phenomenon.

(4) Improvement of the wire oscillation system devised in this work and optimisation of its operational range in terms, principally, of oscillation frequency and amplitude.

(5) Comparison between submerged arc and other processes, on the basis of weld final mechanical properties, susceptibility to solidification cracking and total costs, when welding the class of steels subject of this work.

REFERENCES

/ 1 / FLINTHAM, E. The Development of Metal-Arc Welding During the Past Half-Century. British Welding Journal. 1 (1): 3-10 Jan 1954.

/ 2 / ANON Trials of a Supersub. Time Magazine. 10, 27th July, 1981.

/ 3 / MACHADO, I.G. & ROGERSON, J.H. Determination of Cold Cracking Susceptibility of Q2N and HY100 Steel Plate. Cranfield Progress Reports, 1st August, 1981, 2nd March, 1982, 3rd May, 1982.

/ 4 / SHACKLETON, D.N. Welding HY100 and HY130 Steels - A Literature Review. The Welding Institute, 1973.

/ 5 / HELLER Jr. S.R., FIORITI, I. & VASTA, J. An Evaluation of HY80 Steel as a Structural Material for Submarines. Part I. Naval Engineering Journal. 29-44 February 1965.

/ 6 / DOLBY, R.E. The Metallurgy and Welding of QT35 and HY80 Steels. The Welding Institute, 1974.

/ 7 / DOTY, W.D. Welding of Quenched and Tempered Alloy Steels. Metals Engineering Quarterly, 9 (2) 66-78, February 1969.

/ 8 / BAUMGARDT, H. et al. Special Feactures in the Development of High Strength Steels for Offshore Technology. Paper 46, Sec. Int. Conf. on Offshore Welded Structures. The Welding Institute, London, November 1982.

/ 9 / MOD (NAVY-UK) Specification DG Ships 70, Navy Quality Steel Plates January 1968.

/ 10 / PENSE, A.W. 1980 Adams Lecture: Twenty Years of Pressure Vessel Steel Research. Welding Journal 59 (11): 311s-325s. November 1980.

/ 11 / SUZUKI, H. 1982 Houdremont Lecture: Weldability of Modern Structural Steels.Welding in the World, 20 (7/8), 121-148, 1982.

/ 12 / HAMILTON, I.G. Ferritic Steels Plates for Pressure Vessels in 'Developments in Pressure Vessel Technology - 3'. Ed. R.W. NICHOLS. Applied Science Publishers Ltd., 1980.

/ 13 / PICKERING, F.B. High-Strength, Low-Alloy Steels - A Decade of Progress. MicroAlloying 75. Washington, 1975.

/ 14 / STEPHENSON, E.T. Effect of Recycling on Residuals, Processing and Properties of Carbon and Low-Alloy Steels. Metallurgical Transactions A. 14A (3), 343-353, March, 1983.

/ 15 / DUCKETT, E.J. Resource Recovery and Conservation, 2, 301-328, 1976/1977 (As quoted in / 14 /.)

/ 16 / HONEYCOMBE, R.W.K. Steels-Microstructure and Properties, Edward Arnold, 1981.

/ 17 / ANON Background for the Development of Materials to be used in High-Strength-Steel Structural Weldments. DMIC Report 172, July 1962.

/ 18 / PICKERING, F.B. Ed. Inclusions. The Institution of Metallurgists, Monog. No. 3, 1979.

/ 19 / McLEAN, A. & KAY, D.A.R. Control of Inclusions in High-Strength, Low-Alloy Steels, MicroAlloying 75, Washington, 1975.

/ 20 / WILSON, W.G. Technical Note: Reduced Heat-Affected Zone Cracking and Improved Base Metal Impact through Sulphide Control with Rare Earth Additions. Welding Journal, 50 (1), 42s-46s, January, 1971.

/ 21 / A Guide to the Solidifaction of Steels. Jernkontoret, Stockholm, 1977.

/ 22 / Metals Handbook, Vol. 8, American Society for Metals, 1973.

/ 23 / CHALMERS, B. Principles of Solidifaction. Wiley, N.Y., 1964.

/ 24 / FLEMINGS, M.C. Principles of Control of Soundness and Homogeneity of Large Ingots. Scandinavian Journal of Metallurgy, 5 (1), 1-5, 1976.

/ 25 / FLEMINGS, M.C. Solidification Processing. Mcgraw-Hill, 1974.

/ 26 / KATTAMIS, T.Z. & FLEMINGS, M.C. Dendrite Morphology, Microsegregation and Homogenization of Low-Alloy Steel. Trans. Met. Soc. AIME, 233 (5), 992-999, May 1965.

/ 27 / HONEYCOMBE, R.W.K. The Precipitation of Alloy Carbides in Austenite and Ferrite. Scandinavian Journal of Metallurgy, 8, 21-26, 1979.

/ 28 / ARONSSON, B. Gefugeaufbau und Mechanische Eigenschaften Einiger Martensitischer Stohle Unter Besonderer Berucksichtigung dis Einflusses non Niob un Molybdon, 77-87, Steel Strengthening Mechanisms. Climax Molybdenum Company, 1969.

/ 29 / Study of the Transformation Characteristic and the Weldability of HY80 Steel. Rensselaer Polytechnic Inst., Quart. Report, June 1962.

/ 30 / BAILEY, N. Aspects of the Weldability of HY130.Metal Construction and British Welding Journal, 2 (8), 339-344, August 1970.

/ 31 / STERNE, Jr. R.H. & KEAY, L.K. Nickel-Chromium-Molybdenum Steel Plate for Pressure Vessels. Sec. Int. Conf. on Pres. Vesl. Techn. Part III - Discs, The ASME, San Antonio, USA, October 1973.

/ 32 / WILLIAMS, C.S. Steel Strength and Ductility Response to Arc-Welding Thermal Cycles; Welding Journal 42 (1), 1s-8s, January 1963.

/ 33 / ROSENSTEIN, A.H. & ASCHE, W.H. Stress-Relief Embrittlement of High-Strength Quenched and Tempered Alloy in Steels. Temper Embrittlement in Steel. ASTM STP 407, 1968.

/ 34 / YORKE, D.G. Survey of Structural Steels from 100 to 150 Ksi. Sec. Int. Conf. on Pres. Ves. Techn. Part III - Discs. The ASME, San Antonio, USA, October, 1973.

/ 35 / RADZIMINSKI, J.B.& LAWRENCE, Jr., F.V. Fatigue of High-Yield-Strength Steel Weldments: Welding Journal 49 (8), 365s-375s, August 1970.

/ 36 / BARSOM, J.M. Relationship between Plane - Strain Ductility and K_{IC} for Various Steels. Journal Engineering and Industry, 93, 1208-1215, 1971.

/ 37 / LOGINOW, A.W. Corrosion and Stress Corrosion of HY130 (T) Steel and HY80 Steel in Marine Environments. Applied Res. Lab. U.S. Steel, May 1967.

/ 38 / TAYLOR, D.S. & EVAN, G.M. The Systematic Development of a New Range of MMA Electrodes for Critical Areas of Offshore Fabrication. Sec. Int. Conf. on Offshore Structure. The Welding Institute, London, November 1982.

/ 39 / HAWTHORNE, J.R. & WATSON, H.E. Strength and Notch Ductility of Selected Structural Alloys after High Fluence 550°F (288°C) Irradiation, Properties of Reactor Struct. Alloys after Neutron or Particle Irradiation. ASTM STP 570. ASTM, 1975.

/ 40 / REYNOLDS, M.B. Radiation Effects in Some Engineering Alloys. Journal of Materials, 1, 127-152, March 1966.

/ 41 / WHITMAN, G.D. et al (Eds.) Technology of Steel Pressure Vessel for Water-Cooled Nuclear Reactors. ORNL - NSIC - 21, Oak Ridge Nat. Lab., 1967.

/ 42 / WEEKS, A.F. Discussion on Session II, 212-213 and Session III, 228. Strong Tough Structural Steels. Procds. of the Joint Conf. Iron and Steel Inst., Publ. 104, 1967.

/ 43 /	TILLER, W.A., JACKSON, K.A., RUTTER, J.W. & CHALMERS, B.	The Redistribution of Solute Atoms During the Solidifaction of Metals. Acta Metallurgica, 1, 428-437, July 1953.
/ 44 /	SMITH, V.G., TILLER, W.A. & RUTTER, J.W.	A Mathematical Analysis of Solute Redistribution during Solidifaction. Canadian Journal of Physics, 33, 723-745, 1955.
/ 45 /	TILLER, W.A. & RUTTER, J.W.	The Effect of Growth Conditions Upon the Solidifaction of a Binary Alloy. Canadian Journal of Physics, 34, 96-121, 1956.
/ 46 /	TILLER, W.A.	Solute Segregation during Ingot Solidification. Journal of The Iron and Steel Institute, 192, 338-350, August 1959.
/ 47 /	TURKDOGAN, E.T.	Causes and Effects of Deoxidation Occurring During Cooling and Solidification of Steel. Trans. of The Met. Soc. AIME, 233, 2100-2112, December, 1965.
/ 48 /	BHAMBRI, A.K., KATTAMIS, T.Z. & MORRAL, J. E.	Cast Microstructure of Inconel 713 and its Dependence on Solidification Variables. Metallurgical Transactions B, 6B (4), 523-537, December 1975.
/ 49 /	FERNANDEZ, R., LECOMTE, J.C. & KATTAMIS, T.Z.	Effect of Solidification Parameters on the Growth Geometry of MC Carbide in IN-100 Dendritic Monocrystals. Metallurgical Transactions A, 9A (10), 1381-1386, October 1978.
/ 50 /	GLADSHTEIN, L.I.	Weld Metal Primary Crystallisation. Automatic Welding, (10), 86-99, 1959.
/ 51 /	CALVO, F.A.C. et al.	Growth Substructures in Weld Metal. Acta Metallurgica, 8, 898-900, 1960.
/ 52 /	PROKHOROV, N. N. & MASTRYUKOVA, A.S.	Calculating the Crystallisation Pattern of a Welded Joint. Welding Production, 14 (2), 7-16, 1961.
/ 53 /	RAZIKOV, M.I.	The Problem of Primary Weld Metal Crystallisation in Fusion Weld, Automatic Welding, 11 (8), 57-59, 1958.
/ 54 /	RABKIN, D.M. & NIKITINA, A.V.	The Structures of Welds in Aluminium, Automatic Welding, 15 (9), 42-47, 1962.
/ 55 /	SAVAGE, W.F., LUNDIN, C.D. & ARONSON, A.H.	Weld Metal Solidification Mechanics. Welding Journal, 44 (4), 175s-181s, April 1965.
/ 56 /	SAVAGE, W.F. & ARONSON, A.H.	Preferred Orientation in the Weld Fusion Zone. Welding Journal, 45 (2), 85s-89s, February 1966.

/ 57 / MATSUDA, F., HASHIMOTO, T. & SENDA, T. — Fundamental Investigations on Solidification Structure in Weld Metal. Trans. of Nat. Res. Inst. for Metals (Japan), 11 (1), 43-58, 1969.

/ 58 / SENDA, T. et al. — X-Ray Investigation on Modes of Epitaxial and Dendritic Growth in Weld Metal. Osaka Univ. Techn. Rep. 20 (916), 89-98, 1970.

/ 59 / TERRY, C.A. & TYLER, W.T. — Inert-Gas Tungsten-Arc Welding S.A.E. 4130 Steel Sheet -5. Welding and Metal Fabrication, 26 (3), 103-110. March 1958.

/ 60 / GARLAND, J.G. — The Control of Weld Pool Solidification, PhD. Thesis, Univ. of Cambridge, 1971.

/ 61 / DAVIES, G.J. & GARLAND, J.G. — Solidification Structures and Properties of Fusion Welds, Int. Metall. Reviews, 20, 83-106, 1975.

/ 62 / LOPER, C.R. & GREGORY, J.T. — Non-epitaxial Growth in Weld Metal. Solidification and Casting of Metals. The Metals Society, 1979.

/ 63 / MASTRYUKOVA, A.S. & PROKHOROV, N.N. — Calculating the Crystallisation Isotherms in the Butt Welding of Plates. Welding Production, 10 (8), 8-12, 1963.

/ 64 / PROKHOROV, N.N. & PROKHOROV, N. NIKOL — A General Equation for the Surface of the Solidification Front During Welding. Welding Production, 16, (8), 1-6, 1969.

/ 65 / PROKHOROV, N.N. & PROKHOROV, N. NIKOL — The Spatial Macrostructure of Weld Metal with Various Forms of the Crystallisation Front. Welding Production, 16 (12), 2-7, 1969.

/ 66 / RYKALYN, N.N. — Calculation of Heat Flow in Welding. Moscow, 1951.

/ 67 / ISHIZAKI, K. — Interfacial Tension Theory of the Phenomena of Arc Welding. Trans. Symp. Physics of the Welding Arc, London 1962. The Welding Institute, 1966.

/ 68 / ISHIZAKI, K. — Solidification of Molten Pool and Beat Formation. IIW Doc. 212-368-76, 1976.

/ 69 / ISHIZAKI, K. — Solidification of the Molten Pool and Bead Formation. Int. Conf. on Arc Physics and Weld Pool Behaviour, London 1979. The Welding Institute, 1980.

/ 70 / BACKERUD, L. & EDVARDSSON, T. — Influence of Process Variables During Submerged Arc Welding on the Primary Structure. Scandinavian Journal of Metallurgy, 4 (6), 267-272, 1975.

/ 71 / WOODS, R.A. & MILNER, D.R. — Motion in the Weld Pool in Arc Welding. Welding Journal, 50 (4), 163s-173s, April 1971.

/ 72 / TELFORD, D.G. & MILNER, D.R. — Factors Inherent in Arc Welding which Influence Grain Size. Metal Construction and British Welding Journal, 4 (12), 461-465, December 1972.

/ 73 / SAVAGE, W.F. — Solidification, Segregation and Weld Defects. Conf. Weldments: Physical Metallurgy and Failure Phenomena. General Electric Co., N.Y., 1979.

/ 74 / D'ANNESSA, A.T. — Sources and Effects of Growth Rate Fluctuations During Weld Metal Solidification. Welding Journal, 49 (2), 41s-45s, February 1970.

/ 75 / JESNITZER, F.E. — Interaction of Carbon and Hydrogen on the Brittle Behaviour of Carbon Steels, IIW Doc. X-554-69.

/ 76 / YOSHIMURA, H. & WINTERTON, K. — Solidification Mode of Weld Metal in Inconel 718. Welding Journal, 51 (3), 132s-137s, March 1972.

/ 77 / GARLAND, J.G. & DAVIES, G.J. — Surface Rippling and Growth Perturbations During Weld Pool Solidification. Metal Construction and British Welding Journal, 2 (5), 171-175, May 1970.

/ 78 / KOTECKI, D.J., CHEEVER, D.L. & HOWDEN, D.G. — Mechanism of Ripple Formation During Weld Solidification. Welding Journal 51 (8), 386s-391s, August 1972.

/ 79 / SAVAGE, W.F., NIPPES, E.F. & SZEKERES, E.S. — A Study of Weld Interface Phenomena in a Low Alloy Steel. Welding Journal, 55 (9), 260s-268s, September 1976.

/ 80 / TAKALO, T. & MOISIO, T. — Fusion Line Attack at Low Corrosion Potentials in Austenitic Stainless Steel Welds. IIW Annual Assembly, Israel, July 1975.

/ 81 / BROWN, P.E. & ADAMS, Jr. C.M. — Fusion-Zone Structures and Properties in Aluminium Alloys. Welding Journal, 39 (12), 520s-524s, December 1960.

/ 82 / PALEY, Z., LYNCH, J.N. & ADAMS, Jr., C.M. — Heat Flow in Welding Heavy Steel Plate. Welding Journal, 43 (2), 71s-79s, February 1964.

/ 83 / JORDAN, M.F. & COLEMAN, M.C. — Fused Zone Structures in Arc Welded Deposits of a Commercial Al-Mg-Mn Alloy. British Welding Journal, 15 (11) 553-558, November 1968.

/ 84 / PROKHOROV, N.N. & MASTRYUKOVA, A.A. — Primary Structures and their Importance when Estimating the Strength of Weld Metal. Automatic Welding, 18 (8), 17-25, 1965.

/ 85 / THORNLEY, J.C. Effect of Heat Input on Properties of Inconel Filler Metal 82 Weld Deposits Welding Journal, 52 (8), 355s-358s, August, 1973.

/ 86 / GARLAND, J.G. Weld Pool Solidification Control. Metal Construction and British Welding Journal, 6 (4), 121-127, April, 1974.

/ 87 / BROWN, D.C. et al. The Effect of Electromagnetic Stirring and Mechanical Vibration on Arc Welds. Welding Journal, 41 (6), 241s-250s, June 1962.

/ 88 / YAKUSHIN, B.F. et al. The Hot Cracking Resistance of the Joint Produced by the Submerged Arc Welding of Thick Steel 16G 2AF Using Powdered Filler Metal. Welding Production, 24 (10), 6-9, 1977.

/ 89 / ABRALOV, M.A. & ABDURAKHMANOV, R.U. Mechanism by which Electromagnetic Action Breaks down Primary Structure of Weld Metal. Automatic Welding, 35 (2), 14-17, 1982.

/ 90 / TSENG, C-F. & SAVAGE, W.F. The Effect of Arc Oscillation. Welding Journal, 50 (11), 777-786, November 1971.

/ 91 / MAKARA, A.M. & KUSHNIRENKO, B.N. Weaving the Arc as a Factor in Improving the Structure and Properties of Welded Joints. Automatic Welding, 20 (1), 35-40, 1967.

/ 92 / MATSUDA, F. et al. Effects of Current Pulsation on Weld Solidification Structure of Aluminium Alloys. Trans. Jap. Weld. Res. Inst. 7 (2), 287-289, 1978.

/ 93 / BECKER, D.W. & ADAMS, Jr., C.M. The Role of Pulsed GTA Welding Variables in Solidification and Grain Refinement. Welding Journal, 58 (5), 143s-152s, May 1979.

/ 94 / POKHODNYA, I.K. et al. Improving the Resistance of Weld Metal to Hot Cracking During Welding Using Electrode with Rutile Coatings. Automatic Welding, 31 (10), 14-17, October, 1978.

/ 95 / PATCHETT, B.M., DEMOS, G.A. & APPS, R.L. The Influence of Flux Composition and Welding Parameters on Heat Distribution in Submerged Arc Welding. Welding Research International, 4 (2), 81-94, 1974.

/ 96 / COCHRANE, R.C. Weld Metal Microstructure - A'State-of-the-Art' Review. British Steel Corp. Report T/PP/1131/30/82A, 1982.

/ 97 / HEMSWORTH, B., BONISZEWSKI, T. & EATON, N.F. Classification and Definition of High Temperature Welding Cracks in Alloys. Metal Construction and British Welding Journal, 1 (2s), 5-16, February 1969.

/ 98 / SPRARAGEN, W. & CLAUSSEN, G.E. Weldability - Weld Metal Cracks - A Review of the Literature to July 1, 1939. Welding Journal, 20 (7), 289s-305s, July 1941.

/ 99 / BORLAND, J.C. Generalised Theory of Super-Solidus Cracking in Welds (and Castings). British Welding Journal, 7 (8), 508-512, August 1960.

/ 100 / BORLAND, J.C. Suggested Explanation of Hot Crackings in Mild and Low Alloy Steel Welds. British Welding Journal, 8 (11), 526-540, November 1961.

/ 101 / KAMMER, P.A., MASUBUCHI, K. & MONROE, R.E. Cracking in High-Strength Steel Weldments - A Critical Review. DMIC Report 197, Battele Memorial Institute, Ohio, USA, February 1964.

/ 102 / WIDGERY, D.J. Composition and Solidification Cracking in Ferritic Weld Metals. The Welding Institute, Research Bulletin, 12 (7), 196-200, July 1971.

/ 103 / SIMPSON, M. & TAIT, W.P. Solidification Crackings During the Submerged Arc Welding of Carbon Manganese Steels - A Review. Welding Research International, 7 (3), 177-192, 1977.

/ 104 / BAILEY, N. & JONES, S.B. Solidification Cracking. The Welding Institute, 1977.

/ 105 / BAILEY, N. & JONES, S.B. The Solidification Cracking of Ferritic Steel During Submerged Arc Welding. Welding Journal, 57 (8), 217s-231s, August 1978.

/ 106 / BORLAND, J.C. Fundamentals of Solidification Cracking in Welds, Part 1. Welding and Metal Fabrication, 47 (1), 19-29, January/February 1979.

/ 107 / Ibid, Part 2. Welding and Metal Fabrication, 47 (2), 99-107, March 1979.

/ 108 / DIXON, B.D. Weld Metal Solidification Cracking in Ferritic Steels - A Review. Australian Welding Journal, 26, 23-30, Summer 1981.

/ 109 / BRIGGS, C.W. & GEZELIUS, R.A. Studies on Solidification in Steel Castings. Trans. Amer. Foundrymen's Soc. 42, 449-476, 1934.

/ 110 /	BRIGGS, C.W. & GEZELIUS, R.A.	Studies on Solidification and Contractions in Steel Castings. Trans. Amer. Foundrymen's Soc., 44, 1-31, 1936.
/ 111 /	VERO, J.	The Hot Shortness of Aluminium Alloys. Trans. Met. Ind. 48 (4), 431-494, 1936.
/ 112 /	LUTTS, C.J. & HICKEY, J.P.	Special Low Carbon Steel for Castings. Trans. Amer. Foundrymen's Soc., 52, 904-912, 1944.
/ 113 /	GALPERIN, N.B.	Steel Susceptibility to Hot-ear Formation in Casting. Trans. Amer. Foundrymen's Soc., 54, 724-726, 1946.
/ 114 /	LEES, D.C.G.	The Hot Tearing Tendencies of Aluminium Casting Alloys. The J. of The Inst. of Metals, 72, 343-364, 1946.
/ 115 /	SPRARAGEN, W. & CLAUSSEN, G.E.	The Effect of Sulphur on the Welding of Steel - A Review of the Literature to 1 July, 1937. Welding Journal, 18 (2), 44s-49s, February 1939.
/ 116 /	SINGER, A.R.E. & COTTRELL, S.A.	Properties of the Aluminium - Silicon Alloys at Temperatures in the Region of the Solidus. The J. of The Inst. of Metals, 73, 33-54, 1947.
/ 117 /	SINGER, A.R.E. & JENNINGS, P.H.	Hot-Shortness of Aluminium-Silicon Alloys of Commercial Purity. The J. of The Inst. of Metals, 73, 197-212, 1947.
/ 118 /	PUMPHREY, W.I. & JENNINGS, P.H.	A Consideration of the Nature of Brittleness at Temperatures Above the Solidus in Castings and Welds in Aluminium Alloys. The J. of The Inst. of Metals, 75, 235-256, 1948.
/ 119 /	MEDOVAR, B.I.	On the Nature of Weld Hot Cracking. Automatic Welding, 7 (4), 12-18, 1954.
/ 120 /	PROKHOROV, N.N.	The problem of the Strength of Metals Whilst Solidifying During Welding. Welding Production, 3 (6), 5-11, 1956.
/ 121 /	PROKHOROV, N.N. & BOCHAI, M.P.	Mechanical Properties of Aluminium Alloys in the Crystallisation Temperature Range During Welding. Welding Production, 5 (2), 1-6, 1958.
/ 122 /	PROKHOROV, N.N.	The Technological Strength of Metals While Crystallising During Welding Production, 9 (4), 1-5, 1962.
/ 123 /	PROKHOROV, N.N.	Ductility of Solidifying Metals. Russian Casting Production, 10, 176-179, 1962.
/ 124 /	PROKHOROV, N.N., PROKHOROV, N. NIKOL & GAVRILYUK, M.N.	Strain Behaviour of Metals During Solidification after Welding. Welding Production, 18 (6), 8-13, 1971.

/ 125 / BISHOP, H.F., ACKERLIND, C.E. & PELLINI, W.S. Metallurgy and Mechanics of Hot Tearing. Trans. Amer. Foundrymen's Soc. 60, 818-831, Discussion: 831-833, 1952.

/ 126 / PELLINI, W.S. Strain Theory of Hot Tearing. Foundry, 80, 125-133, 192, 194, 196, 199, (1952.)

/ 127 / APBLETT, W.R. & PELLINI, W.S. Factors which Influence Weld Hot Cracking. Welding Journal, 33 (2), 83s-90s, February, 1954.

/ 128 / SAVEIKO, V.N. Theory of Hot Tearing. Russian Casting Production, 8, 453-456, 1960.

/ 129 / ROGERSON, J.H. & BORLAND, J.C. Effect of The Shapes of Intergranular Liquid on the Hot Cracking of Welds and Castings. Trans. Met. Soc. AIME, 227, 2-7, February 1963.

/ 130 / SMITH, C.S. Grains, Phases and Interfaces: An Interpretation of Microstructure. Trans. Met. Soc. AIME, 175, 15-52, 1948.

/ 131 / MASUBUCHI, K. Analysis of Welded Structures, P.520, Pergamon Press, 1980.

/ 132 / GARLAND, J.G. & BAILEY, N. Solidification Cracking During the Submerged-Arc Welding of Carbon-Manganese Steels - The Effect of Parent Plate Composition: Carbon Manganese, Sulphur and Phosphorus. Welding Research International, 5 (1), 1-33, 1975.

/ 133 / WILKINSON, F.J., COTTRELL, C.L.M. & HUXLEY, H.V. Calculating Hot Cracking Resistance of High Tensile Alloy Steel. British Welding Journal, 5 (12), 557-562, December 1958.

/ 134 / NAKAGAWA, H., MATSUDA, F. & SENDA, T. Effect of Sulphur on Solidification Cracking in Weld Metal of Steel (Report 1.) Trans. Jap. Weld. Soc. 5 (1), 39-46, April 1974.

/ 135 / KEH, A.S. & VAN VLACK, L.H. Microstructure of Iron-Sulphur Alloys. Trans. AIME, 206 (4), 950-958, 1956.

/ 136 / WOLSTENHOLME, D.A. & BONISZEWSKI, T. Effect of Manganese on Solidification Cracking in 2 CrMo Manual Metal-Arc Weld. Welding and Metal Fabrication, 40, (1), 59-67, February, 1972.

/ 137 / OHSHITA, S. et al. Prevention of Solidification Cracking in Very Low Carbon Steel Welds. Welding Journal, 62 (5), 129s-136s, May 1983.

/ 138 / HUXLEY, H.V. The Influence of Composition on Weld Solidification Cracking in Carbon Manganese Steel. Metallurgia, 82, 167-174, November 1970.

/ 139 / JONES, P.W. An Investigation of Hot Cracking in Low-Alloy Steel Welds. British Welding Journal 6 (6), 282-290, June 1959.

/ 140 / NAKAGAWA, H., MATSUDA, F. & SENDA, T. Effect of Sulphur on Solidification Cracking in Weld Metal of Steel (Report 2). Trans. Jap. Weld. Soc. 5 (2), 192-197, September 1974.

/ 141 / NAKAGAWA, H. et al. Ibid (Report 3). Trans. Jap. Weld. Soc. 5 (2), 134-141, September 1974.

/ 142 / Ibid (Report 4). Trans. Jap. Weld. Soc. 5 (2), 126-133, September 1974.

/ 143 / Ibid (Report 5). Trans. Jap Weld. Soc. 6 (1), 3-9, April, 1975.

/ 144 / Ibid (Report 6). Trans. Jap. Weld. Soc. 6 (1), 10-16, April 1975.

/ 145 / MATSUDA, F. & SAVAGE, W.F. Effect of Individual Alloying Element on Hot-Cracking of Two Low Alloy Steels. Techn. Rep. Osaka Univ. 19 (876/907), 467-491, 1969.

/ 146 / KAL'NER, D.A. & RUSSIYAN, A.V. Increasing the Hot Cracking Resistance of Structural Steels During Welding. Welding Production 17, (5), 55-58, 1970.

/ 147 / MASUMOTO, I. & IMAI, K. A Metallurgical Aspect of Hot Cracking and Toughness of Weld Metal. Trans. Jap. Weld Res. Inst. 1 (1), 104-111, April 1970.

/ 148 / WOLSTENHOLME, D.A. & BONISZEWSKI, T. The Susceptibility to Solidification Cracking in 2 1/4 Cr - 1Mo Weld Metal Deposited from Basic Electrodes. Metal Construction, 1 (2s), 78-85, February 1969.

/ 149 / MORGAN-WARREN, E.J. & JORDAN, M.F. Technical Note: Role of Oxygen in Weld Solidification Cracking in Low-Alloy High-Strength Steels. J. of the Iron and Steel Inst. 210 (1), 868-869, November, 1972.

/ 150 / MORGAN-WARREN, E.J. & JORDAN, M.F. A quantitative Study of The Effect of Composition on Weld Solidification Cracking in Low-Alloy Steels. Metals Technology, 1 (6), 271-278, June 1974.

/ 151 / LEINACHUK, E.I. et al. Influence of Titanium on The Resistance of Deposited Metal to Solidification Cracking. Automatic Welding, 27 (7), 19-22, 1974.

/ 152 / MANDEL'BERG, S.E. et al. Resistance of Welded Joints in Tube Steels to Hot Cracking. Automatic Welding, 25 (3), 1-5, 1972.

/ 153 / UL'YANOV, V.I. et al. Effects of Titanium on The Technological Properties of Type SV-08G2S Wire. Automatic Welding, 26 (6), 56-60, 1973.

/ 154 / GARLAND, J.G. & BAILEY, N. Solidification Cracking During the Submerged Arc Welding of Carbon-Manganese Steels - A Detailed Assessment of the Effect of Parent Plate Composition. Welding Research International, 8 (3), 240-281, 1978.

/ 155 / WIDGERY, D.J. The Effects of Copper in Mild Steel Weld Metal. Metal Construction, 10 (10), 480, 481, 483, October, 1978.

/ 156 / LEINACHUK, E.I., PODGAETSKII, V.V. & PARFESSA, G.I. Effects of Molybdenum and Tungsten on the Resistance of Welds to Hot Cracking During Welding. Automatic Welding, 26 (11), 10-15, 1973.

/ 157 / LEINACHUK, E.I. & PARFESSA, G.I. Effects of Vanadium on The Susceptibility of Deposited Metal to Hot Cracking. Automatic Welding, 22 (1), 14-18, 1969.

/ 158 / TOLSTYKH, L.G. The Effect of Cr, Ni and Mo on The Hot Cracking Susceptibility of Steel Okh 6N7M7S. Welding Production, 24 (5), 11-13, 1977.

/ 159 / LEINACHUK, E.I. et al. Effects of Niobium on The Resistance of Welds to Hot Cracking During Welding. Automatic Welding, 27 (9), 8-12, 1974.

/ 160 / ORNICHEV, S.I. et al. Effects of Niobium on Properties of Welded Joints. Welding Production, 19 (4), 51-56, 1972.

/ 161 / AGANAEV, Yu. P., BARMIN, L.N. & KULISHENKO, B.A. The Effect of Structure on the Formation of Solidification Cracks in Iron Boron Alloys. Welding Production, 26 (8), 10-13, 1979.

/ 162 / HUXLEY, H.V. Effect of Sulphur, Phosphorus, Arsenic, Tin and Copper on The Weldability of 2% Ni-Cr-Mo Low Alloy Steel Sheet. Welding and Metal Fabrication, 38 (7), 288-292, July 1970.

/ 163 / GROSS, J.H. The New Development in Steel Weldments. Welding Journal, 47 (6), 241s-270s, June 1968.

/ 164 / VADIVASOV, D.G. et al. Influence of Modifiers on Process Strength of Deposits in Sumberged-Arc Resurfacing. Welding Production 20 (5), 15-18, 1973.

/ 165 / WILKINSON, F.J. & COTTRELL, C.L.M. Factors Affecting Weldability of High Strength One Per Cent Chromium - Molybd enum and Other Steels. Welding and Metal Fabrication, 26 (5), 171-184, May 1958.

/ 166 / OSTROVSKAYA, S.A. Assessing The Resistance of Steel to Hot Cracking in The Weld Metal. Automatic Welding, 17 (1), 1-6, 1964.

/ 167 / HUXLEY, H.V. Phosphorus and The Weldability of High Strength Steel Sheet. Welding and Metal Fabrication, 31 (1), 29-32, January 1963.

/ 168 / COTTRELL, C.L.M. Factors Affecting the Fracture of High-Strength Steels. Journal of the Iron and Steel Inst. 203, 597-604, June 1965.

/ 169 / McKEOWN, D.J. Versatile Weld Metal Cracking Tests. Metal Construction, 2 (8), 351-352, August 1970.

/ 170 / MASUBUCHI, K. Control of Distortion and Shrinkage in Welding. Weld. Res. Council Bulletin 149, USA, 1970.

/ 171 / MASUBUCHI, K. Integration of NASA - Sponsored Studies on Aluminium Welding, NASA CR-2064, June 1972.

/ 172 / KLEIN, K.M. Investigation of Welding Thermal Strains in Marine Steels. M.Sc., Thesis, M.I.T., 1971.

/ 173 / ANON The Physical Properties of a Series of Steels, Part II, Journal of Iron and Steel Institute, 154 (2), 83-121, 1946.

/ 174 / NIPPES, E.F. & SAVAGE, W.F. Development of Specimen Simulating Weld Heat-Affected Zones. Welding Journal, 28 (11), 534s-546s, November 1949.

/ 175 / YENISCAVICH, W. Correlation of Hot Ductility Curves with Cracking During Welding. Proc. of a Symp. Methods of High-Alloy Weldability Evaluation. Welding Res. Council, USA, 1970.

/ 176 / DUVAL, D.S. & OWCZARSKI, W.A. Further Heat-Affected Zone Studies in Heat-Resistant Nickel Alloys. Welding Journal 46 (9), 423s-432s, September 1967.

/ 177 / TALL, L. Residual Stresses in Welded Plates - A Theoretical Study. Welding Journal, 43 (1), 10s-23s, January, 1964.

/ 178 / WELLS, R.L. A Study of Cracking During Welding of Aluminium Alloys. Journal of Basic Eng. Trans. ASME, 89 (1), 40-48, March 1967.

/ 179 / STEENBERGEN, J.E. & THORNTON, H.R. A Quantitative Determination of the Conditions for Hot Cracking During Welding for Aluminium Alloys. Welding Journal, 49 (2), 61s-68s, February 1970.

/ 180 / LOW, Jr. J.R. The Effect of Quench-Aging on the Notch Sensitivity of Steel. Welding Journal, 31 (5), 253s-256s, May 1952.

/ 181 / PROKHOROV, N.N., OSOKINA, T.N. & PROKHOROV, N. NIKOL Plastic Strain Distribution in Welded Joints, Welding Production, 17 (8), 17-20, 1970.

/ 182 / KASATKIN, B.S. & TSARYUK, A.K. — Special Features of Plastic Deformation in the Heat Affected Zone. Automatic Welding, 18 (2), 1-7, 1965.

/ 183 / OUDEN, G. den. — Internal Friction and Ductility in the Heat-Affected Zone. Metal Construction and British Welding Journal, 4 (3), 94-95, March 1972.

/ 184 / WEISS, B., GROTKE, G.E. & STICKLER, R. — Physical Metallurgy of Hot Ductility Testing. Welding Journal, 49 (10), 471s-487s, October 1970.

/ 185 / ERASMUS, L.A. — Effect of Small Additions of Vanadium on the Austenitic Grain Size, Forgeability and Impact Properties of Steel. Journal Iron and Steel Inst, 202, 128-134, February 1964.

/ 186 / BARFORD, J. & MYERS, J. — Structure Related to Hot Ductility of Three Austenitic Steels. Journal Iron and Steel Inst., 201, 1025-1031, December 1963.

/ 187 / WILBERG, G.A. et al. — The Effects of Thermal History and Composition on the Hot Ductility of Low Carbon Steels. Metallurgical Transactions A. 6A (9), 1727-1735, September 1975.

/ 188 / SOETE, W. et al — Exhaustion of Ductility by Hot Straining or Welding. IIW Doc. X - 431-67, 1967.

/ 189 / DE CHAENE, R., DE COCK, J. & DE CALUWE, W. — Measurement of Transient Thermal Plastic Strains. Journal of The Brit. Soc. for Strain Measurement, 4 (4), 1-7, October 1968.

/ 190 / JOHN, R. & RICHARDS, W.G. — Hot Cracking in 5% Nickel Steel Weld-Metal. Metal Construction and British Welding Journal, 4 (4), 127-132, April 1972.

/ 191 / MORGAN-WARREN, E.J. & JORDAN, M.F. — Effects of Travel Speed on Solidification Cracking in Autogenous Tungsten Inert Gas Arc Welding of Low-Alloy Steel Sheet. Metals Technology, 3 (1), 29-39, January 1976.

/ 192 / JOHNSON, L. — Formation of Plastic Strains During Welding of Aluminium Alloys. Welding Journal, 52 (7), 298s-305s, July 1973.

/ 193 / CHIHOSKI, R.A. — Understanding Weld Cracking in Aluminium Sheet. Welding Journal, 51 (1), 24-30, January 1972.

/ 194 / CHIHOSKI, R.A. — The Character of Stress Fields Around a Weld Arc Moving on Aluminium Sheet. Welding Journal, 51 (1), 9s-18s, January 1972.

/ 195 / GARLAND, J.G. — Solidification Cracking During the Submerged Arc Welding of Carbon-Manganese Steels - the relative importance of parent Plate Strength and Composition. Welding Research International, 9, (1), 59-82, 1979.

/ 196 / APPS, R.L., GOURD, L.M. & NELSON, K.A. — Effect of Welding Variables Upon Bead Shape and Size in Submerged Arc Welding. Welding and Metal Fabrication, 31 (11), 453-457, November 1963.

/ 197 / DRAYTON, P.A. — An Examination of the Influence of Process Parameters on Submerged Arc Welding. Welding Research International, 2, (2), 1-19, 1972.

/ 198 / BORLAND, J.C. & ROGERSON, J.H. — Examination of the Patch Test for Assessing Hot Cracking Tendencies of Weld Metal. British Welding Journal, 9 (8), 494-499, August 1962.

/ 199 / ROGERSON, J.H., COTTEREL, B. & BORLAND, J.C. — An Analysis and Evaluation of the Houldcroft Weld Cracking Test. Welding Journal 42 (6), 264s-268s, June 1963.

/ 200 / BORLAND, J.C. & ROGERSON, J.H. — Comparison of Houldcroft and Patch Weld Cracking Tests. Welding Journal, 42 (4), 160s-163s, April 1963.

/ 201 / SAVAGE, W.F., LUNKIN, C.D. & HRUBEC, R.J. — Segregation and Hot Cracking in Low-Alloy Quench and Tempered Steels. Welding Journal, 47 (9), 420s-425s, September 1968.

/ 202 / SAVAGE, W.F. & LUNDIN, C.D. — The Varestraint Test. Welding Journal 44 (10), 443s-442s, October 1965.

/ 203 / TULIANI, S.S. BONISZEWSKI, T. & EATON, N.F. — Notch Toughness of Commercial Submerged-Arc Weld Metal. Welding and Metal Fabrication, 37 (8), 327-339, August 1969.

/ 204 / GARLAND, J.G. & KIRKWOOD, P.R. — Towards Improved Submerged Arc Weld Metal, Part 1. Metal Construction, 7 (5), 275-283, May 1975.

/ 205 / BAILEY, N. — Effect of Wire Composition and Flux Type on Solidification Cracking When Submerged Arc Welding C-Mn Steels. Welding Research International, 8 (3), 215-238, 1978.

/ 206 / BENNETT, A.P. — Submerged-Arc Welding of Q.T. 35. Industrial Production of the N.C.R.E. Flux. NCRE Report R546, May 1968.

/ 207 / TULIANI, S.S., BONISZEWSKI, T. & EATON, N.F. — Carbonate Fluxes for Submerged-Arc Welding of Mild Steel. Welding and Metal Fabrication, 40 (7), 247-259, July 1972.

/ 208 / PATCHETT, B.M., DEMOS, G.A. & APPS, R.L. The Influence of Flux Composition and Welding Parameters on Heat Distribution in Submerged-Arc Welding. Welding Research International, 4 (2), 81-94, 1974.

/ 209 / LEWIS, W.J., FAULKNER, G.E. & RIEPPEL, P.Y. Flux and Filler-Wire Developments for Submerged-Arc Welding HY-80 Steel. Welding Journal, 26 (8), 337s-345s, August 1961.

/ 210 / RICHARDSON, F.D. Physical Chemistry of Melts in Metallurgy, Vol. 1, Academic Press, 1974.

/ 211 / KUBLI, R.A. & SHARAV, W.B. Advancements in Submerged-Arc Welding of High Impact Steels. Welding Journal, 40 (11), 497s-502s, November 1961.

/ 212 / SEKIGUCHI, H. Recent Advancement of CO_2O_2 Arc Welding Process in Japan. IIW December, XII, 127-62, 1962.

/ 213 / BONISZEWSKI, T. Letter to The Editor: Basic Fluxes and Dioxidation in Submerged-Arc Welding of Steel. Metal Construction and British Welding Journal, 6 (4), 128-129, April 1974.

/ 214 / EAGAR, T.W. Sources of Weld Metal Oxygen Contamination During Submerged Arc Welding. Welding Journal, 57 (3), 76s-80s, March 1978.

/ 215 / NORTH, T.H. et al. Slag/Megal Interaction, Oxygen and Toughness in Submerged Arc Welding. Welding Journal 57, (3), 63s-75s, March 1978.

/ 216 / VALETTE, J La Disoxydation du Metal Fondu. Consequences Pratiques. Soudage et Techniques Connexes. 35 (11/12), 412-416, November/December 1981.

/ 217 / GARLAND, J.G. & KIRKWOOD, P.R. A Reappraisal of the Relationship between Flux Basicity and Mechanical Properties in Submerged-Arc Welding. Welding and Metal Fabrication, 44 (4), 217-224, April 1976.

/ 218 / WIDGERY, D.J. Deoxidation Practice and the Toughness of Mild Steel Weld Metal. PhD. Thesis, University of Cambridge, 1974.

/ 219 / FARRAR, R.A. The Role of Inclusions in the Weld Ductile Fracture of Weld Metals. Welding and Metal Fabrication, 44 (8), 578-581, August 1976.

/ 220 / LEVINE, E. & HILL, D.C. Structure-Property Relationships in Lo C Weld Metal. Metallurgical Transactions A. (9), 1453-1463, September 1977.

/ 221 / CHOI, C.L. & HILL, D.C. — A Study of Microstructural Progression in As-Deposited Weld Metal. Welding Journal, 57 (8), 232s-236s, August 1978.

/ 222 / ALCANTARA, N.G. — Weld Metal Hydrogen Cold Cracking. PhD. Thesis, CIT, 1982.

/ 223 / DOS SANTOS, J.F. — Factors Affecting Transformation and Microstructure in High Strength Ferritic MMA Weld Metals. PhD. Thesis, CIT, 1983.

/ 224 / DOLBY, R.E. — Advances in The Welding Metallurgy of Steel. Proc. Int. Conf. Advances in The Physical Metallurgy and Applications of Steels. University of Liverpool. The Metals Soc., September 1981.

/ 225 / ABSON, D.J. DOLBY, R.E. & HART, P.H.M. — The Role of Nonmetallic Inclusions in Ferrite Nucleation in Carbon Steel Weld Metals. The Welding Institute Int. Conf. Trends in Steels and Consumables for Welding. London, 1978.

/ 226 / COCHRANE, R.C. & KIRKWOOD, P.R. — The Effect of Oxygen on Weld Metal Microstructure. The Welding Institute Int. Conf. Trends in Steels and Consumables for Welding, London, 1978.

/ 227 / DOLBY, R.E. — Factor Controlling HAZ and Weld Metal Toughness in C-Mn Steels. Proc. 1st Nat. Conf. on Fracture, Johanesburg, 1979.

/ 228 / DOLBY, R.E. — The Influence of Nanadium on The Microstructure and Toughness of Ferritic Weld Metal - A Review. Metal Construction, 14 (3), 148-153, March 1982.

/ 229 / KEELER, T. & GARLAND, J.G. — How SA Welding Adopted to The Offshore Challenge. Part 1, Welding and Metal Fabrication, 51 (4), 129-133, April 1983.

/ 230 / GRANJON, H. & GAILLARD, R. — Possibilities Offertes par l'analyse Thermique "in situ" pour l'etude des Transformations de l'acier au Cours du Soundage. Revue de Metallurgie, 64 (4), 335-343, 1967.

/ 231 / RODRIQUES, P.E.L.B. — The Relationship between The Welding Conditions, Thermal Cycles, Microstructure and Toughness of Weld Metal in C-Mn Steels, PhD. Thesis, CIT, 1978.

/ 232 / BRITISH STANDARD 18 — Methods for Tensile Testing of Metals, Part 2, 1971.

/ 233 / BRITISH STANDARD 131 — Methods for Notched Bar Tests. Part 2. Charpy V-Notch Impact Test.

/ 234 / DAVIS, M.L.E. & BAILEY, N. — The Influence of Flux on Element Transfer During Submerged-Arc Welding. The Welding Institute Report 66/1978/M, June 1978.

/ 235 /	MILITARY SPECIFICATION	Steel Plate, Alloy, Structural High Yield Strength, MIL-S-16216 (Ships), (USA.)
/ 236 /		American Society for Testing and Materials - ASTM A543 Class 2.
/ 237 /	KIHARA, H. et al.	Weld Cracking Test of High-Strength Steels and Electrodes. Welding Journal, 41 (1), 36s-48s, January 1962.
/ 238 /	WINN, W.H.	Weldability of Low Alloy Steels. British Welding Journal, 11 (8), 366-376, August 1964.
/ 239 /	COOLEN, A. CARON, F. & LECLERC, J.	Developments by Usinor to Meet New Pipeline Requirements. p.209-213, Proc. Int. Conf. Steels for Linepipe and Pipeline Fittings. The Metals Society, London, October 1981.
/ 240 /	DOLBY, R.E.	Welding and Fracture Initiation in QT Low Alloy Steels. Metal Construction and British Welding Journal, 3 (3), 99-103, March, 1971.
/ 241 /	NELSON, K.A.	Personal Communication (Head of the Welding Laboratory - CIT.)
/ 242 /	ABSON, D.J. & DOLBY, R.E.	A Scheme for the Quantitative Description of Ferritic Weld Metal Microstructures. The Welding Institute Research Bulletin, 21 (4), 100-103, April, 1980.
/ 243 /	SMITH, E. CAMPBELL, D.Y. & APPS, R.L.	Submerged-Arc Weld Deposits in Navy Q1 Steels. Welding and Metal Fabrication, 42 (3), 104-110, March 1974.
/ 244 /	BORLAND, J.C.	Cracking Tests for Assessing Weldability, British Welding Journal, 7 (10), 623-637, October 1960.
/ 245 /	STOUT, R.D. & DOTY, W.O.	Weldability of Steels. Welding Research Council, N.York, 1971.
/ 246 /		U.S. Navy Bureau of Ships - Navships 0900-006-9010.
/ 247 /	BAILEY, N.	Solidification Cracking in MIG Fillet Welds. Metal Construction and British Welding Journal, 6 (5), 143-147, May 1974.
/ 248 /		Welding Handbook, Vol. 1. American Welding Society, 1976.
/ 249 /	GRONG, Ø. & CHRISTENSEN, N.	Factors Controlling MIG Weld Metal Chemistry. Scandinavian Journal of Metallurgy, 12 (4), 155-165, 1983.
/ 250 /	ROSENTHAL, D.	Mathematical Theory of Heat Distribution During Welding and Cutting. Welding Journal, 20 (5), 220s-234s, May 1941.

/ 251 / MYERS, P.S. et al. Fundamentals of Heat Flow in Welding. Welding Research Bulletin, No. 123, 1967.

/ 252 / PROKHOROV, N.N. & SHIRSHOV, Yu, V. Influence of Welding Conditions and Chemical Composition of The Base Metal on The Primary Structure of Weld Metal. Automatic Welding, 27 (3), 6-8, 1974.

/ 253 / GANAHA, T. & KERR, H.W. TIG Weld Solidification Structures in Carbon Sheet Steels. Metals Technology, 5 (2), 62-69, February 1978.

/ 254 / FRASER, F.W. & METZBOWER, E.A. Alloy Segregation, Solidification, Microstructure and Hardness of High Strength Weld Metal. Proc. Symp. Physical Metallurgy of Metal Joining, AIME, USA, October 1980.

/ 255 / RUSSEL, J.D. Investigation of Cracking Problem in Electron Beam Welding High Alloy Steel. Welding Research International, 5 (4), 1-19, 1975.

/ 256 / BONISZEWSKI, T., WATKINSON, F. & BAKER, R.G. Heat-Affected Zone Cold Cracking in Low Alloy Steels. Paper M5. Commonwealth Welding Conference, London, 1965.

/ 257 / SAVAGE, W.F. et al. Hydrogen Induced Cracking in H-80 Steel Weldments. Welding Journal 55 (11), 368s-376s, November 1976.

/ 258 / ROBINSON, J.L. & SCOTT, M.H. Liquation Cracking During The Welding of Austenitic Stainless Steels and Nickel Alloys. Phil. Trans. Royal Soc. London, A295, 105-107, 1980.

/ 259 / ABSON, D.J. & DOLBY, R.E. Microstructural Transformations in Steel Weld Metals - A Reappraisal. The Welding Institute Research Bulletin, 19 (7), 202-207, July 1978.

/ 260 / IRVINE, K.J. A Comparison of The Bainite Transformation with Other Strengthening Mechanisms in High-Strength Structural Steel. Symp. Steel-Strengthening Mechanisms. Glimax Molybdenum Company, May 1969.

/ 261 / COCHRANE, R.C. Weld Metal Microstructures and Terminology. British Steel Corporation Report T/PDM/462/1/77/C, November 1977.

/ 262 / CHRISTENSEN, N. & SIMONSEN, T. Transformation Behaviour of Weld Metal. Scandinavian Journal of Metallurgy, 10 (4), 147-156, 1981.

/ 263 / IIW Commission IX J 'Weld Metal Microstructure Classification Exercise'. Robin Round No. 3, April 1983.

/ 264 / MACHADO, I.G. Weld Solidification Cracking in a Naval Constructional Steel. MSc. Thesis, UFRGS, Brazil, 1980 (in Portuguese).

/ 265 / ROBERTS, D.K. & WELLS, A.A. Fusion Welding of Aluminium Alloys. British Welding Journal, 1 (12), 553-560, December 1954.

/ 266 / HOULDCROFT, P.T. A Simple Cracking Test for Use with Argon-Arc Welding. British Welding Journal, 2 (10), 471-475, October 1955.

/ 267 / HOULDCROFT, P.T. Part III - Dilution and Uniformity in Aluminium Alloy Weld Beads. British Welding Journal, 1 (10), 468-472, October 1954.

/ 268 / BARRY, B.A. Errors in Practical Measurement in Science Engineering and Technology. Ed. M.D. MORRIS, John Willey & Sons, Inc., 1978.

APPENDIX A

DILUTION AND EXPECTED CONTENT

The weld bead dilution (D) can be calculated through the nickel (or copper) content, which recovery is taken as 100%. Thus, from HOULDCROFT / 267 /:

$$D = 100 \frac{(Ni_w - Ni_f)}{(Ni_p - Ni_f)}$$

where Ni_w = actual % of Ni in the weld metal.

Ni_f = actual % of Ni in the filler.

Ni_p = actual % of Ni in the parent metal.

Considering the 'standard deviations' given for the nickel analysis, the error for the dilution is:

$$E_D = 100\left(\frac{Ni_w - Ni_f}{Ni_p - Ni_f}\right)\sqrt{\left(\frac{0.04}{Ni_w - Ni_p}\right)^2 + \left(\frac{0.04}{Ni_p - Ni_f}\right)^2}$$

Then, the expected (EXP) content for any element is:

$$EXP = \frac{D\,(A_p - A_f)}{100} + A_f$$

where A_p = actual % of element A in the parent metal

A_f = actual % of element A in the filler

The error for EXP is:

$$E_{EXP} = \frac{D\,(A_p - A_f)\sqrt{\left(\frac{E_D}{D}\right)^2 + \left(\frac{E_{A_p - A_f}}{A_p - A_f}\right)^2}}{100} + E_{A_p}$$

where $E_{A_p - A_f}$ = error for the difference between the % of element A in the parent metal and filler, respectively.

E_{A_f} = error for the % of element A in the filler

The different (DIF) is between the actual analysed (ANA) content for the element A in the weldmetal, less its expected (EXP) content:

Thus:

$$DIF = ANA - EXP$$

$$E_{DIF} = E_{ANA} + E_{EXP}$$

In these derivations it was assumed that the maximum error for the sum or difference is the sum of the errors of each quantity. See, for example, BARRY / 268 /.

APPENDIX B

ISOTHERMIC PATTERN

This model of weld heat flow was based on the approach given by MYERS et al / 251 /.

The basic equation that gives the material temperature at any time or position around the weld pool is:

$$T = T_o + \frac{Q}{4\pi KR} \text{ EXP } (-LV(R + W))$$

where

T_o = preheat temperature (^oC)

Q = power input (U x I = watts)

K = thermal conductivity (0.05 J/mm.s.^oC for steels)

R = $(W^2 + Y^2 + Z^2)^{1/2}$

W = moving coordinate (with the arc) in the welding direction (mm)

Y,Z = distance measured at right angles to the axis of the arc (mm)

V = welding speed (mm/s)

a = thermal diffusivity (7.5 mm^2/s for steels)

L = $\frac{1}{2a}$ = 0.0667 (s/mm^2)

Note: The Y and W axes are in a plane parallel to the plate surface. The axis Z extends into the plate.

As it is wellknown, the only way to get the isothermic pattern in a plane parallel to the plate surface is through interactive methods. In this work the coordinate Z was chosen to be 0 at the mid plate thickness and the preheat (T_o) constant and equal to 120^oC, leaving, therefore, only the W and Y coordinates to be calculated, depending on the welding parameters.

First of all, we decided that the isotherms of 1400, 1200, 900, 700, 500 and 300^oC would illustrate the model. After this, a time interval of 0.5 s between the events was found to be convenient. Then, the W values were calculated at each interval (it is the product of speed and time elapsed, and has a negative signal), until the only existing isotherm was the 300^oC. From its values, and the Y values calculated at each 0.001 mm interval, the isotherms were plotted using the program enclosed (Program Isothermic - DISOT).

```
C**** PROGRAM ISOTHERMIC (DISOT)
C
C**** A PROGRAM TO PLOT ON THE SAME SHEET OF PAPER THREE
C      DIFFERENT ISOTHERMIC PATTERN FOR THE CONDITIONS 641,
C      674 AND 1371 ( Z=0,  PH=120C)
C
       DIMENSION AX1(8),BY1(8),AX2(8),BY2(8),AX3(10),BY3(10
      1),AX4(13),BY4(13),AX5(16),BY5(16),AX6(20),BY6(20),
      1CX1(13),DY1(13),CX2(14),DY2(14),CX3(15),DY3(15),CX4
      1(16),DY4(16),CX5(19),DY5(19),CX6(19),DY6(19),EX1(7),
      1FY1(7),EX2(8),FY2(8),EX3(10),FY3(10),EX4(12),FY4(12)
      1,EX5(14),FY5(14),EX6(14),FY6(14)
       DATA AX1,BY1/2.251,0.,-3.15,-5.,-6.3,-9.45,-12.6,
      1-14.921,0.,3.471,4.53,4.685,4.655,4.161,2.941,0./
       DATA AX2,BY2/2.384,0.,-3.15,-6.3,-9.45,-12.6,-15.75,
      1-17.684,0.,3.714,4.872,5.162,4.923,4.198,2.755,0./
       DATA AX3,BY3/2.647,0.,-3.15,-6.3,-9.45,-12.6,-15.75
      1,-18.9,-22.05,-24.485,0.,4.197,5.523,6.07,6.18,
      15.963,5.446,4.582,3.154,0./
       DATA AX4,BY4/2.894,0.,-3.15,-6.3,-9.45,-12.6,-15.75
      1,-18.9,-22.05,-25.2,-28.35,-31.5,-32.929,0.,4.656,
      16.112,6.85,7.193,7.264,7.116,6.772,6.226,5.443,
      14.323,2.475,0./
       DATA AX5,BY5/3.256,0.,-3.15,-6.3,-9.45,-12.6,-15.75
      1,-18.9,-22.05,-25.2,-28.35,-31.5,-34.65,-37.8,
      1-47.25,-50.259,0.,5.337,6.953,7.912,8.512,8.874,
      19.06,9.102,9.023,8.833,8.54,8.14,7.616,6.966,3.616,
      10./
       DATA AX6,BY6/3.924,0.,-3.15,-6.3,-9.45,-12.6,-15.75
      1,-18.9,-22.05,-25.2,-28.35,-31.5,-34.65,-37.8,
      1-47.25,-56.7,-75.6,-94.5,-103.95,-106.103,0.,6.607,
      18.449,9.704,10.636,11.352,11.912,12.353,12.7,12.962
      1,13.158,13.3,13.381,13.419,13.28,12.815,10.9,7.082,
      13.14,0./
       DATA CX1,DY1/2.884,0.,-3.15,-6.3,-9.45,-12.6,-15.75,
      1-18.9,-22.05,-25.2,-28.35,-31.5,-32.55,0.,4.637,
      16.09,6.821,7.156,7.218,7.059,6.7,6.136,5.326,4.157,
      12.134,0./
       DATA CX2,DY2/3.028,0.,-3.15,-6.3,-9.45,-12.6,-15.75,
      1-18.9,-22.05,-25.2,-28.35,-31.5,-37.8,-38.58,0.,
      14.907,6.428,7.254,7.702,7.894,7.889,7.716,7.386,
      16.898,6.231,5.333,1.848,0./
       DATA CX3,DY3/3.309,0.,-3.15,-6.3,-9.45,-12.6,-15.75
      1,-18.9,-22.05,-25.2,-28.35,-31.5,-37.8,-50.4,
      1-53.413,0.,5.437,7.076,8.063,8.695,9.092,9.316,
      19.401,9.368,9.231,8.995,8.663,7.689,3.65,0./
       DATA CX4,DY4/3.571,0.,-3.15,-6.3,-9.45,-12.6,-15.75
      1,-18.9,-22.05,-25.2,-28.35,-31.5,-37.8,-50.4,-63.,
      1-71.835,0.,5.934,7.667,8.781,9.555,10.106,10.49,
      110.75,10.905,10.973,10.963,10.882,10.526,9.042,
      16.155,0./
       DATA CX5,DY5/3.953,0.,-3.15,-6.3,-9.45,-12.6,-15.75
      1,.,6.664,8.514,9.784,
```

```
     110.728,11.457,12.031,12.485,12.844,13.123,13.335,
     113.488,13.644,13.459,12.711,11.411,8.063,3.368,0./
      DATA CX6,DY6/4.65,0.,-3.15,-6.3,-9.45,-12.6,-15.75
     1,-18.9,-22.05,-25.2,-28.35,-31.5,-37.8,-50.4,-63.,
     1-75.6,-94.5,-107.1,-130.,0.,8.004,10.023,11.516,
     112.7,13.678,14.505,15.216,15.835,16.378,16.857,
     117.283,18.,19.01,19.615,19.916,19.919,19.667,
     118.772/
      DATA EX1,FY1/1.627,0.,-6.9,-13.8,-20.7,-27.6,-32.552
     1,0.,2.703,4.747,4.965,4.424,3.089,0./
      DATA EX2,FY2/1.697,0.,-6.9,-13.8,-20.7,-27.6,-34.5,
     1-38.58,0.,2.836,5.03,5.452,5.2,4.409,2.852,0./
      DATA EX3,FY3/1.832,0.,-6.9,-13.8,-20.7,-27.6,-34.5,
     1-41.4,-48.3,-53.399,0.,3.095,5.546,6.294,6.443,
     16.211,5.656,4.732,3.216,0./
      DATA EX4,FY4/1.957,0.,-6.9,-13.8,-20.7,-27.6,-34.5,
     1-41.4,-48.3,-55.2,-69.,-71.839,0.,3.335,5.994,
     16.987,7.409,7.497,7.341,6.973,6.395,5.574,2.44,0./
      DATA EX5,FY5/2.139,0.,-6.9,-13.8,-20.7,-27.6,-34.5,
     1-41.4,-48.3,-55.2,-69.,-82.8,-103.5,-109.648,0.,
     13.686,6.609,7.892,8.622,9.04,9.25,9.295,9.215,9.015,
     18.283,7.068,3.56,0./
      DATA EX6,FY6/2.467,0.,-6.9,-13.8,-20.7,-27.6,-34.5,
     1-41.4,-48.3,-55.2,-69.,-82.8,-103.5,-130.,0.,4.323,
     17.623,9.329,10.471,11.303,11.932,12.415,12.787,
     113.076,13.428,13.547,13.412,12.728/
      WRITE(2,*)'PENS:BLACK(0.50)=1 , BLACK(0.35)=2'
      WRITE(2,*)'NO. OF PLOTS REQUIRED ?'
      READ(1,*)NPLOT
      CALL TERM
      DO 10 KPLOT=1,NPLOT
      CALL DEVHEA(1)
      CALL WINDOW(2)
C**** TO LABEL AXIS
      CALL CHASIZ(2.,2.)
      CALL PENSEL(1,0.0,0)
      CALL MOVTO2(49.,208.)
      CALL CHAHOL('*L(A)- *UW*LELDING *UP*LARAMETERS: *U1.9
     1 KJ/*LMM , *U30 V , 400 A , 6.3 *LMM/S*.')
      CALL MOVTO2(49.,134.)
      CALL CHAHOL('*L(B)- *UW*LELDING *UP*LARAMETERS: *U4.1
     1 KJ/*LMM , *U34 V , 770 A , 6.3 *LMM/S*.')
      CALL MOVTO2(49.,60.)
      CALL CHAHOL('*L(C)- *UW*LELDING *UP*LARAMETERS: *U1.9
     1 KJ/*LMM , *U30 V , 770 A , 13.8 *LMM/S*.')
      CALL MOVTO2(30.,42.)
      CALL CHASIZ(3.,3.)
      CALL CHAHOL('FIGURE      -  COMPUTED  ISOTHERMIC  PA
     1TTERN  FOR  THREE*.')
      CALL MOVTO2(30.,36.)
      CALL CHAHOL('DIFFERENT WELDING CONDITIONS (120 *LDEG
     1 *UC PREHEAT) ON THE*.')
```

```
      CALL MOVTO2(30.,30.)
      CALL CHAHOL('X-Y  PLANE AND  Z=0  ( HALF THICKNESS
     1 OF A  33*LMM*U  STEEL*.')
      CALL MOVTO2(30.,24.)
      CALL CHAHOL('PLATE ). PLEASE, SEE FIGURE*.')
C**** TO PLOT THE CURVES AND DRAW THE AXIS
      CALL CHASIZ(2.,2.)
      CALL EIXS(222.,214.)
      CALL PENSEL(2,0.0,0)
      CALL GRACUR(AX1,BY1,8)
      CALL GRACUR(AX2,BY2,8)
      CALL GRACUR(AX3,BY3,10)
      CALL GRACUR(AX4,BY4,13)
      CALL GRACUR(AX5,BY5,16)
      CALL GRACUR(AX6,BY6,20)
      CALL PENSEL(1,0.0,0)
      CALL EIXS(148.,140.)
      CALL PENSEL(2,0.0,0)
      CALL GRACUR(CX1,DY1,13)
      CALL GRACUR(CX2,DY2,14)
      CALL GRACUR(CX3,DY3,15)
      CALL GRACUR(CX4,DY4,16)
      CALL GRACUR(CX5,DY5,19)
      CALL GRACUR(CX6,DY6,19)
      CALL PENSEL(1,0.0,0)
      CALL EIXS(74.,66.)
      CALL PENSEL(2,0.0,0)
      CALL GRACUR(EX1,FY1,7)
      CALL GRACUR(EX2,FY2,8)
      CALL GRACUR(EX3,FY3,10)
      CALL GRACUR(EX4,FY4,12)
      CALL GRACUR(EX5,FY5,14)
      CALL GRACUR(EX6,FY6,14)
      CALL PENSEL(1,0.0,0)
      CALL RISK(222.)
      CALL RISK(148.)
      CALL RISK(74.)
10    CONTINUE
      CALL DEVEND
      STOP
      END
C
C**** SUBROUTINES
C
      SUBROUTINE TERM
100   WRITE(2,*)'TERMINAL: 1=T4014 , 2=CALCOMP'
      READ(1,*)BCALL
      GOTO(110,120),BCALL
      GOTO 100
110   CALL T4014
      CALL DEVSPE(4800)
      CALL WINDOW(2)
```

```
      CALL DEVPAP(215.,300.,0)
      GOTO 130
120   CALL CC81
      CALL DEVSPE(2400)
      CALL DEVPAP(215.,300.,0)
      CALL WINDOW(2)
130   CALL PICCLE
      RETURN
      END
C
C
      SUBROUTINE EIXS(YOR,Y)
      CALL AXIPOS(1,49.,YOR,143.,1)
      CALL AXIPOS(1,49.,YOR,50.,2)
      CALL AXISCA(1,14,10.,-130.,1)
      CALL AXISCA(1,5,0.,25.,2)
      CALL AXIDRA(-2,1,1)
      CALL AXIDRA(2,-1,2)
      C=YOR+50.
      CALL MOVTO2(192.,C)
      CALL LINTO2(49.,C)
      CALL MOVTO2(90.,Y)
      CALL CHAHOL('DISTANCE FROM ENERGY SOURCE *L(MM)*.')
      B=Y
      B=B+20.
      CALL CHAANG(90.)
      CALL MOVTO2(38.,B)
      CALL CHAHOL('DISTANCE FROM*.')
      B=B-8.
      CALL MOVTO2(42.,B)
      CALL CHAHOL('WELD CENTRE LINE *L(MM)*.')
      CALL CHAANG(0.)
      RETURN
      END
C
C
      SUBROUTINE RISK(YOR2)
      CALL AXIPOS(1,192.,YOR2,50.,2)
      CALL AXISCA(1,5,0.,25.,2)
      CALL AXIDRA(-2,0,2)
      A=YOR2+3.
      CALL MOVTO2(192.,YOR2)
      CALL LINTO2(195.,A)
      A=A+50.
      CALL LINTO2(195.,A)
      A=A-3.
      CALL LINTO2(192.,A)
      CALL LINTO2(49.,A)
      A=A+3.
      CALL LINTO2(52.,A)
      CALL LINTO2(195.,A)
      RETURN
```

APPENDIX C

LIST OF THE MOST COMMON SYMBOLS, ABBREVIATIONS AND UNITS USED IN THIS WORK

CE	Carbon equivalent
DS	Actual dendrite size (mm)
Energy input	U x I/V (KJ/mm)
HAZ	Heat Affected Zone
HV5	Vickers hardness (136°, 5 Kg load)
HY	High Yield (strength steels)
I	Welding current (A)
SC	Solidification Cracking
SD	Standard Deviation
Sp	Specimen
Q & T	Quenched and Tempered
U	Welding voltage (V)
V	Welding speed (mm/s)
WC	Welding Condition
Z	Apparent dendrite size (mm)
α	Angle between the dendrite growth direction and weld centreline
Wt%	Weight %
TEM	Transmission Electron Microscope
SEM	Scanning Electron Microscope